A Visible Light Driven Nickel Catalyst for Carbonylative Coupling Reactions

Kristian El Chami

A thesis submitted to McGill University in partial fulfillment of the requirements of the degree of Master of Science

Department of Chemistry

McGill University

Montreal, Quebec, Canada

H3A 0B8

August 2022

Abstract

Metal-catalyzed coupling reactions with carbon monoxide offer one of the most efficient methods for the introduction of a carbonyl-containing functionality into organic products. While many variants of the reaction have been developed, these typically rely upon the use of precious metal catalysts, and in particular palladium catalysts, to mediate the coupling of organic halide electrophiles, carbon monoxide and nucleophiles. This is due in part to the ability of palladium catalysts to undergo well-balanced 2-electron oxidative addition and reductive-elimination steps in the presence of coordinating carbon monoxide. Although earth-abundant metals such as nickel complexes were among the earliest catalysts explored in carbonylative coupling reactions, the more strong coordination of nickel(0) to carbon monoxide usually requires high temperatures to overcome in catalysis and limits the scope of these transformations relative to more active palladium catalysts.

Recent research has shown that visible light excitation, either of exogenous photoredox catalysts in concert with metal catalysts, or directly on active metal catalysts, can open new, often radical-based pathways to the oxidative addition/reductive elimination cycle in coupling reactions. This includes results from our lab that demonstrate the direct excitation of palladium catalysts can be used to carry out carbonylations in a versatile fashion. Described herein are our efforts to determine if these principles of visible light excitation might be applied to more earth abundant nickel catalysts. The results show that a rigid, bidentate phosphine ligand coordinated to nickel can allow the carbonylation of alkyl halides with blue light irradiation. Performing the reaction in the presence of a chloride salt has opened a nickel catalyzed route to form acid chlorides, and acid chloride derived products, at ambient temperature and often ambient pressure. Preliminary mechanistic studies have been carried out, which implicate a phosphine-coordinated nickel complex as a plausible photocatalyst. In this, the presence of coordinated carbon monoxide is not inhibitory, and instead light excitation of the carbon monoxide coordinated nickel appears to allow the activation typically unreactive alkyl halides via a radical pathway.

Résumé

Les réactions de couplage catalysées par un métal avec du monoxyde de carbone offrent l'une des méthodes les plus efficaces pour l'introduction d'une fonctionnalité contenant du carbonyle dans des produits organiques. Bien que de nombreuses variantes de la réaction aient été développées, celles-ci reposent généralement sur l'utilisation de catalyseurs de métaux précieux, et en particulier de catalyseurs au palladium, pour assurer le couplage d'électrophiles halogénures organiques, de monoxyde de carbone et de nucléophiles. Cela est dû en partie à la capacité des catalyseurs au palladium à subir des étapes d'addition oxydante et d'élimination réductrice à 2 électrons bien équilibrées en présence de monoxyde de carbone coordinant. Bien que les métaux riches en terre tels que les complexes de nickel aient été parmi les premiers catalyseurs explorés dans les réactions de couplage carbonylatif, la coordination plus forte du nickel (0) au monoxyde de carbone nécessite généralement des températures élevées pour surmonter la catalyse et limite la portée de ces transformations par rapport à plus. catalyseurs au palladium actif.

Des recherches récentes ont montré que l'excitation par la lumière visible, soit de catalyseurs photoredox exogènes de concert avec des catalyseurs métalliques, soit directement sur des catalyseurs métalliques actifs, peut ouvrir de nouvelles voies, souvent radicalaires, vers le cycle d'addition oxydative/élimination réductrice dans les réactions de couplage. Cela inclut les résultats de notre laboratoire qui démontrent que l'excitation directe des catalyseurs au palladium peut être utilisée pour effectuer des carbonylations de manière polyvalente. Décrits ici sont nos efforts pour déterminer si ces principes d'excitation de la lumière visible pourraient être appliqués à des catalyseurs au nickel plus abondants en terre. Les résultats montrent qu'un ligand phosphine bidenté rigide coordonné au nickel peut permettre la carbonylation d'halogénures d'alkyle avec une irradiation à la lumière bleue. La réalisation de la réaction en présence d'un sel de chlorure a ouvert une voie catalysée par le nickel pour former des chlorures d'acide et des produits dérivés de chlorure d'acide, à température ambiante et souvent à pression ambiante. Des études mécanistes préliminaires ont été réalisées, qui impliquent un complexe de nickel coordonné à la phosphine comme photocatalyseur plausible. En cela, la présence de monoxyde de carbone coordonné n'est pas inhibitrice, et à la place, une excitation lumineuse du nickel coordonné au monoxyde de carbone semble permettre l'activation des halogénures d'alkyle généralement non réactifs via une voie radicalaire.

Table of Contents

List of Schemes

List of Figures

List of Tables

List of Abbreviations

^{1}H: Proton

^{19}F: 19-Fluorine

^{31}P: 31-Phosphorus

[^{11}C]CO: Carbon-11 labelled carbon monoxide

[^{11}C]CH2O: Carbon-11 labelled formaldehyde

Å: Angstrom

acac: Acetylacetone

ADMAL: allyloxydimethylaluminum

$AlMe_3$: Trimethylaluminum

Alk: Alkyl

aq.: Aqueous

Ar: Aryl

$AsPh_3$: Triphenylarsine

atm.: Atmosphere

B.B.: Benzyl benzoate

BF_4^-: Tetrafluoroborate cation

Bn: Benzyl

Bu_4NBF_4: Tetrabutylammonium tetrafluoroborate

Bu_4NCl: Tetrabutylammonium chloride

cat.: catalyst

δ : Chemical Shift

°C: Degrees Celsius

°K: Degrees Kelvin

C_6D_6: Deuterated benzene

CD_3CN: Deuterated acetonitrile

CN: Cyano

CF_3: Trifluoromethyl

CO: Carbon monoxide

CO_2: Carbon dioxide

COOEt: Ethoxycarbonyl

CsCl: Caesium chloride

CTAB: Cetyltrimethylammonium bromide

Cy: Cyclohexyl

CyJohnPhos: (2-Biphenyl)dicyclohexylphosphine

d(5-F)ppe: 1,3-bis(bis(6,6,6,6,6-pentafluoro-6l8-hexa-1,3,5-triyn-1-yl)phosphaneyl)propane

DCH-DPEPhos: (oxybis(2,1-phenylene))bis(dicyclohexylphosphane)

dcpe: 1,2-bis(dicyclohexylphosphaneyl)ethane

DI: Deionized

diMebpy: 4,4'-dimethyl-2,2'-bipyridine

diMeObpy: 4,4'-dimethoxy-2,2'-bipyridine

DMA: Dimethylacetamide

DME: Dimethoxyethane

DMF: Dimethylformamide

DMSO: Dimethylsufoxide

DOT-DPE-Phos: (oxybis(2,1-phenylene))bis(di-o-tolylphosphane)

DPE-Phos: Bis(2-diphenylphosphinophenyl)ether

dppb: 1,4-bis(diphenylphosphino)butane

dppp : 1,3-bis(diphenylphosphino)propane

dppe: 1,2-bis(diphenylphosphino)ethane

dppf: 1,1'-Bis(diphenylphosphino)ferrocene

dtbbpy: 4,4'-di-*tert*-butyl-2,2'-bipyridine

DTBP: Di-*tert*-butyl peroxide

Eq., equiv.: Equivalent

Et: Ethyl

ESI: Electrospray Ionization

Fig.: Figure

HMBC: Heteronuclear multiple bond coherence

HMPA: Hexamethylphosphoramide

HRMS: High-Resolution Mass Spectrometry

Hz: Hertz

h: Hour

^{i}Pr: Isopropyl

JohnPhos : (2-Biphenylyl)di-tert-butylphosphine

K_2CO_3 : Potassium carbonate

KCl : Potassium chloride

L: Ligand

LED : Light-Emitting Diode

LiCl : Lithium chloride

[M]: Metal (where M=Pt, Pd, Ni)

m: Multiplet

m/z: Mass-to-charge ratio

Me: Methyl

mg: Milligram

$MgSO_4$: Magensium sulfate

min: Minute

MHz: Megahertz

mL: Milliliter

M: mole per liter

mol: Mole

MorDalphos: Di(1-adamantyl)-2-morpholinophenylphosphine

mmol: Millimole

mTorr: millitorr

Me: Methyl

MeCN: Acetonitrile

n: Unspecified number

Na_2CO_3: Sodium carbonate

Na_2SO_3: Sodium thiosulfate

Na_3PO_4: Sodium phosphate

nm: Nanometer

NaCl: Sodium chloride

NaOH: Sodium hydroxide

NEt^iPr_2: *N*,*N*-Diisopropylethylamine

$Ni(CO)_4$: Nickel tetracarbonyl

$Ni(COD)_2$: Bis(cyclooctadiene)nickel(0)

NiI_2: Nickel diiodide

$[Ni(\pi^3\text{-allyl})halide]_2$: Nickel allyl halide dimer

NMP: *N*-methyl-2-pyrrolidone

NMR: Nuclear Magnetic Resonance

Nu: Nucleophile

OAc: Acetyl

OMe: Methoxy

OH: Hydroxyl

OTf: Triflate (Trifluoromethanesulfonyl)

Ph: Phenyl

phen: 1,10-Phenanthroline

Ph_3BnPCl: Benzyltriphenylphosphonium chloride

P(*o*-methoxy-Ph)$_3$: Tris(o-methoxyphenyl)phosphine

p-$MeOC_6H_4$: *para*-methoxybenzene

PhDavePhos: 2′-(Diphenylphosphino)-N,N′-dimethyl-(1,1′-biphenyl)-2-amine

$PhNH_2$: Aniline

PMe_3: Trimethylphosphine

PPh_3: Triphenylphosphine

ppm: Parts per Million

Pr: Propyl

PrCN : Isobutyronitrile

q: Quadruplet

R: Substituent

r.t.: Room Temperature

rac- BINAP: (±)-2,2′-Bis(diphenylphosphino)-1,1′-binaphthalene

RuPhos: dicyclohexyl(2',6'-diisopropoxy-[1,1'-biphenyl]-2-yl)phosphane

s: Singlet

SPhos: 2-Dicyclohexylphosphino-2′,6′-dimethoxybiphenyl

t: Triplet

^{t}Bu: *tert*-Butyl

*t*BuDavePhos: 2-Di-tert-butylphosphino-2′-(N,N-dimethylamino)biphenyl

*t*BuMePhos: 2-Di-tert-butylphosphino-2′-methylbiphenyl

*t*BuOH: *tert*-butanol

*t*BuXPhos: t-Bu XPhos, 2-Di-tert-butylphosphino-2′,4′,6′-triisopropylbiphenyl

TEMPO: (2,2,6,6-Tetramethylpiperidin-1-yl)oxyl

THF: Tetrahydrofuran

TRiP: 4-hydroxy-2,6-bis(2,4,6-triisopropylphenyl)dinaphtho[2,1-d:1',2'-f][1,3,2]dioxaphosphepine 4-oxide

UV-Vis: Ultraviolet-Visible

W: Watt

X: Halogen

Xantphos: 4,5-Bis(diphenylphosphino)-9,9-dimethylxanthene

XPhos: 2-Dicyclohexylphosphino-2′,4′,6′-triisopropylbiphenyl

Contributions of Co-Authors

This thesis is made up of three chapters. Chapter 1 is a summary of nickel-catalyzed carbonylative cross-couplings systems. Chapter 2 is a manuscript that is currently being submitted, and describes a visible light driven nickel carbonylation catalyst for acid chloride synthesis. All experiments detailed in Chapter 2 were performed by me under the supervision of Dr. Bruce Arndtsen for the completion of the degree of Master of Science in chemistry, apart from the catalytic reactions for the formation of and isolation of **3o**, **3p**, **3r**, **3s**, **3u**, **3w**, **3x**, **3y**, **4a**, **4j, 4k**, **4l**, **4m** and **4n** (in Figures 3 & 4) which were performed by labmate and undergraduate researcher Mohammed Amin Belahouane. Fluorescence measurements were taken with the aid of Cory Ruchlin, a researcher from the Perepichka lab. My supervisor throughout my degree, Dr. Arndtsen, assisted in the editing of this thesis. Chapter 3 is a brief conclusion to the work described in this thesis.

1. Nickel-Catalyzed Carbonylative Cross-Coupling Reactions

1.1 Perspective

Carbon monoxide (CO) gas is one of the most heavily used building blocks in industrial and academic chemical synthesis. The broad use of carbon monoxide is driven in part by its availability. Carbon monoxide is generated as a product of methane reforming, CO_2 reduction, or the partial oxidation of most hydrocarbons. Examples of the use of carbon monoxide in synthesis, referred to as carbonylation reactions, include the Reppe carbonylations, the Oxo synthesis, and methanol carbonylation (to name a few, Scheme 1.1A),[1] all of which are performed on multi-million ton scale per year.[2] Since carbon monoxide by itself is kinetically inert, its use in these transformations requires transition metal catalysts. While the role of the catalyst can vary, the incorporation of carbon monoxide usually involves its initial coordination to the metal catalyst followed by migratory insertion into a metal-ligand bond (Scheme 1.1B).

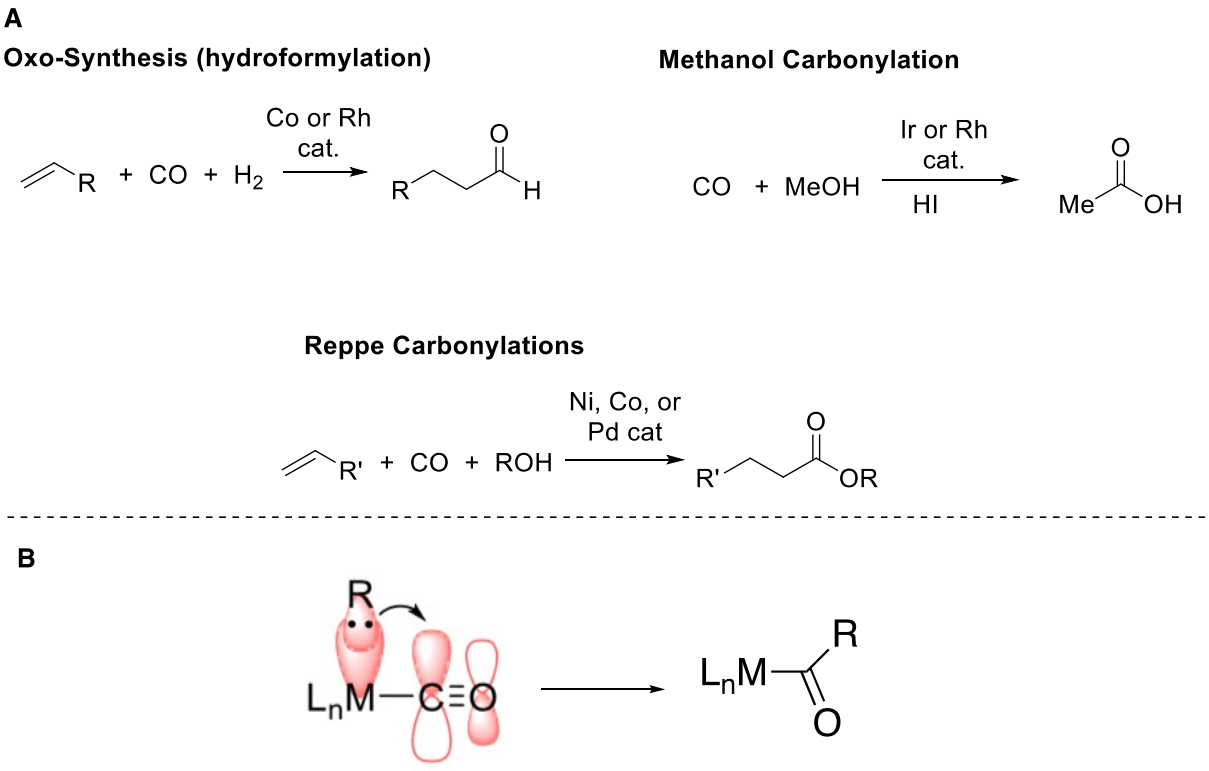

Scheme 1.1 - A. Chemical processes using CO; B. CO insertion into a M-R bond.

One of the most versatile methods to use carbon monoxide is palladium-catalyzed carbonylative coupling reactions. Introduced by Richard Heck in the 1970's, the reaction involves the coupling of an organic halide (I^-, Br^- or Cl^-) or pseudohalide (tosylate, mesylate, triflate etc.), CO and a nucleophile to form a carbonyl-containing compound (Scheme 1.2A).[3] Varying the nucleophilic reaction component allows for the construction of a multitude of carbonyl-containing functionalities, including carboxylic acids, esters, amides, thioesters, aldehydes and ketones.[4] The electrophilic substrate can also be modulated to tune these structures. While early work predominately employed C(sp^2) hybridized aryl- or vinyl-halides, more recent studies have shown C(sp)- and C(sp^3)-halides can also be used.[5] Catalytic carbonylative coupling reactions are thought

to proceed via the mechanism shown in Scheme 1.2, where a ligated Pd(0) catalyst undergoes oxidative addition of the organic halide followed by carbon monoxide coordination and insertion into the palladium-carbon bond. The nucleophile then reacts with this intermediate through initial coordination followed by reductive elimination of the final product.

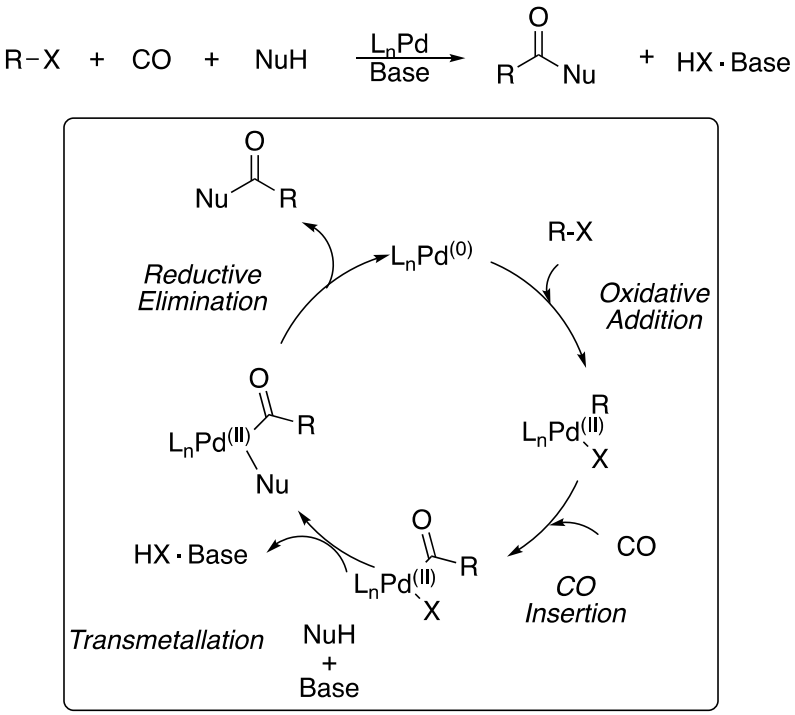

Scheme 1.2 - A classical palladium catalyzed carbonylative cross-coupling reaction

One of the intrinsic limitations of carbonylative coupling chemistry is its reliance on palladium catalysts. Palladium is a precious metal of low abundance in the earth's crust. As such, it is not only expensive, but its mining has tremendous environmental impact. Efforts to replace the widespread use of palladium in catalysis with more earth abundant metals, such as the isoelectronic nickel catalysts, have seen significant efforts and success in the last decade.[6] However, doing so in carbonylation reactions has been much slower to develop. The reliance on precious metals in

carbonylations is somewhat ironic, as many of the early examples employed earth abundant metal catalysts. Examples include the initial industrial processes developed by Reppe in the 1930's,[7] as well as works of Chiusoli on nickel-catalyzed Reppe-type carbonylations.[8]

A common rationale for the lack of potent nickel catalysts in carbonylation reactions is its high affinity for carbon monoxide coordination. Unlike the weak coordination of carbon monoxide to palladium catalysts, the less electronegative Ni(0) associates strongly to CO via backbonding interactions to form $Ni(CO)_4$. The latter is a coordinatively saturated volatile liquid (boiling point: 43°C) and extremely toxic.[9] Moreover, this association to carbon monoxide inhibits the formation of an empty site on nickel for the first step in carbonylative coupling reactions: oxidative addition of the organic halide substrate. In addition, strong backbonding from nickel to carbon monoxide makes the nickel electron poor, which also slows this step. While donor ligand association to palladium has proven powerful in creating more active catalysts for this first step, doing so with nickel catalysts further stabilizes carbon monoxide association and often completely inhibits catalysis.

The following section will provide an overview of nickel catalyst use in carbonylative cross-coupling reactions. The latter will include highlights of both early studies in the area and more recent advances. This will serve as background for the research presented in Chapter 2 on developing a new method to use nickel in carbonylation chemistry.

1.2 Nickel Catalysts for Carbonylative Coupling Reactions

1.2.1 Early Nickel-Catalyzed Carbonylative Cross-Coupling Reactions

One of the first reports of carbonylative coupling reactions using aryl halides came from Yamamoto and Sato in 1954 (Scheme 1.3).[10] This employed NiI_2 as a catalyst for the conversion of aryl iodides into carboxylic acids. While the transformation proceeds in good yields with a number of substrates, it employed extremely high temperatures and pressures (250 °C, 300 atm).

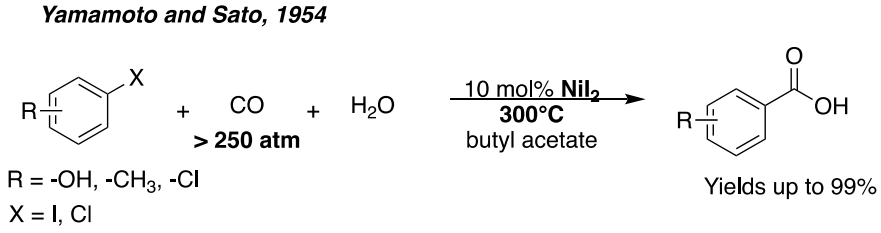

Scheme 1. 3 - Carbonylative synthesis of carboxylic acids using a NiI_2 catalyst

Subsequent studies described a number of related nickel catalyzed carbonylations.[10,11,12] For example, Prichard noted in 1956 the carbonylation of aryl halides using $Ni(CO)_4$ catalyst under 100-600 atm with up to 325°C affords anhydrides (Scheme 1.4).[13] The formation of anhydride presumably proceeds via the initial formation of a benzoate derivative, which serves as the nucleophile for the carbonylation of a second aryl halide. While the mechanism of this and Yamamoto and Sato's reactions were not discussed, the ability of a Ni(0) source to catalyze the reaction, and their similarity to palladium catalyzed carbonylations, suggests both reactions proceed via a $Ni(CO)_4$ catalyst and a cycle similar to that shown in section 1.1.

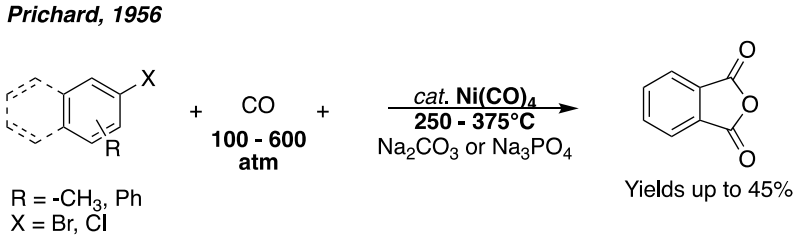

Scheme 1. 4 - $Ni(CO)_4$-catalyzed carbonylative synthesis of phthalic anhydrides.

A number of related stoichiometric nickel mediated reactions were performed at a similar time. For example, Chiusoli reported in 1959 that the reaction of allylic halides, acetylene and CO in alcohol solvents with $Ni(CO)_4$ could be used to form esters of dienoic acids (Scheme 1.5A)[8]. Their systems also used temperatures and pressures above 100°C and 50 atm CO. In studies that shed light on the mechanism of this reaction, Heck reported in 1963 that the stoichiometric reaction of $[Ni(\eta^3\text{-allyl})halide]_2$ complexes with CO and acetylene formed the corresponding acyl halides under much milder conditions (0 °C, Scheme 1.5B).[14] These results showed that Ni(II)-allyl complexes are likely intermediates in the reaction of Chiusoli, and their insertion of acetylene and carbon monoxide, and reductive elimination, are all rapid.

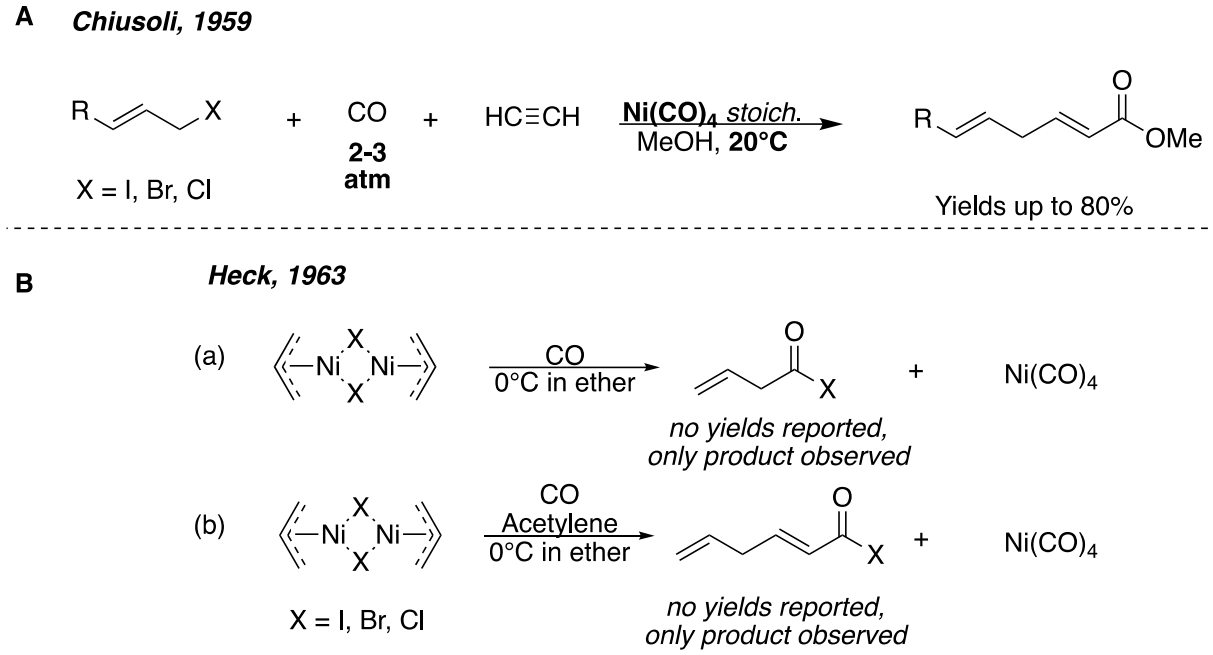

Scheme 1. 5 - A. Stoichiometric nickel mediated carbonylative synthesis of esters.; B. Reaction of (π^3-allyl)Ni(X) with CO to form acyl halides.

In 1968, Chiusoli demonstrated catalytic allyl halide carbonylation could be performed under mild conditions when using a Ni(0) catalyst generated in situ from Ni(II) chloride reduction by iron-manganese alloys in the presence of thiourea (Scheme 1.6)[15]. This system permitted the synthesis of dienoic esters from allylic chlorides in yields up to 80% under 1 atm mixture of 1:1 CO and acetylene at room temperature. The authors postulate the rapid generation of a thiourea-coordinated nickel-allyl complex under these reducing conditions, and presumably before $LNi(CO)_n$ is formed, which is regenerated after acetylene/CO insertion and reaction with methanol.

Chiusoli, 1968

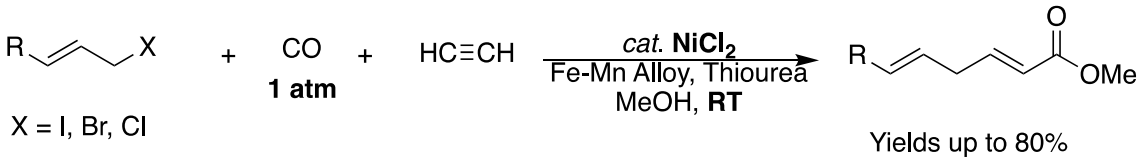

Scheme 1. 6 - Nickel-catalyzed carbonylative synthesis of dienoic esters.

In the area of aryl halide carbonylation, Mizoroki and Nakayama reported in 1969 an in-depth analysis of the nickel catalyzed carbonylative synthesis of carboxylic acids from aryl bromides (Scheme 1.7).[16] This showed that both Ni(II) acetate and $Ni(CO)_4$ worked similarly as catalysts. A more thorough analysis of the carbonylation of α-bromonapthalene with Ni(II) acetate showed that both low and high pressures of CO led to low reaction yields, with a CO pressure between 80-160 atm proving optimal. The authors proposed that low CO pressures prevented adequate conversion of Ni(II) acetate into the active $Ni(CO)_4$ but that higher pressures inhibited CO loss from a coordinatively saturated $Ni(CO)_4$, thereby blocking its reaction with the substrate. Their optimized conditions (200°C and 100 atm of CO) allowed the formation of carboxylic acids in high yields.

Mizoroki and Nakayama, 1969

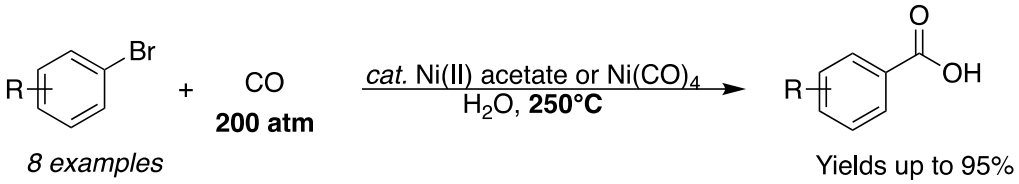

Scheme 1. 7- Nickel-catalyzed aryl bromide carbonylation to carboxylic acids.

Nickel catalyzed aryl halide carbonylations can also be employed in amide synthesis. One report in the area came from Pannacciulli in 1987 and also sheds light on the possible active nickel catalyst (Scheme 1.8).[17] Seven Ni(0) and Ni(II) catalysts were tested: $(Ni(CO)_2(PPh_3)_2$,

$NiBr_2(PMe_3)_2$, $NiCl_2(PPh_3)_2$, $NiI_2(PPh_3)_2$, $NiI_2(PhNH_2)_4$, $NiI_2(CO)(PPh_3)_2$ and $Ni(CO)_2(PPh_3)_2$). In situ IR analysis shows that regardless of the precursor, the same set of bands characteristic of $Ni(CO)_2L_2$ and $Ni(CO)_3L$ complexes were always generated, implying that reduction of Ni(II) to Ni(0) occurs in the presence of CO. Similar to the results of Mizoroki and Nakayama,[18] an optimal CO pressure is observed, and attributed to the need of CO pressure to both reduce Ni(II) to Ni(0) and enable CO insertion into the Ni-aryl intermediate, while too much pressure inhibited CO loss from Ni(0) to enable substrate oxidative addition. The optimal conditions for aminocarbonylation were 180 °C and 40 atm of CO, which formed amide products in up to 90% yield. In general, aryl iodides reacted more effectively than aryl bromides under the same conditions, with aryl chlorides proving unreactive.

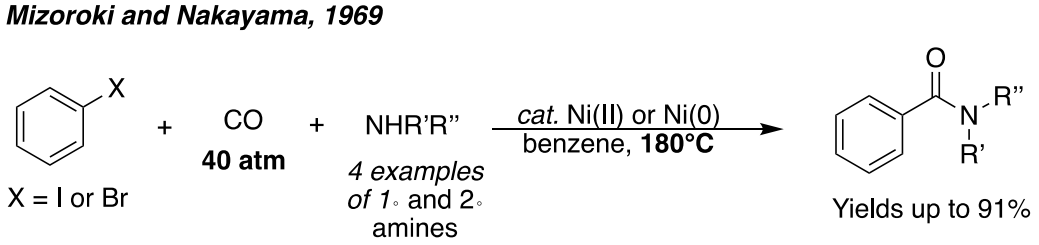

Scheme 1. 8 - Nickel-catalyzed carbonylative amide synthesis from aryl halides.

Ketones are also viable products of this chemistry. Tanaka showed in 1981 an effective carbonylative cross coupling between aryl iodides and tetramethyltin under 20 atm CO and at 120°C using $Ni(CO)_2(PPh_3)_2$ as catalyst (Scheme 1.9).[19] The authors noted that different nickel precursors could be used under their conditions, including $Ni(CO)_3(PPh_3)$ and $Ni(CO)_4$.

Tetraphenyltin failed to provide the analogous diaryl ketone product, limiting the transformation to the formation of aryl methyl ketones.

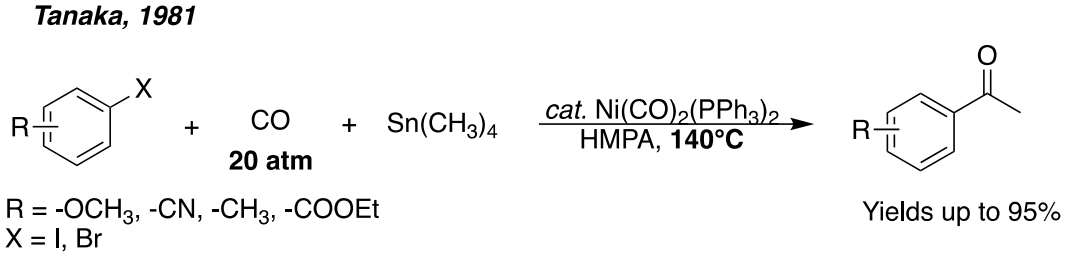

Scheme 1. 9 - Nickel-catalyzed carbonylative cross coupling of aryl halides and Me_4Sn.

Cassar and Foà were among the first to note that aryl bromide and aryl chloride carbonylations could be performed under more mild conditions (as low as 100°C at 1 atm CO). The reaction here also exploited a $Ni(CO)_4$ catalyst and $Ca(OH)_2$ as base in polar aprotic solvents (Scheme 1.10).[20] Based on the relative rates of reactivity of various aryl bromides, they proposed that the activation of the aryl bromide occurs by oxidative addition to a nucleophilic nickel catalyst. In addition, kinetic studies showed an induction period to catalysis, but this could be shortened upon addition of chloride and bromide anions. This led the authors to propose that halides, which are generated as by-products of carbonylation, have a role in forming an anionic nickelate species that may be

the active catalyst. Consistent with this postulate, the dianionic $[Ni_3(CO)_8]^{2-}$ is also an active catalyst for the reaction.

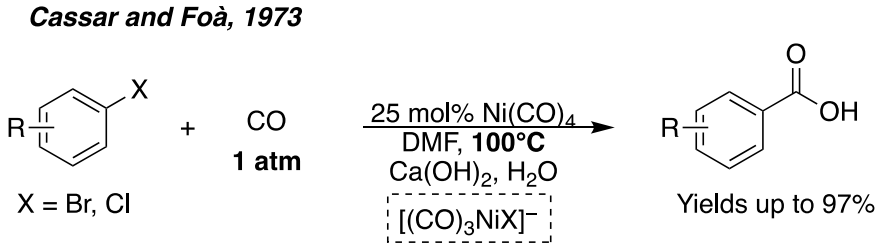

Scheme 1. 10 - Mild $Ni(CO)_4$ catalyzed synthesis of carboxylic acids from aryl bromides and chlorides

It was over a decade later, 1989, that the group of Alper used a similar concept to access more potent nickel catalyst systems. They showed that bromo- and chlorostyrene derivatives could be carbonylated to their corresponding α,β-unsaturated carboxylic acids when subjected to a system consisting of catalytic $Ni(CN)_2{\cdot}4H_2O$ in the presence of phase-transfer reagent cetyltrimethylammonium bromide (CTAB) in a toluene/saturated aqueous NaOH mixed solvent system (Scheme 1.11A).[21] The transformation occurred under 1 atm of CO at 100°C and formed products in up to 97% yield within 5 h. Subsequent studies showed that the products of double carbonylation could be obtained using 2-bromo-butadiene substrates under similarly mild conditions (80°C, Scheme 1.11B).[22] The authors postulate that the unusually high activity observed, and the need for a cyanide in the nickel precursor, are consistent with the in situ formation of a more reactive anionic $[Ni(CN)(CO)_3]^-$ catalyst, whose high electron density may

better undergo rate limiting oxidative addition. Rosas and coworkers have used this catalyst system in a number of related carbonylation reactions.

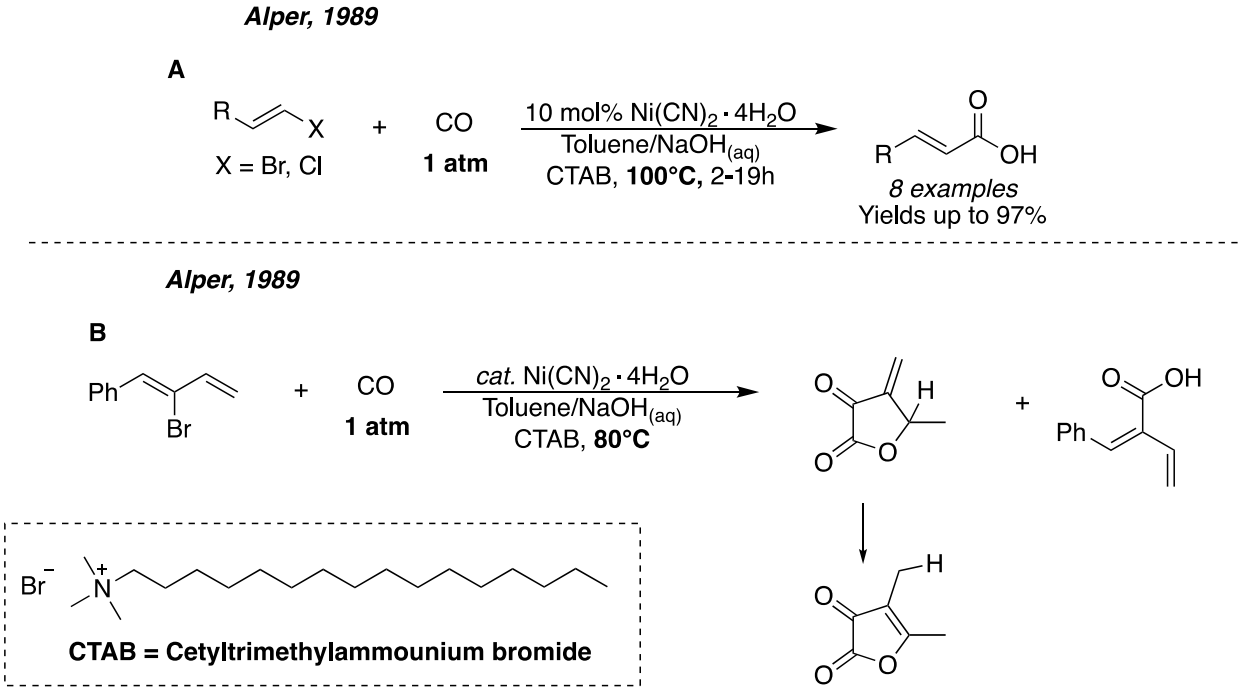

Scheme 1. 11 - Nickel-catalyzed carbonylation under phase-transfer conditions

In different direction, the group of Watanabe published in 1988 the first account of a photochemical transition metal-catalyzed carbonylation of alkyl halides using UV-irradiation. Fourteen different transition metal-carbonyl complexes from Groups 6-10 were tested as catalysts for the alkoxycarbonylation of cyclohexyl iodide. Of those tested, $Ni(CO)_4$ showed to be moderately effective, delivering 47% yield of ester (Scheme 1.12).[23] Mechanistic insight into the role of UV light in the reaction is limited, and may involve either the postulated light induced loss of carbon monoxide from the catalyst or, as shown by Ryu[24] the excitation of the alkyl halide

reagent itself to form alkyl radicals. The reaction offers an usual pathway to carry out nickel catalyzed carbonylation at ambient conditions with only UV light as the added energy source.

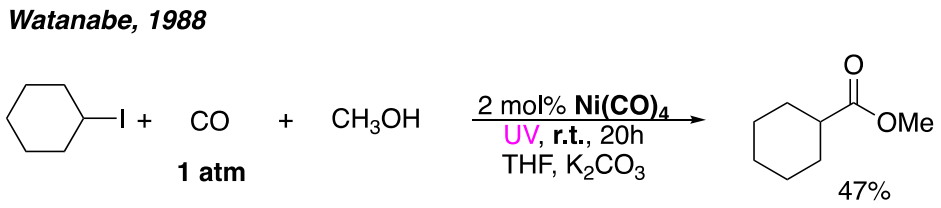

Scheme 1. 12 - UV-irradiated, nickel catalyzed carbonylation of cyclohexyl iodide.

1.2.2 Modern Nickel Catalyzed Carbonylation Chemistry

The early studies in nickel catalyzed carbonylative coupling reactions shows that while these are viable systems, they often require much more pressing conditions than the analogous palladium catalyzed reactions. In addition, the active catalyst systems often entail the in situ formation of highly toxic $Ni(CO)_4$, which can further limit its utility. The past 2 decades have seen various efforts to circumvent these challenges. These often involve using ligands other than simply carbon monoxide on the nickel center, and in many cases involve either highly reactive reagents or alternative mechanistic pathways beyond the cycle common with palladium catalysts.

In 2016, the groups of Långström and Halldin showed that stoichiometric $Ni(COD)_2$ with a 2,2'bipyridyl ligand derivative could allow the aminocarbonylation of alkyl iodides with ^{11}CO, and does so within 5 min at 100 ^{o}C (Scheme 1.13).[25] The reaction employed low concentration of carbon monoxide (nanomolar), which may contribute to the activity of this nickel catalyst, although the mechanism and source of catalytic activity was not discussed.

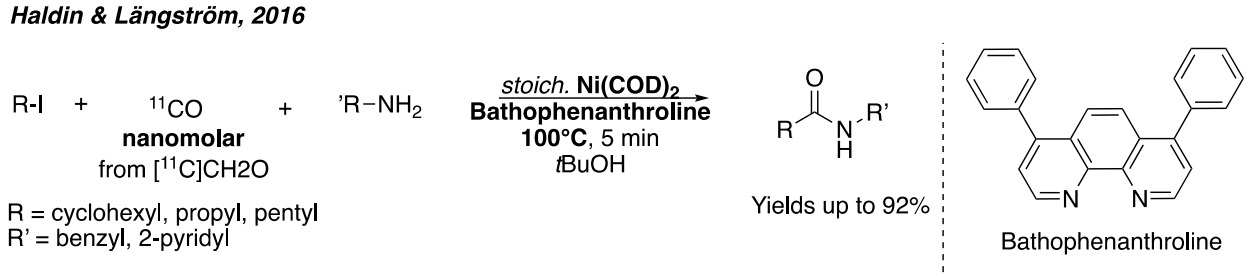

Scheme 1. 13 - ^{11}CO aminocarbonylation catalyzed by a Nickel-bathophenathroline system

In 2015, our lab reported a tandem carbonylative synthesis of isoindolinones from aryl iodides and imines using a ligand-free $Ni(COD)_2$ catalyst at 1 atm CO and 120 ºC (Scheme 1.14).[26] A variety of aryl iodides and imines could be used in the reaction, which involves a tandem carbonylation/C-H functionalization. The reaction is believed to proceed via the formation of acid chlorides, as suggested by the critical role of the Bu_4NCl salt. The electron deficient $Ni(CO)_4$ catalyst generated in situ is believed to be key in driving this challenging reductive elimination, in analogy to earlier stoichiometric reactions (Scheme 1.4, 1.5).

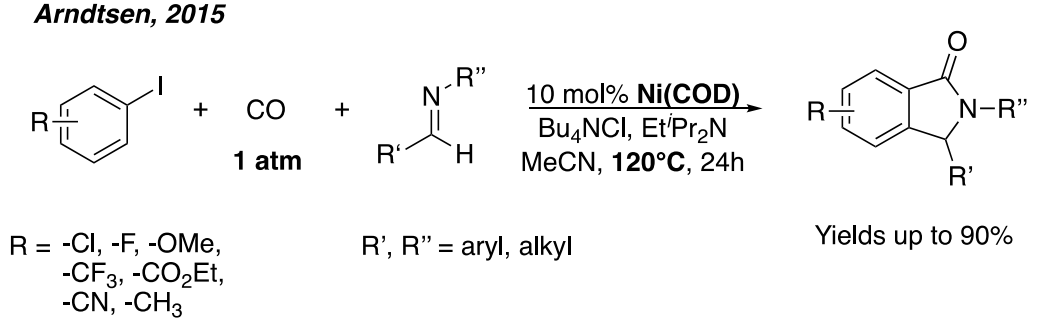

Scheme 1. 14 - Isoindolinone synthesis from multicomponent carbonylative coupling of aryl iodides and imines.

The Wu group has described a number of nickel catalyzed carbonylations that operate under relatively mild conditions. These often use low concentrations of carbon monoxide, which could be key to catalyst activity. For example, they reported in 2021 the carbonylative synthesis of thiochromenones from phenylacetylenes and 2-bromoarylsulfonyl chlorides (Scheme 1.15A).[27]

The catalyst consisted of $NiCl_2$ and terpyridine ligand and used slow CO release from 1.5 equiv. $Mo(CO)_6$ to form cyclized products in high overall yields. In this, reduction of the sulfur to a thiol by PPh_3 is believed to be key to initiate a sequence of aryl bromide oxidative addition, CO and alkyne insertion, followed by reductive elimination of a S-C bond to form the observed product. The related transformation of alkyne-tethered nitroarenes (reduced in situ by Zn) was later found to afford N-acyl indoles under nickel catalyzed conditions with $Co_2(CO)_8$ as the CO source (Scheme 1.15B)[28], and in 2022 they showed that in situ reduction of sulfonyl chlorides by $Mo(CO)_6$

could both slowly release CO and generate thiols in situ for the nickel catalyzed thiocarbonylation of vinyl triflates (Scheme 1.15C).[29]

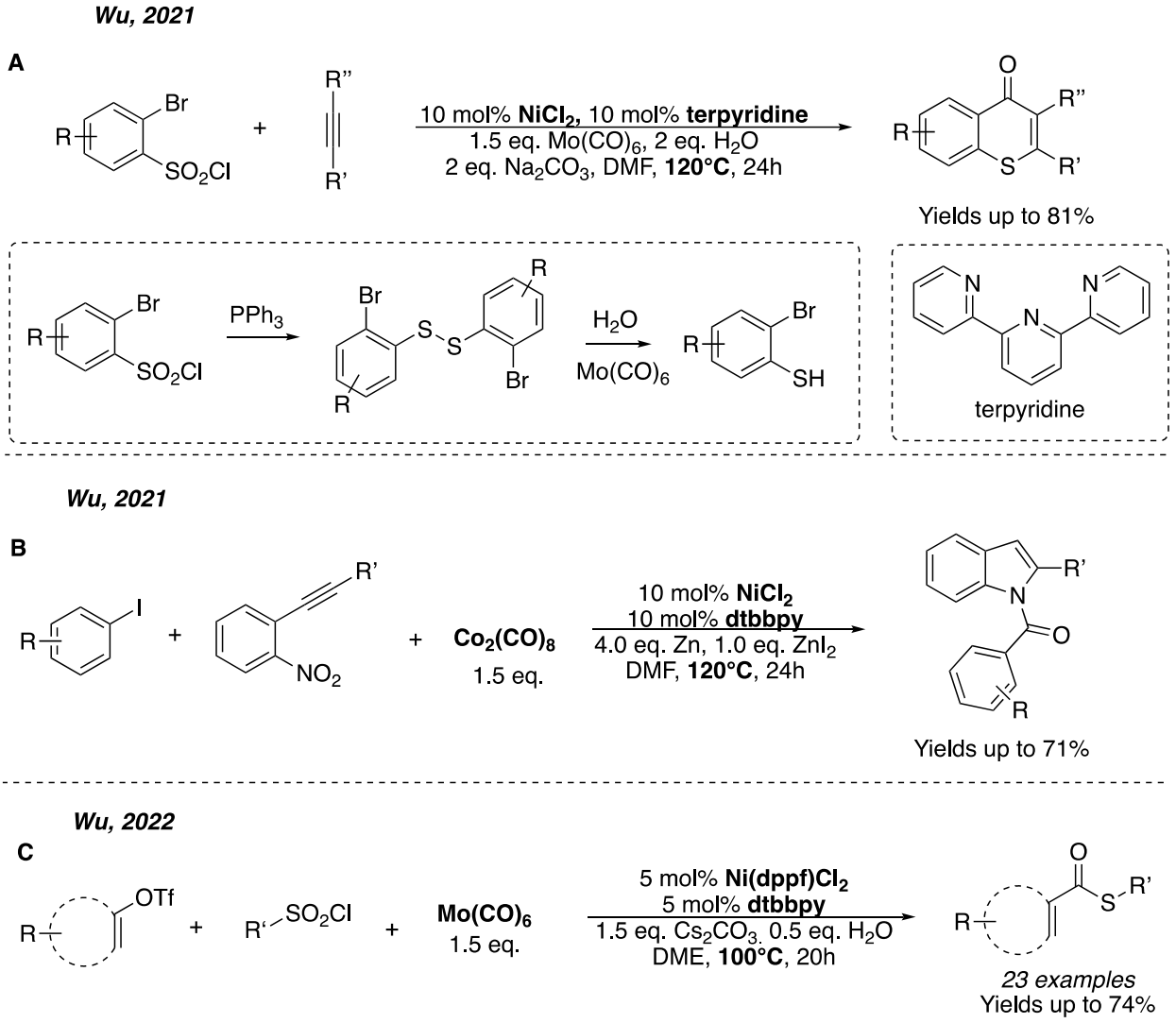

Scheme 1. 15 - Nickel-catalyzed carbonylative transformations by the Wu group.

Likely the most potent nickel carbonylation catalysts developed to date involve variants of cross-coupling reactions to form ketones. As will be discussed later, their potency may come from pathways that avoid the formation of CO-ligated Ni(0) intermediates. One of the earliest examples in the field came in 1995, when the group of Troupel reported the nickel-catalyzed electrochemical reductive carbonylative coupling of aryl or alkyl halides to form ketones (Scheme 1.16A).[30] Their

catalytic system consisted of nickel embedded cathodes and anodes which on the addition of 2,2'-bipyridine (bpy) is believe to form in situ (bpy)Ni(0). Mechanistic data suggested that low CO concentrations (not exceeding a ratio of 1:1 CO to Ni(0)) were key to creating potent catalysts, and is believed to generate the coordinatively unsaturated (bpy)Ni(CO) complex necessary for efficient carbonylative coupling to occur. Subsequent studies by their lab extended this approach to unsymmetrical ketone synthesis (Scheme 1.16B).[31] In this case, the oxidation of $Fe(CO)_5$ was used to complete the electrochemical cycle and also allowed the controlled release of CO into the reaction.

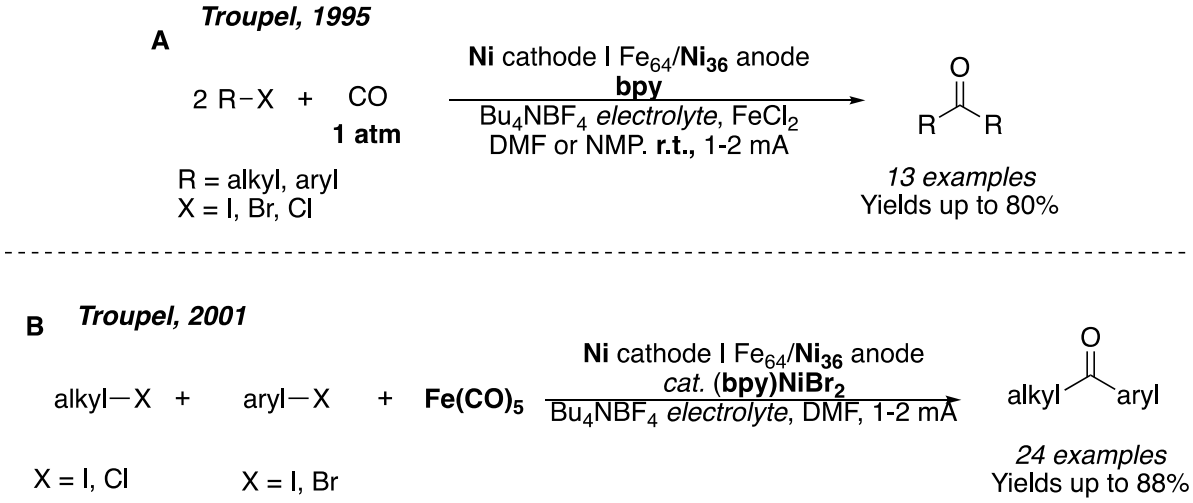

Scheme 1. 16 - Nickel-catalyzed electrochemical reductive carbonylative coupling of aryl or alkyl halides to form ketones

A carbonylative Stille reaction between diaryl hypervalent iodonium tetrafluoroborate salts and vinyl, alkynyl or aryl organostannanes was reported by Lee in 1999 (Scheme 1.17A).[32] This exploited a $Ni(acac)_2$ catalyst without any added ligand, and formed ketones at only 80°C and 1 atm CO. The mild conditions reported in their system is at odds with previously discussed nickel catalyzed carbonylations, and in particular lack the high CO pressures that have been suggested to generate an active Ni(0) catalyst. Although the authors did not propose a mechanism for the

reaction, it could involve a Ni(I)/Ni(III) bimetallic pathway suggested in later works (*vide infra*). Subsequent studies by a number of labs described related carbonylative ketone syntheses under relatively mild conditions. Examples include the work of Chen[33] involving vinyl triflates and organozinc reagents, Etemadi-Davan on carbonylative Stille coupling reactions using aryl iodides

and $Cr(CO)_6$ as the CO source, and Korupolu[34] and Das[35] on carbonylative variants of Sonogashira reactions with terminal alkynes (Scheme 1.17B-E).

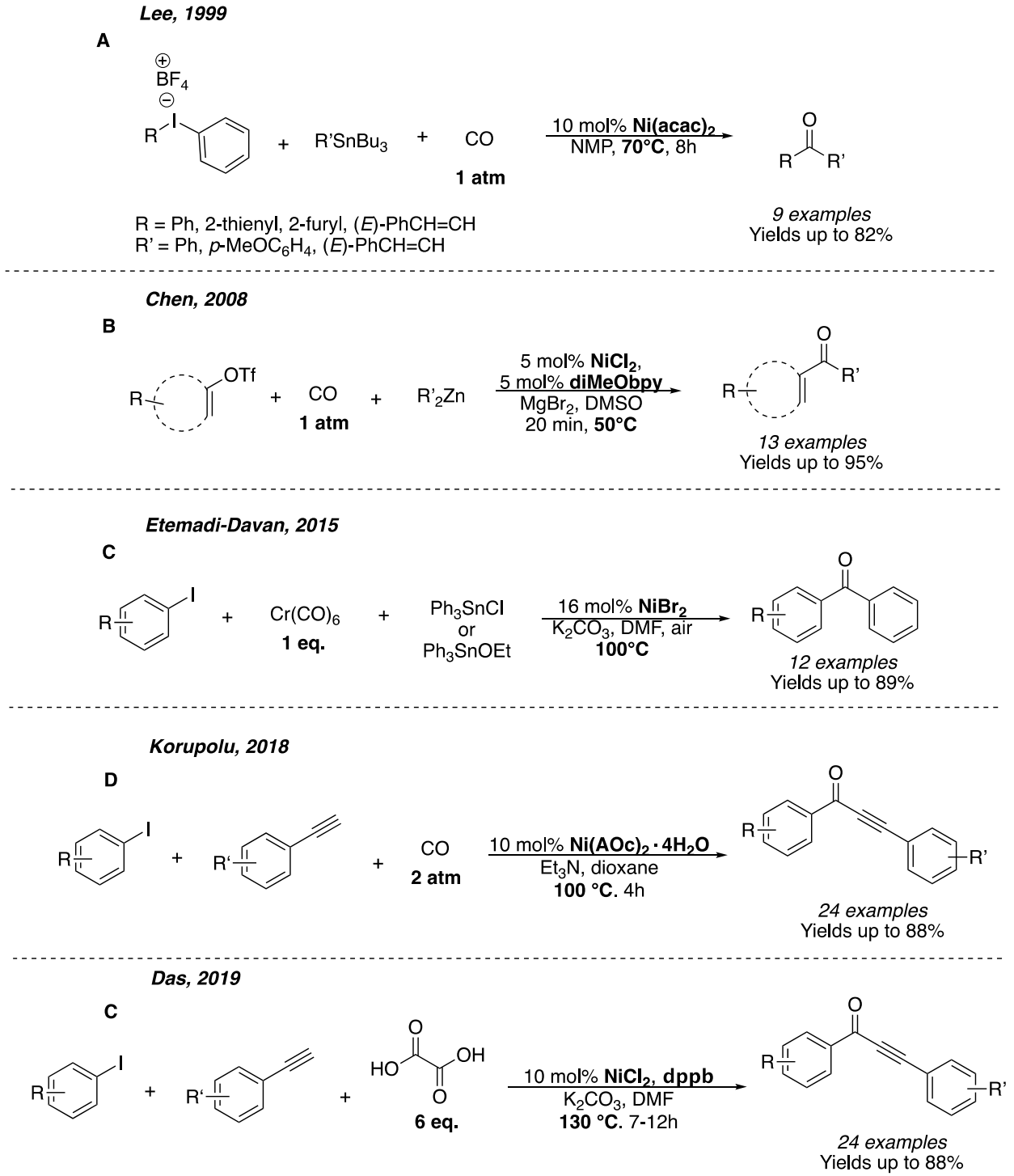

Scheme 1. 17 - Nickel-catalyzed cross-coupling reactions to form ketones.

In 2018, the group of Skrydstrup reported the novel use of a tridentate pincer ligand in nickel-catalyzed carbonylation (Scheme 1.18).[36] In this, the three-point binding ligand was proposed to prevent unwanted CO coordination and deactivation of the nickel catalyst. This transformation employed a dual-chamber reactor, where the controlled release of carbon monoxide by the palladium catalyzed decarbonylation of an acid chloride (COgen) allowed the production of just 1.5 equiv. CO for diffusion to the second chamber and nickel catalyzed coupling with benzyl bromide and organozinc nucleophiles. Based upon a number of control experiments, and the unusual ability of the tridentate ligand to mediate catalysis, the authors put forward a different mechanism from that typically postulated for palladium catalysis. This does not invoke a Ni(0) intermediate, and instead involves the reaction of the Ni(II) complex first with the organozinc reagent and CO to form a Ni(II)-acyl complex **C** that undergoes a bimetallic radical oxidative addition with benzyl bromide. The latter generates Ni(III) intermediates that reductively eliminate ketone and disproportionate back to Ni(II). Overall, this provides a pathway to employ typically challenging C(sp^3)-halide substrates (via radical oxidative addition to a relatively electron rich Ni(II) intermediate), and avoids the need for organic halides to oxidatively add to Ni(0)-carbon

monoxide coordinated intermediates. This pathway could well be involved in many of the more active nickel catalysts above for carbonylative ketone synthesis.

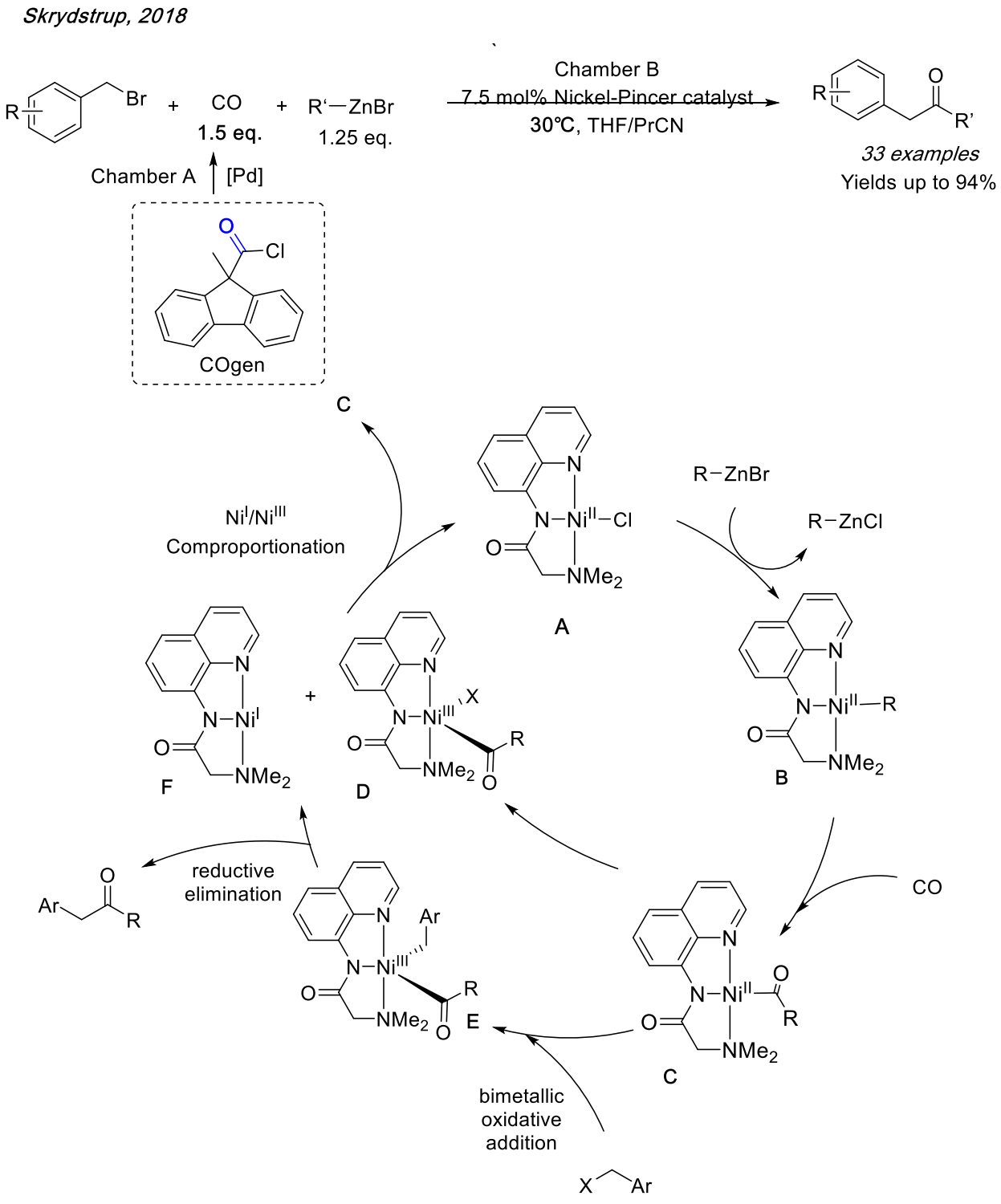

Scheme 1. 18 - A pincer-type ligand in nickel-catalyzed carbonylative cross-coupling via a Ni(I)/Ni(III) pathway.

Skrydstrup later demonstrate this same approach in the carbonylative cross-coupling of α-bromonitriles to alkylzinc reagents with a nickel-pincer catalyst (Scheme 1.19).[37] This transformation occurs at only 30°C with a range of reagents and can be adapted to radiolabelling by the use of labeled carbon monoxide releasing precursors.

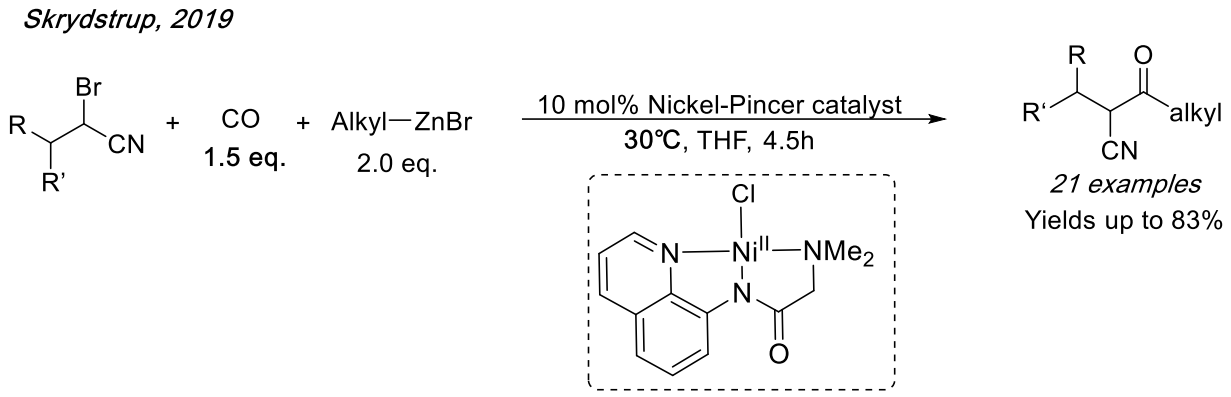

Scheme 1. 19 - Mild alkyl bromide carbonylation to ketones with a nickel pincer catalyst.

A number of related carbonylative ketone syntheses with C(sp^3)-halides with Ni(II) catalysts have been reported, many of which are believed to proceed via a similar pathway avoiding Ni(0) intermediates. For example, Zhang reported in 2019 a carbonylative cross-coupling of arylboronic acids with propargyl bromides using a $NiCl_2$·DME-dtbbpy (dtbbpy = 4,4'-di-*tert*-butyl-2,2'-bipyridine) catalyst (Scheme 1.20A).[38] Here, 1 atm of CO at 65°C was sufficient for the synthesis of the corresponding ketones in moderate to high yields. A mechanism was postulated following the general scheme in Scheme 1.18. The same group reported a related coupling with secondary

alkyl iodides and a phenanthroline coordinated nickel catalyst,[39] as well as a four-component coupling involving the intermediate insertion of terminal alkenes (Scheme 1.20B-C).[40]

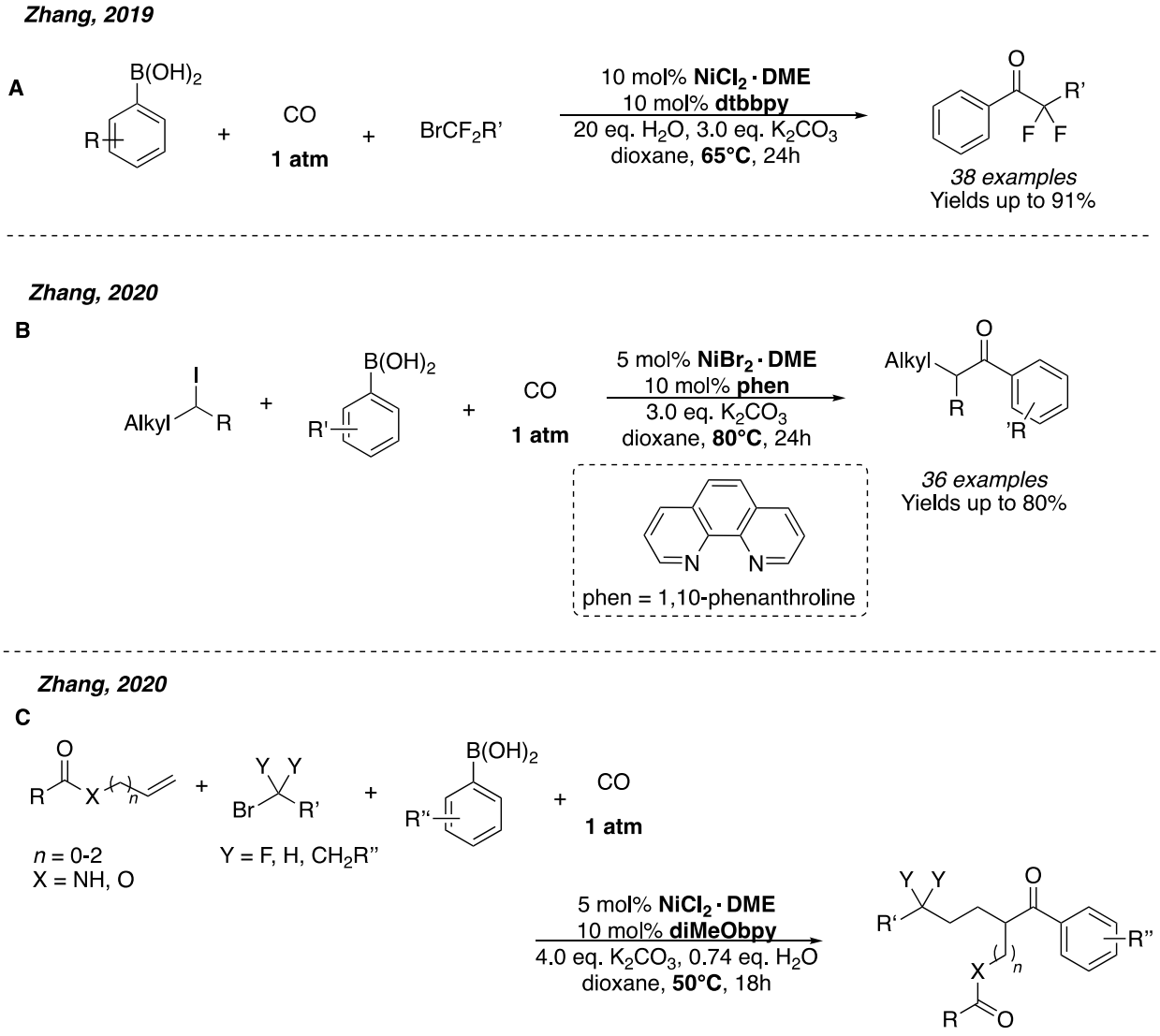

Scheme 1. 20 - Nickel-catalyzed carbonylative ketone syntheses from C(sp³)-halides.

The Ni(II) catalyzed carbonylative coupling of allylic alcohols and organoaluminum reagents was described by Chen (Scheme 1.21A).[41] In this, the aluminium reagent serves the dual role of providing a nucleophilic alkyl group for the coupling reaction, and, through association to the

allylic alcohol, activating the substrate toward reaction. A Ni(0) catalyst was proposed to undergo oxidative addition of the activated allylic alcohol to initiate the reaction, although a Ni(II) cycle involving an initial reaction of the organoaluminium reagent similar to Scheme 1.18 may instead be active. Chen also reported in 2022 the carbonylative synthesis of cyclopentenone derivatives from benzyl bromides and cyclopropanols with a related $NiCl_2$·DME-4,4'-dimethyl-2,2'-bipyridine catalyst (Scheme 1.21B).[42] In this case, alcohol association and β-carbon elimination forms a carbon-bonded nickel intermediate for 1,4-diketone synthesis. The latter undergo

intramolecular aldol condensation under the reaction conditions to yield the 2,3-diaryl substituted cyclopentenones.

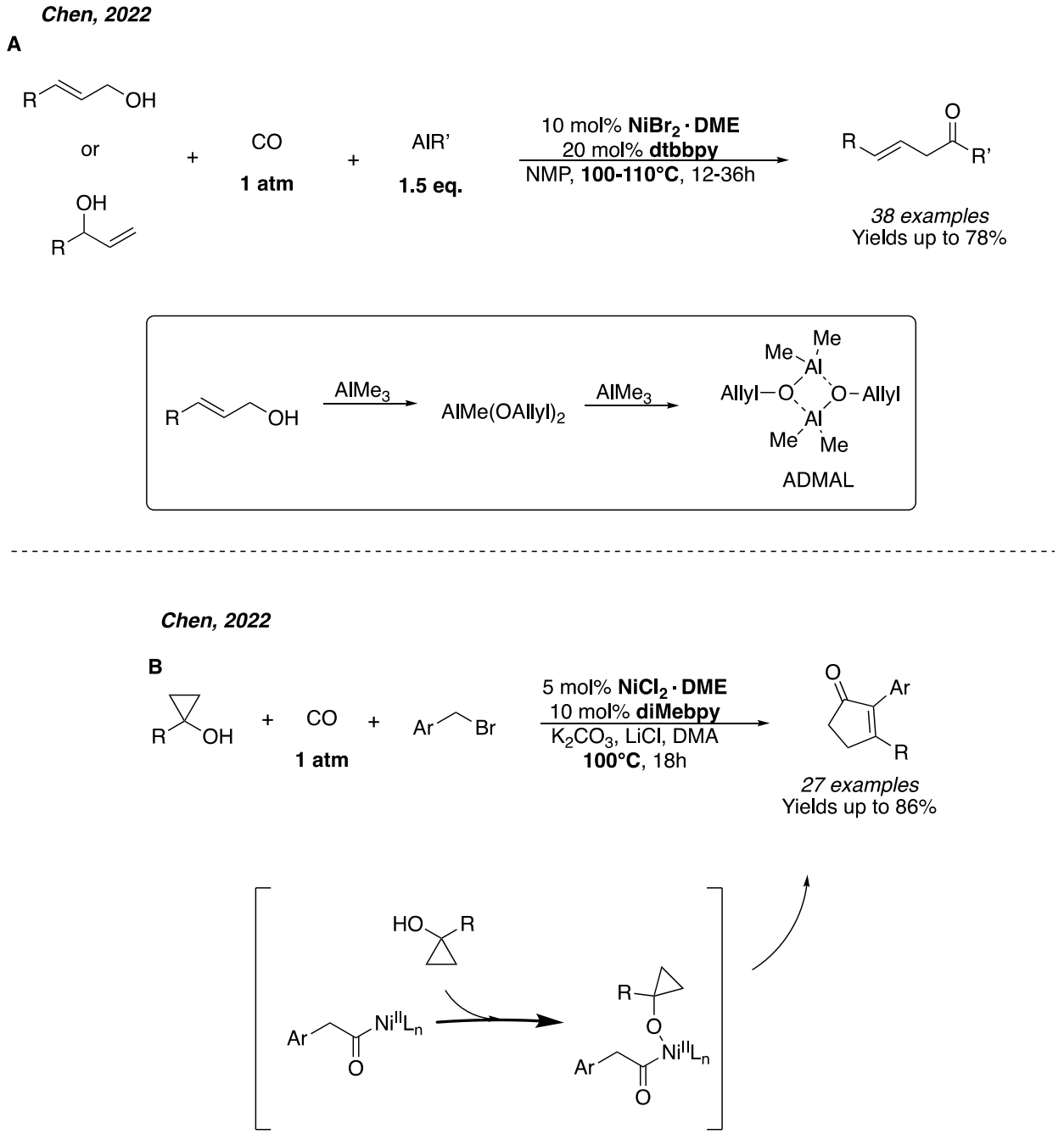

Scheme 1. 21 - Ni-catalyzed carbonylative coupling with allylic- and cyclopropyl alcohols.

In a different direction, Wu reported in 2022 a four-component nickel-catalyzed carbonylative C-H functionalization reaction of ethers (Scheme 1.21).[43] The reaction employed a $Ni(acac)_2$-4,4'-dimethyl-2,2'-bipyridine catalyst and di-*tert*-butyl peroxide (DTBP) as a radical initiator. Fragmentation of the peroxide to a *tert*-butoxide radical is believed to initiate the reaction by hydrogen-abstraction from the ether to furnish a carbon radical. Coupling of the latter with alkene and a CO coordinated to nickel can form a Ni(II)-acyl intermediate for reaction with the

nucleophile. Moderate to high yields of product were observed with a range of ether, olefin, and nucleophile components.

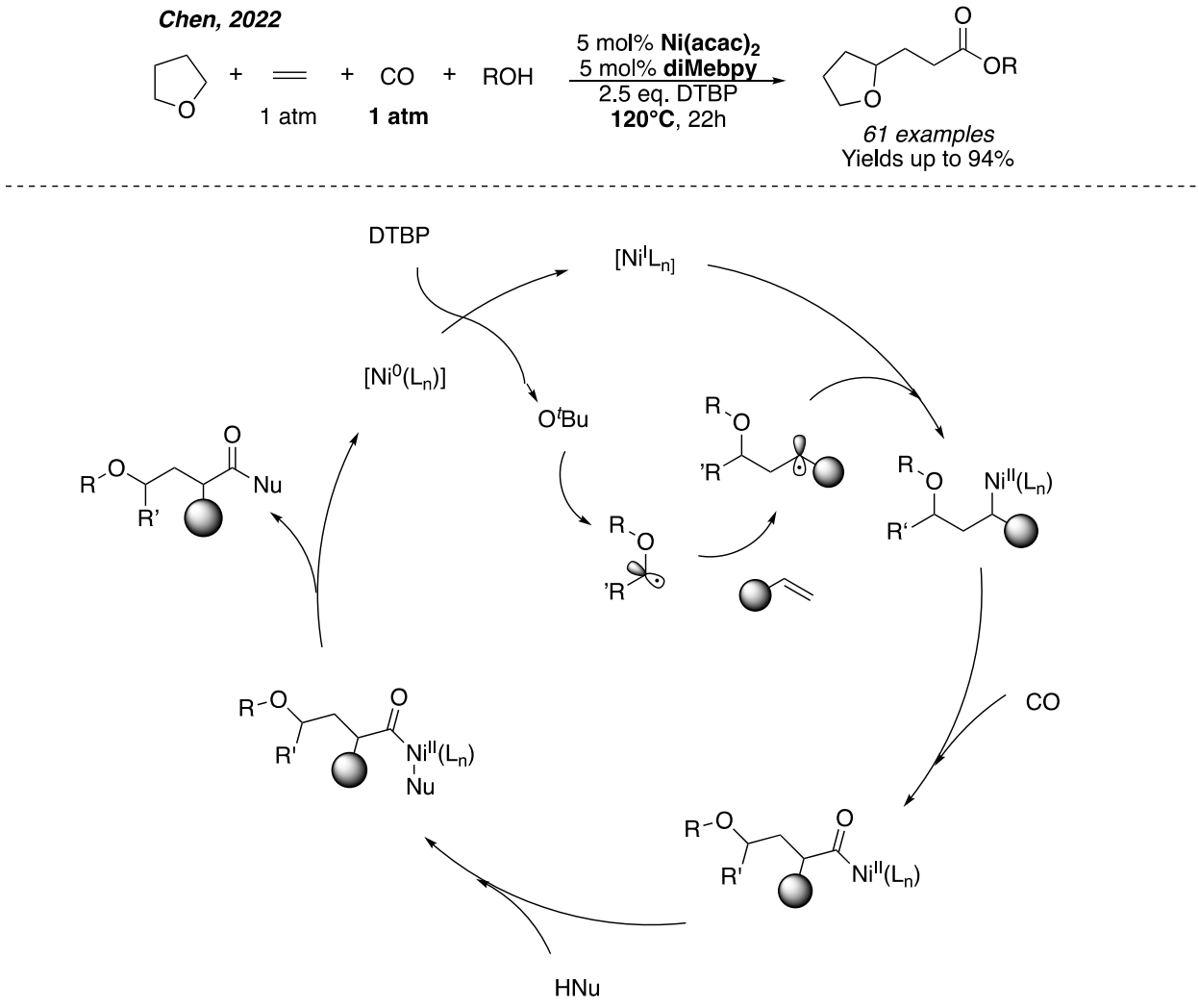

Scheme 1. 22 - The four-component nickel-catalyzed carbonylative C-H functionalization reaction of ethers.

1.3 Overview of Thesis

As discussed above, nickel catalysts provide a potentially useful alternative to the use of palladium catalysts in carbonylative coupling reactions. Early studies in the field required pressing conditions in nickel catalyzed version of these reactions. This can be attributed in part to the formation of coordinatively saturated and electron deficient $LNi(CO)_n$ catalysts under the reaction conditions that presumably slows substrate oxidative addition. However, more recent work has demonstrated that some variants of these reactions, in particular nickel catalyzed cross coupling reactions to form ketones, can occur under mild conditions with Ni(II) catalysts associated to polydentate ligands. These systems appear to avoid the need to generate Ni(0) for oxidative addition and instead exploit the rapid *in situ* formation of $L_nNi(II)$-COR intermediates for electron transfer to alkyl halides to mediate catalysis.

Despite these advances, nickel catalyzed carbonylation reactions to form products besides ketones still typically require pressing conditions and are often limited in their scope to reactive nucleophiles and activated aryl or vinyl halide substrates. To try to address this limitation, we describe in chapter 2 how visible light can instead be employed to activate Ni(0) complexes toward carbonylative coupling reactions under mild conditions. A wide array of alkyl halides can carbonylated in high yields to corresponding acid chlorides with the system, and these products trapped to form esters, amides and thioesters. Overall, this system offers a route to use nickel catalysts in carbonylative coupling reactions with classically challenging alkyl halide and nucleophilic components at ambient temperature and often ambient pressure.

1.4 References to Chapter 1

(1) J.-B. Peng, H.-Q. Geng, X.-F. Wu, The chemistry of CO: carbonylation. *Chem.* **2019**, *5*, 526-552.

(2) Y. Liu, D. Deng, X. Bao, Catalysis for selected C1 chemistry, *Chem.* **2020**, *6*, 2497-2514.

(3) J. Tsuji. Reactions of organic halides and pseudohalides. In *Transition metal reagents and catalysts: Innovations in organic synthesis.* John Wiley & Songs, Ltd.; Baffins Lane, Chichester, West Sussex, England, 2002; pp. 27-96.
(4) C. F. J. Barnard, Palladium-catalyzed carbonylation – a reaction come of age. *Organometallics*. **2008**, *27*, 5402-5422.
(5) L. Wu, X. Fang, Q. Liu, R. Jackstell, M. Beller, X.-F. Wu, Palladium-Catalyzed Carbonylative Transformation of C(sp3)-X Bonds. *ACS Catal*. **2014**, *4*, 2977-2989.
(6) S. Z. Tasker, E. A. Standley, T. F Jamison, Recent advances in homogeneous nickel catalysis. Nature, 2014, 509, 299-309.
(7) P. J. T. Morris. Science and industry. In *Determinants in the evolution of the European chemical industry, 1900-1939: New technologies, political frameworks, markets and companies*. Springer – Science + Business Media, B.V.; 1998; pp. 89-123.
(8) G. P. Chiusoli, G. Cometti, G. Sacchelli, V. Bellotti, G. D. Andreetti, G. Bocelli, P. Sgarabotto, Nickel-catalysed stereospecific cyclocarbonylation of cyclopentadiene dimer. Crystal and molecular structure of 2-(tetracyclo[5.5.1.0.0]tridec-9-en-4-yl)propionic acid. *J. Chem. Soc.* **1977**, 389-392.
(9) M., Zhou, H.-Y., Zhao, S., Zhang, Y., Zhang, X., Zhang, Nickel-Catalyzed Four-Component Carbocarbonylation of Alkenes under 1 atm of CO. *J. Am. Chem. Soc.* **2020**, *142*, 18191-18199.
(10) H. Adkins and R. W. Rosenthal, Carbonylation of Alcohols with Nickel Carbonyl Catalyst. *J. Am. Chem. Soc.* **1950**, *72*, 4550-4553.
(11) R. W., Rosenthal, L. H., Schwartzman, N. P, Greco, R. Proper, Carboxylation of propargyl alcohol. *J. Org. Chem.*, **1963**, *28*, 2835-2838.
(12) G. P., Mueller, F. L., Macartor, The anomalous carbonylation of diphenylacetylene. *J. Am. Chem. Soc.* **1954**, *76*, 4621-4622.
(13) W. W., Prichard, Reactions of carbon monoxide at high temperatures. I. A new synthesis of phthalic anhydrides. *J. Am. Chem. Soc.* **1956**, *78*, 6137-6139.
(14) R. F. Heck, The Mechanism of the Allyl Halide Carboxylation Reaction Catalyzed by Nickel Carbonyl. *J. Am. Chem. Soc.* **1963**, *85*, 2013-2013.
(15) G. P. Chiusoli, M. Dubini, M. Ferraris, F. Guerrieri, S. Merzoni and G. Mondelli, A simple Method for the Carbonylation of Allylic Halides with Insertion of Acetylene. *J. Chem. Soc. C.* **1968**, (0), 2889-2890.
(16) N., Nakayama, T., Mizoroki, Synthesis of carboxylic acid from aryl halide and carbon monoxide catalyzed by nickel carbonyl. *Bull. Chem. Soc. Jpn.* **1969**, *42*, 1124-1129.
(17) P. Giannoccaro, E. Pannacciulli, Nickel-catalyzed amidation of bromo- and iodobenzene. *J. Organomet. Chem.* **1987**, *319*, 119-127.
(18) N., Nakayama, T., Mizoroki, Synthesis of carboxylic acid from aryl halide and carbon monoxide catalyzed by nickel carbonyl. *Bull. Chem. Soc. Jpn.* **1969**, *42*, 1124-1129.
(19) M., Tanaka, Nickel Complex-Catalyzed Methyl Ketone Synthesis via Carbonylation of Organic Halides with Tetramethyltin. *Synth.* **1981**, *1981*, 47-48.
(20) L., Cassar, M., Foà, Nickel-catalyzed carbonylation of aromatic halides at atmospheric pressure of carbon monoxide. *J. Organomet. Chem.* **1973**, *51*, 381-393.

(21) H., Alper, I., Amer, G., Vasapollo, Stereospecific nickel and phase transfer catalyzed carbonylation of vinyl bromides and chlorides. *Tetrahedron Lett.* **1989**, *30*, 2615
(22) H., Alper, G., Vasapollo, Novel nickel catalyzed conversion of 2-bromo-1-phenyl-1,3-butadiene to an α-keto lactone. An example of double carbonylation of a halodiene. *Tetrahedron Lett.* **1989**, *30*, 2617.
(23) T., Kondo, Y., Tsuji, Y., Watanabe, Photochemical carbonylation of alkyl iodides in the presence of various metal carbonyls. *Tetrahedron Lett*., **1988**, *29*, 3833-3936.
(24) I. Ryu, N. Sonoda, Free-radical carbonylations: then and now. *Angew. Chem., Int. Ed.* **1996**, *35*, 1050-1066.
(25) O., Rahman, B., Längström, C., Halldin, Alkyl Iodides and [11C]CO in Nickel-Mediated Cross-Coupling Reactions: Successful Use of Alkyl Electrophiles containing a β Hydrogen Atom in Metal-Mediated [11C] Carbonylation. *Chemistry Select*. **2015**, *1*, 2498-2501.
(26) J., Tjutrins, L., Shao, V., Yempally, A. A., Bengali, B. A., Arndtsen, A Nickel-Based, Tandem Catalytic Approach to Isoindolinones from Imines, Aryl Iodides, and CO. *Organometallics*. **2015**, *34*, 1802-1805.
(27) W., Wang, Z.-P., Bao, X., Qi, X.-F., Wu, Nickel-Catalyzed One-Pot Carbonylative Synthesis of 2-Mono- and 2,3-Disubstituted Thiochromenones from 2-Bromobenzenesulfonyl Chlorides and Alkynes. *Org. Lett*. **2021**, *23*, 6589-6593.
(28) L., Yao, J., Ying, X.-F., Wu, Nickel-catalyzed cascade carbonylative synthesis of *N*-benzoyl indoles from 2-nitroalkynes and aryl iodides. *Org. Chem. Front.* **2021**, *8*, 6541-6545.
(29) Y.-W., Huo, X., Qi, X.-F., Wu, Nickel-Catalyzed Carbonylative Synthesis of α,β-Unsaturated Thioesters from Vinyl Triflates and Arylsulfonyl Chlorides. *Org. Lett.* **2022**, *24*, 4009-4013.
(30) M., Oçafrain, M., Devaud, M., Troupel, J., Périchon, New electrochemical synthesis of ketones from organic halides and carbon monoxide. *J. Chem. Soc., Chem. Commun.* **1995**, 2331-2332.
(31) E., Dolhem, R., Barhdadi, J. C., Folest, J. Yves., Nédelec, M., Troupel, Nickel catalysed electrosynthesis of ketones from organic halides and iron pentacarbonyl. Part 2: Unsymmetrical ketones. *Tetrahedron*. **2001**, *57*, 525-529.
(32) S.-K., Kang, H.-C., Ryu, S.-W., Lee, Ni(acac)$_2$-catalyzed cross-coupling and carbonylative cross-coupling of organostannanes with hypervalent iodonium salts. *J. Chem. Soc., Perkin Trans.* **1999**, 2661-2663.
(33) Q., Wang, C., Chen, Nickel-catalyzed carbonylative Negishi cross-coupling reactions. *Tetrahedron Lett*. **2008**, *49*, 2916-2921.
(34) R., Charugandla, M. S., Vangala, S., Chidara, R. B., Korupolu, Nickel catalysed carbonylative Sonogashira reaction for the synthesis of diarylalkynones and 2-substituted flavones. *Tetrahedron Lett.* **2018**, *59*, 3283-3287.

(35) Shaifali, S., Ram, V., Thakur, P., Das, Synthesis of α,β-alkynyl ketones via the nickel catalysed carbonylative Sonogashira reaction using oxalic acid as a sustainable C1 source. *Org. Biomol. Chem.* **2019**, *17*, 7036-7041.
(36) T. L., Andersen, A. S., Donslund, K. T., Neumann, T., Skyrdstrup, *Angew. Chem., Int. Ed.* **2018**, *57*, 800-804.
(37) A. S. Donslund, K. T. Neumann, N. P. Corneliussen, E. K. Grove, D. Herbstritt, K. Daasbjerg, T. Skrydstrup, Access to β-Ketonitriles through Nickel-Catalyzed Carbonylative Coupling of α-Bromonitriles with Alkylzinc Reagents *Chem. Eur. J.* **2019**, *25*, 9856.
(38) H.-Y., Zhao, X., Gao, S., Zhang, X., Zhang, Nickel-Catalyzed Carbonylation of Difluoroalkyl Bromides with Arylboronic Acids. *Org. Lett.* **2019**, *21*, 1031-1036.
(39) R., Cheng, H.-Y., Zhao, S., Zhang, X., Zhang, Nickel-Catalyzed Carbonylation of Secondary Trifluoromethylated, Difluoromethylated, and Nonfluorinated Aliphatic Electrophiles with Arylboronic Acids under 1 atm of CO. *ACS Catal.* **2020**, *10*, 36-42.
(40) M., Zhou, H.-Y., Zhao, S., Zhang, Y., Zhang, X., Zhang, Nickel-Catalyzed Four-Component Carbocarbonylation of Alkenes under 1 atm of CO. *J. Am. Chem. Soc.* **2020**, *142*, 18191-18199.
(41) C., Wang, X., Wu, H., Li, J., Qu, Y., Chen, Carbonylative Cross-Coupling Reaction of Allylic Alcohols and Organoalanes with 1 atm CO Enabled by Nickel Catalysis. *Angew. Chem., Int. Ed.* **2022**, Accepted author manuscript. DOI: 10.1002/anie.202210484
(42) L., Hou, H., WEnyi, X., Wu, J., Qu, Y., Chen, Nickel-Catalyzed Carbonylation of Cyclopropanol with Benzyl Bromide for Multisubstituted Cyclopentenone Synthesis. *Org. Lett.* **2022**, *24*, 2699-2704.
(43) L. C., Wang, B., Chen, Y., Zhang, X.-F., Wu, Nickel-Catalyzed Four-Component Carbonylation of Ethers and Olefins: Direct Access to γ-Oxy Esters and Amides. *Angew. Chem., Int. Ed.* **2022**, *61*, e2022079.

2. A Visible Light Driven Nickel Carbonylation Catalyst for Acid Chloride Synthesis

Chapter 1 described how nickel catalysts can be employed in carbonylative coupling reactions. In some variants of these transformations, such as carbonylative cross coupling reactions to form ketones, recent studies have shown that nickel complexes of polydentate nitrogen donor ligands can be active catalysts that function under mild conditions. However, for carbonylative coupling reactions to form esters, amides and related derivatives, the use of nickel catalysts usually requires very pressing conditions and is limited in scope relative to reactions using palladium catalysts. Described in this chapter are our studies toward using visible light excitation as an alternative avenue to create active nickel catalysts for carbonylative coupling reactions. This has opened a route to perform these reactions under often ambient conditions and with a range of classically challenging substrates.

2.1 Introduction

Metal catalyzed carbonylation reactions offer one of the most efficient methods to assemble carbonyl-containing compounds.[1] A powerful variant are carbonylative coupling reactions, which can form various amides, esters and related products directly from broadly available carbon monoxide and other stable reagents (Figure 1a). Nevertheless, there remain significant aspects limiting the utility of carbonylation chemistry. One of the most intrinsic is the catalyst. While there has been advances in related cross coupling reactions using more earth abundant nickel catalysts,[2,3] most carbonylative coupling reactions still rely upon precious metal palladium systems. The relatively high affinity of nickel to carbon monoxide is believed to inhibit carbonylation with these catalysts, requires high temperatures to overcome, and even with this often only proceeds with relatively activated aryl halide substrates (Figure 1b).[4-6] A number of important recent advances have been made in the use of more earth abundant metals, including nickel catalysts, in

carbonylations.[5-13] This includes key works in nickel catalysis by Skrydstrup,[8] Zhang,[9] Troupel[10] and others[11-13] that have shown how ligand design can be used to inhibit CO coordination in ketone synthesis (Figure 1b). However, the latter often employ an alternative Ni(II) mechanism that functions with strong carbon nucleophiles, meaning most carbonylative coupling products still rely on palladium catalysts. In addition to the metal, carbonylative coupling reactions are often limited to the use of reactive C(sp^2)-halide and/or simple nucleophilic components. These can be attributed to the inhibitory effect of CO coordination with palladium, as well as the need for nucleophiles that are strongly coordinating to allow product reductive elimination.[14,15] As a result, many carbonyl-containing products are instead prepared by the more classical use of high energy, synthetic acylating agents.

We and others have recently noted that visible light excitation of active palladium catalysts can offer an avenue to address a number of these issues in carbonylation reactions (Figure 1c).[16-23] In this, photolysis of Pd(0) in the presence of carbon monoxide can induce rapid oxidative addition of a range of substrates, while a concurrent light excitation of Pd(II) favors the reductive elimination of acid chloride electrophiles. The combination of these two steps can open a fully light driven catalytic cycle, and from this a versatile method to perform carbonylations with combinations of challenging reagents. Ryu, Odell, Alexanian and others have shown other important avenues to use UV or visible light, including with metals, in carbonylative coupling chemistry.[7a,23,24]

In considering these features, we questioned if visible light may offer an avenue to use nickel catalysts more generally in carbonylations. While the ability of precious metals to undergo well-defined oxidative addition and reductive elimination has made them valuable as catalysts in thermal chemistry, photoexcitation offers a mechanism to drive these operations that is less

dependent on balancing metal steric and electronic properties, and potentially less inhibited by CO coordination. There has been significant recent use of visible light photoredox chemistry in concert with nickel catalysts,[25-27] including examples of the direct excitation of Ni(II) enabling new reactivity.[28,29] However, the ability of simple visible light excitation to allow a nickel catalyst to function in a similar fashion to palladium in carbonylation chemistry, especially as a route to drive the formation of reactive acyl electrophiles, is not known. Combining these features could prove useful in expanding the applicability of carbonylation chemistry.

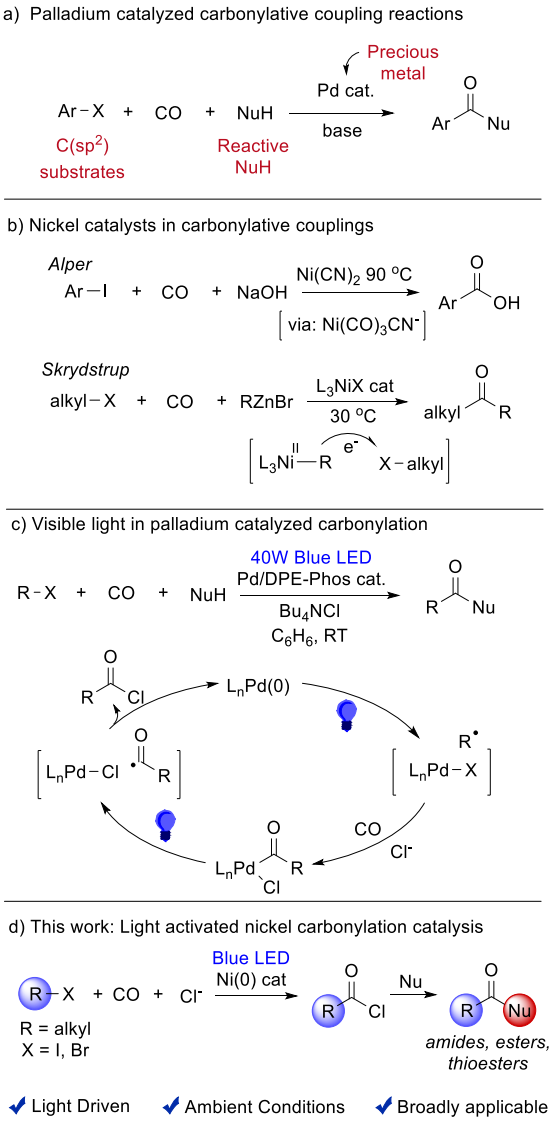

Figure 1 - Carbonylative Coupling Reactions with Group 10 Metal Catalysts

We describe below our studies toward such a nickel catalyst. This shows that the correctly ligated nickel can allow visible light driven, ambient temperature carbonylation reactions (Figure 1d). Carbon monoxide does not appear inhibitory in the system, and instead a carbon monoxide-ligated Ni(0) is the potent catalyst for the reaction. This system can be employed to carbonylate a range of C(sp^3)-alkyl iodides to build-up reactive acid chloride electrophiles. Coupling the latter with nucleophiles offers a versatile and general earth abundant metal catalyzed route to form amides, esters and thioesters of classically challenging reagents at ambient temperature.

2.2 Results and Discussion

Our initial studies toward this system probed the nickel catalyzed carbonylation of n-butyl iodide into an acid chloride in the presence of blue light. As shown in Figure 2a, the use of chelating nitrogen donor ligands with $Ni(COD)_2$ catalyst leads to minimal reaction (See Figure S1 for full screening). This includes a 2,2'-bipyridyl derivative systems that have proven effective in light-based nickel coupling chemistry.[25,28] We next moved to phosphorus donor ligands. Several of these ligands do show evidence for catalyst turnover in the presence of light, and form acid chloride formation in up to 31% yield with the bidentate Xantphos ligand. Closer examination of the reaction mixture shows that a contributing factor to the low yield with these systems is a background reaction of the substrate and Bu_4NCl to form a catalytically inactive n-butyl chloride as a side product (Figure S1). The latter can be inhibited by the use of a less soluble Ph_3BnPCl salt to slow anion metathesis, and with Xantphos as ligand leads to acid chloride **1a** in high yield (see Figure S2 for other chloride salts).

While carrying out these reactions, we noted significant variation in the yield depending upon how the reaction was performed. After examining several variables, it was found that pre-mixing the

alkyl iodide and nickel catalyst for > 30 min before the addition of carbon monoxide and light led to lower yields (Figure S3), implying a background reaction may be deactivating the catalyst. Evidence can be seen in the reaction of $Ni(COD)_2$, 2,2'-bipyridyl and butyl iodide without CO, which leads to the formation of the disproportionation product octane within minutes at ambient temperature and catalytically inactive nickel(II) halides (Figure S4). A solution is to exploit the ability of nickel to form stable carbon monoxide coordinated complexes. The reaction of $Ni(COD)_2$ and Xantphos followed by CO leads to the near quantitative formation of $XantphosNi(CO)_2$, **2**, which can be isolated as an air stable solid and has been structurally characterized (Figure 2b). Of note, the nickel resides in a pseudo-tetrahedral environment in the complex, and the two CO ligands display slightly lengthened C-O bonding (1.140(3) Å),[30] consistent with weak backbonding to the Ni(0). Complex **2** offers a stable, easily handled, and reproducible catalyst for the near quantitative carbonylative formation of acid chloride (Figure 2c). The reaction with this catalyst is also effective at 1 atm CO in slightly lower yield. No product is observed in the absence of light or the nickel catalyst, suggesting that the combination the nickel complex, alkyl halide and light, without an exogenous photocatalyst, is responsible for reactivity (*vide infra*).

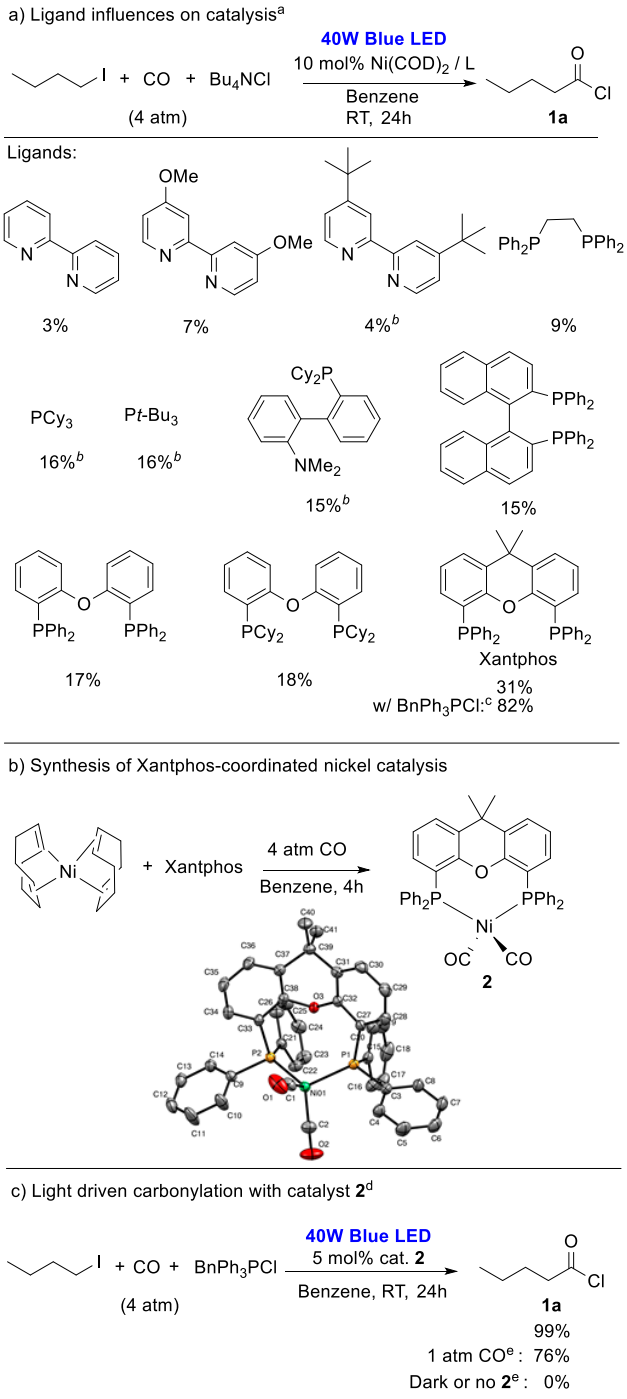

Figure 2. Catalyst Development for Visible Light Driven Nickel Catalyzed Carbonylation. [a] 1-iodobutane (0.08 mmol), Bu_4NCl (0.08 mmol), $Ni(COD)_2$ (0.008 mmol), Ligand (0.008 mmol), 0.8 mL benzene, 40W Blue LED, ^1H NMR yield after conversion to benzylamide.. [b] 20% L [c] 1.5 eq. $BnPh_3PCl$ with stirring. [d] 0.25 mmol scale,1.5 eq. $BnPh_3PCl$. [e] 10 mol% 2

With a potent light driven nickel catalyst for carbonylation in hand, we next explored the generality of the transformation. As shown in Figure 3, a range of primary alkyl iodides can be carbonylated to form acid chlorides (**1b-d**), including more sterically encumbered b- and g-branched substrates. Secondary alkyl iodides (**1e, f**) can also be employed as reagents, as can the tertiary tert-butyl iodide (**1g**) in slightly lower yield. The introduction of functionality does not appear to affect catalysis. Examples here include the □-electron withdrawing trifluoromethyl functionality (**1i**), as well as potentially reactive alkyl halides (**1j**) or terminal alkynes (**1v**). Coordinating functionalities such as esters (**1k**), dioxolanes (1l), ethers (**1o, s, w**), ketones (**1u**), nitriles (**1p, q**) and a phosphonate group (**1m**) are each tolerated. □-Ester substituted alkyl iodides are also viable reagents (**1n**) and provide access to protected a-hydroxy-acid chloride derivatives. The reaction can be extended to heteroaromatic containing reagents such as those with coordinating thiophene (**1y**) and pyridine (**1x**) substituents with 10 mol% nickel catalyst. In addition to alkyl iodides, activated alkyl bromides can also be employed as substrates, including β-cyano ethyl- (**1z**) and benzyl-bromide (**1aa**), although the use of less activated substrates leads to lower yields (**1bb**).

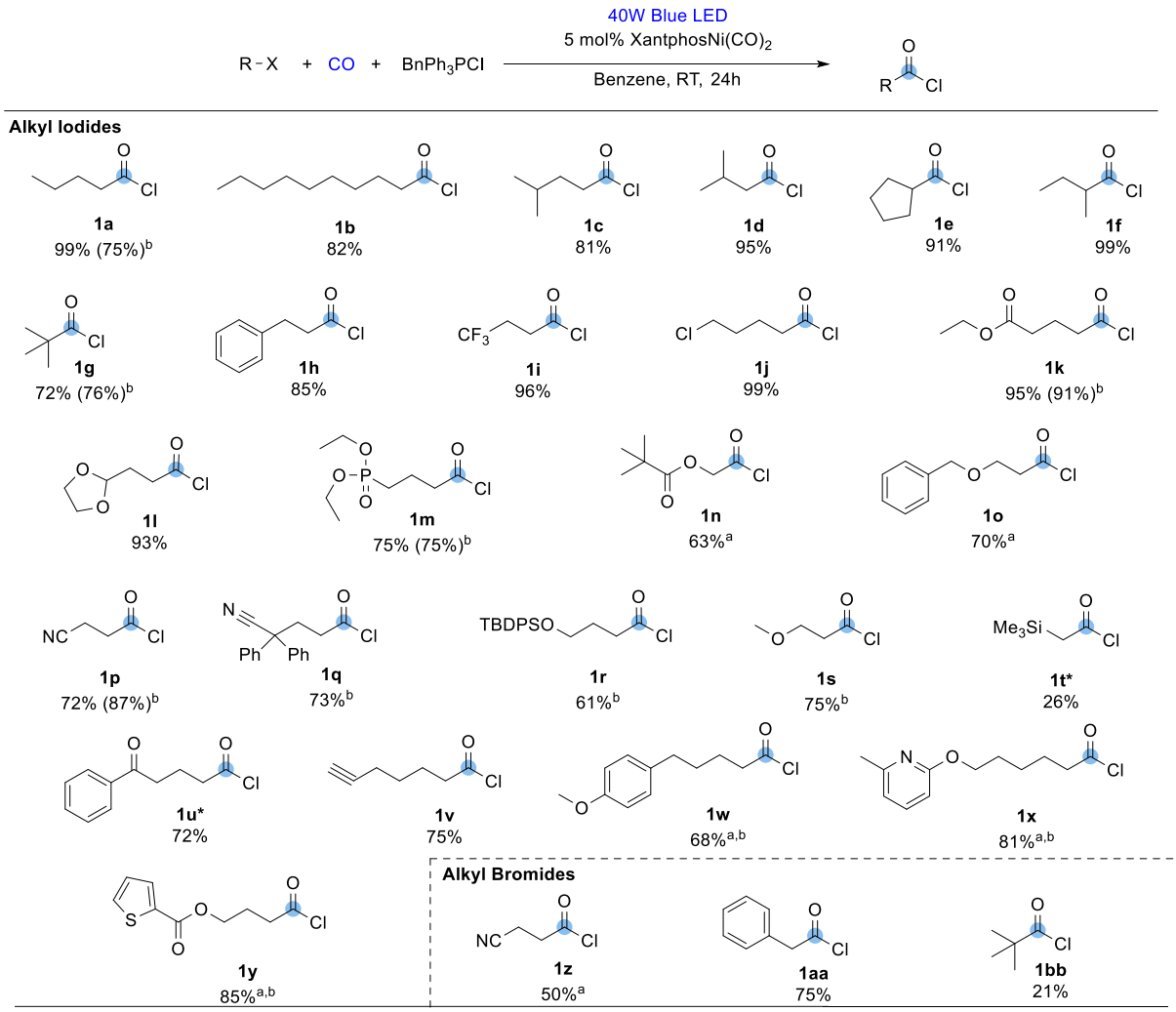

Figure 3. Versatile Nickel Catalyzed Carbonylative Acid Chloride Synthesis with Light. Conditions: Alkyl iodide (0.25 mmol), $BnPh_3PCl$ (0.38 mmol), $XantphosNi(CO)_2$ (0.013 mmol), 4 atm CO, 3 mL benzene, 24h, 40W blue LED; isolated yields as determined by conversion to benzylamide. [a] 10 mol% 1. [b]1 atm CO.

Coupling the formation of acid chlorides with their electrophilic reactivity can allow the synthesis of a range of carbonylation products. Representative examples are shown in Figure 4, and include the synthesis of primary and secondary amides, such as those of sterically encumbered amines often not viable in carbonylations (**4b**) or with nickel-reactive functionalities (**4g**). Esters (**4d-f, j-l**) can also be prepared upon alcohol addition. The latter includes bioactive compounds such as the

phytosteroid diosgenin (**4f**) or icaridin (**4k**), and phenols containing coordinating or reactive functionalities (**4e, l**). Alternatively, the addition of thiols can offer access to alkyl-thioesters (**4a**, **h**). To our knowledge, none of these products has been previously generated by nickel catalyzed carbonylations.

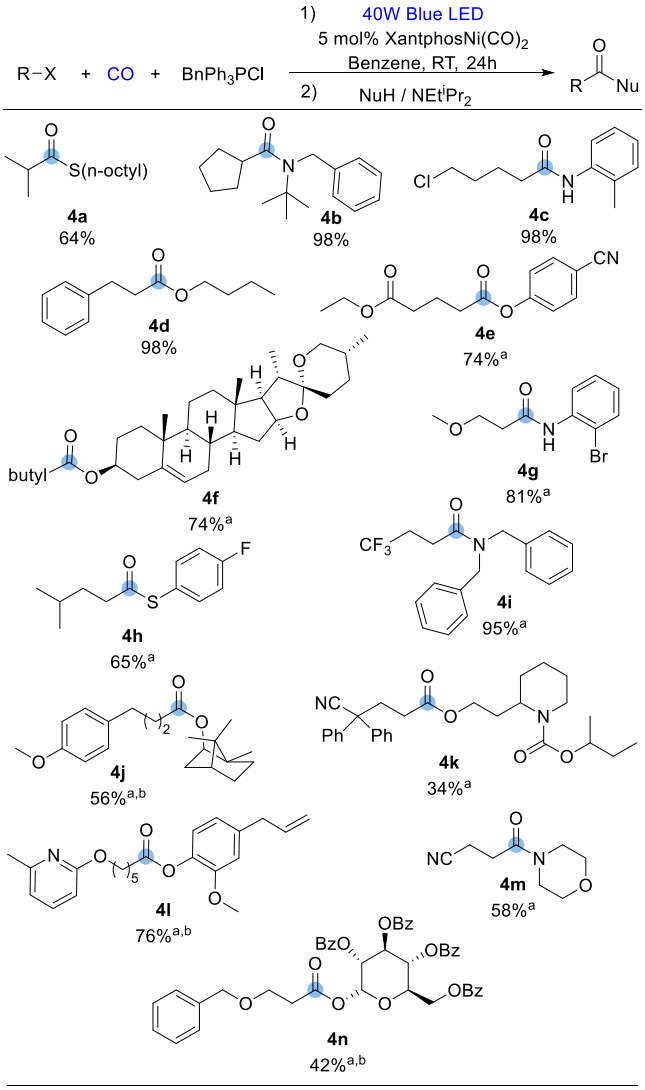

Figure 4. Nickel Catalyzed Carbonylative Synthesis of Amides, Esters and Thioesters with Visible Light. Conditions of Figure 3. [a] 1 atm CO. [b] 10 mol% 2.

We have performed several preliminary studies to probe the role of light in these transformations. Monitoring the catalytic reaction by in situ ^{1}H and ^{31}P NMR analysis shows that complex **2** is

rapidly generated from $Ni(COD)_2$/Xantphos and is the major catalyst resting state throughout the transformation (Figure 5A). UV/Vis analysis shows that complex **2** does absorb light in the blue region of the visible spectrum, and is also weakly emissive (Figure S5), in analogy to previous reports with $(PPh_3)_2Ni(CO)_2$.[31] More important, the blue light photolysis of **2** in the presence of n-butyl iodide and TEMPO leads to the rapid generation of the butyl radical trapping-TEMPO adduct in near quantitative yield (Figure 5B). No reaction is observed without the nickel complex or without light. The latter suggests that the combination of blue light and nickel complex **2** is required for the activation of the alkyl iodide substrate. Interestingly, and unlike the related palladium systems,[16] the CO coordinated complex **2** shows no evidence for reaction with the acid chloride product, even with irradiation with blue light (Figure 5C). However, performing the latter experiment in the presence of TEMPO leads to the acyl-TEMPO radical trapping product, implying that electron transfer from nickel to the acid chloride product may occur, but its overall addition to the electron deficient nickel complex **2** is disfavored.

Together, this data is consistent with light excitation in the presence of the nickel catalyst leading to activation of the alkyl halide substrate via alkyl radical formation (Figure 5D). This could occur by electron transfer from the Ni(0) photoexcited state, although a radical chain mechanism, potentially involving Ni(II) intermediates,[29] cannot be ruled out. The trapping of this radical by CO would generate a Ni(II) intermediate that appears to strongly favor reductive elimination even without light (Figure 2C). In this, carbon monoxide does not appear to inhibit catalysis, and the reaction proceeds in higher yields with more CO (Figure 2C), which may result from the more favored regeneration of the nickel-carbonyl complex **2** resting state. The high reductive elimination propensity of the nickel catalyst **2** can be clearly seen by monitoring the catalytic reaction in the absence of chloride anion, which leads to the build-up of acyl iodide in up to 33% yield (Figure

5E). Acyl iodides are much more potent electrophiles than acyl chlorides. Their formation as catalytic products is unknown with group 10 metals,[32] and highlights the ability of these nickel-carbonyl catalysts in driving the chemistry toward reactive product formation.

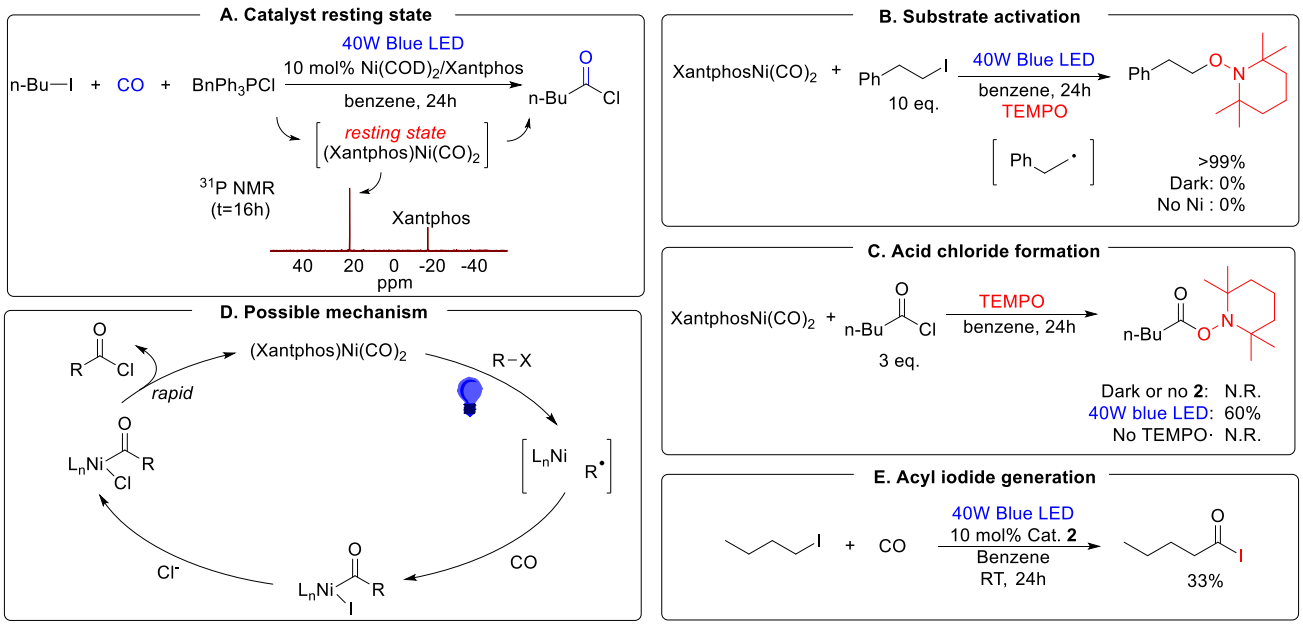

Figure 5. Mechanistic Studies on Light Driven Nickel Catalyzed Carbonylation.

2.3 Conclusion

In conclusion, visible light excitation has been found to offer a powerful avenue to activate nickel(0) catalyst toward carbonylation chemistry. This has been used to synthesize electrophilic acid chlorides from alkyl iodides or activated alkyl bromides, and from these an variety of ester, thioester and amide products, all of which occur at ambient conditions. Considering the broad use of group 10 metals in catalysis, the ability to activate nickel(0) systems with light could prove a useful tool to carry out coupling reactions with available nickel catalysts.

2.4 Experimental Section

All experimental details for experiments performed, supplementary figures, and NMR spectra are provided in Appendix I (Supplementary material in the paper to be submitted).

2.5 References to Chapter 2

(1) For reviews: a) M., Beller, X.-F., Wu, Transition Metal Catalyzed Carbonylation Reactions: Carbonylative Activation of C-X Bonds, 1st ed.; Springer: Amsterdam, 2013. b) L., Kollär, Modern Carbonylation Methods; Wiley-VCH: Weinheim, 2008. c) Q., Liu, H., Zhang, A., Lei, *Angew. Chem., Int. Ed*. **2011**, *50*, 10788−10799, d) Peng, J.-B.; Geng, H.-Q. & Wu, X.-F. Chem **2019,** *3*, 526-552.e) R. Skoda-Földes, L. Kollár. *Curr. Org. Chem.* **2002**, *6*, 1097-1119.

(2) S. Z. Tasker, E. A. Standley, T. F Jamison, *Nature*, **2014**, *509*, 299-309.

(3) Lin C.-Y., Power P.P. *Chem. Soc. Rev*. **2017**, *46*, 5347-5399

(4) For example: H. Alper, I. Amer, G. Vasapollo, *Tetrahedron Lett.* **1989**, *30*, 2615-2617.

(5) Y. Li, Y. Hu, X.-F. Wu, *Chem. Soc. Rev*. **2018**, *47*, 172-194.

(6) J.-B. Peng, F.-P. Wu, X.-F. Wu. *Chem. Rev*. **2019**, *119*, 2090-2127.

(7) For recent examples of non-nickel first row metal carbonylations: a) A. M. Veatch, E. J. Alexanian. *Chem. Sci.* **2020**, *11*, 7210-7213; b) L.-J. Cheng, N. P. Mankad. *Acc. Chem. Res.* **2021**, *54*, 2261-2274; c) Y. Li, F. Zhu, Z. Wang, J. Rabeah, A. Bruckner, X.-F. Wu *ChemCatChem* **2017**, *9,* 915-919.

(8) a) T. L. Andersen, A. S. Donslund, K. T. Neumann, T. Skrydstrup. *Angew. Chem., Int. Ed*. **2018**, *57*, 800-804. b) A. S., Donslund, K. T., Neumann, N. P., Corneliussen, E. K., Grove, D., Herbstritt, K., Daasbjerg, T., Skrydstrup. *Chem. Eur. J.* **2019**, *25*, 9856-9860

(9) M., Zhou, H.-Y., Zhao, S., Zhang, Y., Zhang, X., Zhang. *J. Am. Chem. Soc.* **2020**, *142*, 18191-18199.

(10) M., Oçafrain, M., Devaud, M., Troupel, J., Périchon. *J. Chem. Soc., Chem. Commun.* **1995**, 2331-2332

(11) Q., Wang, C., Chen. *Tetrahedron Lett*. **2008**, *49*, 2916-2921.

(12) Y.-W., Huo, X., Qi, X.-F., Wu. *Org. Lett.* **2022**, *24*, 4009-4013.

(13) H., Yu, B., Gao, B., Hu, H., Huang. *Org. Lett.* **2017**, *19*, 3520-3523.

(14) a) K. D., Dobbs, W. J., Marshall, V. V., Grushin. *J. Am. Chem. Soc.* **2007**, *129*, 30-31. b) J. S., Quesnel, S., Moncho. K. E. I., Ylijoki, G. M., Torres, E. N., Brothers, A. A., Bengali, B. A., Arndtsen. *Chem. Eur. J.* **2016**, *22*, 15107-15118. c) J. Y., Wang, A. E., Storm, J. F., Hartwig. *J. Am. Chem. Soc.* **2018**, *140*, 7979-7993.

(15) Examples of catalytic acyl electrophile formation or palladium catalyzed carbonylations with alkyl halides: a) J. S., Quesnel, B. A., Arndtsen. *J. Am. Chem. Soc.* **2013**, *135*, 16841-16844. b) J. S., Quesnel, L. V., Kayser, A., Fabrikant, A. B., Arndtsen. *Chem. Eur. J.* **2015**, *21*, 9550-9555. c) B. T., Sargent, E. J., Alexanian, *J. Am. Chem. Soc.* **2016**, *138*, 7520-7523.

(16) G. M. Torres, Y. Liu and B. A. Arndtsen. *Science*. **2020**, *368*, 318-323.

(17) Y., Liu, C., Zhou, M., Jiang, B. A., Arndtsen. *J. Am. Chem. Soc.* **2022**, *144*, 9413-9420.

(18) M. Parasram, P. Chuentragool, D. Sarkar, V. Gevorgyan. *J. Am. Chem. Soc*. **2016**, *138*, 6340–6343.

(19) M. A. Fredricks, M. Drees, K. Köhler. *ChemCatChem*. **2010**, *2*, 1467-1476.

(20) G.-Z. Wang, R. Shang, W.-M. Cheng, Y. Fu. *J. Am. Chem. Soc*. **2017**, *139*, 18307-18312.

(21) R. Kancherla, K. Muralirajan, B. Maity, C. Zhu, P. E. Krach, L. Cavallo, M. Rueping. *Angew. Chem., Int. Ed*. **2019**, *58*, 3412-3416.

(22) P., Chuentragool, D., Kurandina, V., Gevorgyan. *Angew. Chem. Int. Ed.* **2019**, *58*, 11586-11598.

(23) S. Roslin and L. R. Odell. *Chem. Commun*. **2017**, *53*, 6895-6898.

(24) For UV light induced alkyl iodide radical carbonylation: a) I. Ryu, N. Sonoda. *Angew. Chem., Int. Ed*. **1996**, *35*, 1050-1066. b) S. Sumino, A. Fusano, T. Fukuyama, I. Ryu *Acc. Chem. Res.* **2014**, *47*, 1563-1574. Including in concert with nickel complexes: c) T. Kondo, Y. Sone, Y. Tsuji, Y. Watanabe. *J. Organomet. Chem*. **1994**, *473*, 163-173.

(25) For reviews: a) A. Y. Chan, I. B. Perry, N. B. Bissonnette, B. F. Buksh, G. A. Edwards, L. I. Frye, O. L. Garry, M. N. Lavagnino, B. X. Li, Y. Liang, E. Mao, A. Millet, J. V. Oakley, N. L. Reed, H. A. Sakai, C. P. Seath, D. W. C. MacMillan, *Chem. Rev.* **2022**, *122*, 1485−1542. b) J. A. Milligan, J. P. Phelan, S. O. Badir, G. A. Molander, *Angew. Chem., Int. Ed.* **2019**, *58*, 6152−6163. c) K. L. Skubi, T. R. Blum, T. P. Yoon, *Chem. Rev.* **2016**, *116*, 10035−10074. d) C., Zhu, H., Yue, J., Jia, M., Rueping. *Angew. Chem. Int. Ed.* **2021**, *60*, 17810-17831. e) C., Zhu, H., Yue, L., Chu, M., Rueping. *Chem. Sci*. **2020**, *11*. 4051-4064. f) M. M. Mastandrea, M. A. Pericas, Photoredox *Eur. J. Inorg. Chem*. **2021**, 2021, 3421−3431. g) T. Noel, E. Zysman-Colman, *Chem Catalysis* **2022**, *2*, 468−476.

(26) Early reports: a) J. C., Tellis, D. N., Primer, G. A., Molander. *Science*. **2014**, *345*, 433-436. b) Z., Zuo, D. T., Ahneman, L., Chu, J. A., Terrett, A. G., Doyle, D. W. C., MacMillan. *Science*. **2014**, *345*, 437-440.

(27) Recent examples: a) E. R. Welin, C. Le, D. M. Arias-Rotondo, J. McCusker and D. W. C. MacMillan. *Science*. **2017**, *355*, 380-385; b) D.N. Primer, I. Karakaya, J. C. Tellis, G. A. Molander, *J. Am. Chem. Soc.* **2015**, *137*, 2195−2198 c) B. J. Shields, A. G. Doyle *J. Am. Chem. Soc.* 2016, *138*, 12719−12722 d) Y., Shen, T., Rovis. *J. Am. Chem. Soc.* **2021**, *143*, 16364-16369. e) L. Peng, Z. Li, G. Yin *Org. Lett.* **2018**, *20*, 1880−1883. f) S. Cao, W. Hong, Z. Ye, L. Gong, *Nat. Commun.* **2021**, *12*, No. 2377. g) L. Cavallo, M. Rueping, B. Maity, C. Zhu, H. Yue, L. Huang,M. Harb, Y. Minenkov *J. Am. Chem. Soc.* **2020**, *142*, 16942−16952. h) H. M. Huang, P. Bellotti, J. E. Erchinger, T. O. Paulisch, F. Glorius, F. *J. Am. Chem. Soc.* **2022**, *144*, 1899−1909. i) Y Ben-Tal, G. C. Lloyd-Jones *J. Am. Chem. Soc.* **2022**, *144*, 15372-15382

(28) Reviews: a) K. P. S., Cheung, S., Sarkar, V., Gevorgyan. *Chem. Rev.* **2022**, *122*, 1543-1625. b) S. K. Kariofillis, A. G. Doyle *Acc. Chem. Res.* **2021**, *54*, 988−1000.

(29) Examples: a) B. J. Shields, B. Kudisch, G. D. Scholes, A. G. Doyle. *J. Am. Chem. Soc*. **2018**, *140*, 3035-3039. b) S. I. Ting, S. Garakyaraghi, C. M. Taliaferro, B. J. Shields, G. D. Scholes, F. N. Castellano, A. G. Doyle. *J. Am. Chem. Soc*. **2020**, *142*, 5800-5810. c) C.-H. Lim, M. Kudisch, B. Liu and G. M. Miyake. *J. Am. Chem. Soc*. **2018**, *140*, 7667-7673. d) G., Song, D.-Z., Nong, J.-S., Li, G., Li, W., Zhang, R., Cao, C., Wang,, J., Xiao, D., Xue. *J. Org. Chem.* **2022**, *87*, 10285-10297. e) L., Yang, H.-H., Lu, C.-H., Lai, G., Li, W., Zhang, R., Cao, F., Liu, C., Wang, J., Xiao, D., Xue. *Angew. Chem. Int. Ed.* **2020**, *59*, 12714-12719. f) S. Wang, P. Ma, S. Shaik, H Chen *J. Am. Chem. Soc.* **2022,** *144*, 14607-14613

(30) Deposition numbers 2205625 for **2**) contain the supplementary crystallographic data for this paper. These data are provided free of charge by the joint Cambridge Crystallographic Data Centre and Fachinformationszentrum Karlsruhe Access Structures service.

(31) **2** is also emissive (Figure S5), but the weak signal inhibited the study of its quenching with alkyl iodides. For similar emission with $(PPh_3)_2Ni(CO)_2$, see:, Kunkley, A., Vogler. *Inorg. Chem. Commun.* **2000**, *3*. 143-144.

(32) The related acetyl iodide is a well-known intermediate in methanol carbonylation using rhodium and iridium catalysts.

3. Conclusions and Contributions to Knowledge

In conclusion to the completion of a Master's degree in Chemistry, the work undertaken in efforts of reaching this point have been demonstrated in Chapters 1 and 2.

A nickel-catalyzed carbonylative cross-coupling reaction that is driven by visible light is a novel achievement in the field of chemistry.

The classic carbonylative manifold established by palladium is the status quo in carbonylation chemistry. The well-understood fundamental processes governing the reactivity of those systems are characterized by balanced oxidative-addition/reductive-elimination steps, occurring via 2-electron mechanisms. The electronics of these palladium catalysts make them well-suited to operate under CO atmospheres as they do not appear to majorly inhibit activity, as is usually the case with nickel catalysts.

The system operating in this thesis invokes the special role of visible light irradiation in the observed catalytic efficiency. Whereas CO usually appears to inhibit nickel, the discovery of a CO-ligated nickel complex capable of reacting under a CO atmosphere represents an innovative method for circumventing its traditionally encountered limitations.

Evidence proposing that XantphosNi$(CO)_2$ is photoactive, with emission being detected when excited at low temperatures, invokes nickel as the system's sole photocatalytic component. Its ability to activate alkyl iodides can therefore be postulated to occur by pathways involving photoexcited states; an emerging – but nevertheless rare – occurrence in the field of chemistry.

The high yield catalytic build-up of reactive acid chloride electrophiles, as well as evidence demonstrating the formation of the even more reactive acid iodide, are promising results for future applications of this catalyst.

Where and how nickel photochemistry will be exploited in future chemical transformations remains to be seen, with XantphosNi$(CO)_2$ undoubtedly holding promise in aiding in unlocking the secrets that this special Earth Abundant metal has to hide.

4. Appendix I: Experimental Procedures and Spectra

4.1 General materials and methods

All manipulations were conducted in a glovebox under a nitrogen atmosphere. All reagents were purchased from commercial sources, unless otherwise noted. Prior to use in catalysis, all liquid substrates were degassed, transferred to a glovebox, and dried with 4Å molecular sieves. Solid reagents were transferred to a glovebox under nitrogen, dissolved in dichloromethane, stirred over 4Å molecular sieves, then filtered and the solvent removed *in vacuo*. Solvents were dried by filtration through 4Å molecular sieves under nitrogen on an MBraun solvent purification system, and then stored over activated 4Å molecular sieves inside the glovebox. Deuterated acetonitrile and benzene were stirred over calcium hydride, vacuum transferred, degassed, and stored over 4Å molecular sieves. Research grade carbon monoxide (99.99%) was used as received. Warning: CO is a poisonous gas that requires all the experiments to be conducted in well-ventilated fume hoods. For reactions performed in a J-Young NMR tube, carbon monoxide was added by attaching the J-Young tube to a Schlenk line of a known internal gas volume (67 mL) and equipped with a pressure gauge. The NMR tube solution was frozen in liquid nitrogen, the headspace evacuated, the tube closed, and the Schlenk line was filled with 800 mTorr of CO. In order to condense 4 atm CO into the 2.2 mL headspace of the NMR tube, the tube was opened until a pressure drop of 120 mTorr was recorded on the Schlenk line (corresponding to 0.44 mmol of CO; which equals 4 atm CO in the J-Young NMR tube based on the idea gas law). For reaction in Schlenk bombs at 1 atm CO, the solution was frozen in liquid nitrogen, evacuated, thawed, and the tube was pressurized to 1 atm CO. For reaction in Schlenk bombs at 4 atm CO, 4 atm CO was added to the existing atmosphere of nitrogen.

Kessil 40W A160WE Tuna Blue LED lamps were purchased from Reef Supplies. Nuclear magnetic resonance (NMR) characterization was performed on 400, 500 or 800 MHz spectrometers for proton, 126 or 201 MHz for carbon, 162 MHz for phosphorus and 377 or 471 MHz for ^{19}F NMR. ^{1}H and ^{13}C NMR chemical shifts were referenced to residual solvent. Mass spectra were recorded on a high-resolution electrospray ionization quadrupole mass spectrometer. UV-Vis was recorded on a Jasco V-670 spectrophotometer. Fluorescence spectra were recorded on a Cary Eclipse fluorescence spectrophotometer.

4.2 Supplementary Figures

Figure S1 – Full ligand screening

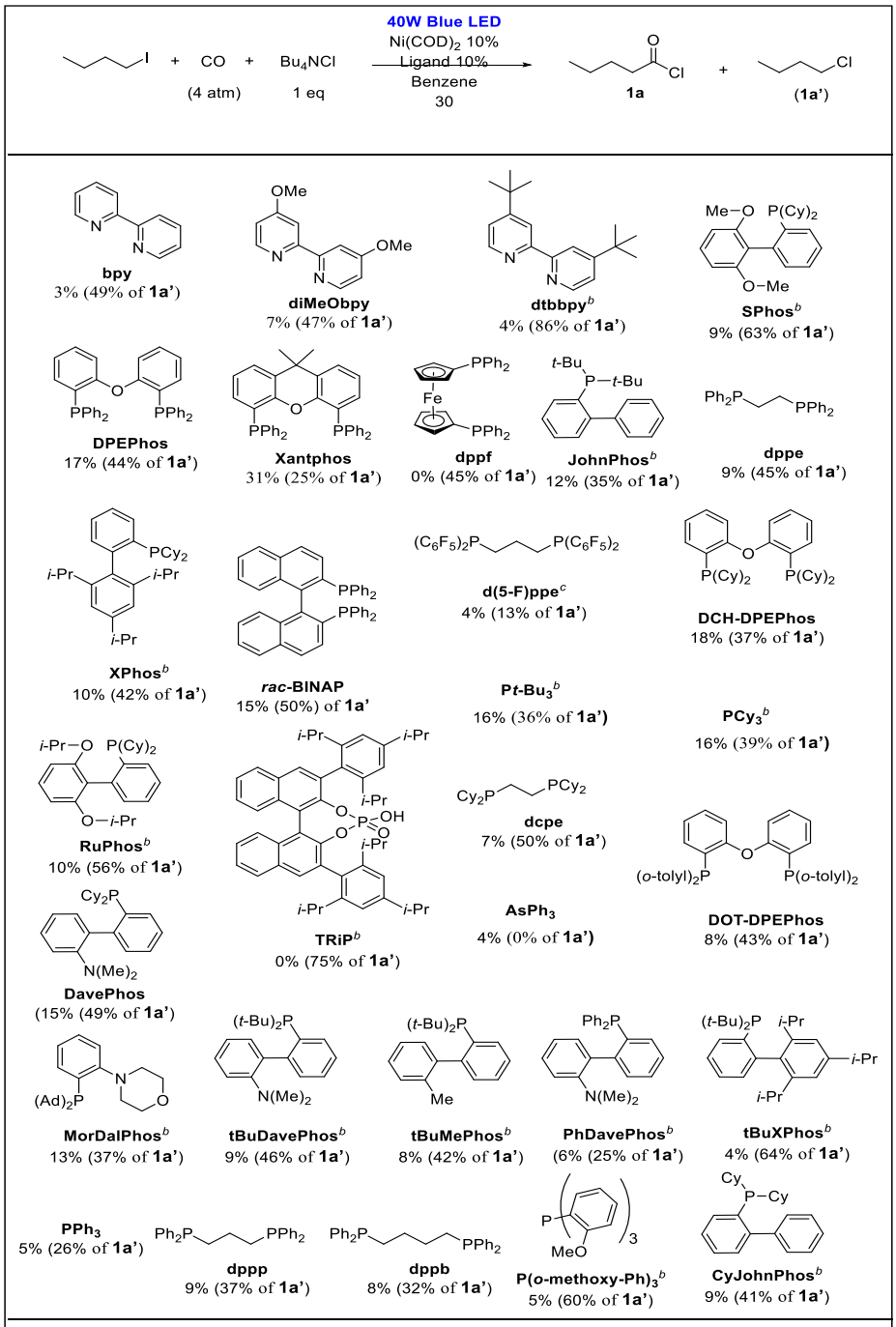

[a]1-iodobutane (0.08 mmol), Bu_4NCl (0.08 mmol), $Ni(COD)_2$ (0.008 mmol), Ligand (0.008 mmol), 0.8 mL benzene, 40W Blue LED, 24h; yield determined by ^1H NMR after conversion to benzylamide with benzylamine.[b] 20% ligand [c]Acetonitrile instead of Benzene, LiCl instead of Bu_4NCl, in bomb w/ stirring

Figure S2 - Influence of chloride source on acyl chloride formation

Cl^- source	Yield **1a** (**1a'**)
LiCl	21%(0%)
KCl	23%(0%)
NaCl	25%(0%)
CsCl	27%(0%)
$BnPh_3PCl$	64%(4%)
$BnPh_3PCl$ (1.5 equiv)	82%

Figure S3 – Influence of time spent pre-mixing prior to CO loading and light irradiation[a]

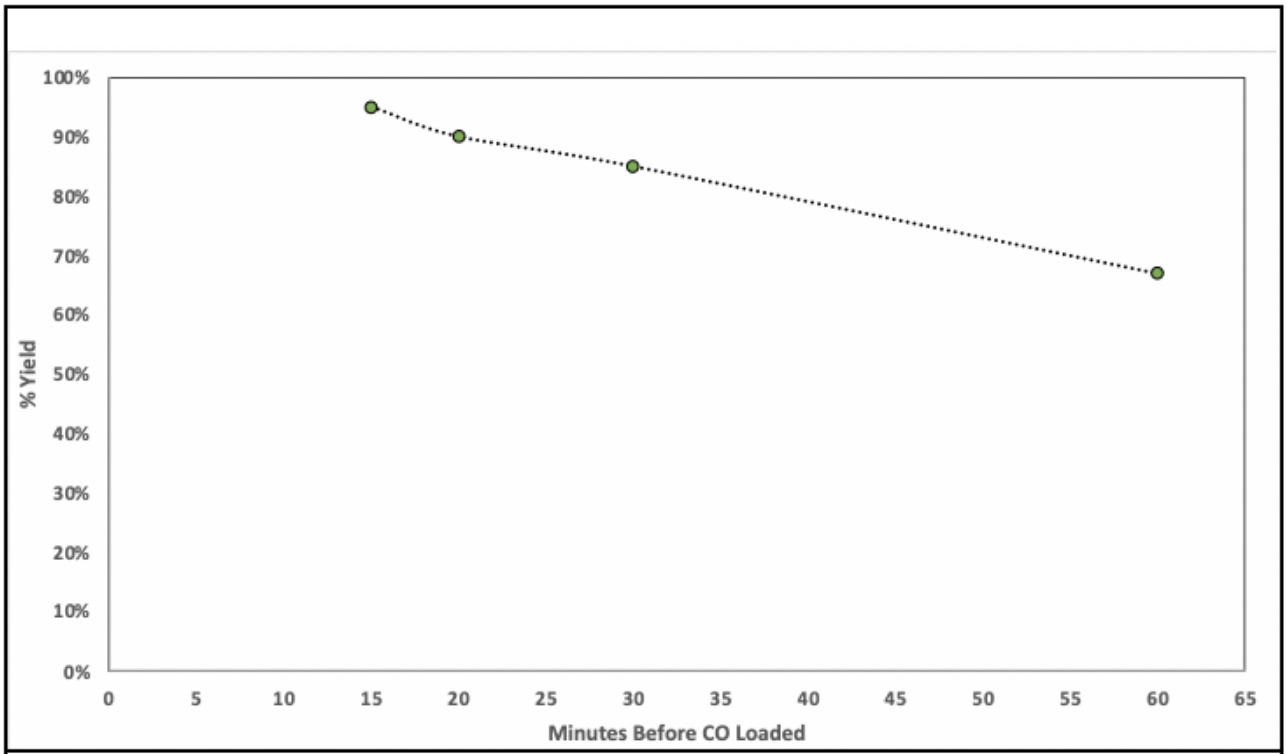

[a] 1-iodobutane (0.08 mmol), Bu_4NCl (0.08 mmol), $Ni(COD)_2$ (0.008 mmol), Ligand (0.008 mmol), $BnPh_3PCl$ (0.12 mmol) 0.8 mL benzene, 40W Blue LED, 24h; yield determined by ^1H NMR after conversion to benzylamide with benzylamine.

Figure S4 - Reaction of $Ni(COD)_2$, 2,2'-bipyridyl and *n*-butyl iodide without CO

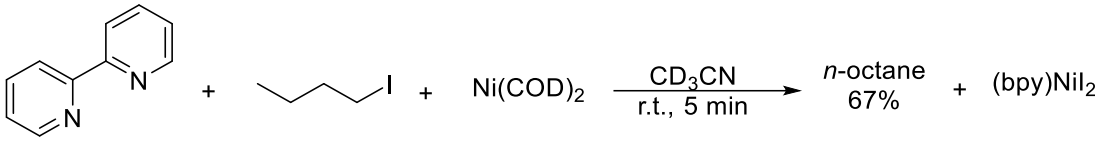

^{1}H NMR (t = 5 min)

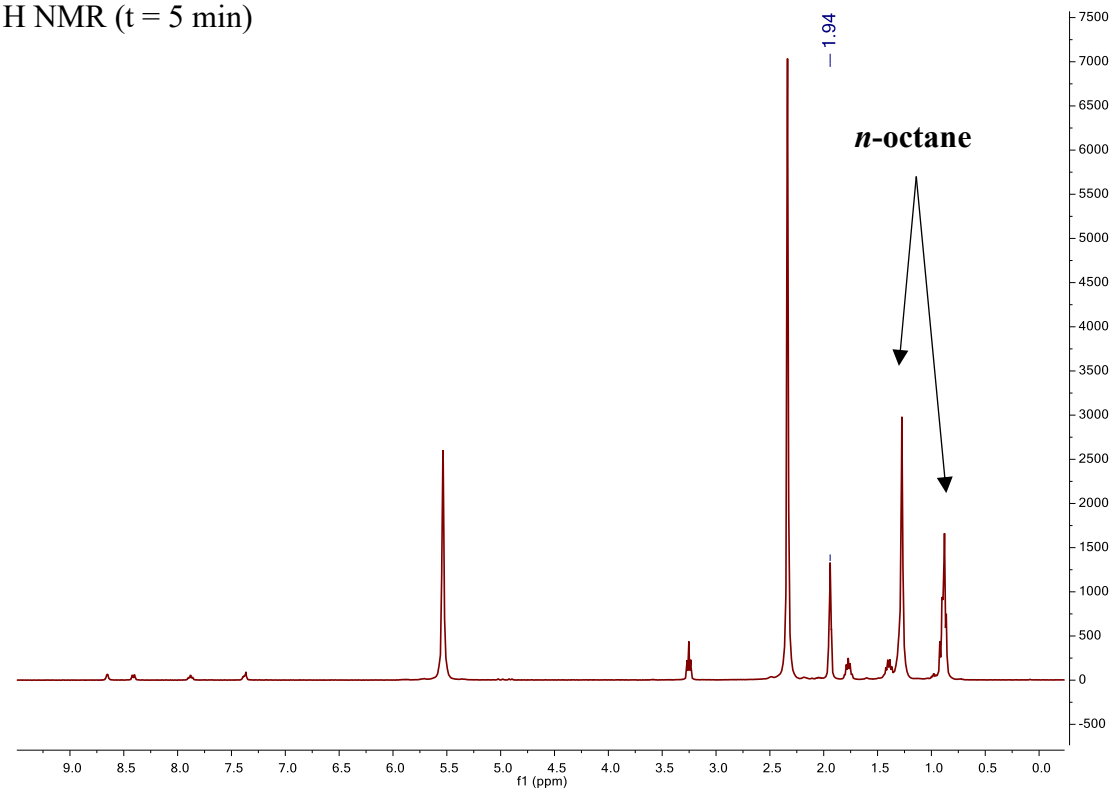

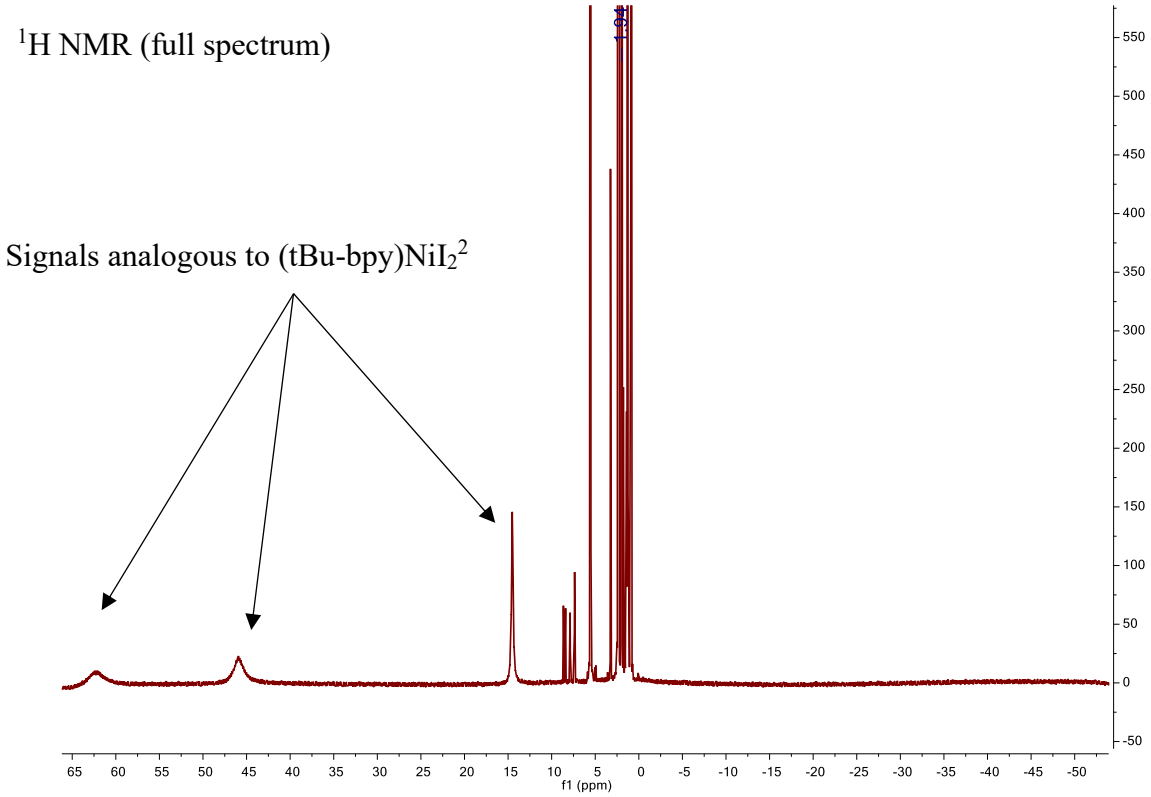

Figure S5 – UV-Vis of XantphosNi(CO)$_2$in benzene [9.5x10^{-5}M]

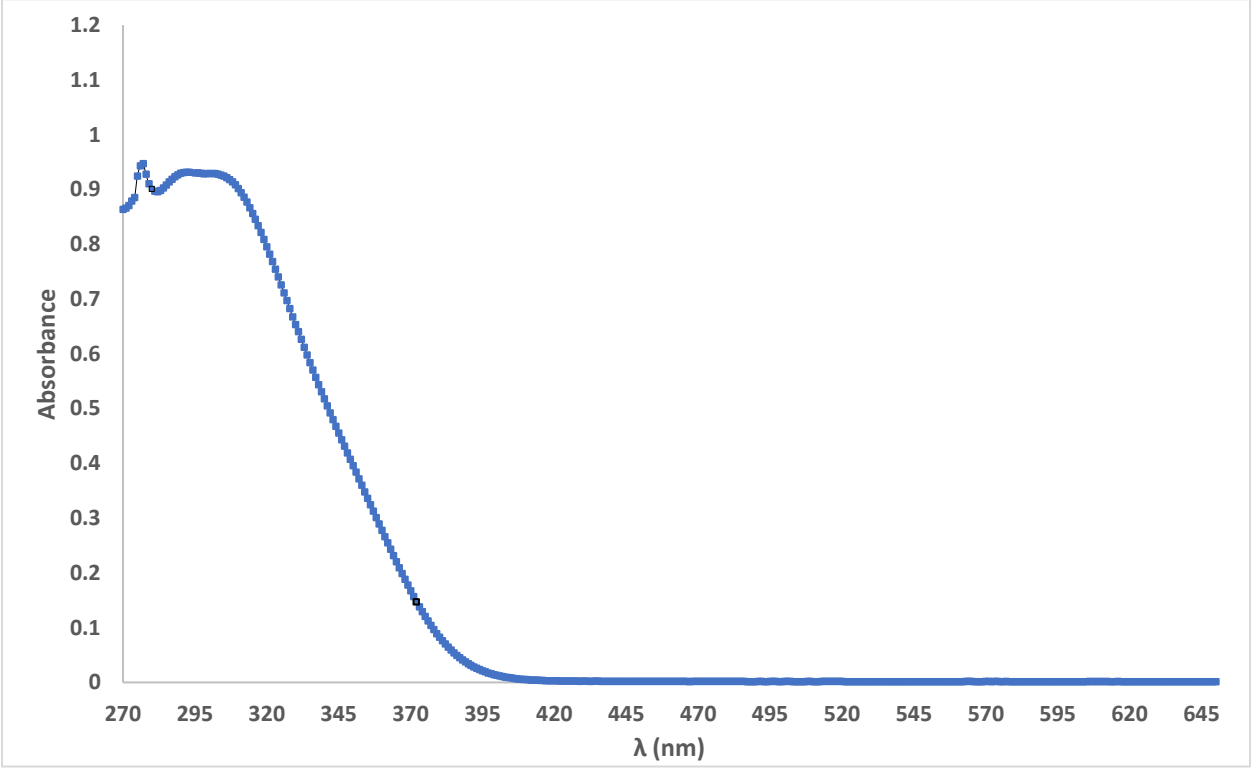

Emission from XantphosNi(CO)$_2$ [4.6x10^{-3}M] in benzene at 77K from excitation at 365 nm.

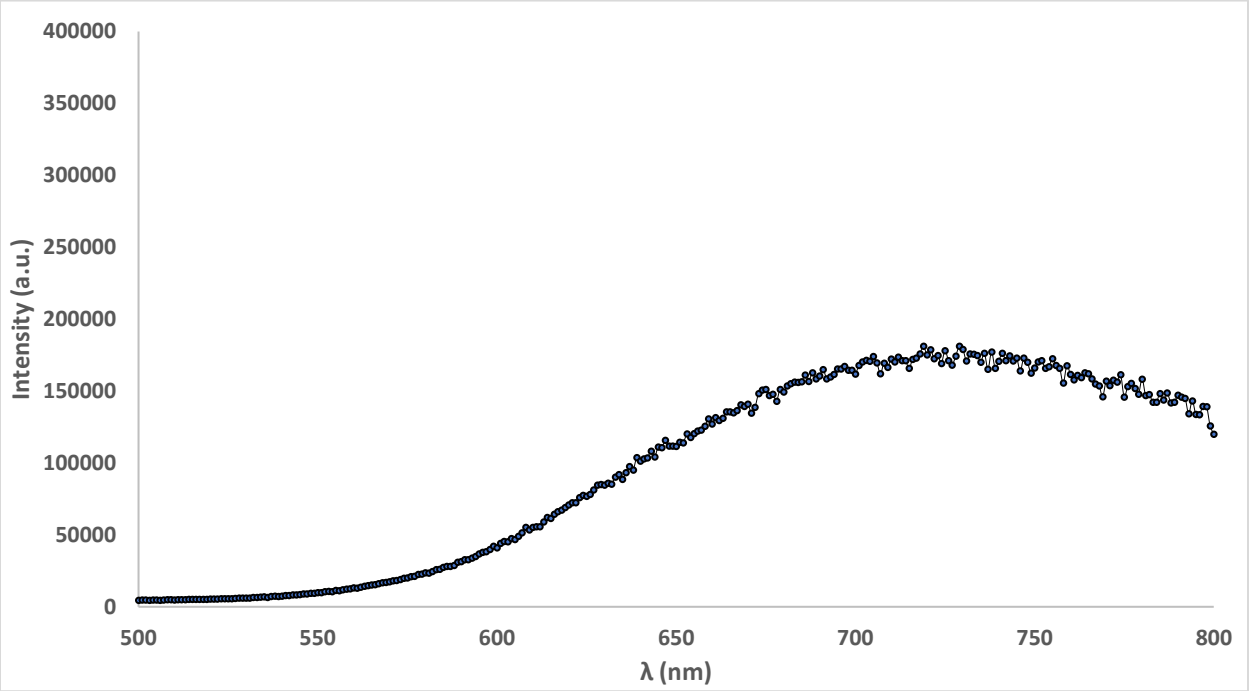

Emission from XantphosNi(CO)$_2$ [4.6x10^{-3}M] in benzene at room temperature from excitation at 380 nm.

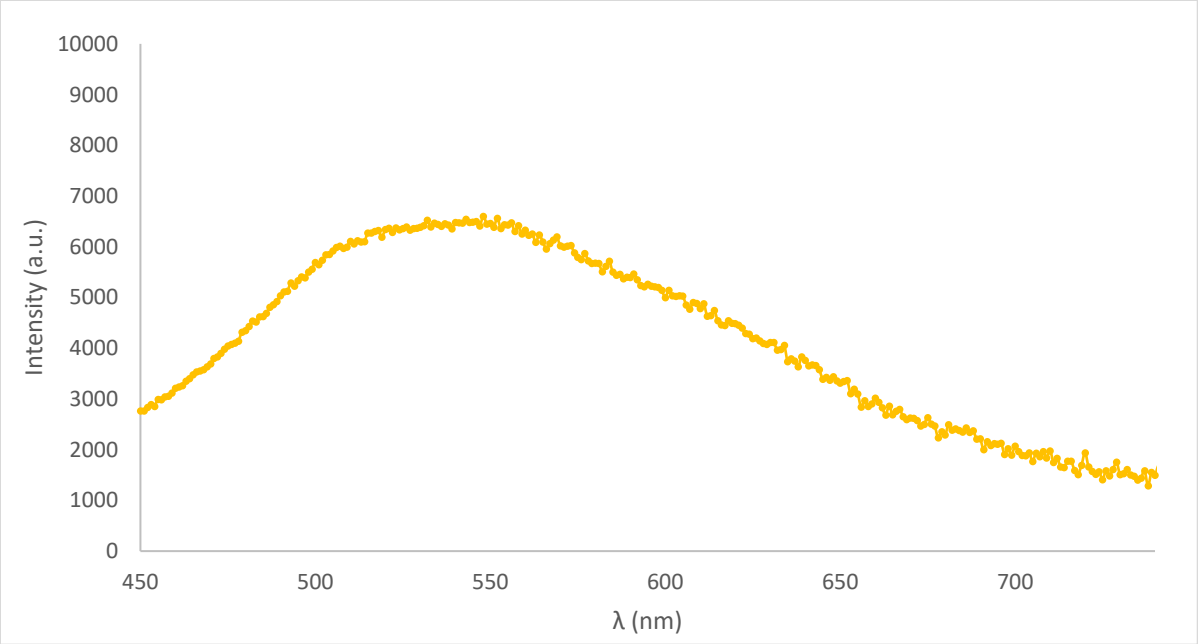

4.3 Procedure for reaction development (Figure 2)

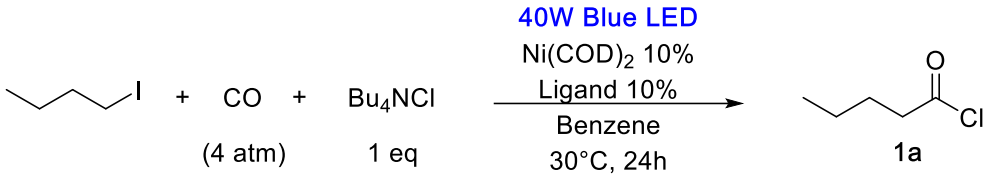

In a glovebox, *n*-butyl iodide (15 mg, 0.080 mmol), $Ni(COD)_2$ (2 mg, 0.0080 mmol), ligand (0.0080 mmol) and benzyl benzoate standard (8.5 mg, 0.040 mmol) were dissolved in 0.6 mL of C_6D_6. The mixture was transferred into a J-Young NMR tube. A suspension of Bu_4NCl (22 mg, 0.080 mmol) was prepared in 0.2 mL of C_6D_6 and transferred to the NMR tube. The J-Young was sealed, taken out of the glovebox and attached to a CO line. Before opening the vessel, the connecting line was evacuated and backfilled with carbon monoxide three times. The J-Young was frozen under liquid nitrogen and pressurized with 4 atm carbon monoxide. This was done by attaching the J-Young tube to the Schlenk line of a known internal gas volume (67 mL) and equipped with a pressure gauge. The NMR tube solution was frozen in liquid nitrogen, the headspace evacuated, the tube closed, and the Schlenk line was filled with 800 mTorr of CO. In order to condense 4 atm CO into the 2.2 mL headspace of the NMR tube, the tube was opened until a pressure drop of 120 mTorr was recorded on the Schlenk line (corresponding to 0.44 mmol of CO; which equals 4 atm CO in the J-Young NMR tube based on the idea gas law). The J-Young was closed and clamped on top of a stirring plate, and the solution was irradiated using a 40W Blue LED lamp. Fans were used to keep the temperature below 30 ºC (**see the picture of setup in Figure S6**). After 24 hours, the J-Young was taken out of the irradiation system and ^1H and ^{13}C NMR analysis was conducted to determine the yield of acyl chloride **1a** formed. The mixture was then frozen by liquid nitrogen, and the excess CO was removed by opening the cap to vacuum. The J-Young was brought into the glovebox. To confirm the yield of the acid chloride, benzylamine (13 mg, 0.12 mmol) and EtN^iPr_2 base (21 mg, 0.16 mmol) were added, and the yield of the amide calculated based on the internal standard.

Figure S5 – Blue light irradiation setup. System is enclosed on the sides by a foil lined box.

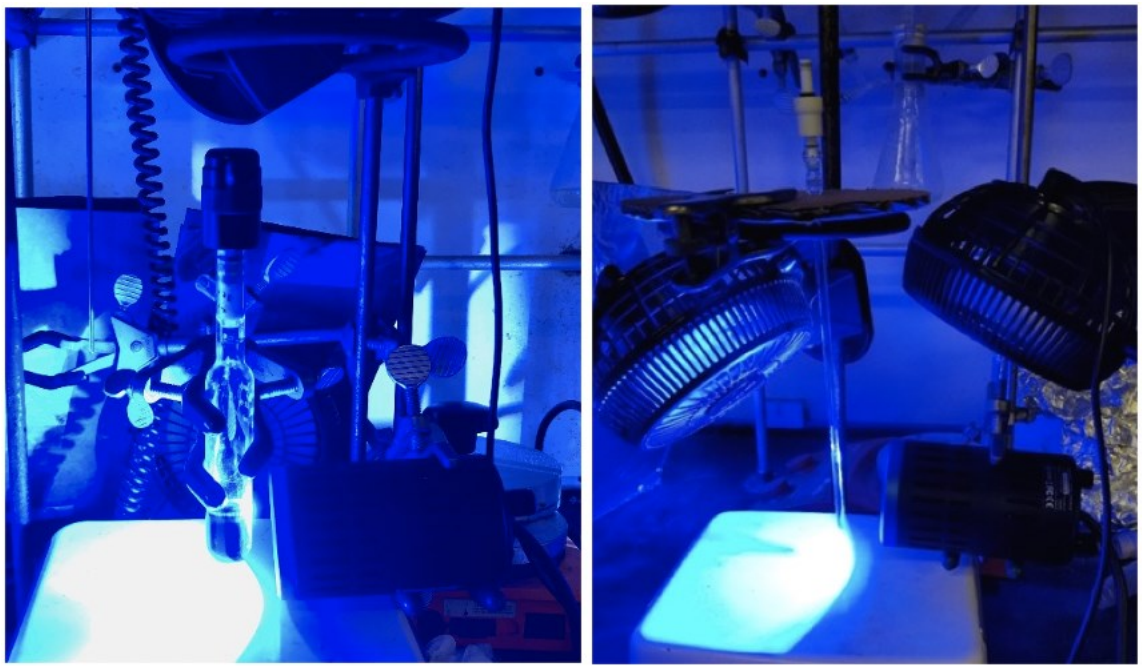

4.4 Synthesis and Characterization of XantphosNi(CO)2

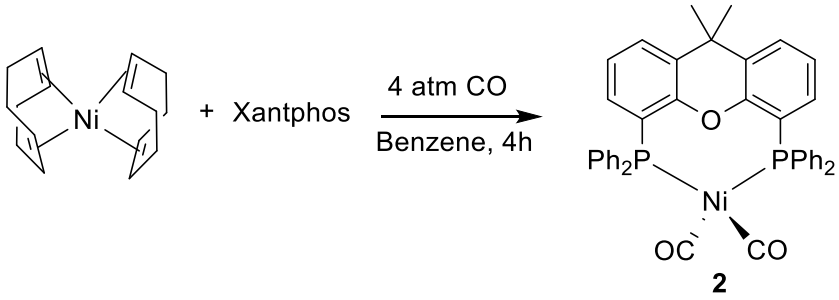

Under a nitrogen atmosphere, $Ni(COD)_2$ (55 mg, 0.20 mmol) and Xantphos (127 mg, 0.22 mmol) were dissolved in 3 mL of C_6H_6 and transferred to a thick-walled 50 mL glass reaction vessel equipped with a magnetic stir bar and a Teflon cap. The vessel was closed, taken out of the glovebox, and attached to a CO line. Before opening the vessel, the connecting tubing was evacuated and backfilled with carbon monoxide three times, and finally, the vessel was opened

and pressurized with 4 atm CO (on top of 1 atm of nitrogen). The vessel was closed and clamped on top of a stirring plate. A white suspension appears after 1 hour of stirring. The stirring was stopped after an additional 23 hours of stirring and attached to a Schlenk line. The mixture was frozen by liquid nitrogen, and the excess CO was removed by opening the cap to vacuum. The vessel was brought into the glovebox. The resulting suspension was poured into a 50 mL round bottom flask, and pentane (10 mL) was used to transfer the remaining solid out. Upon settling, the upper pentane solution was removed by pipette. 2 x 10 mL pentane were used to wash the solid. Pentane (5 mL) was added and the suspension was transferred to a 20 mL vial. Residual solvent was removed *in vacuo* for 10 minutes, affording **2** (111 mg, 0.16 mmol) as a white solid. ^{1}H NMR (400 MHz, C_6D_6) δ 7.69 – 7.60 (m, 8H), 7.09 – 7.01 (m, 3H), 7.00 – 6.87 (m, 11H), 6.79 – 6.70 (m, 4H), 1.37 (s, 6H). ^{13}C NMR (126 MHz, C_6D_6) δ 199.5, 199.4, 155.7, 155.7, 135.8, 135.8, 135.6, 135.5, 134.5, 133.5, 133.4, 129.8, 128.7, 128.2, 128.1, 128.0, 127.9, 127.7, 127.5, 126.4, 126.1, 125.4, 123.8, 123.8, 36.1. ^{31}P NMR (162 MHz, C_6D_6) δ 20.62.

4.5 Catalytic carbonylative generation of acid chlorides (Figures 3 and 4)

4.5.1 Typical generation of acid chloride for in situ characterization (Figure 3)

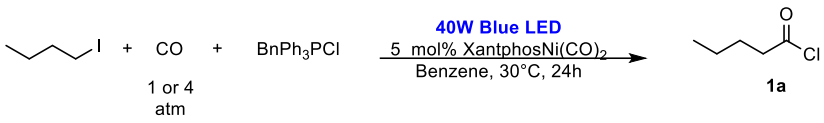

In a glovebox, *n*-butyl iodide (15 mg, 0.08 mmol), XantphosNi(CO)$_2$ (2.8 mg, 0.004 mmol) and benzyl benzoate standard (8 mg, 0.04 mmol) were dissolved in 0.8 mL of C_6D_6 and put in a 25 mL glass reaction vessel equipped with a magnetic stir bar and a Teflon cap, followed by dry transfer addition of benzyltriphenylphosphonium chloride (47 mg, 0.12 mmol). A 1 dram vial containing the benzyltriphenylphosphonium chloride was inverted over the opening of the vessel to ensure complete transfer of the solid. The vessel was closed, frozen in liquid nitrogen and attached to a CO filled Schlenk line. Before opening the vessel, the connecting tubing was evacuated and backfilled with carbon monoxide three times. Then the reaction vessel was opened to *vacuum* and evacuated. The Teflon cap was closed, the tube thawed, and the CO tubing was opened to 1 atm CO using a mineral-oil bubbler to establish atmospheric pressure. The Teflon cap was then opened for 30 seconds and then closed. The vessel was closed and clamped on top of a stirring plate, and the solution was irradiated using a 40W Blue LED lamp. Fans were used to keep the temperature

below 30°C **(see the picture of setup in Figure S6)**. After 24 hours, the vessel was taken out of the irradiation system and attached to a Schlenk line. The mixture was frozen by liquid nitrogen, and the excess CO was removed by opening the cap to vacuum. The vessel was brought into the glovebox. An aliquot was taken, and the acyl chloride product 1**a** was characterized in situ by ^{1}H and ^{13}C NMR analysis.

4.5.2 Typical synthesis of acid chlorides and isolation of benzylamide (Figure 3)

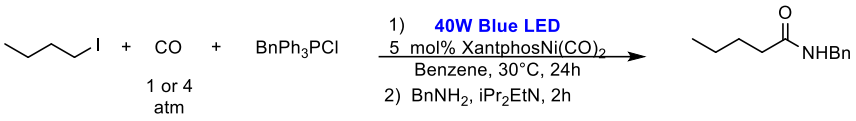

In a glovebox, *n*-butyl iodide (46 mg, 0.25 mmol), XantphosNi(CO)$_2$ (8.7 mg, 0.013 mmol) and benzyl benzoate standard (26 mg, 0.13 mmol) were dissolved in 3 mL of C_6H_6 and transferred into a thick-walled 50 mL glass reaction vessel equipped with a magnetic stir bar and a Teflon cap. Benzyltriphenylphosphonium chloride (146 mg, 0.38 mmol) was dry transferred into the vessel. A 1 dram vial containing the benzyltriphenylphosphonium chloride was inverted over the opening of the vessel to ensure complete transfer of the solid. The vessel was closed, taken out of the glovebox, and attached to a CO line. Before opening the vessel, the connecting tubing was evacuated and backfilled with carbon monoxide three times, and finally, the vessel was opened and pressurized with 4 atm CO (on top of 1 atm of nitrogen). The vessel was closed and clamped on top of a stirring plate, and the solution was irradiated using a 40W Blue LED lamp. Fans were used to keep the temperature below 30°C (**see the picture of setup in Figure S6**). After 24 hours, the vessel was taken out of the irradiation system and attached to a Schlenk line. The mixture was frozen by liquid nitrogen, and the excess CO was removed by opening the cap to vacuum. The vessel was brought into the glovebox. Benzylamine (40.7 mg, 0.38 mmol) and Et$N^{i}Pr_2$ base (64.6 mg, 0.50 mmol) were added. The mixture was allowed to stir at room temperature for 2 hours. The product was isolated by column chromatography on silica gel using 35% hexane/ethyl acetate solvent. Benzylamide **3a** was isolated in 99% yield (47 mg, 0.25 mmol).

[For reaction performed at 1 atm CO. The reaction vessel was frozen in liquid nitrogen and attached to a CO filled Schlenk line. Before opening the vessel, the connecting tubing was evacuated and backfilled with carbon monoxide three times. Then the reaction vessel was opened

to *vacuum* and evacuated. The Teflon cap was closed, the tube thawed, and the CO tubing was opened to 1 atm CO using a mineral-oil bubbler to establish atmospheric pressure. The Teflon cap was then opened for 30 seconds and then closed.]

4.5.3 Typical carbonylative coupling reaction (Figure 4)

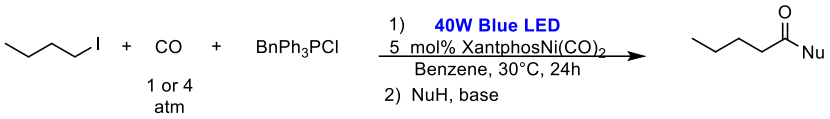

In a glovebox, *n*-butyl iodide (46 mg, 0.25 mmol), XantphosNi(CO)$_2$ (8.7 mg, 0.013 mmol) and benzyl benzoate standard (27 mg, 0.13 mmol) were dissolved in 4 mL of C_6H_6 and put in a 50 mL glass reaction vessel equipped with a magnetic stir bar and a Teflon cap, followed by dry transfer addition of benzyltriphenylphosphonium chloride (146 mg, 0.38 mmol). A 1 dram vial containing the benzyltriphenylphosphonium chloride was inverted over the opening of the vessel to ensure complete transfer of the solid. The vessel was closed, taken out of the glovebox, frozen in liquid nitrogen and attached to a CO filled Schlenk line. Before opening the vessel, the connecting tubing was evacuated and backfilled with carbon monoxide three times. Then the reaction vessel was opened to *vacuum* and evacuated. The Teflon cap was closed, and the CO tubing was opened to 1 atm CO using a mineral-oil bubbler to establish atmospheric pressure. The Teflon cap was then opened for 30 seconds and then closed. The vessel was closed and clamped on top of a stirring plate, and the solution was irradiated using a 40W Blue LED lamp. Fans were used to keep the temperature below 30°C (**see the picture of setup in Figure S6**). After 24 hours, the vessel was taken out of the irradiation system and attached to a Schlenk line. The mixture was frozen by liquid nitrogen, and the excess CO was removed by opening the cap to vacuum. The vessel was brought into the glovebox. Diosgenin (156 mg, 0.38 mmol) and EtN^iPr_2 base (64.6 mg, 0.50 mmol) were added. The mixture was allowed to stir at 50°C for 24 hours. The product was isolated by column chromatography on silica gel using hexane/ethyl acetate (10%) solvent. Ester **4f** was isolated in 74% yield (92 mg, 0.19 mmol).

A similar procedure was used for all other products, except **4a-d** used 5 mol% catalyst, 4 atm CO, and **4k, n, o** used 10 mol% catalyst, 1 atm CO.

4.6 Mechanistic studies (Figure 5)

4.6.1 Catalyst resting state (Figure 5A)

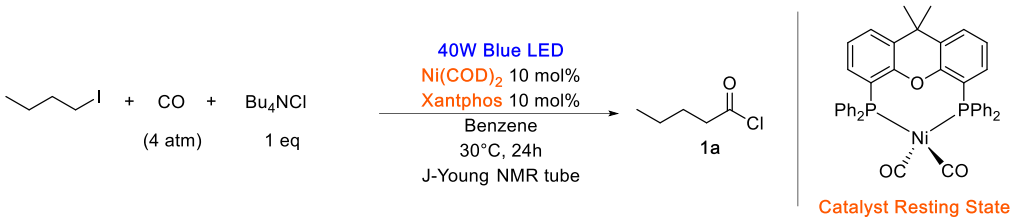

Figure S6 - ^{1}H NMR spectra of catalyst resting state

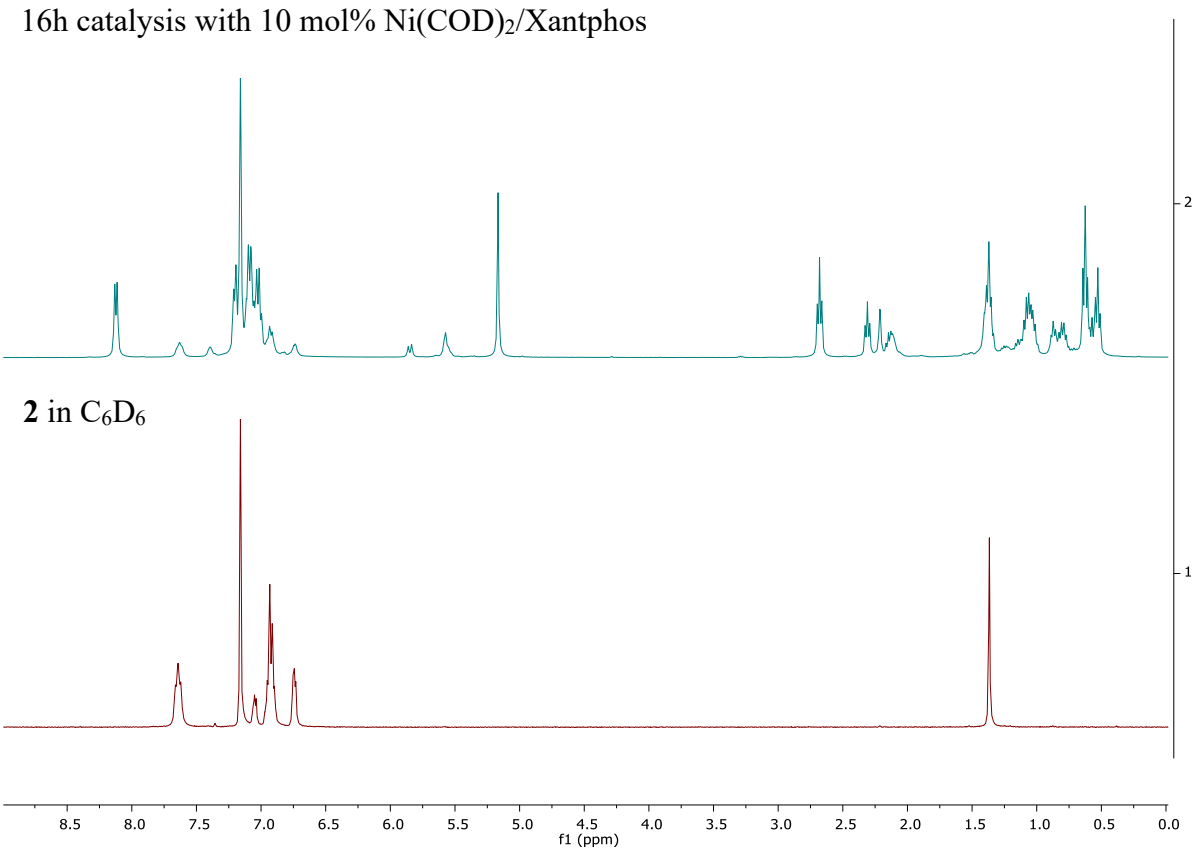

Figure S7 - ^{31}P NMR spectra of catalyst resting state

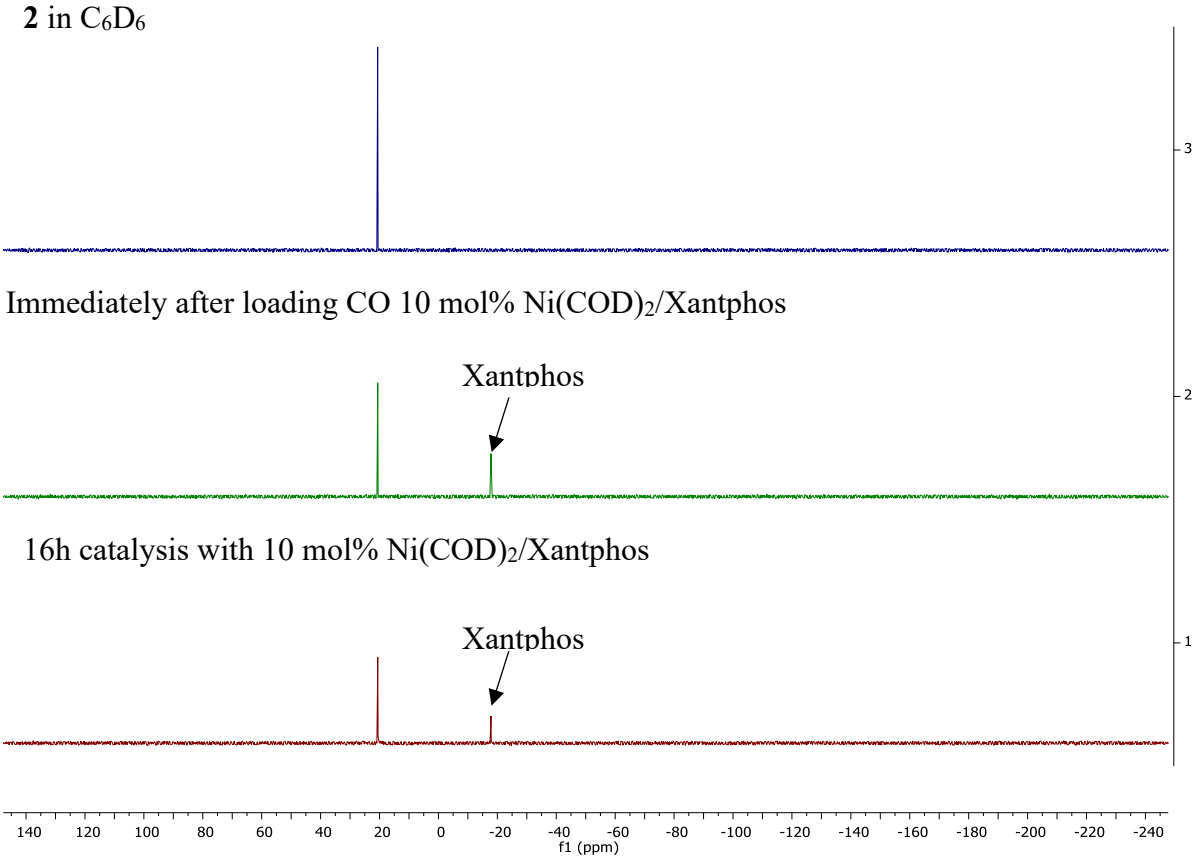

4.6.2 UV-Vis of XantphosNi(CO)$_2$

In the glovebox, XantphosNi(CO)$_2$ (1.6 mg, 0.0024 mmol) was dissolved in 25 mL of degassed and dry C_6H_6 to prepare a 9.5x10^{-5}M solution. 3 mL of the solution was transferred to a 1 cm pathlength quartz cuvette with a sealable screw cap. Once closed, the cuvette was taken out of the glovebox and submitted to a Jasco V-670 spectrophotometer for measurement of the UV-Vis spectrum.

Figure S8 – UV-Vis of XantphosNi(CO)$_2$in benzene [9.5x10^{-5}M]

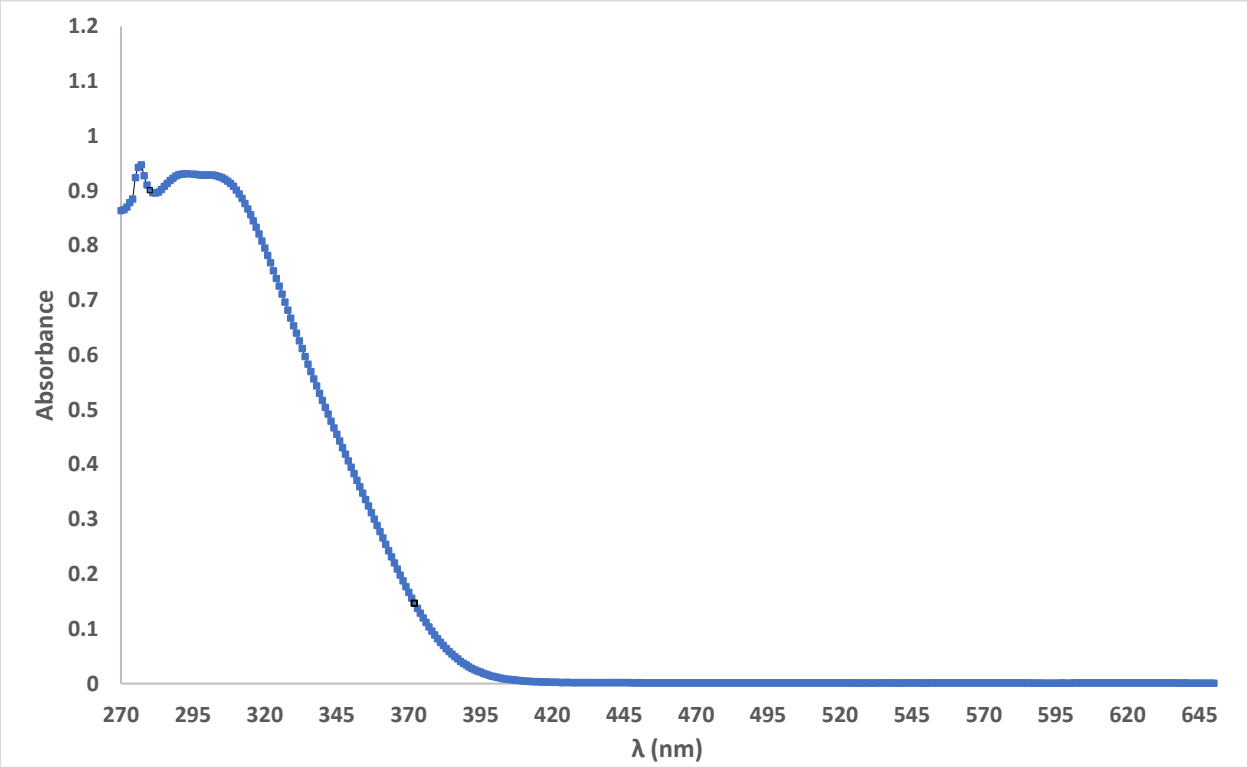

4.6.3 Fluorescence of XantphosNi(CO)$_2$ at 77K

In the glovebox, XantphosNi(CO)$_2$(80 mg, 0.12 mmol) was dissolved in 25 mL of degassed and dry C_6H_6 to prepare a 4.6x10^{-3}M solution. 0.5 mL of the solution was transferred to a clear fused-quartz EPR tube and fitted with a 4mm NMR tip-off manifold to achieve an air-tight seal. The EPR tube was placed in a dewar fitted into a Jasco V-670 spectrophotometer, frozen to 77K with liquid nitrogen and fluorescence measured from excitation at 365 nm (see Figure S5).

4.6.4 Fluorescence of XantphosNi(CO)$_2$ at ambient temperature

In the glovebox, XanphosNi(CO)$_2$ (80 mg, 0.12 mmol) was dissolved in 25 mL of degassed and dry C_6H_6 to prepare a 4.6x10^{-3}M solution. 0.5 mL of the solution was transferred to a clear fused-quartz EPR tube and fitted with a 4mm NMR tip-off manifold to achieve an air-tight seal. The EPR tube was placed into a Jasco V-670 spectrophotometer and fluorescence measured from excitation at 380 nm (see Figure S5).

4.6.5 TEMPO trapping radical experiments

4.6.5.1 TEMPO in the catalytic reaction (Figure 5B)

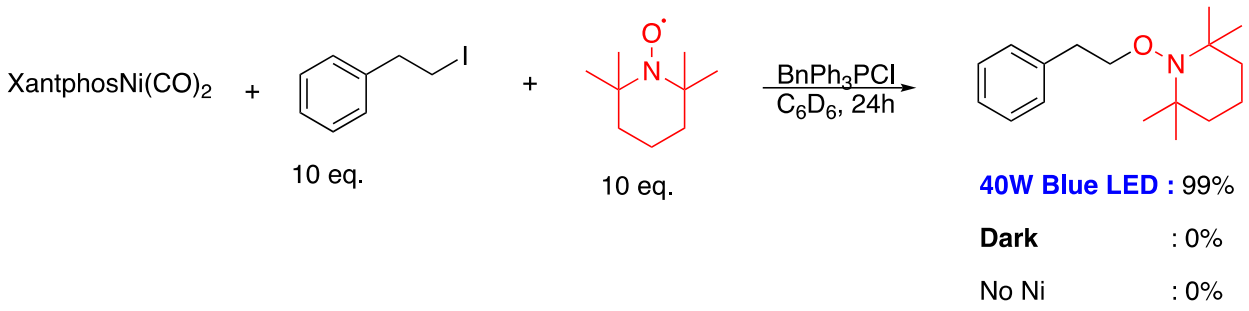

(2-iodoethyl)benzene (116 mg, 0.5 mmol), $XantphosNi(CO)_2$ (35 mg, 0.05 mmol), TEMPO (62 mg, 0.5 mmol), benzyl benzoate standard (53 mg, 0.25 mmol) were dissolved in 6 mL C_6H_6 and transferred to a 50 mL Teflon cap sealable thick walled glass reaction bomb. Benzyl triphenylphosphonium chloride (292 mg, 0.75 mmol) was dry transferred into the reaction. A 1 dram vial containing the benzyltriphenylphosphonium chloride was inverted over the opening of the vessel to ensure complete transfer of the solid. The vessel was closed, taken out of the glovebox**,** clamped on top of a stirring plate, and the solution was irradiated using a 40W Blue LED lamp. Fans were used to keep the temperature below 30°C (**see the picture of setup in Figure S6**). After 24 hours, the vessel was taken out of the irradiation system. The vessel was brought into the glovebox and an aliquot was taken and yield of the TEMPO ether (99% relative to $XantphosNi(CO)_2$) was determined by ^1H NMR analysis of the crude mixture relative to the internal standard. The TEMPO ether was separated from most of the other compounds by column chromatography (silica support using 10:1 ratio of hexane: ethyl acetate) and collected together with benzyl benzoate. *In situ* ^1H and ^{13}C NMR confirm its formation. A similar reaction without blue light irradiation led to no TEMPO ether, nor did the reaction without the nickel complex.

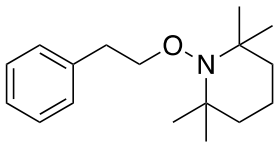

2,2,6,6-Tetramethyl-1-phenethoxypiperidine. 64% yield (6.7 mg, 0.03 mmol). Colorless oil. Spectral data correlated with that previously reported in the literature.[1] ^1H NMR (500 MHz, $CDCl_3$) δ 7.31 – 7.26 (m, 2H), 7.25 – 7.21 (m, 2H), 7.21 – 7.16 (m, 1H), 3.95 (t, J = 7.0 Hz, 2H), 2.83 (t, J = 7.0 9 Hz, 2H), 1.48 - 1.59 (m, 1H), 1.48 – 1.38 (m, 4H), 1.35 – 1.24 (m, 1H), 1.07 (s, 12H). ^{13}C NMR (126 MHz, $CDCl_3$) δ 139.6, 129.1, 128.1, 125.9, 59.7, 39.6, 35.4, 33.0, 20.1, 17.2. HRMS of partially separated mixture: calculated for $C_{17}H_{28}NO^+$ ($M+H^+$): 262.2165, found: 262.2165.

Figure S10 – ^{1}H NMR of catalytic reaction after 24h

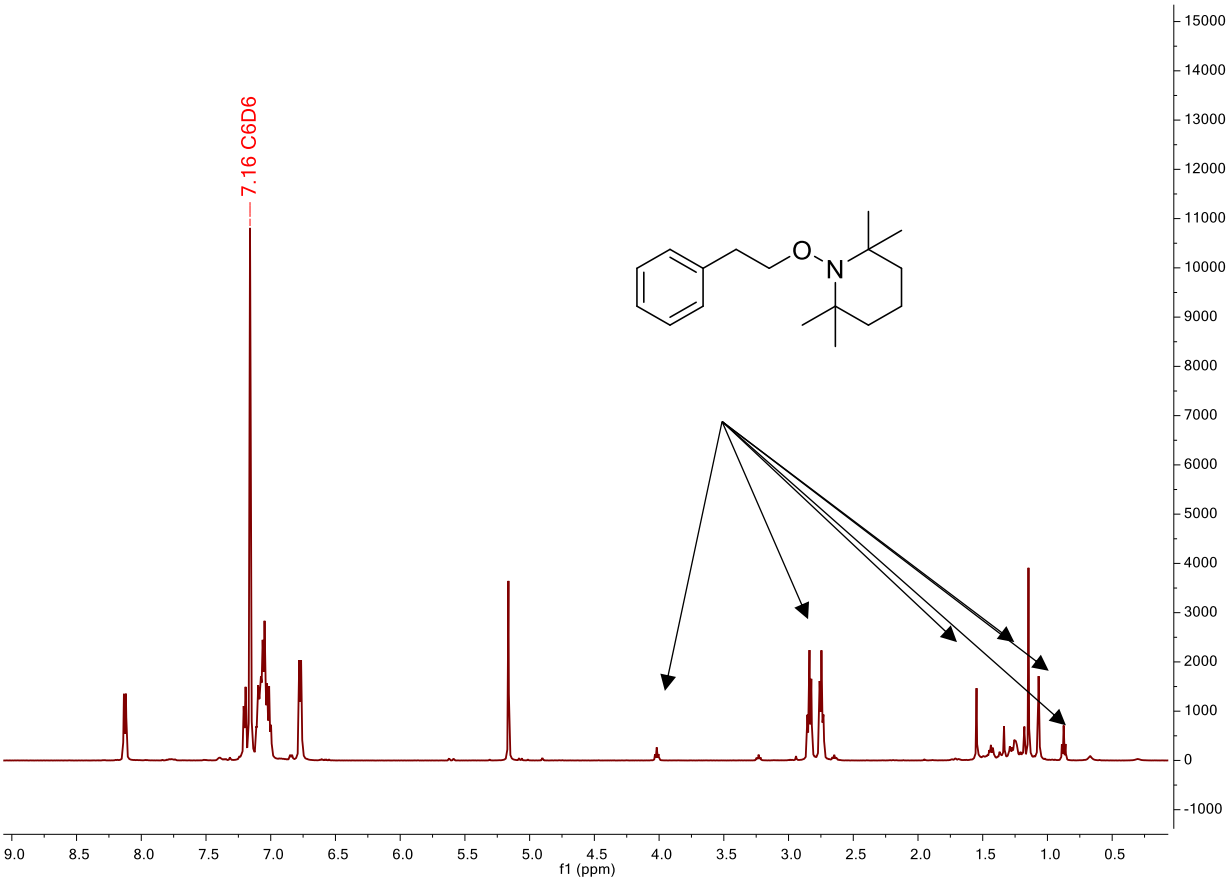

Figure S11 - ^{13}C NMR of catalytic reaction after 24h

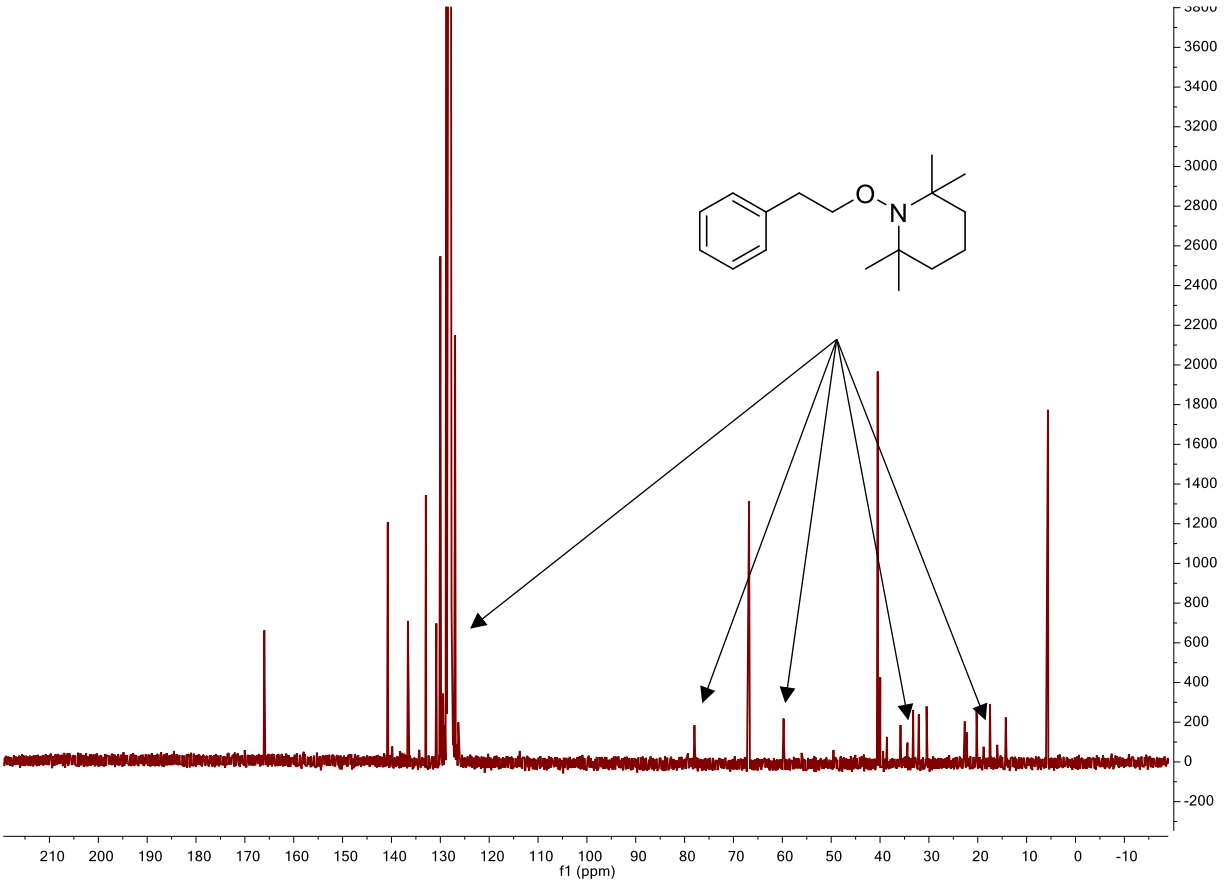

Figure S12 - ^{1}H and ^{13}C NMR of 2,2,6,6-Tetramethyl-1-phenethoxypiperidine with BnOBz

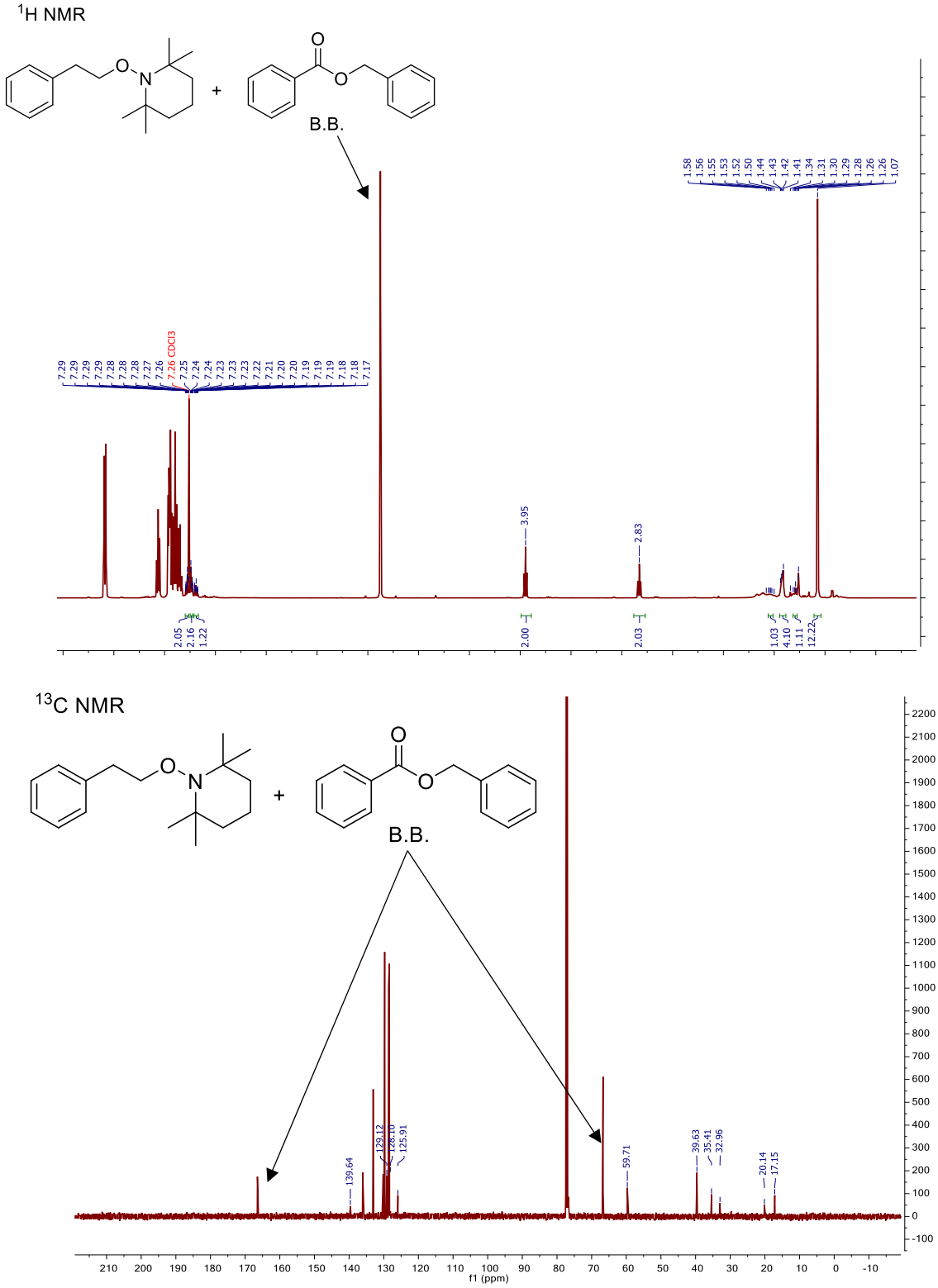

4.6.5.2 TEMPO trapping of pentanoyl chloride and XantphosNi(CO)$_2$ (Figure 5C)

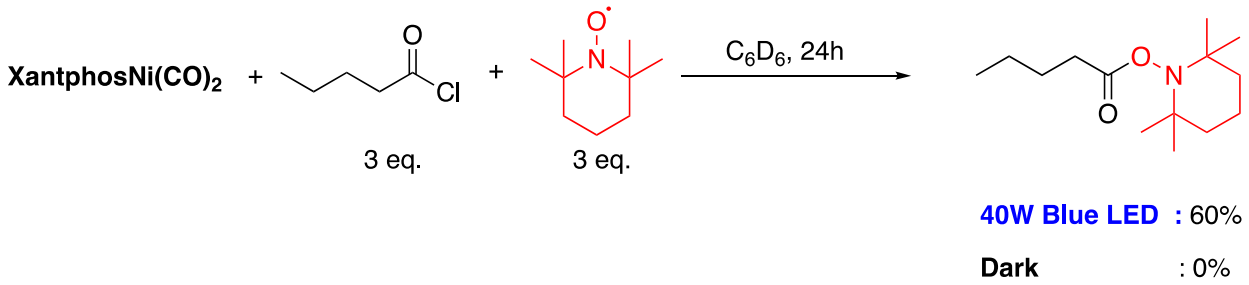

Pentanoyl chloride (3.6 mg, 0.03 mmol), XantphosNi(CO)$_2$ (6.9 mg, 0.010 mmol), TEMPO (4.7 mg, 0.030 mmol), benzyl benzoate standard (3.2 mg, 0.015 mmol) and 6 mL C_6H_6 and transferred to a 50 mL Teflon cap sealable thick walled glass reaction bomb. The vessel was closed, taken out of the glovebox**,** clamped on top of a stirring plate, and the solution was irradiated using a 40W Blue LED lamp. Fans were used to keep the temperature below 30°C **(see the picture of setup in Figure S6**). After 24 hours, the vessel was taken out of the irradiation system. The vessel was brought into the glovebox and an aliquot was taken and yield of the TEMPO adduct (60% relative to XantphosNi(CO)$_2$) was determined by ^{1}H NMR analysis of the crude mixture relative to the internal standard. A similar reaction without blue light irradiation led to no TEMPO ether, nor did the reaction without the nickel complex. An authentic sample of the TEMPO adduct was prepared and characterized as described below.

Figure S13 - ^{1}H NMR of catalytic reaction at 24h

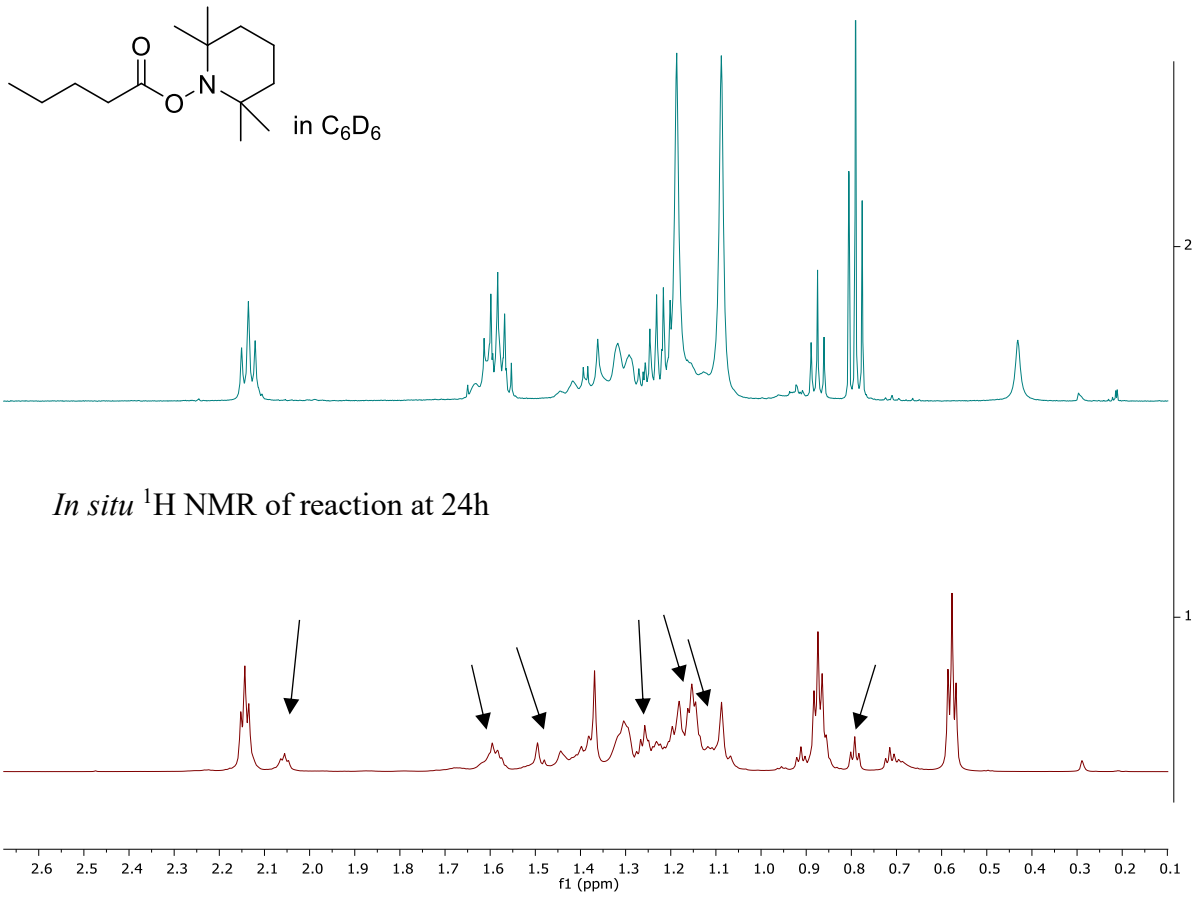

Figure S14 - ^{1}H NMR spectrum of 2,2,6,6-tetramethylpiperidin-1-yl pentanoate in $CDCl_3$

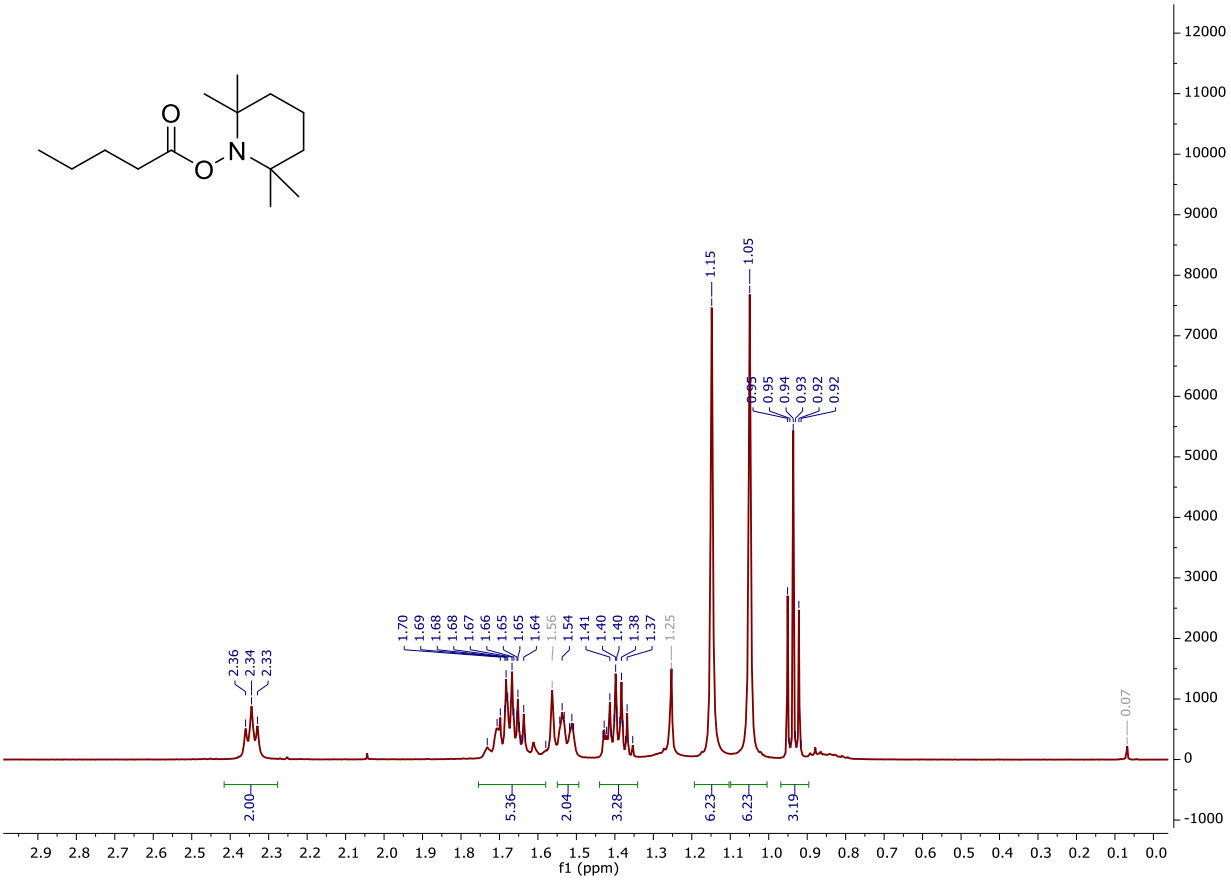

Figure S15 – HMBC of *in situ* catalytic reaction at 24h

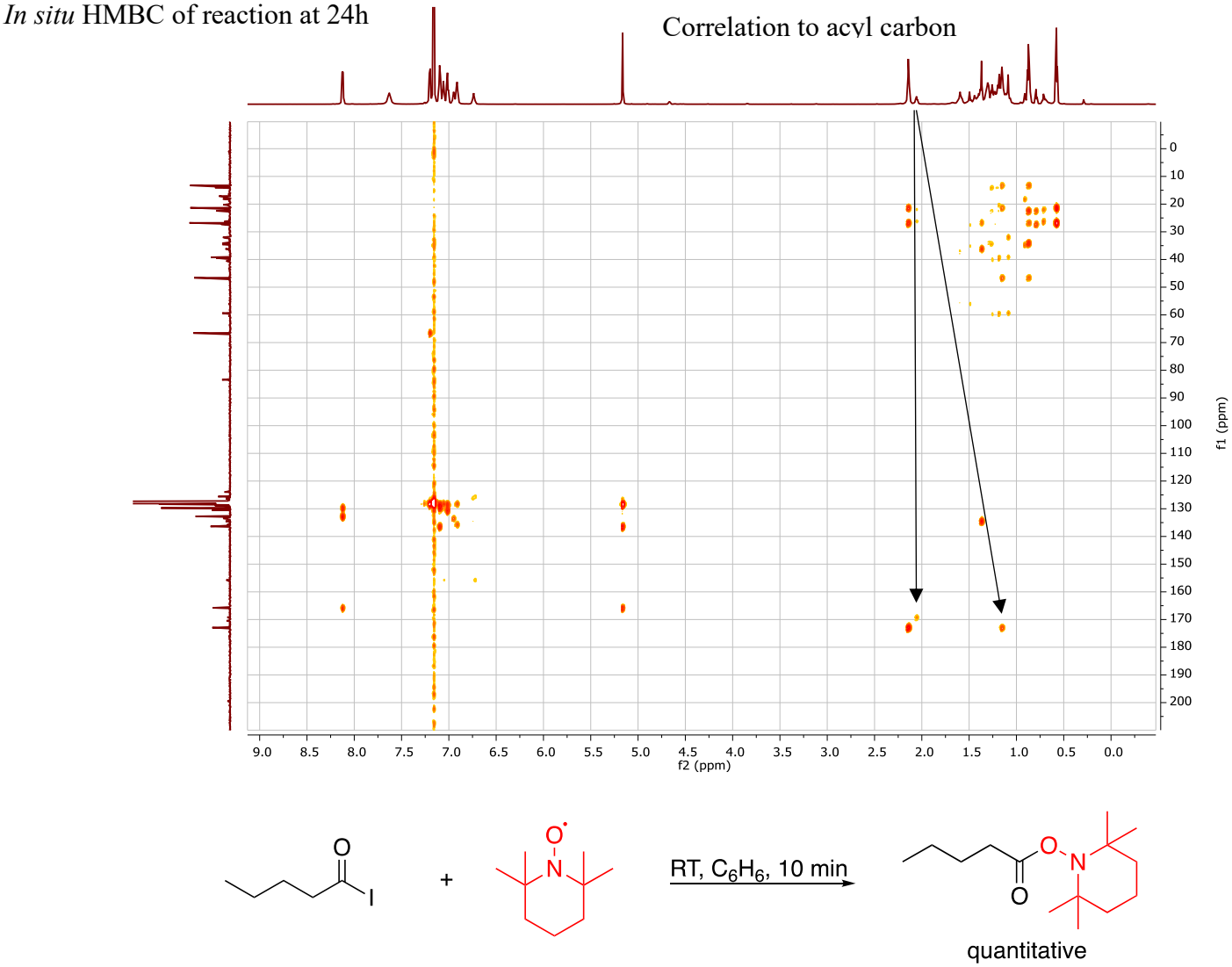

In order to isolate the TEMPO adduct, pentanoyl iodide (42.4 mg, 0.2 mmol) and TEMPO (31.3 mg, 0.2 mmol) were mixed in 3 mL C_6H_6 at room temperature in the glovebox. After 10 minutes, the reaction was taken out of the glovebox, diluted to 10 mL 0.5M Na_2SO_3 (aq) and extracted with 20 mL ethyl acetate. The organic layer was washed further with brine (20 mL), followed by deionized water (20 mL). The organic layer was dried on $MgSO_4$, filtered, and the solvent was removed *in-vacuo* to afford the pure product as a red oil in 56% yield (27 mg, 0.11 mmol).

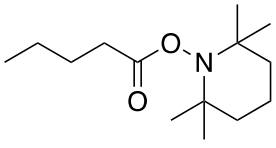

2,2,6,6-tetramethylpiperidin-1-yl pentanoate. Red oil. ^{1}H NMR (500 MHz, $CDCl_3$) δ 2.34 (t, J = 7.7 Hz, 2H), 1.75 – 1.61 (m, 5H), 1.52 (dt, J = 12.0, 2.6 Hz, 2H), 1.45 – 1.34 (m, 3H), 1.15 (s, 6H), 1.05 (s, 6H), 0.94 (t,

J = 7.4 Hz, 3H). ^{13}C NMR (201 MHz, $CDCl_3$) δ 173.3, 77.2, 77.2, 77.0, 76.9, 59.9, 39.0, 32.0, 27.4, 22.5, 20.5, 17.0, 13.7. HRMS: calculated for $C_{14}H_{28}NO_2$+ (M+H+): 242.21200, found: 242.21094.

4.6.6 Irradiation of XantphosNi(CO)$_2$ in the presence of excess *n*-butyl iodide

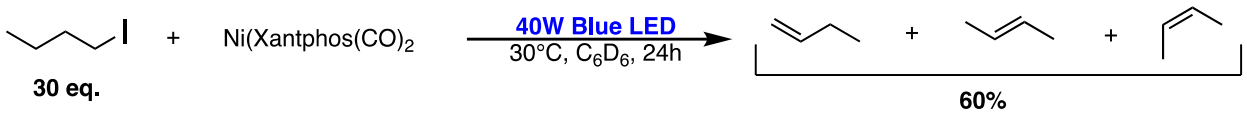

In a glovebox, *n*-butyl iodide (55 mg, 0.30 mmol) and XantphosNi(CO)$_2$ (6.9 mg, 0.010 mmol) were transferred to a J-Young NMR tube with 0.8 mL of C_6D_6. Benzyl benzoate (32 mg 0.15 mmol) was used as an internal standard. The tube was closed, taken out of the glovebox. The reaction mixture was irradiated with a 40W Blue LED lamp and monitored over time via ^{1}H NMR. 24h irradiation leads to 60% conversion of *n*-butyl iodide and isomers of butene (1-butene, *Z*-butene and *E*-butene) in 60% total yield.

Figure S169 – Reaction mixture at 24h irradiation

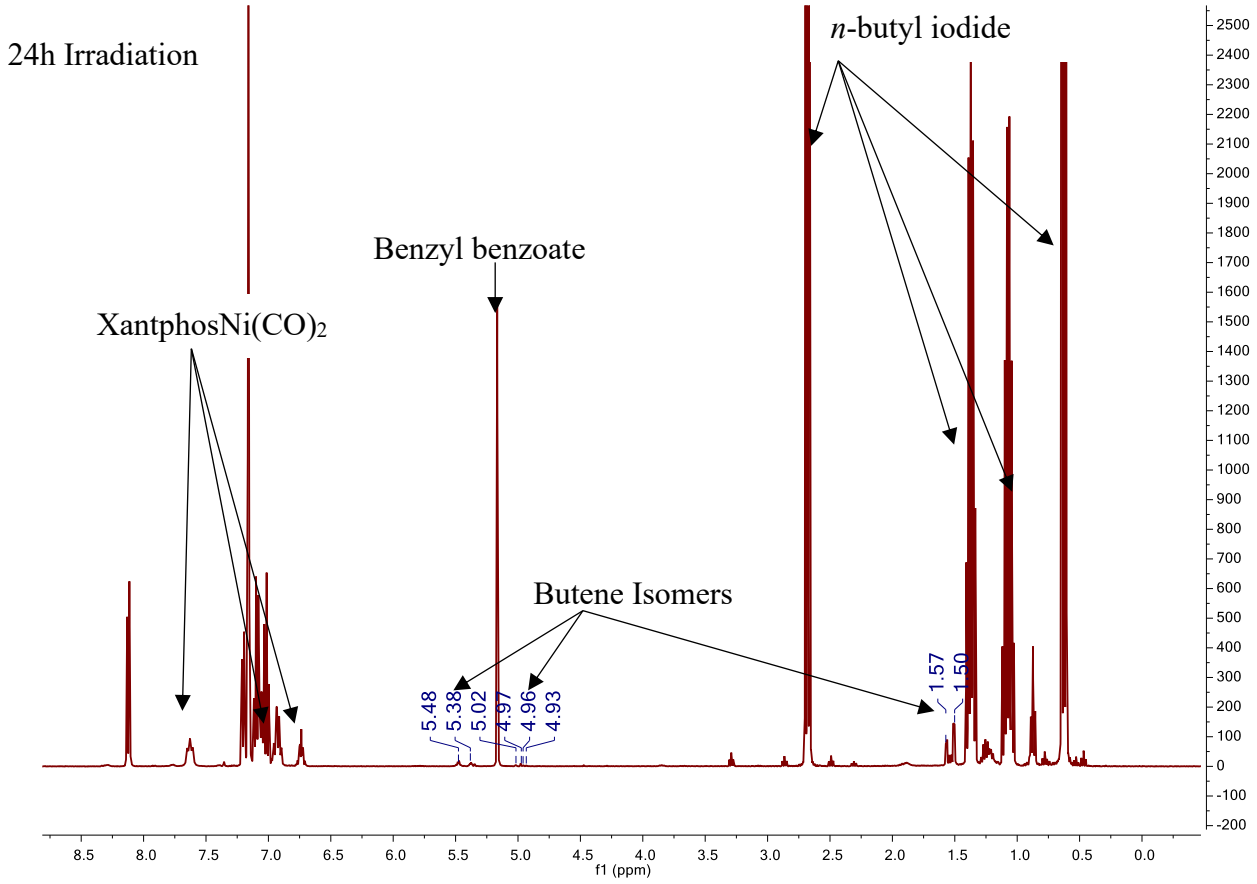

4.6.7 Catalytic formation of acyl iodide (Figure 5E)

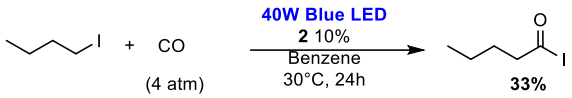

In a glovebox, *n*-butyl iodide (14.7 mg, 0.08 mmol), $Ni(COD)_2$ (2.2 mg, 0.0080 mmol) and benzyl benzoate standard (8.5 mg, 0.040 mmol) were dissolved in 0.8 mL of C_6D_6. The mixture was transferred into a J-Young NMR tube. The J-Young was sealed, taken out of the glovebox and attached to a CO line. Before opening the vessel, the connecting line was evacuated and backfilled with carbon monoxide three times, the J-Young was frozen under liquid nitrogen, evacuated then opened and pressurized with 4 atm CO. This was done by attaching the J-Young tube to the Schlenk line of a known internal gas volume (67 mL) and equipped with a pressure gauge. The NMR tube solution was frozen in liquid nitrogen, the headspace evacuated, the tube closed, and the Schlenk line was filled with 800 mTorr of CO. In order to condense 4 atm CO into the 2.2 mL headspace of the NMR tube, the tube was opened until a pressure drop of 120 mTorr was recorded

on the Schlenk line (corresponding to 0.44 mmol of CO; which equals 4 atm CO in the J-Young NMR tube based on the idea gas law). The J-Young was closed and clamped on top of a stirring plate, and the solution was irradiated using a 40W Blue LED lamp. Fans were used to keep the temperature below 30 ºC (**see the picture of setup in Figure S6**). After 24 hours, the J-Young was taken out of the irradiation system and ^{1}H and ^{13}C NMR analysis shows the formation of pentanoyl iodide. The mixture was then frozen in liquid nitrogen, and the excess CO was removed by opening the cap to vacuum. The J-Young was brought into the glovebox. To confirm the yield of the acyl iodide, benzylamine (12.9 mg, 0.12 mmol) and $EtN^{i}Pr_2$ base (20.7 mg, 0.16 mmol) were added, and the yield of the amide was determined by ^{1}H NMR analysis of the crude mixture relative to the internal standard (33%).

Synthesis of pentanoyl iodide

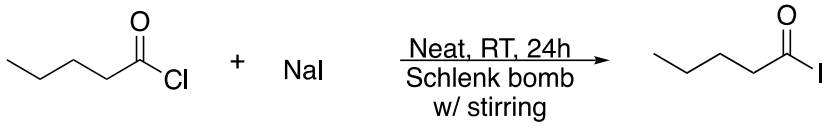

An authentic sample of pentanoyl iodide was synthesized in the following manner.[4] In a glovebox, pentanoyl chloride (1.0g, 9.7 mmol) was added to a 25 mL Schlenk bomb containing NaI (2.2g, 15 mmol) and charged with a magnetic stir bar. The mixture let to stir over night covered in aluminum foil to protect from light. (1.3 g, 6.1 mmol) of pentanoyl iodide (63% yield) was obtained from the reaction by vacuum distillation (60°C, static vacuum, 60 mTorr) as a red liquid.

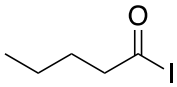

Pentanoyl iodide. ^{1}H NMR (400 MHz, C_6D_6) δ 2.30 (t, J = 7.3 Hz, 2H), 1.08 – 0.97 (m, 2H), 0.79 (dq, J = 14.4, 7.3 Hz, 2H), 0.52 (t, J = 7.3 Hz, 3H). ^{13}C NMR (126 MHz, C_6D_6) δ 162.1, 59.5, 27.1, 20.7, 13.0.

Figure S17 - ^{1}H & ^{13}C NMR of the catalytic formation of pentanoyl iodide after 24h.

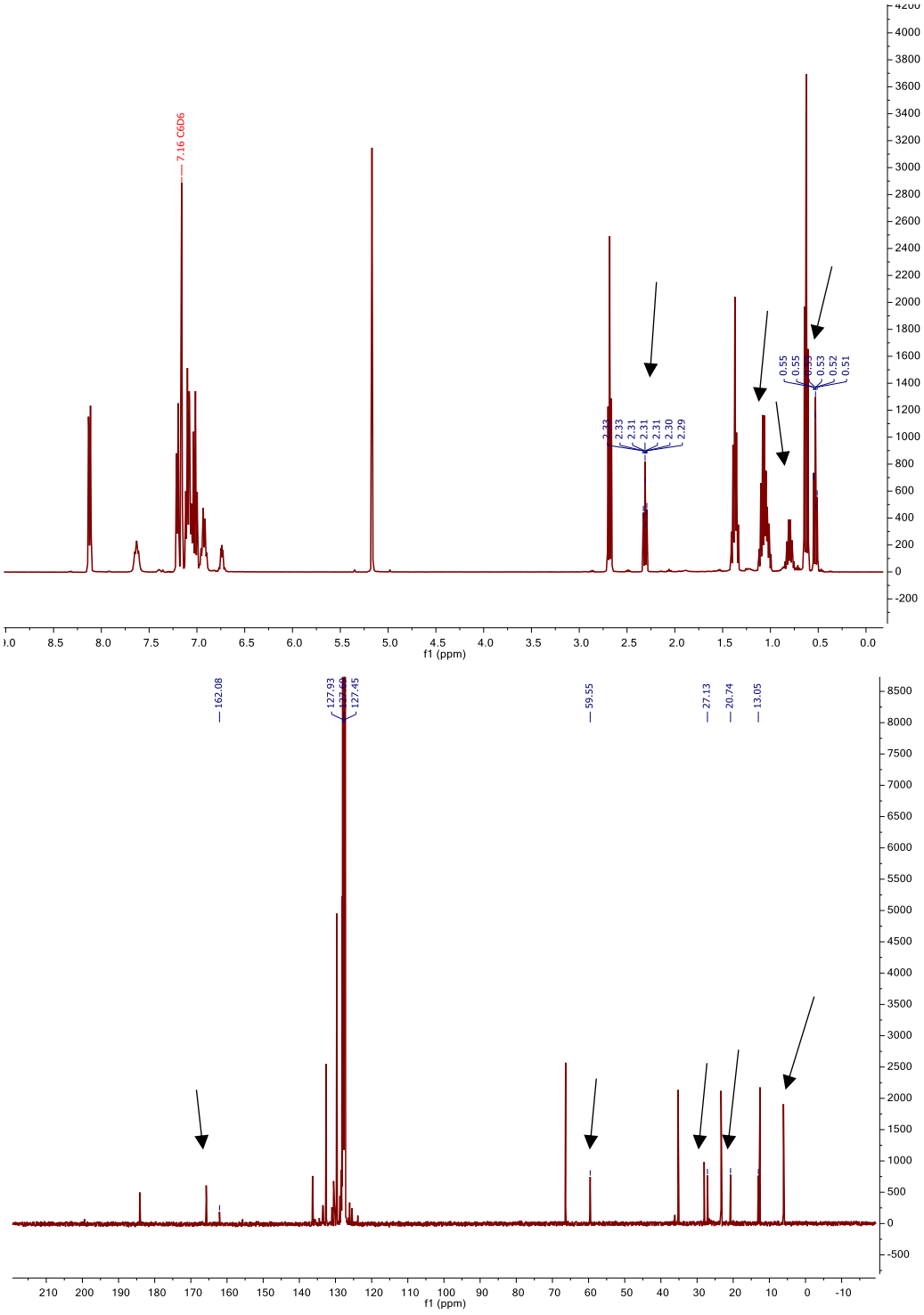

4.7 Synthesis of alkyl iodides

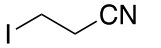 **3-iodopropanenitrile.** To an N_2-purged flask containing 3 eq. NaI was added 3-bromopropanenitrile (2.5 g, 18.7 mmol) along with acetone (20 mL) and stirred under reflux for 48h. The acetone is removed *in vacuo*, the crude diluted with 20 mL water and extracted with 30 mL ethyl acetate. The organics are washed with 1M $Na_2S_2O_3$ and a saturated $NaHCO_3$ solution then dried with $MgSO_4$ and filtered. The solvent was removed *in vacuo* and the crude mixture distilled under reduced pressure (60 mTorr, 85°C) to yield the product as a yellow oil (500 mg, 2.8 mmol, 15% yield). ^{1}H NMR (400 MHz, $CDCl_3$) δ 3.18 (s, 2H), 2.91 (s, 2H). ^{13}C NMR (126 MHz, C_6D_6) δ.8, 21.5, -6.1. HRMS (ESI) calculated for C3H5NI *m/z* 181.9467 ($[M+H+]^+$), found: *m/z* 181.9461 ($[M+H+]^+$).

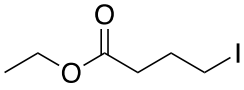 **4-ethyl-4-bromobutanoate**. This procedure was adapted from the literature.[5] To an N_2-purged flask containing 3 eq. NaI was added ethyl 4-bromobutanoate (2.0 g, 6.4 mmol) along with acetone (20 mL) and stirred under reflux for 48h. After 48h, the acetone was removed *in vacuo*, the crude diluted with 20 mL water and extracted with 30 mL ethyl acetate. The organics are washed with 1M $Na_2S_2O_3$ and a saturated $NaHCO_3$ solution then dried with $MgSO_4$ and filtered. The solvent was removed *in vacuo* and the crude distilled under reduced pressure (60 mTorr, 95°C to yield the as a yellow oil (1g, 4.1 mmol, 65% yield). ^{1}H NMR (500 MHz, C_6D_6) δ 3.87 (q, J = 7.1 Hz, 2H), 2.69 (t, J = 6.8 Hz, 2H), 2.02 (t, J = 7.2 Hz, 2H), 1.71 (p, J = 7.0 Hz, 2H), 0.91 (t, J = 7.1 Hz, 3H). ^{13}C NMR (126 MHz, C_6D_6) δ 171.2, 59.9, 34.3, 28.4, 13.8, 5.0.

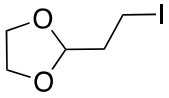 **2-(2-iodoethyl)-1,3-dioxolane**. This procedure was adapted from the literature.[6] To an N_2-purged flask containing 3 eq. NaI was added 2-(2-bromoethyl)-1,3-dioxolane (1.0 g, 5.5 mmol) along with acetone (20mL) and stirred under reflux for 48h. After 48h, the acetone was removed *in vacuo*, the crude diluted with 20 mL water and extracted with 30 mL ethyl acetate. The organics are washed with 1M $Na_2S_2O_3$ and a saturated $NaHCO_3$ solution then dried with $MgSO_4$ and filtered. The solvent was removed *in vacuo* and the crude purified by column chromatography (silica gel, hexanes: ethyl acetate, 10) to yield a colorless oil (1.0 g, 4.4 mmol, 80% yield). ^{1}H NMR (500 MHz, C_6D_6) δ 4.72 (t, J = 4.6 Hz, 1H), 3.40 – 3.30 (m, 2H), 3.28 – 3.18 (m, 2H), 2.90 (t, J = 7.4 Hz, 2H), 1.99 (td, J = 7.3, 4.6 Hz, 2H). ^{13}C NMR (126 MHz, C_6D_6) δ 172.9, 46.3, 26.6, 21.2, 13.1.

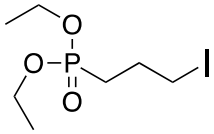

Diethyl (3-iodopropyl)phosphonate. This procedure was adapted from the literature.[7] To a flask containing neat boiling (167℃) 1,3-dibromopropane (3.0 g, 15 mmol) ℃ was added triethylphosphite (0.83 g, 5 mmol) over the course of 30 minutes. This crude mixture was allowed to cool to room temperature and used directly in the next step (procedure for 2k). To an N_2-purged flask containing 3 eq. NaI was added the reaction mixture along with acetone (20mL) and stirred under reflux for 48h. After 48h, the acetone was removed *in vacuo*, the crude diluted with 20 mL water and extracted with 30 mL ethyl acetate. The organics were washed with 1M $Na_2S_2O_3$ and a saturated $NaHCO_3$ solution then dried with $MgSO_4$ and filtered. The solvent was removed *in vacuo* and the crude distilled under reduced pressure (60mTorr, 130℃) to yield an orange oil.^{1}H NMR (500 MHz, C_6D_6) δ 3.97 – 3.74 (m, 1H), 2.71 (td, J = 6.9, 0.9 Hz, 0H), 1.92 – 1.76 (m, 0H), 1.59 – 1.45 (m, 0H), 1.01 (t, J = 7.1 Hz, 1H). ^{13}C NMR (126 MHz, C_6D_6) δ 60.9, 60.9, 27.5, 27.0, 26.9, 26.3, 16.2, 16.2, 6.4, 6.2. ^{31}P NMR (203 MHz, C_6D_6) δ 29.22.

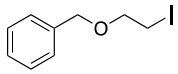

((2-iodoethoxy)methyl)benzene. This procedure was adapted from the literature.[8] A flask containing 2-(Benzyloxy)ethanol (1.5 g, 9.86 mmol), triethylamine (1.3 g, 12.8 mmol) were dissolved in dichloromethane (15 mL) and the flask was cooled to 0℃. Methanesulfonyl chloride (0.56 mL, 7.23 mmols) was added dropwise whilst still at 0 ºC. The resulting solution was stirred at room temperature for 1 h. The reaction mixture was poured into 20 mL water and ice, basified with a saturated NaHCO3 aqueous solution, and extracted with 30 mL dichloromethane. The organic extracts were washed with 20 mL brine, dried over $MgSO_4$, filtered and concentrated to give the crude 2-(benzyloxy)ethyl methanesulfonate as a yellow oil, which was used in the next step without purification. To an N_2-purged flask containing 3 eq. NaI was added the reaction mixture along with acetone (20mL) and stirred under reflux for 48h. After 48h, the acetone was removed *in vacuo*, the crude diluted with 20 mL water and extracted with 30 mL ethyl acetate. The organics are washed with 1M $Na_2S_2O_3$ and a saturated $NaHCO_3$ solution then dried with $MgSO_4$ and filtered. The solvent was removed *in vacuo* and the crude purified via column chromatography (silica gel, hexanes: ethyl acetate, 9:1) to yield an orange oil (1.0g, 3.8 mmol, 39% yield). ^{1}H NMR (500 MHz, C_6D_6) δ 7.20 (d, J = 7.3 Hz, 1H), 7.16 – 7.12 (m, 2H), 7.11 – 7.06 (m, 2H), 4.15 (s, 2H), 3.26 (t, J = 6.6 Hz, 2H), 2.79 (t, J = 6.6 Hz, 2H). ^{13}C NMR (126 MHz, C_6D_6) δ 138.3, 129.7, 128.2, 127.4, 72.3, 70.5, 2.7.

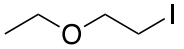 **1-iodo-2-methoxyethane**. This procedure was adapted from the literature.[9] A flask under positive N_2-pressure containing a 5M aqueous solution of NaOH (0.75 g, 18.8 mmol in 3.75 mL H_2O) was cooled to 0°C. Maintaining this temperature, 2-methoxyethanol (0.95 g, 12.5 mmol) was added, by syringe followed by 4-methyl-benzenesulfonyl chloride (2.62 g, 13.8 mmol) and 4 mL of THF. The reaction was stirred for 3h on ice. The resultant mixture was diluted with 200 mL ice water and extracted with 30 mL dichloromethane. The organic phase was washed with 1M hydrochloric acid and brine followed by drying over $MgSO_4$. The solvent was removed *in vacuo* and subjected to the next step without further purification. To an N_2-purged flask containing 3 eq. NaI was added the reaction mixture along with acetone (20mL) and stirred under reflux for 48h. After 48h, the acetone was removed *in vacuo*, the crude diluted with 20 mL water and extracted with 30 mL ethyl acetate. The organics are washed with 1M $Na_2S_2O_3$ and a saturated $NaHCO_3$ solution then dried with $MgSO_4$ and filtered. The solvent was removed *in vacuo* and the product obtained by distillation under reduced pressure (85°C at 60 mTorr) to yield an orange oil (0.8 mg, 4.0 mmol, 32% yield). ^{1}H NMR (500 MHz, C_6D_6) δ 3.12 (t, J = 6.6 Hz, 2H), 2.90 (s, 3H), 2.74 (t, J = 6.6 Hz, 2H). ^{13}C NMR (126 MHz, C_6D_6) δ 72.7, 57.5, 22.4.

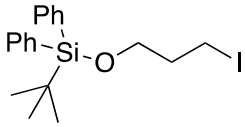

tert-Butyl(3-iodopropoxy)diphenylsilane. This procedure was adapted from the literature.[10] A flask was charged with a solution of *tert*-butyl(chloro)diphenylsilane (1.10 g, 4 mmol) in 10 mL DMF. propan-1,3-diol (3.05 g, 40 mmol) was added dropwise followed by imidazole (0.330 g, 4.8 mmol) and allowed to stir at room temperature for 24 h. The crude was diluted with a 20 mL of a 1:1 mixture of brine: H_2O and extracted with 30 mL ethyl acetate. The organic layer was washed again with H_2O, and then dried over $MgSO_4$. After removing the solvent *in vacuo*, the next step was performed with further purification. An iodine (1.53 g, 6 mmol) solution in dichloromethane (15 mL) was charged to a flask and allowed to cool to 0°C over an ice bath. Whilst maintaining the temperature, triphenylphosphine (1.57 g, 6 mmol) was added and stirred for 20 minutes. The ice bath was removed, and the solution was allowed to cool to room temperature. Then, imidazole (0.82 g, 12 mmol) was added and stirred for an additional 10 minutes. Then, the crude from the previous step was added in with an additional 10 mL dichlormethane. The mixture was stirred at room temperature for 2h. Once complete, the crude was diluted with 0.5M Na_2SO_3, extracted with 30 mL dicholormethane. The organics were dried over $MgSO_4$, the solvent removed *in vacuo* and the compound purified by column chromatography (silica gel, hexanes: ethyl acetate, 50:1) to yield a

colorless oil (1.2g, 2.8 mmol, 71% yield). ^{1}H NMR (500 MHz, $CDCl_3$) δ 7.73 – 7.66 (m, 1H), 7.48 – 7.38 (m, 1H), 3.74 (t, *J* = 5.7 Hz, 0H), 3.37 (t, *J* = 6.8 Hz, 0H), 2.10 – 2.01 (m, 0H), 1.08 (s, 2H). ^{13}C NMR (126 MHz, None) δ 135.9, 133.8, 130.0, 128.0, 63.3, 36.2, 27.0, 19.3, 3.0.

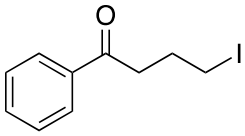

4-iodo-1-phenylbutan-1-one. This procedure was adapted from the literature.[11] To an N_2-purged flask containing 3 eq. NaI was added 4-bromo-1-phenylbutan-1-one (1.5 g, 6.6 mmol) along with acetone (20mL) and stirred under reflux for 48h. After 48h, the acetone was removed *in vacuo*, the crude diluted with 20 mL water and extracted with 30 mL ethyl acetate. The organics are washed with 1M $Na_2S_2O_3$ and a saturated $NaHCO_3$ solution then dried with $MgSO_4$ and filtered. The solvent was removed *in vacuo* and the crude purified via column chromatography (silica gel, hexanes: ethyl acetate, 100:1) to a red solid (1.0 g, 3.6 mmol, 55% yield). ^{1}H NMR (500 MHz, C_6D_6) δ 7.78 – 7.73 (m, 2H), 7.15 – 7.08 (m, 1H), 7.03 (ddd, *J* = 8.2, 6.6, 1.3 Hz, 2H), 2.80 (t, *J* = 6.7 Hz, 2H), 2.48 (t, *J* = 6.9 Hz, 2H), 1.89 (p, *J* = 6.8 Hz, 2H). ^{13}C NMR (126 MHz, C_6D_6) δ 196.9, 136.9, 132.5, 128.3, 127.8, 38.5, 27.5, 6.3.

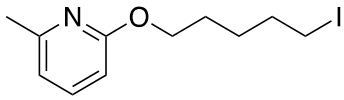

2-((5-iodopentyl)oxy)-6-methylpyridine. This procedure was adapted from the literature.[12] A 50 mL flame-dried round-bottom flask charged with a stir bar was sealed with a rubber septum and placed under positive N_2 pressure with a needle. The rubber septum was partly removed and sodium tert-butoxide (1.36 g. 14.1 mmol) was added. The rubber septum was replaced and DMF (30 mL), and 1,5-pentanediol (6.7 g, 64 mmol) were added via syringe under positive N_2 pressure. The mixture stirred for 10 minutes at room temperature and 2-bromo-6-methylpyridine (2.2 g, 12.8 mmol) was then added via syringe. The flask was placed in an oil bath at 120 °C and stirred for 7 h under nitrogen. After cooling to room temperature, 30 mL ethyl acetate was added and the organic phase was washed with 20 mL water, dried over MgSO4, filtered and the solvents removed *in vacuo*. The product was obtained via column chromatography (hexanes: ethyl acetate, 50:50) to yield a colorless oil (0.5 g, 1.6 mmol, 13% yield). 1H NMR (500 MHz, C6D6) δ 7.42 – 7.35 (m, 1H), 6.53 (dt, *J* = 8.2, 0.7 Hz, 1H), 6.39 (dt, *J* = 7.2, 0.7 Hz, 1H), 4.29 (t, *J* = 6.6 Hz, 2H), 2.64 (t, *J* = 7.1 Hz, 2H), 2.36 (s, 3H), 1.53 – 1.36 (m, 4H), 1.30 – 1.15 (m, 2H). ^{13}C NMR (126 MHz, C_6D_6) δ 156.0, 138.4, 133.8, 115.2, 107.7, 65.0, 33.1, 27.9, 26.9, 23.9, 6.0. [11]

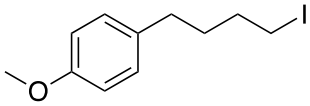

1-(4-iodobutyl)-4-methoxybenzene. This procedure was adapted from the literature.[12] An iodine (2.1 g, 8.3 mmol) solution in dichloromethane (50 mL) was charged to a flask and allowed to cool to 0°C over an ice bath. Whilst maintaining the temperature, triphenylphosphine (2.2 g, 8.3 mmol) was added and stirred for 20 minutes. The ice bath was removed, and the solution was allowed to cool to room temperature. Then, imidazole (0.95 g, 13.9 mmol) was added and stirred for an additional 10 minutes. Then, 4-methoxy benzenebutanol (1.0 g, 5.6 mmol) was added in with an additional 15 mL dichloromethane. The mixture was stirred at room temperature for 2h. Once complete, the crude was diluted with 0.5M Na_2SO_3, extracted with 30 mL dicholormethane. The organics were dried over $MgSO_4$, the solvent removed *in vacuo* and the compound purified by column chromatography (silica gel, hexanes: ethyl acetate, 95:5) to yield a colorless oil (1.0 g, 3.4 mmol, 62% yield). ^{1}H NMR (500 MHz, C_6D_6) δ 6.92 – 6.86 (m, 2H), 6.81 – 6.75 (m, 2H), 3.34 (s, 3H), 2.67 (t, *J* = 6.8 Hz, 2H), 2.25 (t, *J* = 7.4 Hz, 2H), 1.48 – 1.32 (m, 2H). ^{13}C NMR (126 MHz, C_6D_6) δ 158.2, 133.6, 129.2, 113.9, 54.4, 33.7, 32.8, 32.2, 6.1.

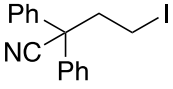

4-iodo-2,2-diphenylbutanenitrile. This procedure was adapted from the literature.[13] To an N_2-purged flask containing 3 eq. NaI was added 4-bromo-2,2-diphenylbutanenitrile (2.0 g, 6.7 mmol) along with acetone (20mL) and stirred under reflux for 48h. After 48h, the acetone is pumped off, the crude diluted with 20 mL water and extracted with 30 mL ethyl acetate. The organics are washed with 1M $Na_2S_2O_3$ and a saturated $NaHCO_3$ solution then dried with $MgSO_4$ and filtered. The solvent was removed *in vacuo* and the pure compound crystallized to yield a white crystalline solid (1.5 g, 4.3 mmol, 65%). ^{1}H NMR (500 MHz, C_6D_6) δ 7.08 – 7.00 (m, 1H), 6.94 – 6.86 (m, 1H). ^{3}C NMR (126 MHz, C_6D_6) δ 139.0, 128.9, 127.9, 127.8, 127.7, 127.5, 126.6, 120.9, 53.4, 44.0, -3.5.

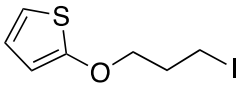

3-iodopropyl thiophene-2-carboxylate. This procedure was adapted from the literature.[14] 2-thiophenecarboxylic acid (2.0 g, 15.6 mmol) was dissolved in acetone (3 mL). 1,2-Dibromoethane (9.23 g, 31.2 mmol) and K_2CO_3 were added and the mixture refluxed for 2 days. The reaction mixture was cooled to room temperature, diluted with dichloromethane and washed with water. After drying over $MgSO_4$ and evaporation of volatiles, the crude product was purified by column chromatography (silica gel, hexanes: ethyl acetate 20:1),

which was used in the next step. To an N_2-purged flask containing 3 eq. NaI was added the reaction mixture along with acetone (20mL) and stirred under reflux for 48h. After 48h, the acetone is pumped off, the crude diluted with water and extracted with ethyl acetate. The organics are washed with 1M $Na_2S_2O_3$ and a saturated $NaHCO_3$ solution then dried with $MgSO_4$ and filtered. The solvent was pumped off and the product obtained by column chromatography (hexanes: ethyl acetate, 80:20) to yield a yellow oil (1.4 g, 5.2 mmol, 33% yield).. ^{1}H NMR (500 MHz, $CDCl_3$) δ 7.81 (dd, *J* = 3.8, 1.3 Hz, 1H), 7.56 (dd, *J* = 5.0, 1.3 Hz, 1H), 7.11 (dd, *J* = 5.0, 3.7 Hz, 1H), 4.37 (t, *J* = 6.0 Hz, 2H), 3.29 (t, *J* = 6.9 Hz, 2H), 2.31 – 2.24 (m, 2H).^{13}C NMR (126 MHz, $CDCl_3$) δ 161.99, 133.62, 133.46, 132.61, 127.85,64.70, 32.50, 1.40. HRMS (ESI) calculated for C8H9IO2NaS: *m/z* 318.9266 ($[M+Na]^+$), found: *m/z* 318.9264 ($[M+Na]^+$).

4.8 Characterization data on acid chlorides and their isolated N-benzylamides

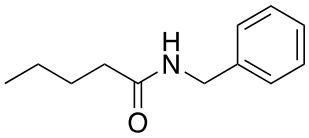

***N*-benzylpentanamide, 3a.** Data matches that previously reported in the literature.[15] 97% yield (47 mg, 0.25 mmol). Brown solid. ^{1}H NMR (500 MHz, $CDCl_3$) δ 7.42 – 7.29 (m, 2H), 7.27 (td, *J* = 5.7, 5.2, 3.2 Hz, 3H), 5.82 (s, 1H), 4.43 (d, *J* = 5.7 Hz, 2H), 2.37 – 2.08 (m, 2H), 1.74 – 1.53 (m, 2H), 1.35 (dq, *J* = 14.8, 7.4 Hz, 2H), 0.91 (t, *J* = 7.4 Hz, 3H). ^{13}C NMR (126 MHz, $CDCl_3$) δ 172.99, 138.47, 128.71, 127.82, 127.49, 43.58, 36.53, 27.86, 22.45, 13.81.

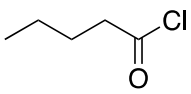

Pentanoyl Chloride, 1a. *In situ* spectra ^{1}H NMR (500 MHz, C_6D_6) δ 2.18 – 2.11 (m, 1H), 1.18 – 1.11 (m, 1H), 0.91 – 0.80 (m, 1H), 0.57 (t, *J* = 7.4 Hz, 1H). ^{13}C NMR (126 MHz, C_6D_6) δ 172.88, 46.26, 21.19, 13.09.

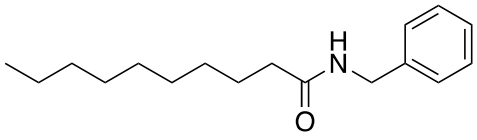

***N*-benzyldecanamide, 3b.** Data matches that previously reported in the literature.[1] 81% isolated yield (53 mg, 0.20 mmol). White solid. ^{1}H NMR (500 MHz, $CDCl_3$) δ 7.37 – 7.30 (m, 1H), 7.28 (dp, *J* = 4.9, 1.8 Hz, 2H), 5.71 (s, 0H), 4.44 (d, *J* = 5.6 Hz, 1H), 2.25 – 2.16 (m, 1H), 1.65 (p, *J* = 7.5 Hz, 1H), 1.35 – 1.21 (m, 7H), 0.88 (t, *J* = 6.9 Hz, 2H). ^{13}C NMR (126 MHz, $CDCl_3$) δ 173.0, 138.5, 128.7, 127.8, 127.5, 43.6, 36.9, 31.9, 29.5, 29.4, 29.3, 29.3, 25.8, 22.7, 14.1.

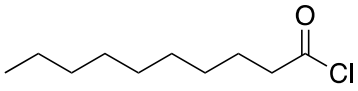

decanoyl chloride, 1b. *In situ* spectra ^{1}H NMR (500 MHz, C_6D_6) δ 2.20 (t, 2H), 1.28 − 0.98 (m, 14H), 0.92 (t, 3H). ^{13}C NMR (126 MHz, C_6D_6) δ 172.9, 127.9, 127.7, 127.5, 46.6, 31.8, 29.2, 29.2, 28.9, 28.1, 24.8, 22.7, 14.0.

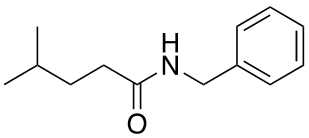

***N*-benzyl-4-methylpentanamide, 3c.** Data matches that previously reported in the literature.[1] 81% (45 mg, 0.22 mmol). Yellow-white solid. ^{1}H NMR (500 MHz, $CDCl_3$) δ 7.35 (ddt, *J* = 7.8, 5.6, 1.3 Hz, 2H), 7.33 – 7.26 (m, 3H), 5.80 (s, 1H), 4.45 (d, *J* = 5.7 Hz, 2H), 2.27 – 2.20 (m, 2H), 1.67 – 1.51 (m, 3H), 0.92 (d, *J* = 6.2 Hz, 6H). ^{13}C NMR (126 MHz, $CDCl_3$) δ 173.1, 138.5, 128.7, 127.8, 127.5, 43.6, 34.8, 34.6, 27.9, 22.3.

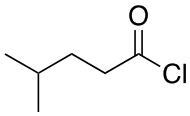

4-methylpentanoyl chloride, 1c. *In situ* spectra ^{1}H NMR (500 MHz, C_6D_6) δ 2.22 (t, 2H), 1.13 (m, 3H), 0.56 (d, 6H). ^{13}C NMR (126 MHz, C_6D_6) δ 173.0, 127.9, 127.7, 127.5, 44.8, 33.2, 26.8, 21.5.

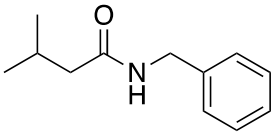

***N*-benzyl-3-methylbutanamide, 3d.** Data matches that previously reported in the literature.[16] 95% (45 mg, 024 mmol). ^{1}H NMR (500 MHz, $CDCl_3$) δ 7.36 – 7.29 (m, 1H), 7.30 – 7.23 (m, 2H), 5.82 (s, 0H), 4.43 (d, *J* = 5.7 Hz, 1H), 2.14 (dh, *J* = 8.2, 6.5 Hz, 1H), 2.09 – 2.04 (m, 1H), 0.96 (d, *J* = 6.5 Hz, 3H). ^{13}C NMR (126 MHz, $CDCl_3$) δ 172.3, 138.5, 128.7, 127.8, 127.5, 46.1, 43.6, 26.2, 22.5.

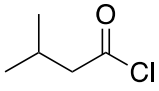

3-methylbutanoyl chloride, 1d. *In situ* spectra ^{1}H NMR (500 MHz, C_6D_6) δ 2.08 (d, 2H), 1.75 (m, 1H), 0.54 (d, 6H). ^{13}C NMR (126 MHz, C_6D_6) δ 172.1, 127.9, 127.7, 127.5, 54.9, 25.5, 21.1.

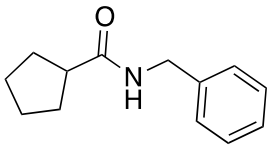

***N*-benzylcyclopentanecarboxamide,** Data matches that previously reported in the literature.[17] 91% isolated yield (46 mg, 0.23 mmol). White solid. ^{1}H NMR (500 MHz, $CDCl_3$) δ 7.36 – 7.31 (m, 1H), 7.31 – 7.25 (m, 2H), 5.72 (s, 0H), 4.44 (d, *J* = 5.6 Hz, 1H), 2.54 (p, *J* = 8.1 Hz, 1H), 1.94 – 1.70 (m, 3H), 1.65 – 1.52 (m, 1H). ^{13}C NMR (126 MHz, $CDCl_3$) δ 176.0, 138.6, 128.7, 127.8, 127.5, 45.9, 43.6, 30.5, 25.9.

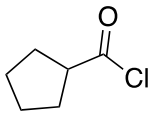

Cyclopentanecarbonyl chloride, 1e. *In situ* spectra ^{1}H NMR (500 MHz, C_6D_6) δ 2.59 (tt, *J* = 8.7, 7.0 Hz, 1H), 1.67 – 1.56 (m, 2H), 1.43 – 1.34 (m, 2H), 1.31 – 1.19 (m, 2H), 1.12 – 1.00 (m, 2H). ^{13}C NMR (126 MHz, C_6D_6) δ 176.1, 55.6, 29.7, 25.1.

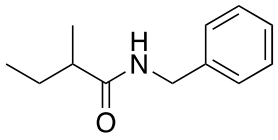

***N*-benzyl-2-methylbutanamide, 3f** Data matches that previously reported in the literature.[18] 98% isolated yield (46 mg, 0.24 mmol). Brown solid.^{1}H NMR (500 MHz, $CDCl_3$) δ 7.35 – 7.30 (m, 2H), 7.30 – 7.24 (m, 3H), 5.80 (s, 1H), 4.54 – 4.34 (m, 2H), 2.13 (h, *J* = 6.9 Hz, 1H), 1.70 (dt, *J* = 13.4, 7.4 Hz, 1H), 1.45 (ddd, *J* = 13.7, 7.7, 6.4 Hz, 1H), 1.16 (d, *J* = 6.8 Hz, 3H), 0.91 (t, *J* = 7.4 Hz, 3H). ^{13}C NMR (126 MHz, $CDCl_3$) δ 176.3, 138.6, 128.7, 127.8, 127.5, 43.4, 43.3, 27.4, 17.6, 12.0.

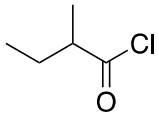

2-methylbutanoyl chloride, 1f. *In situ* spectra ^{1}H NMR (500 MHz, C_6D_6) δ 2.24 (q, *J* = 6.8 Hz, 1H), 1.42 – 1.35 (m, 1H), 1.09 (dqd, *J* = 13.9, 7.4, 6.3 Hz, 1H), 0.78 (d, *J* = 6.9 Hz, 4H), 0.57 (t, *J* = 7.5 Hz, 4H). ^{13}C NMR (126 MHz, C_6D_6) δ 52.5, 26.1, 15.8, 10.5.

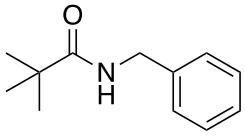

***N*-benzylpivalamide, 3g** and **1bb** Data matches that previously reported in the literature.[19] 72% isolated from alkyl iodide and 21% from alkyl bromide (34 mg, 0.18 mmol). Brown solid. ^{1}H NMR (500 MHz, $CDCl_3$) δ 7.33 (tt, *J* = 6.9, 1.1 Hz, 1H), 7.27 (tt, *J* = 8.0, 1.4 Hz, 2H), 5.94 (s, 0H), 4.43 (d, *J* = 5.6 Hz, 1H), 1.23 (s, 5H). ^{13}C NMR (126 MHz, $CDCl_3$) δ 178.3, 138.7, 128.7, 127.7, 127.4, 43.6, 38.7, 27.6.

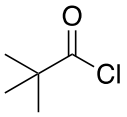

Pivaloyl chloride, 1g. *In situ* spectra ^{1}H NMR (500 MHz, C_6D_6) δ 0.89 (s, 1H). ^{13}C NMR (126 MHz, C_6D_6) δ 179.6, 39.9, 26.3.

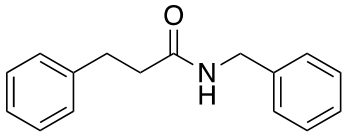

***N*-benzyl-3-phenylpropanamide, 3h.** Data matches that previously reported in the literature.[20] 85% (51 mg, 0.21 mmol). White solid. ^{1}H NMR (500 MHz, $CDCl_3$) δ 7.36 – 7.24 (m, 1H), 7.27 – 7.19 (m, 1H), 7.21 – 7.14 (m, 0H), 5.68 (s, 0H), 4.42 (d, *J* = 5.7 Hz, 0H), 3.02 (t, *J* = 7.6 Hz, 0H), 2.54 (dd, *J* = 8.2, 7.0 Hz, 0H). ^{13}C NMR (126 MHz, $CDCl_3$) δ 171.9, 140.8, 138.2, 128.7, 128.6, 128.4, 127.8, 127.5, 126.3, 43.6, 38.5, 31.7, 30.9.

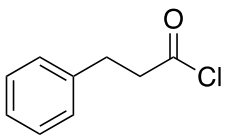

3-phenylpropanoyl chloride, 1h. *In situ* spectra ^{1}H NMR (500 MHz, C_6D_6) δ 7.03 (m, 3H), 6.75 (m, 3H), 2.44 (s, 4H). ^{13}C NMR (126 MHz, C_6D_6) δ 172.2, 128.5, 128.1, 126.5, 47.9, 30.6.

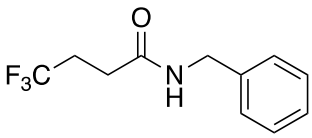

***N*-benzyl-4,4,4-trifluorobutanamide, 3i.** Data matches that previously reported in the literature.[1] 94% isolated yield (54 mg, 0.23 mmol). White solid. ^{1}H NMR (500 MHz, $CDCl_3$) δ 7.36 – 7.31 (m, 1H), 7.32 – 7.22 (m, 2H), 5.95 (s, 0H), 4.43 (d, *J* = 5.7 Hz, 1H), 2.57 – 2.38 (m, 2H). ^{13}C NMR (126 MHz, $CDCl_3$) δ 169.6, 137.8, 128.8, 127.8, 127.7, 43.9, 29.6 (q, *J* = 29.8 Hz), 28.8 (q, *J* = 3.0 Hz). ^{19}F NMR (471 MHz, $CDCl_3$) δ -66.79.

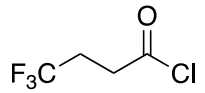

4,4,4-trifluorobutanoyl chloride, 1i. *In situ* spectra ^{1}H NMR (500 MHz, C_6D_6) δ 2.11 (dd, *J* = 8.2, 7.0 Hz, 1H), 1.61 – 1.50 (m, 1H). ^{13}C NMR (126 MHz, C_6D_6) δ 170.7, 38.7 (d, *J* = 3.2 Hz), 28.5 (q, *J* = 30.3 Hz). ^{19}F NMR (471 MHz, C_6D_6) δ -66.67.

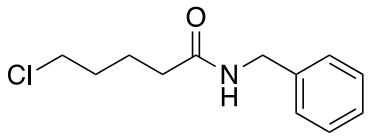

***N*-benzyl-5-chloropentanamide, 3j.** Data matches that previously reported in the literature.[1] 98% isolated yield (55 mg, 0.25 mmol). Yellow-brown solid. ^{1}H NMR (500 MHz, $CDCl_3$) δ 7.37 – 7.30 (m,

1H), 7.28 (td, *J* = 6.7, 6.2, 1.6 Hz, 2H), 5.77 (s, 1H), 4.44 (d, *J* = 5.7 Hz, 1H), 3.60 – 3.46 (m, 1H), 2.30 – 2.17 (m, 1H), 1.85 – 1.80 (m, 2H). ^{13}C NMR (126 MHz, $CDCl_3$) δ 172.1, 138.3, 128.8, 127.9, 127.6, 44.6, 43.7, 35.7, 32.0, 23.0.

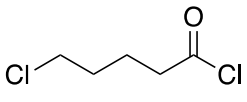

5-chloropentanoyl chloride, 1j. *In situ* spectra ^{1}H NMR (500 MHz, C_6D_6) δ 2.80 (t, 1H), 1.98 (t, 1H), 1.13 (m, 1H), 1.02 (m, 1H). ^{13}C NMR (126 MHz, C_6D_6) δ 172.5, 127.9, 127.7, 127.5, 45.9, 43.4, 30.5, 21.9.

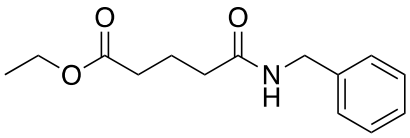

ethyl 5-(benzylamino)-5-oxopentanoate, 3k. Data matches that previously reported in the literature.[21] 95% isolated yield (0.24 mmol, 59 mg). Orange-red oil. ^{1}H NMR (500 MHz, $CDCl_3$) δ 7.37 – 7.31 (m, 2H), 7.30 – 7.26 (m, 3H), 5.78 (s, 1H), 4.44 (d, *J* = 5.7 Hz, 2H), 4.12 (q, *J* = 7.1 Hz, 2H), 2.38 (t, *J* = 7.1 Hz, 2H), 2.28 (t, *J* = 7.4 Hz, 2H), 1.99 (p, *J* = 7.2 Hz, 2H), 1.25 (t, *J* = 7.1 Hz, 3H). ^{13}C NMR (126 MHz, $CDCl_3$) δ 14.2, 20.9, 33.3, 35.5, 43.7, 60.4, 127.6, 127.9, 128.8, 138.3, 171.9, 173.2.

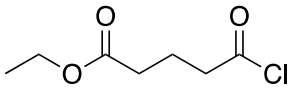

ethyl 5-chloro-5-oxopentanoate, 1k. *In situ* spectra ^{1}H NMR (500 MHz, C_6D_6) δ 3.87 (t, 2H), 2.23 (t, 2H), 1.79 (m, 2H), 1.49 (t, 2H), 0.91 (t, 3H). ^{13}C NMR (126 MHz, C_6D_6) δ 172.6, 171.3, 127.9, 127.7, 127.5, 59.9, 45.5, 31.8, 19.9, 13.8.

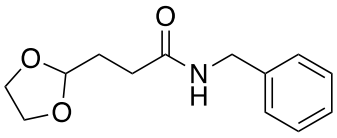

***N*-benzyl-3-(1,3-dioxolan-2-yl)propenamide, 3l.** Data matches that previously reported in the literature.[1] 93% isolated yield (0.23 mmol, 55 mg). ^{1}H NMR (500 MHz, $CDCl_3$) δ 7.35 – 7.28 (m, 1H), 7.28 – 7.21 (m, 2H), 3.96 – 3.76 (m, 2H), 2.33 (t, *J* = 7.4 Hz, 1H), 2.03 (td, *J* = 7.4, 4.4 Hz, 1H). ^{13}C NMR (126 MHz, $CDCl_3$) δ 172.2, 138.4, 128.7, 127.8, 127.5, 103.4, 77.3, 77.2, 77.0, 76.8, 65.0, 43.7, 30.6, 29.3.

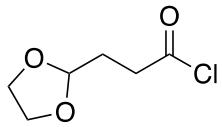

3-(1,3-dioxolan-2-yl)propanoyl chloride, 1l. *In situ* spectra ^{1}H NMR (500 MHz, C_6D_6) δ 4.54 (t, *J* = 3.9 Hz, 1H), 3.37 – 3.29 (m, 2H), 3.25 – 3.13 (m, 2H), 2.49 (t, *J* = 7.0 Hz, 2H), 1.72 (td, *J* = 7.1, 3.9 Hz, 2H). ^{13}C NMR (126 MHz, C_6D_6) δ 172.7, 127.9, 127.7, 127.5, 101.8, 64.6, 40.5, 28.7

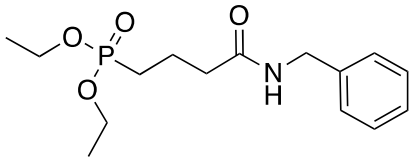

diethyl (4-(benzylamino)-4-oxobutyl)phosphonate, 3m. Data matches that previously reported in the literature.[22] 82% Isolated yield (61 mg, 0.20 mmol). Yellow-orange oil. ^{1}H NMR (500 MHz, $CDCl_3$) δ 7.31 (dtd, *J* = 16.9, 8.7, 7.9, 6.6 Hz, 5H), 6.26 (s, 1H), 4.44 (d, *J* = 5.7 Hz, 2H), 4.12 – 3.97 (m, 4H), 2.39 (t, *J* = 7.1 Hz, 2H), 2.05 – 1.92 (m, 2H), 1.77 (dt, *J* = 18.1, 7.4 Hz, 2H), 1.30 (t, *J* = 7.1 Hz, 6H). ^{13}C NMR (126 MHz, $CDCl_3$) δ 16.4, 16.5, 18.9, 19.0, 23.8, 24.9, 36.1, 36.2, 43.6, 61.6, 61.6, 127.5, 127.9, 128.7, 138.4, 171.9. ^{31}P NMR (203 MHz, $CDCl_3$) δ 31.41.

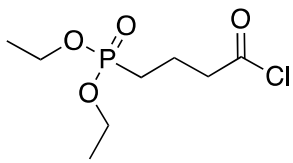

diethyl (4-chloro-4-oxobutyl)phosphonate, 1m. *In situ* spectra ^{1}H NMR (500 MHz, C_6D_6) δ 3.85 (t, 4H), 2.32 (t, 2H), 1.60 (m, 2H), 1.33 (t, 2H), 1.01 (t, 6H). ^{13}C NMR (126 MHz, C_6D_6) δ 172.7, 66.4, 61.0, 60.9, 46.4, 46.3, 24.7, 23.6, 18.3, 18.3, 16.2, 16.1. ^{13}C NMR (126 MHz, C_6D_6) δ 172.7, 66.4, 61.0, 60.9, 46.4, 46.3, 24.7, 23.6, 18.3, 18.3, 16.2, 16.1.

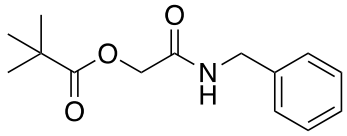

2-(benzylamino)-2-oxoethyl pivalate, 3n. Data matches that previously reported in the literature.[1] 63% isolated yield (0.16 mmol, 39 mg). Yellow oil. ^{1}H NMR (500 MHz, $CDCl_3$) δ 7.34 (m, 2H), 7.27 (m, 3H), 6.29 (br. s, 1H), 4.60 (s, 2H), 4.49 (d, 2H), 1.22 (s, 9H). ^{13}C NMR (126 MHz, $CDCl_3$) δ 177.0, 167.2, 137.6, 128.8, 127.7, 127.6, 77.3, 77.1, 76.8, 63.0, 43.2, 38.8, 27.

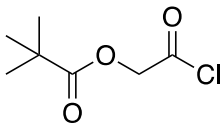

2-chloro-2-oxoethyl pivalate, 1n. *In situ* spectra ^{1}H NMR (500 MHz, C_6D_6) δ 5.20 (s, 1H), 1.02 (s, 5H). ^{13}C NMR (126 MHz, C_6D_6) δ 176.2, 168.9, 127.9, 127.7, 127.5, 66.4, 38.3, 26.3.

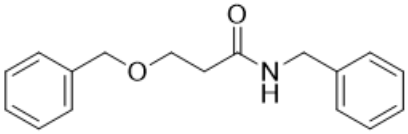

N-benzyl-3-(benzyloxy)propanamide, 3o. Data matches that previously reported in the literature.[1] 70% Yield (47 mg, 0.18 mmol). Orange oil. ^{1}H NMR (500 MHz, $CDCl_3$) δ 7.33 – 7.28 (m, 3H), 7.22 (dd, *J* = 7.3, 2.2 Hz, 1H), 4.51 (s, 1H), 4.44 (d, *J* = 5.6 Hz, 1H), 3.80 – 3.74

(m, 1H), 2.55 (t, J = 5.7 Hz, 1H). ^{13}C NMR (126 MHz, $CDCl_3$) δ 171.30, 138.30, 137.54, 128.69, 128.52, 127.89, 127.83, 127.73, 127.4173.41, 66.43, 43.52, 37.20.

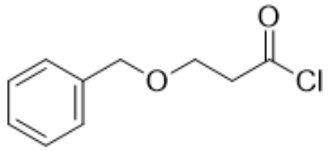

3-(benzyloxy)propanoyl chloride, 1o. *In situ* spectra ^{1}H NMR (500 MHz, C_6D_6) δ 7.17 – 7.08 (m, 4H), 4.11 (s, 1H), 3.13 (t, J = 5.9 Hz, 1H), 2.38 (t, J = 5.9 Hz, 1H). ^{13}C NMR (126 MHz, C_6D_6) δ 171.1, 137.8, 128.3, 128.0, 127.9, 127.7, 127.6, 127.5, 127.5, 72.8, 64.3, 46.8.

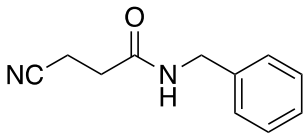

N-benzyl-3-cyanopropanamide, 3p and **3z.** Data matches that previously reported in the literature.[1] 87% Isolated yield from alkyl iodide (**3p,** 0.22mmol, 42 mg). 50% from alkyl bromide (**3z**). Yellow solid.1H NMR (500 MHz, CDCl3) δ 7.49 – 7.22 (m, 6H), 5.87 (s, 1H), 4.46 (d, J = 5.6 Hz, 2H), 2.71 (t, J = 7.5 Hz, 2H), 2.56 (t, J = 7.4 Hz, 2H). 13C NMR (126 MHz, CDCl3) δ 168.49, 137.57, 128.87, 127.92, 127.83, 118.95, 44.00, 31.67, 13.21.

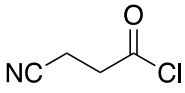

3-cyanopropanoyl chloride, 1p *In situ* spectra ^{1}H NMR (500 MHz, C_6D_6) δ 5.17 (s, 1H), 1.73 (t, 2H), 1.22 (t, J = 7.2 Hz, 2H). ^{13}C NMR (126 MHz, C_6D_6) δ 170.45, 116.19, 22.36, 13.91.

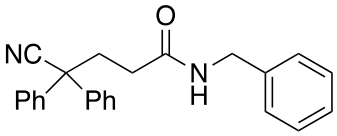

***N*-benzyl-4-cyano-4,4-diphenylbutanamide, 3q.** Data matches that previously reported in the literature.[1] 73% Isolated yield (65 mg, 0.18 mmol). White crystalline solid.^{1}H NMR (500 MHz, $CDCl_3$) δ 7.43 – 7.26 (m, 13H), 7.25 – 7.22 (m, 2H), 5.66 (s, 1H), 4.39 (d, J = 5.7 Hz, 2H), 2.86 – 2.79 (m, 2H), 2.37 – 2.30 (m, 2H). ^{13}C NMR (126 MHz, $CDCl_3$) δ 32.7, 34.8, 43.8, 51.1, 122.0, 126.8, 127.7, 127.9, 128.1, 128.8, 129.0, 137.9, 139.5, 170.8.

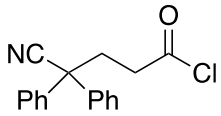

4-cyano-4,4-diphenylbutanoyl chloride, 1q. *In situ* spectra ^{1}H NMR (500 MHz, C_6D_6) δ 7.06 (m, 5H), 6.91 (m, 5H), 2.66 (m, 2H), 2.28 (m, 2H). ^{13}C NMR (126 MHz, C_6D_6) δ 172.0, 139.0, 128.9, 128.0, 126.6, 120.9, 50.2, 43.2, 34.0.

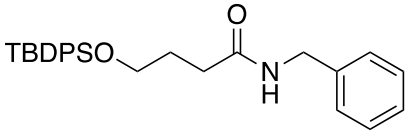

N-benzyl-4-((tert-butyldiphenylsilyl)oxy)butanamide, 3r. 61% Isolated yield (66 mg, 0.15mmol). yellow wax-like solid ^{1}H NMR (500 MHz, $CDCl_3$) δ 7.63 (dd, *J* = 8.1, 1.5 Hz, 1H), 7.45 – 7.38 (m, 0H), 7.38 – 7.31 (m, 1H), 7.29 – 7.23 (m, 0H), 5.77 (s, 0H), 4.41 (d, *J* = 5.8 Hz, 1H), 3.72 (t, *J* = 6.0 Hz, 1H), 2.36 (t, *J* = 7.5 Hz, 1H), 1.96 – 1.87 (m, 0H), 1.03 (s, 2H). ^{13}C NMR (126 MHz, $CDCl_3$) δ 172.67, 138.39, 135.53, 133.70, 129.69, 128.72, 127.85, 127.71, 127.50, 77.28, 77.03, 76.77, 63.04, 43.62, 33.20, 28.43, 26.89. HRMS (ESI) calculated for $C_{27}H_{33}NNaO_2Si$: *m/z* 454.2178 ($[M+Na]^+$), found: *m/z* 454.2173 ($[M+Na]^+$). [Note: acid chloride not observed due to overlap with solvent signals.]

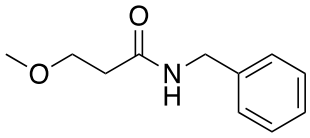

N-benzyl-3-methoxypropanamide, 3s. 75% Isolated yield (36 mg, 0.19 mmol). Orange oil. ^{1}H NMR (500 MHz, $CDCl_3$) δ 7.35 – 7.29 (m, 1H), 7.26 (s, 1H), 6.48 (s, 1H), 4.44 (d, *J* = 5.7 Hz, 1H), 3.64 (t, *J* = 5.8 Hz, 1H), 3.33 (s, 1H), 2.48 (t, *J* = 5.7 Hz, 1H). ^{13}C NMR (126 MHz, $CDCl_3$) δ 171.36, 138.43, 128.67, 127.58, 127.38, 68.69, 58.81, 43.40, 37.05. **HRMS (ESI)** calculated for $C_{11}H_{15}NNaO_2$: *m/z* 216.1000 ($[M+Na]^+$), found: *m/z* 216.0995($[M+Na]^+$).

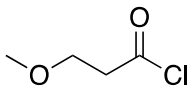

3-methoxypropanoyl chloride, 1s. *In situ* spectra ^{1}H NMR (500 MHz, C_6D_6) δ 3.02 (t, *J* = 5.9 Hz, 1H), 2.86 (s, 2H), 2.35 (t, *J* = 5.8 Hz, 1H). ^{13}C NMR (126 MHz, C_6D_6) δ 171.05, 66.66, 66.37, 58.05.

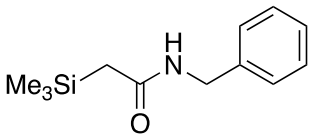

***N*-benzyl-2-(trimethylsilyl)acetamide, 3t.** Data matches that previously reported in the literature.[23] 29% isolated yield (16 mg, 0.074 mmol). Red oil. ^{1}H NMR (500 MHz, $CDCl_3$) δ 7.36 – 7.28 (m, 1H), 7.30 – 7.23 (m, 2H), 5.54 (s, 0H), 4.41 (d, *J* = 5.7 Hz, 1H), 1.80 (s, 1H), 0.12 (s, 4H). ^{13}C NMR (126 MHz, $CDCl_3$) δ 171.9, 138.8, 128.7, 127.9, 127.4, 43.8, 29.2, -1.3.

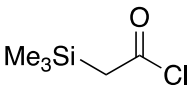

2-(trimethylsilyl)acetyl chloride, 1t. *In situ* spectra ^{1}H NMR (500 MHz, C_6D_6) δ 1.59 (s, 1H), 0.17 (s, 5H). ^{13}C NMR (126 MHz, C_6D_6) δ 179.5, 127.9, 127.7, 127.5, 66.4, 2.6.

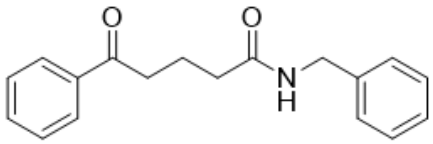

N-benzyl-5-oxo-5-phenylpentanamide, 3u. 50% Isolated yield (35 mg, 0.13 mmol). White solid with a hint of yellow. ^{1}H NMR (500 MHz, $CDCl_3$) δ 8.00 – 7.88 (m, 2H), 7.60 – 7.51 (m, 1H), 7.45 (t, *J* = 7.7 Hz, 2H), 7.34 – 7.29 (m, 2H), 7.27 (d, *J* = 1.5 Hz, 2H), 7.25 (dd, *J* = 4.0, 2.7 Hz, 1H), 5.95 (s, 1H), 4.44 (d, *J* = 5.7 Hz, 2H), 3.06 (t, *J* = 6.9 Hz, 2H), 2.34 (t, *J* = 7.2 Hz, 2H), 2.11 (p, *J* = 7.0 Hz, 2H). ^{13}C NMR (126 MHz, $CDCl_3$) δ 199.92, 172.32, 138.32, 136.77, 133.17, 128.73,128.64, 128.09, 127.82, 127.51, 77.31, 77.05, 76.80, 43.61, 37.38, 35.49, 20.24. **HRMS (ESI)** calculated for C18H19nNaO2: *m/z* 304.1313($[M+Na]^+$), found: *m/z* 304.1310($[M+Na]^+$).

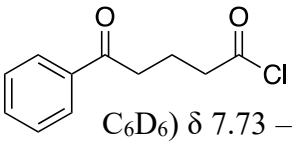

5-oxo-5-phenylpentanoyl chloride, 1u. *In situ* spectra ^{1}H NMR (500 MHz, C_6D_6) δ 7.73 – 7.68 (m, 1H), 7.09 – 6.97 (m, 2H), 2.32 (t, *J* = 7.1 Hz, 1H), 2.25 (t, *J* = 7.0 Hz, 1H), 1.66 (p, *J* = 7.0 Hz, 1H). ^{13}C NMR (126 MHz, C_6D_6) δ 197.01, 196.98, 136.73, 132.62, 128.36, 127.99,45.79, 35.87, 19.05.

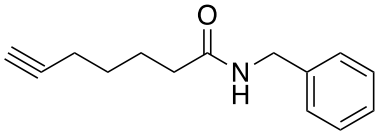

***N*-benzylhept-6-ynamide, 3v.** Data matches that previously reported in the literature.[24] 41% (22 mg, 0.10 mmol). Yellow-white solid. ^{1}H NMR (500 MHz, $CDCl_3$) δ 7.40 – 7.32 (m, 2H), 7.30 (td, *J* = 6.1, 1.4 Hz, 3H), 5.87 (s, 1H), 4.45 (d, *J* = 5.7 Hz, 2H), 2.29 – 2.20 (m, 4H), 1.96 (t, *J* = 2.7 Hz, 1H), 1.85 – 1.75 (m, 2H), 1.63 – 1.55 (m, 2H). ^{13}C NMR (126 MHz, $CDCl_3$) δ 172.4, 138.4, 128.7, 127.8, 127.5, 84.1, 68.6, 43.6, 36.1, 28.0, 24.8, 18.2.

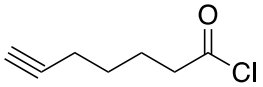

hept-6-ynoyl chloride, 1v. *In situ* spectra ^{1}H NMR (500 MHz, C_6D_6) δ 2.08 – 2.03 (m, 2H), 1.89 (tq, *J* = 7.0, 1.5 Hz, 1H), 1.67 (td, *J* = 6.9, 2.6 Hz, 2H), 1.26 – 1.17 (m, 2H), 0.99 – 0.89 (m, 2H). ^{13}C NMR (126 MHz, C_6D_6) δ 172.6, 127.9, 127.7, 127.5, 69.1, 66.4, 45.9, 26.6, 23.7, 17.6.

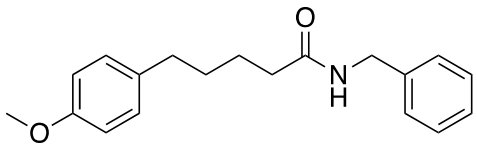

N-benzyl-5-(4-methoxyphenyl)pentanamide, 3w. Found 68% yield (51 mg, 0.17 mmol). Light orange solid. ^{1}H NMR (500 MHz, $CDCl_3$) δ 7.37 – 7.30 (m, 2H), 7.30 – 7.27 (m, 2H),7.26 (s, 1H), 7.10 – 7.03 (m, 2H), 6.84 – 6.78 (m, 2H), 5.63 (s, 1H), 4.43 (d, *J* = 5.7 Hz, 2H), 3.78 (s, 3H), 2.57 (t, *J* = 7.4 Hz, 2H), 2.22 (t, *J* = 7.3 Hz, 2H), 1.75 – 1.66 (m, 2H), 1.66 – 1.59 (m, 2H). ^{13}C NMR (126 MHz, $CDCl_3$) δ 157.7, 138.4, 134.3, 129.3, 128.7, 127.8, 127.5, 113.8, 77.3, 77.1, 76.8, 55.3, 43.6, 36.6, 34.7, 31.3, 25.4. HRMS (ESI) calculated for $C_{19}H_{24}NO_2$: *m/z* 298.1807 ($[M+H]^+$), found: *m/z* 298.1806($[M+H]^+$).

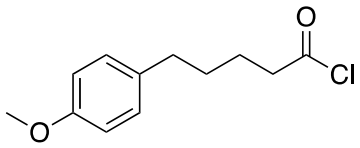

5-(4-methoxyphenyl)pentanoyl chloride, 1w. *In situ* spectra ^{1}H NMR (500 MHz, C_6D_6) δ 6.88 (d, *J* = 8.7 Hz, 2H), 6.80 (d, *J* = 8.7 Hz, 2H), 3.35 (s, 3H), 2.21 (t, *J* = 7.3 Hz, 2H), 2.17 – 2.12 (m, 2H), 1.28 – 1.11 (m, 4H). ^{13}C NMR (126 MHz, C_6D_6) δ 172.84, 158.23, 133.35, 129.15, 113.88, 54.48, 46.43, 34.25, 30.01, 24.23.

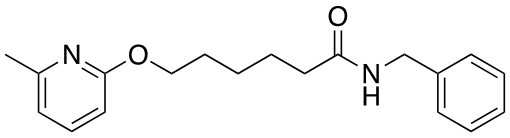

N-benzyl-6-((6-methylpyridin-2-yl)oxy)hexanamide, 3x. Found 81% yield (63.3mg, 0.20mmol). Light orange solid. ^{1}H NMR (500 MHz, $CDCl_3$) δ 7.49 – 7.42 (m, 1H), 7.39 7.32 (m, 2H), 7.30 (d, *J* = 5.5 Hz, 3H), 6.71 (d, *J* = 7.2 Hz, 1H), 6.51 (d, *J* = 8.2 Hz, 1H), 5.75 (s, 1H), 4.47 (d, *J* = 5.8 Hz, 2H), 4.27 (t, *J* = 6.5 Hz, 2H), 2.44 (s, 3H), 2.30 – 2.22 (m, 2H), 1.87 – 1.70 (m, 4H), 1.53 (p, *J* =7.5 Hz, 2H). ^{13}C NMR (126 MHz, $CDCl_3$) δ 172.74, 163.49, 156.34, 138.75, 138.39, 128.73, 128.35, 127.85, 127.53, 115.62, 106.94, 77.28, 77.03, 76.78, 65.53, 43.63, 36.72, 30.94, 28.83, 25.88, 25.52, 24.21. HRMS (ESI) calculated for C19H25N2O2: *m/z* = 313.1916 ($[M+H]^+$), found: *m/z* = 313.1920($[M+H]^+$). [Note: acid chloride not observed due to overlap with solvent signals.]

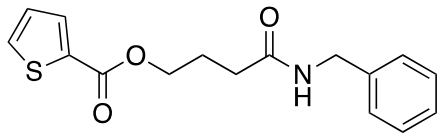

4-(benzylamino)-4-oxobutyl thiophene-2-carboxylate, 3y. Found 88% yield (67 mg, 0.22 mmol). Yellow solid. ^{1}H NMR (500 MHz, $CDCl_3$) δ 7.79 (dd, *J* = 3.8, 1.3 Hz, 1H), 7.55 (dd, *J* = 5.0, 1.3 Hz, 1H), 7.32 (ddt, *J* = 7.7, 5.0, 1.3 Hz, 2H), 7.30 – 7.23 (m, 4H), 7.09 (dd, *J* = 5.0, 3.8 Hz, 1H), 5.86 (s, 1H), 4.44 (d, *J* = 5.7 Hz, 2H), 4.35 (t, *J* = 6.2 Hz, 2H), 2.36 (dd, *J* = 8.0, 6.8 Hz, 2H), 2.18 – 2.09 (m, 2H). ^{13}C NMR (126 MHz, $CDCl_3$) δ 171.64, 162.27, 138.17,

133.66, 133.54, 132.46, 128.77, 127.88, 127.81, 127.59, 77.28, 77.03, 76.77, 64.28, 43.75, 32.98, 24.85. HRMS (ESI) calculated for $C_{16}H_{17}O_3NNaS$: *m/z* 326.0827 ($[M+Na]^+$), found: *m/z* 326.0671 ($[M+Na]^+$).

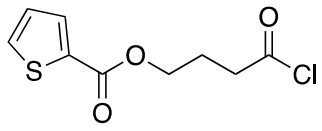

4-chloro-4-oxobutyl thiophene-2-carboxylate, 1y. *In situ* spectra ^1H NMR (500 MHz, C_6D_6) δ 7.68 (dd, *J* = 3.7, 1.3 Hz, 1H), 6.80 (dd, *J* = 5.0, 1.3 Hz, 1H), 6.53 (dd, *J* = 5.0, 3.7 Hz, 1H), 3.75 (t, *J* = 6.3 Hz, 2H), 2.17 (t, *J* = 7.2 Hz, 2H), 1.41 – 1.35 (m, 2H). ^{13}C NMR (126 MHz, C_6D_6) δ 172.43, 161.28, 133.68, 133.34, 132.14, 128.22, 127.88, 127.69, 127.50, 62.64, 43.20, 23.92.

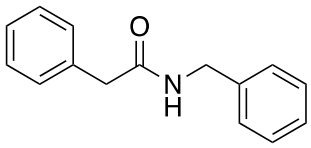

***N*-benzyl-2-phenylacetamide, 3aa**. Data matches that previously reported in the literature.[18] 75% isolated yield (42 mg, 0.20 mmol). White solid. ^1H NMR (500 MHz, $CDCl_3$) δ 7.35 − 7.18 (m, 10H), 5.68 (br. s, 1H), 4.41 (d, 2H), 3.63 (s, 2H). ^{13}C NMR (126 MHz, $CDCl_3$) δ 170.2, 138.6, 135.3, 129.5, 129.1, 128.7, 127.5, 77.3, 77.0, 76.8, 43.9, 43.6.

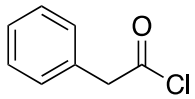

2-phenylacetyl chloride, 1aa. ^1H NMR (500 MHz, C_6D_6) δ 6.99 (dd, *J* = 5.0, 1.9 Hz, 1H), 6.79 – 6.76 (m, 1H), 3.38 (s, 1H). ^{13}C NMR (126 MHz, C_6D_6) δ 171.1, 131.3, 129.3, 128.6, 127.9, 127.7, 127.5, 125.4, 52.3, 43.1.

4.9 Characterization data of amides, esters and thioesters (Figure 4)

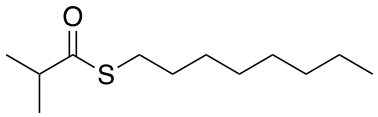

S-octyl 2-methylpropanethioate, 4a. 64% isolated yield (35 mg, 0.16 mmol); isolated by column: ethyl acetate/hexane = 5%. Dark brown oil. ^1H NMR (500 MHz, $CDCl_3$) δ 2.87 (t, *J* = 7.4 Hz, 2H), 2.75 (hept, *J* = 6.9 Hz, 1H), 1.65 – 1.51 (m, 3H), 1.37 (q, *J* = 7.0 Hz, 2H), 1.34 – 1.24 (m, 7H), 1.21 (d, *J* = 6.9 Hz, 6H), 0.90 (t, *J* = 6.9 Hz, 3H). ^{13}C NMR (126 MHz, CDCl3) δ 204.4, 77.2, 43.1, 31.8, 29.6, 29.2, 29.1, 28.9, 28.6, 22.6, 19.4, 14.1. HRMS (ESI) calculated for $C_{12}H_{25}OS$: *m/z* 217.1626($[M+H]^+$), found: *m/z* 217.1558($[M+H]^+$).

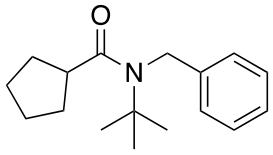

***N*-benzyl-*N*-(*tert*-butyl)cyclopentanecarboxamide, 4b**. 98% isolated yield (63 mg, 0.25 mmol). Isolated by column: ethyl acetate/hexane = 20%. Yellow-white solid. ^{1}H NMR (500 MHz, $CDCl_3$) δ 7.37 − 7.21 (m, 5H), 4.63 (s, 2H), 2.71 (m, 1H), 1.82 (m, 2H), 1.74 (m, 2H), 1.48 (m, 2H), 1.42 (s, 9H). ^{13}C NMR (126 MHz, $CDCl_3$) δ 178.4, 140.1, 128.7, 126.9, 125.6, 57.6, 49.3, 43.6, 31.2, 28.9, 26.3. HRMS (ESI) calculated for $C_{17}H_{25}NNaO$: *m/z* = 282.1834 ($[M+Na]^+$),found: *m/z* = 282.1828 ($[M+Na]^+$).

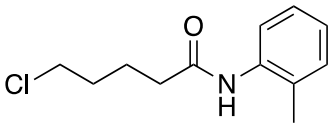

5-chloro-*N*-(*o*-tolyl)pentanamide, 4c. 95% isolated yield (54 mg, 0.24 mmol). isolated by column: ethyl acetate/hexane = 35%. Off-yellow solid. ^{1}H NMR (500 MHz, $CDCl_3$) δ 7.8 (d, 1H), 7.2 − 7.0 (m, 3H), 3.6)t, 2H), 2.4 (m, 2H), 2.2 (s, 3H), 1.9 (m, 4H). ^{13}C NMR (126 MHz, $CDCl_3$) δ 170.6, 135.6, 130.5, 129.2, 126.8, 125.3, 124.0, 44.6, 36.5, 31.9, 23.0, 17.1. HRMS (ESI) calculated for $C_{12}H_{16}ClNNaO$: *m/z* =248.0818 ($[M+Na]^+$),found: *m/z* = 248.0813($[M+Na]^+$).

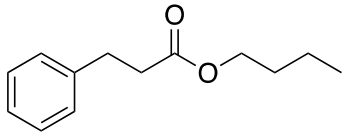

butyl 3-phenylpropanoate, 4d. Data matches that previously reported in the literature.[25] 87% isolated yield (45 mg, 0.22 mmol). Isolated by column: ethyl acetate/hexane = 10%. Red oil. ^{1}H NMR (500 MHz, $CDCl_3$) δ 7.29 − 7.21 (m, 5H), 4.07 (t, 2H), 2.95 (t, 2H), 2.63 (t, 2H), 1.58 (m, 2H), 1.33 (m, 2H), 0.92 (t, 3H). ^{13}C NMR (126 MHz, $CDCl_3$) δ 173.0, 139.6, 128.5, 128.3, 126.2, 77.3, 77.0, 76.8, 64.4, 36.0, 31.0, 30.7, 20.0, 13.7.

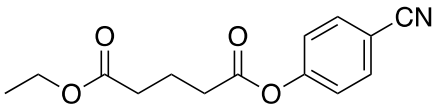

4-cyanophenyl ethyl glutarate, 4e. 74% isolated yield (48 mg, 0.19 mmol). Isolated by column: ethyl acetate/hexane = 15%.^{1}H NMR (400 MHz, $CDCl_3$) δ 7.72 – 7.66 (m, 1H), 7.28 – 7.20 (m, 2H), 4.16 (q, *J* = 7.1 Hz, 1H), 2.68 (t, *J* = 7.4 Hz, 1H), 2.45 (t, *J* = 7.2 Hz, 1H), 2.08 (p, *J* = 7.3 Hz, 1H), 1.27 (t, *J* = 7.1 Hz, 2H). ^{13}C NMR (126 MHz, $CDCl_3$) δ 172.7, 170.6, 153.9, 133.7, 122.7, 109.8, 77.3, 77.2, 77.0, 76.8, 60.6, 33.3, 33.1, 19.9, 14.2. HRMS (ESI) calculated for $C_{16}H_{23}NNaO_2$: *m/z* =284.0899 ($[M+Na]^+$),found: *m/z* = 284.1621 ($[M+Na]^+$).

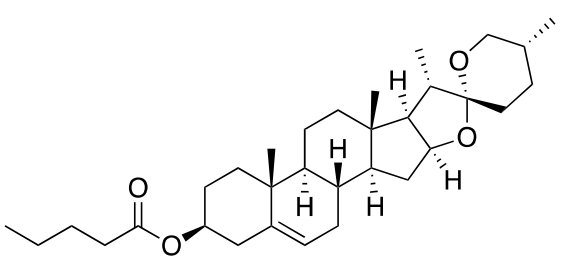

(4*S*,5'*R*,6a*R*,6b*S*,8a*S*,8b*R*,9*S*,10*R*,11a*S*,12a*S*,12b*S*)-5',6a,8a,9-tetramethyl-1,3,3',4,4',5,5',6,6a,6b,6',7,8,8a,8b,9,11a,12,12a,12b-icosahydrospiro[naphtho[2',1':4,5]indeno[2,1-*b*]furan-10,2'-pyran]-4-yl pentanoate, 4f. 77% isolated yield (96 mg, 0.19 mmol). Isolated by column: ethyl acetate/hexane = 10%. White-brown solid. ^{1}H NMR (500 MHz, $CDCl_3$) δ 5.37 (dd, *J* = 4.6, 2.7 Hz, 1H), 4.61 (dtt, *J* = 14.8, 6.2, 3.2 Hz, 1H), 4.41 (ddd, *J* = 8.7, 7.5, 6.4 Hz, 1H), 3.47 (ddd, *J* = 10.8, 4.4, 2.0 Hz, 1H), 3.37 (t, *J* = 11.0 Hz, 1H), 2.36 – 2.29 (m, 2H), 2.27 (t, *J* = 7.6 Hz, 2H), 1.99 (ddt, *J* = 17.4, 7.5, 5.2 Hz, 2H), 1.90 – 1.81 (m, 3H), 1.81 – 1.69 (m, 2H), 1.69 – 1.56 (m, 8H), 1.55 – 1.48 (m, 2H), 1.44 (ddd, *J* = 17.9, 8.8, 5.1 Hz, 2H), 1.39 – 1.31 (m, 2H), 1.29 (ddd, *J* = 13.9, 6.9, 4.6 Hz, 1H), 1.24 – 1.07 (m, 3H), 1.04 (s, 3H), 0.97 (d, *J* = 7.0 Hz, 4H), 0.91 (t, *J* = 7.4 Hz, 3H), 0.79 (t, *J* = 3.2 Hz, 6H). ^{13}C NMR (126 MHz, $CDCl_3$) δ 173.3, 139.8, 122.3, 109.3, 80.8, 77.3, 77.2, 77.0, 76.8, 73.6, 66.9, 62.1, 56.4, 50.0, 41.6, 40.3, 39.7, 38.1, 37.0, 36.8, 34.4, 32.1, 31.9, 31.4, 31.4, 30.3, 28.8, 27.8, 27.2, 22.3, 20.8, 19.4, 17.1, 16.3, 14.5, 13.8. HRMS (ESI) calculated for $C_{32}H_{50}NaO_4$: *m/z* = 521.36068 ($[M+Na]^+$),found: *m/z* = 521.35938 ($[M+Na]^+$).

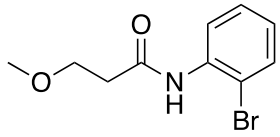

***N*-(2-bromophenyl)-3-methoxypropanamide, 4g**. 81% isolated yield (52 mg, 0.20 mmol). Isolated by column: ethyl acetate/hexane = 30%.^{1}H NMR (500 MHz, $CDCl_3$) δ 8.92 (s, 1H), 8.39 (dd, *J* = 8.3, 1.6 Hz, 2H), 7.53 (dd, *J* = 8.0, 1.5 Hz, 2H), 7.30 (ddd, *J* = 8.6, 7.2, 1.5 Hz, 2H), 6.96 (td, *J* = 7.7, 1.6 Hz, 2H), 3.78 – 3.71 (m, 4H), 3.48 (s, 5H), 2.73 – 2.67 (m, 3H). ^{13}C NMR (126 MHz, $CDCl_3$) δ 170.1, 136.4, 132.3, 128.3, 124.9, 122.1, 113.1, 77.3, 77.0, 76.8, 68.3, 59.1, 38.3. HRMS (ESI) calculated for $C_{10}H_{12}BrNNaO_2$: *m/z* = 279.9949 ($[M+Na]^+$),found: *m/z* = 279.9944 ($[M+Na]^+$).

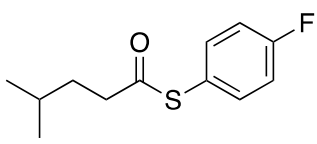

***S*-(4-fluorophenyl) 4-methylpentanethioate, 4h**. 65% isolated yield (37 mg, 0.16 mmol). Isolated by column: ethyl acetate/hexane = 30%.Yellow oil. ^{1}H NMR (500 MHz, $CDCl_3$) δ 7.37 (m, 2H), 7.10 (m, 2H), 2.66 (t, 2H), 1.61 (m, 3H), 0.93 (s, 6H). ^{13}C NMR (126 MHz, $CDCl_3$) δ 197.7, 164.4, 162.4, 136.6, 136.5, 116.5, 116.3, 41.8, 34.3, 27.6, 22.2. ^{19}F NMR (471 MHz, $CDCl_3$) δ -111.40. HRMS (ESI) calculated for $C_{12}H_{15}FNaOS$: *m/z* = 249.0725 ($[M+Na]^+$),found: *m/z* = 249.0708 ($[M+Na]^+$).

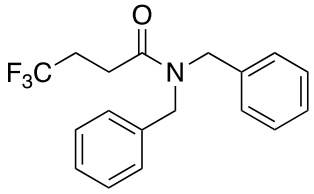

***N*,*N*-dibenzyl-4,4,4-trifluorobutanamide, 4i**. 95% isolated yield (76 mg, 0.24 mmol). isolated by column: ethyl acetate/hexane = 20%.^{1}H NMR (400 MHz, $CDCl_3$) δ 7.43 – 7.26 (m, 3H), 7.25 – 7.18 (m, 1H), 7.18 – 7.11 (m, 1H), 4.63 (s, 1H), 4.46 (s, 1H), 2.71 – 2.52 (m, 2H). ^{13}C NMR (126 MHz, $CDCl_3$) δ 170.4, 137.0, 135.9, 129.1, 128.7, 128.3, 127.9, 127.6, 126.3, 77.3, 77.0, 76.8, 49.9, 48.6, 30.1, 29.8, 29.6, 26.1, 26.0. ^{13}C NMR (126 MHz, $CDCl_3$) δ 170.4, 137.0, 135.9, 129.1, 128.7, 128.3, 127.9, 127.6, 126.3, 77.3, 77.0, 76.8, 49.9, 48.6, 30.1, 29.8, 29.6, 26.1, 26.0. HRMS (ESI) calculated for $C_{18}H_{18}F_3NNaO$: *m/z* = 344.1238 ([M+Na]$^+$),found: *m/z* = 344.1227 ([M+Na]$^+$).

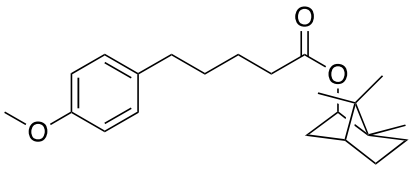

(2*R*,4*S*)-1,7,7-trimethylbicyclo[2.2.1]heptan-2-yl5-(4-methoxyphenyl)pentanoate, 4j. 56% isolated yield (51 mg, 0.14 mmol). Isolated by column: ethyl acetate/hexane = 15%.Yellow oil.^{1}H NMR (500 MHz, $CDCl_3$) δ 7.08 (d, *J* = 8.7 Hz, 2H), 6.82 (d, *J* = 8.7 Hz, 2H), 4.71 – 4.63 (m, 1H), 3.81 – 3.76 (m, 3H), 3.54 (t, *J* = 6.5 Hz, 1H), 2.56 (t, *J* = 7.3 Hz, 2H), 2.29 (t, *J* = 7.2 Hz, 2H), 1.87 – 1.50 (m, 9H), 1.21 – 1.02 (m, 2H), 0.96 (s, 3H), 0.83 (d, *J* = 4.1 Hz, 5H). ^{13}C NMR (126 MHz, $CDCl_3$) δ 173.16, 157.74, 134.28, 129.26, 113.74, 80.78, 55.27, 48.63, 46.92, 45.05, 38.86, 34.68, 34.66, 33.76, 31.18, 27.05, 24.65, 20.13, 19.92, 11.47. HRMS (ESI) calculated for $C_{22}H_{32}NaO_3$: *m/z* = 367.22492 ([M+Na]$^+$), found: *m/z* = 367.22444([M+Na]$^+$).

***sec*-butyl 2-(2-((4-cyano-4,4 diphenylbutanoyl)oxy)ethyl)piperidine-1-carboxylate, 4k**. 34% isolated yield (41 mg, 0.090 mmol). isolated by column: ethyl acetate/hexane = 20%.Clear oil. ^{1}H NMR (500 MHz, $CDCl_3$) δ 7.45 – 7.28 (m, 10H), 4.78 – 4.66 (m, 1H), 4.38 (s, 1H), 4.03 (dp, *J* = 15.5, 4.5 Hz, 3H), 2.86 – 2.67 (m, 3H), 2.55 – 2.37 (m, 2H), 2.11 – 2.00 (m, 1H), 1.75 – 1.66 (m, 1H), 1.64 – 1.58 (m, 3H), 1.56 – 1.45 (m, 4H), 1.29 – 1.23 (m, 1H), 1.17 (dd, *J* = 6.3, 3.3 Hz, 3H), 0.87 (t, *J* = 7.4 Hz, 3H). ^{13}C NMR (126 MHz, $CDCl_3$) δ 172.14, 155.49, 139.41, 129.04, 128.13, 126.85, 121.73, 77.28, 77.03, 76.77, 73.00, 72.93, 62.48, 50.91, 47.71, 34.35, 30.73, 29.12, 29.08, 28.72, 19.83, 19.78, 19.05, 9.74, 9.69. HRMS (ESI) calculated for $C_{29}H_{36}O_4N_2Na$: *m/z* 499.25728 ([M+Na]$^+$), found: *m/z* 499.26711 ([M+Na]$^+$).

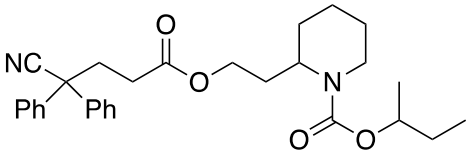

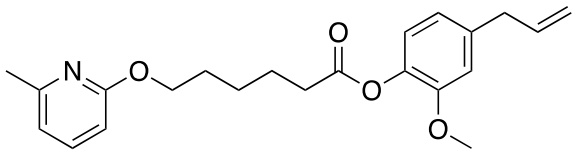

4-allyl-2-methoxyphenyl 6-((6-methylpyridin-2-yl)oxy)hexanoate, 4l. 76% isolated yield (70 mg, 0.19 mmol) Isolated by column: ethyl acetate/hexane = 25%.^{1}H NMR (500 MHz, $CDCl_3$) δ 7.44 (dd, *J* = 8.2, 7.2 Hz, 1H), 6.93 (d, *J* = 7.9 Hz, 1H), 6.83 – 6.72 (m, 2H), 6.69 (d, *J* = 7.2 Hz, 1H), 6.54 – 6.43 (m, 1H), 5.96 (ddt, *J* = 16.8, 10.1, 6.7 Hz, 1H), 5.22 – 4.99 (m, 2H), 4.29 (t, *J* = 6.5 Hz, 2H), 3.80 (s, 3H), 3.37 (dt, *J* = 6.8, 1.5 Hz, 2H), 2.60 (t, *J* = 7.5 Hz, 2H), 2.43 (s, 3H), 1.84 (dtd, *J* = 14.3, 7.1, 4.7 Hz, 4H), 1.64 – 1.57 (m, 2H). ^{13}C NMR (126 MHz, $CDCl_3$) δ 171.89, 163.51, 156.31, 150.90, 138.87, 138.72, 138.06, 137.11, 122.53, 120.67, 116.12, 115.58, 112.71, 107.07, 65.50, 55.80, 40.10, 33.99, 28.83, 25.66, 24.86, 24.22. HRMS (ESI) calculated for $C_{22}H_{28}O_4N$: *m/z* 370.20183 ($[M+H]^+$), found: *m/z* 370.20126 ($[M+H]^+$)

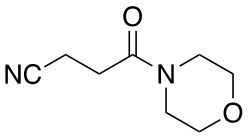

4-morpholino-4-oxobutanenitrile, 4m. 58% isolated yield (24 mg, 0.14 mmol). Isolated by column: ethyl acetate/hexane = 15%.Clear oil, hint of yellow. ^{1}H NMR (500 MHz, $CDCl_3$) δ 3.69 (q, *J* = 4.4 Hz, 4H), 3.66 – 3.57 (m, 2H), 3.49 – 3.37 (m, 2H), 2.78 – 2.62 (m, 4H). ^{13}C NMR (126 MHz, $CDCl_3$) δ 167.44, 119.27, 66.76, 66.39, 45.60, 42.24, 29.04, 13.05. HRMS (ESI) calculated for $C_8H_{12}O_2N_2Na$: *m/z* 191.07965 ($[M+Na]^+$), found: *m/z* 191.07885 ($[M+Na]^+$).

(2*R*,3*R*,4*S*,5*R*,6*R*)-2-((benzoyloxy)methyl)-6-((3 (benzyloxy)propanoyl)oxy)tetrahydro-2*H*-pyran-3,4,5-triyl tribenzoate, 4n. 42% isolated yield (74 mg, 0.11 mmol). Isolated by column: ethyl acetate/hexane = 10%. Yellow Oil. ^{1}H NMR (500 MHz, $CDCl_3$) δ 7.43 – 7.26 (m, 22H), 7.26 – 7.20 (m, 1H), 7.19 – 7.08 (m, 2H), 6.39 (d, *J* = 3.5 Hz, 1H), 5.13 – 4.32 (m, 10H), 3.98 – 3.51 (m, 8H), 2.80 – 2.50 (m, 2H). ^{13}C NMR (126 MHz, $CDCl_3$) δ 170.13, 169.99, 138.66, 138.41, 138.11, 138.05, 137.98, 137.93, 137.85, 137.66, 128.46, 128.41, 128.38, 128.12, 127.98, 127.93, 127.89, 127.88, 127.80, 127.78, 127.75, 127.70, 127.69, 127.65, 127.63, 94.19, 90.19, 84.78, 81.71, 80.98, 78.85, 75.73, 75.67, 75.55, 75.28, 75.02, 74.97, 73.54, 73.15, 72.84, 68.11, 67.98, 65.59, 65.12, 35.30, 35.21. HRMS (ESI) calculated for $C_{44}H_{46}O_8Na$: *m/z* 725.310904 ($[M+Na]^+$), found: *m/z* 725.30751 ($[M+Na]^+$).

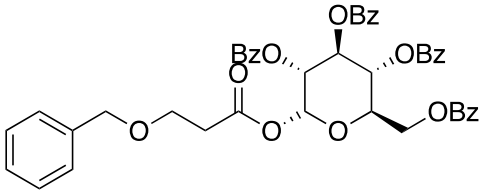

4.10 X-Ray Structural Data of XantphosNi(CO)$_2$

X-ray quality crystals of XantphosNi(CO)$_2$ were grown by dissolving 45 mg in 20 mL of benzene and allowing slow evaporation of the solvent. Suitable crystals for x-ray analysis were taken out of a glovebox and submerged in paratone oil, placed onto a mounting loop. Single crystal X-ray diffraction (SCXRD) data were measured on a Bruker D8 Venture diffractometer equipped with a Photon 200 area detector, and IμS microfocus X-ray source (Bruker AXS, CuKα source). Data were collected in a series of φ- and ω-scans. APEX3 software was used for data collection, integration and reduction.[26] Multi-scan absorption correction was applied using SADABS-2016/2.[27] Intrinsic phasing was used to generate the initial solutions. Final solution refinements were solved by full-matrix least-squares methods on F^2 of all data,[27] by using SHELXLE software.[28] All of the nonhydrogen atoms were refined with anisotropic thermal parameters. All hydrogen atom thermal parameters were constrained to ride on the carrier atom. SHELX restraints such as, EADP, DFIX, were applied in order to model the disordered benzene solvent in the structure as well as using fractional occupancy when it applies. Measurements for XantphosNi(CO)$_2$ were performed at -20(2) °C. The ORTEP representations of the structures were produced by MERCURY 4.0.[29] Olex2 was used to model the disorder and generate the data tables and report.[30]

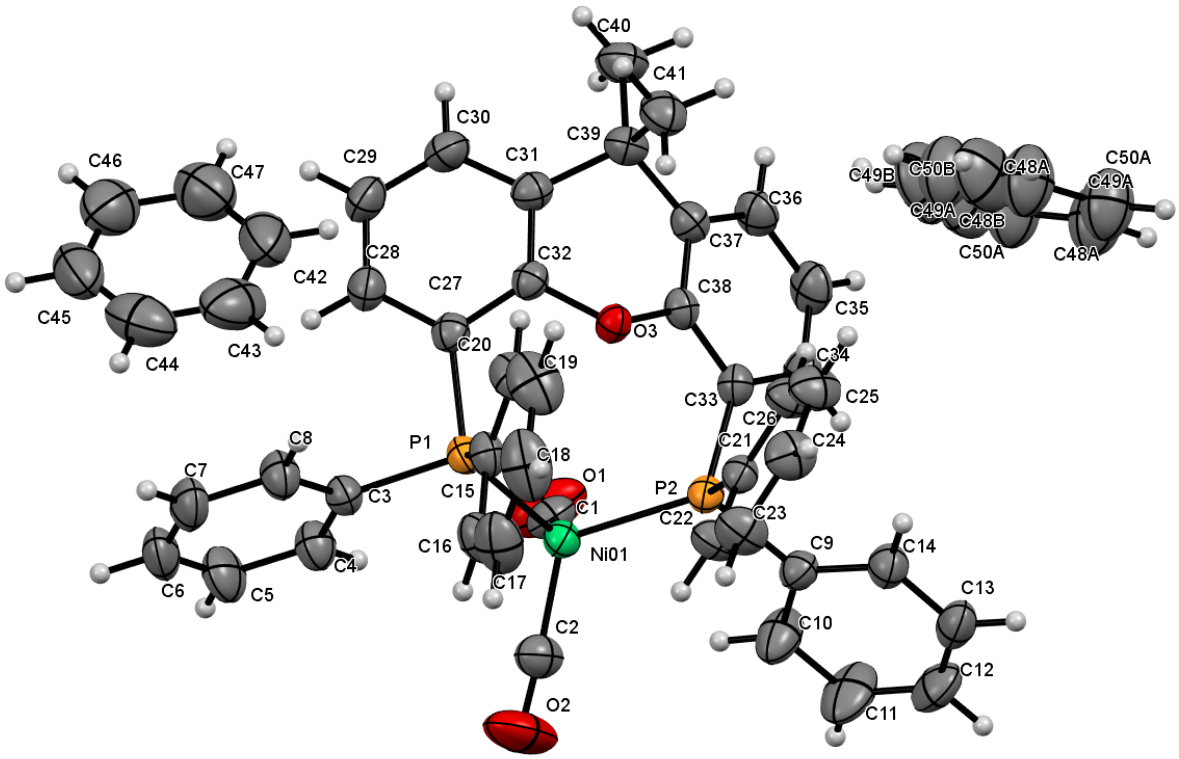

Table 1 - Crystal data and structure refinement for XantphosNiCO2.

Identification code	XantphosNiCO2
Empirical formula	$C_{50}H_{41}NiO_3P_2$
Formula weight	810.48
Temperature/K	253(2)
Crystal system	triclinic
Space group	P-1
a/Å	9.6574(2)
b/Å	14.3559(4)
c/Å	16.3303(4)
α/°	105.7660(10)
β/°	102.8050(10)
γ/°	95.3450(10)
Volume/Å^3	2096.11(9)
Z	2
ρ_{calc}g/cm^3	1.284
μ/mm^{-1}	1.713
F(000)	846.0
Crystal size/mm^3	0.322 × 0.218 × 0.198
Radiation	CuKα (λ = 1.54178)
2Θ range for data collection/°	5.82 to 144.908

Index ranges	$-11 \leq h \leq 10$, $-17 \leq k \leq 17$, $-20 \leq l \leq 20$
Reflections collected	78133
Independent reflections	8204 [R_{int} = 0.0378, R_{sigma} = 0.0174]
Data/restraints/parameters	8204/10/511
Goodness-of-fit on F^2	1.099
Final R indexes [I>=2σ (I)]	R_1 = 0.0383, wR_2 = 0.0927
Final R indexes [all data]	R_1 = 0.0437, wR_2 = 0.0971
Largest diff. peak/hole / e $Å^{-3}$	0.33/-0.29

Table 2 - Fractional Atomic Coordinates (×10^4) and Equivalent Isotropic Displacement Parameters (Å^2×10^3) for XantphosNiCO2. U_{eq} is defined as 1/3 of of the trace of the orthogonalised U_{IJ} tensor.

Atom	*x*	*y*	*z*	U(eq)
Ni01	6772.3(3)	7866.5(2)	7886.6(2)	36.23(9)
P1	5278.4(5)	6581.7(3)	7895.0(3)	35.35(11)
O1	8521(2)	7402.0(16)	6641.1(14)	94.6(7)
C1	7802(2)	7548.4(15)	7114.5(15)	50.1(5)
O2	8658(2)	8660.2(18)	9656.9(13)	98.2(7)
P2	5442.4(5)	8895.8(3)	7410.6(3)	34.72(11)
C2	7875(2)	8372.7(17)	8975.6(15)	53.3(5)
O3	3538.6(13)	7108.6(8)	6458.3(8)	35.0(3)
C3	6179(2)	5753.6(14)	8436.2(12)	40.5(4)
C4	7623(2)	5737.3(16)	8484.6(15)	51.5(5)
C5	8331(3)	5095.8(19)	8858.5(18)	65.8(7)
C6	7605(3)	4473.4(18)	9191.7(17)	62.7(6)
C7	6175(3)	4489.3(17)	9149.6(16)	61.3(6)
C8	5457(2)	5124.8(16)	8777.2(15)	52.0(5)
C9	6385(2)	10131.8(13)	7591.0(13)	40.3(4)
C14	5677(2)	10919.8(15)	7549.9(14)	47.8(5)
C12	7894(3)	11979.5(17)	7855.5(18)	66.3(7)
C10	7863(3)	10293.9(18)	7785(2)	72.3(8)
C11	8611(3)	11217(2)	7909(3)	92.1(11)
C13	6434(3)	11837.6(15)	7685.7(15)	54.6(5)
C15	3904(2)	6872.7(14)	8495.7(13)	40.9(4)
C16	4366(3)	7337.2(18)	9396.3(15)	55.6(5)
C17	3380(3)	7603(2)	9885.7(17)	70.4(7)
C19	1474(3)	6986(2)	8593(2)	74.6(8)
C18	1938(3)	7429(2)	9481(2)	77.3(8)
C20	2444(2)	6698.1(19)	8092.4(16)	56.1(5)
C21	3860.9(19)	9173.2(13)	7813.1(12)	36.4(4)

C22	4005(2)	9392.5(16)	8712.1(14)	49.6(5)
C23	2862(3)	9635.6(19)	9063.4(15)	58.6(6)
C24	1561(2)	9647.8(18)	8528.9(16)	56.9(6)
C25	1392(2)	9417.3(18)	7631.4(16)	58.5(6)
C26	2539(2)	9184.1(16)	7276.7(14)	48.6(5)
C27	4267(2)	5719.4(13)	6828.7(12)	38.0(4)
C28	4269(2)	4707.0(15)	6565.1(15)	48.8(5)
C29	3634(3)	4150.8(15)	5703.3(16)	57.0(6)
C30	2994(2)	4574.7(15)	5082.2(15)	52.8(5)
C31	2933(2)	5571.2(14)	5315.1(13)	41.0(4)
C32	3566.7(19)	6106.2(13)	6188.5(12)	35.4(4)
C33	4712(2)	8476.6(13)	6214.7(12)	36.8(4)
C34	5064(2)	8938.7(15)	5618.7(14)	48.0(5)
C35	4539(3)	8487.2(17)	4720.8(15)	56.1(6)
C36	3641(3)	7589.9(16)	4392.9(14)	50.8(5)
C37	3251(2)	7107.7(14)	4962.6(12)	40.7(4)
C38	3827(2)	7569.5(13)	5854.4(12)	35.7(4)
C39	2248(2)	6127.2(15)	4699.3(13)	44.5(4)
C40	2008(3)	5550.7(18)	3727.9(14)	61.4(6)
C41	777(2)	6335.3(18)	4869.6(16)	56.1(5)
C42	1654(4)	3704(2)	7622(2)	98.7(12)
C43	1816(3)	3847(2)	8523(2)	100.1(12)
C44	2214(4)	3140(2)	8882(2)	98.7(11)
C45	2462(3)	2259(2)	8346(2)	95.8(11)
C46	2270(4)	2117(2)	7477(2)	94.7(10)
C47	1871(4)	2856(2)	7107(2)	97.4(10)
C48A	646(11)	9151(5)	4895(7)	93.3(19)
C49A	-511(12)	9235(7)	5229(5)	93.3(19)
C50A	1162(9)	9956(9)	4647(6)	93.3(19)
C48B	-1023(11)	9622(14)	5372(7)	110(3)
C49B	-28(18)	9073(7)	5149(8)	110(3)
C50B	981(15)	9484(13)	4786(8)	110(3)

Table 3 - Anisotropic Displacement Parameters ($Å^2 \times 10^3$) for XantphosNiCO2. The Anisotropic displacement factor exponent takes the form: $-2\pi^2[h^2a^{*2}U_{11}+2hka^*b^*U_{12}+\ldots]$.

Atom	U_{11}	U_{22}	U_{33}	U_{23}	U_{13}	U_{12}
Ni01	31.17(17)	35.45(17)	41.75(18)	11.83(13)	8.24(13)	6.15(12)
P1	32.0(2)	37.2(2)	39.5(2)	16.27(19)	8.21(18)	6.55(18)
O1	90.7(15)	85.3(14)	92.4(14)	-18.5(11)	60.3(13)	-12.9(11)
C1	46.9(12)	40.1(10)	55.6(12)	2.3(9)	15.8(10)	-1.5(9)
O2	80.2(14)	124.1(18)	54.2(11)	-10.1(11)	-12.9(10)	23.5(13)
P2	31.3(2)	32.4(2)	41.0(2)	12.12(18)	8.89(18)	5.27(17)
C2	46.8(12)	55.0(13)	51.2(12)	5.7(10)	8.8(10)	14.7(10)
O3	39.4(7)	32.0(6)	35.6(6)	11.8(5)	11.7(5)	5.4(5)
C3	41.7(10)	40.4(10)	40.6(10)	16.9(8)	6.9(8)	7.6(8)
C4	45.4(12)	55.1(12)	62.5(13)	27.4(11)	16.0(10)	15.6(10)
C5	54.1(14)	70.7(16)	82.1(17)	33.1(14)	15.2(12)	31.4(12)
C6	77.0(17)	53.3(13)	64.0(14)	27.5(11)	10.5(12)	29.8(12)
C7	79.9(17)	49.3(12)	63.6(14)	31.6(11)	17.3(12)	13.9(12)
C8	49.8(12)	51.3(12)	63.1(13)	29.8(10)	14.6(10)	11.1(9)
C9	39.5(10)	34.8(9)	44.9(10)	10.8(8)	10.3(8)	2.5(7)
C14	49.3(12)	41.9(10)	54.4(12)	18.5(9)	12.6(9)	7.4(9)
C12	77.4(18)	41.4(12)	75.1(16)	14.8(11)	21.5(14)	-12.1(11)
C10	41.6(12)	47.1(13)	127(2)	25.7(14)	21.6(14)	4.9(10)
C11	47.2(15)	59.0(16)	164(3)	31.0(19)	25.1(18)	-8.4(12)
C13	76.9(16)	37.2(10)	51.8(12)	15.6(9)	18.8(11)	7.8(10)
C15	41.9(10)	43.2(10)	46.6(10)	23.0(8)	15.9(8)	11.9(8)
C16	60.2(14)	65.7(14)	48.6(12)	23.9(11)	17.2(10)	19.9(11)
C17	97(2)	79.4(18)	55.8(14)	32.0(13)	38.7(14)	36.1(16)
C19	49.4(14)	106(2)	93(2)	50.3(18)	36.9(14)	25.1(14)
C18	85(2)	98(2)	90(2)	55.3(18)	60.0(17)	45.7(17)
C20	40.4(11)	72.6(15)	62.9(14)	29.3(12)	17.5(10)	9.0(10)
C21	33.6(9)	31.6(8)	44.3(10)	11.4(7)	10.7(7)	5.4(7)
C22	41.8(11)	61.5(13)	42.6(11)	12.4(9)	7.1(9)	13.6(9)
C23	58.5(14)	71.9(15)	47.6(12)	13.5(11)	19.9(10)	20.0(12)
C24	43.4(12)	63.5(14)	64.8(14)	11.6(11)	22.8(10)	14.8(10)
C25	36.2(11)	68.7(15)	63.7(14)	10.3(12)	8.2(10)	15.8(10)
C26	38.8(10)	57.1(12)	45.1(11)	9.1(9)	7.1(8)	11.9(9)
C27	35.1(9)	35.2(9)	44.4(10)	13.5(8)	10.8(8)	3.2(7)
C28	50.6(12)	38.4(10)	58.1(12)	18.4(9)	9.9(10)	8.9(9)
C29	61.9(14)	33.1(10)	68.3(14)	8.5(10)	9.5(11)	7.9(9)
C30	54.9(13)	41.0(11)	50.7(12)	3.0(9)	5.3(10)	3.5(9)
C31	37.8(10)	40.5(10)	42.1(10)	9.5(8)	9.5(8)	4.4(8)

C32	33.9(9)	33.1(9)	40.1(9)	11.2(7)	11.6(7)	4.2(7)
C33	37.8(9)	34.9(9)	41.8(10)	14.9(8)	13.0(8)	9.4(7)
C34	56.5(12)	39.9(10)	54.0(12)	20.7(9)	19.4(10)	6.7(9)
C35	75.7(16)	55.2(13)	50.0(12)	29.2(10)	24.8(11)	11.3(11)
C36	65.5(14)	53.2(12)	37.5(10)	18.0(9)	13.9(9)	13.2(10)
C37	41.4(10)	43.9(10)	38.4(10)	14.1(8)	10.1(8)	9.8(8)
C38	37.2(9)	37.3(9)	38.4(9)	16.6(7)	13.3(7)	9.6(7)
C39	43.5(11)	47.0(11)	38.5(10)	10.8(8)	5.3(8)	5.2(8)
C40	69.3(16)	62.3(14)	40.1(11)	8.3(10)	1.2(10)	0.8(12)
C41	42.1(12)	62.1(14)	63.3(14)	23.0(11)	6.3(10)	8.7(10)
C42	77(2)	79(2)	127(3)	45(2)	-15(2)	3.9(17)
C43	62.2(19)	94(2)	113(3)	1(2)	-3.7(18)	20.0(17)
C44	71(2)	135(3)	80(2)	36(2)	2.7(17)	-4(2)
C45	71(2)	90(2)	123(3)	60(2)	-9.7(19)	-2.1(17)
C46	73(2)	87(2)	110(3)	18(2)	7.5(19)	20.2(17)
C47	91(2)	110(3)	90(2)	41(2)	11.3(19)	7(2)
C48A	91(3)	85(3)	125(4)	44(3)	48(3)	33(2)
C49A	91(3)	85(3)	125(4)	44(3)	48(3)	33(2)
C50A	91(3)	85(3)	125(4)	44(3)	48(3)	33(2)
C48B	101(4)	122(5)	121(5)	36(4)	37(4)	68(4)
C49B	101(4)	122(5)	121(5)	36(4)	37(4)	68(4)
C50B	101(4)	122(5)	121(5)	36(4)	37(4)	68(4)

Table 4 - Bond Lengths for XantphosNiCO2.

Atom	Atom	Length/Å	Atom	Atom	Length/Å
Ni01	C1	1.765(2)	C21	C22	1.387(3)
Ni01	C2	1.772(2)	C22	C23	1.382(3)
Ni01	P2	2.2299(5)	C23	C24	1.367(3)
Ni01	P1	2.2383(5)	C24	C25	1.380(3)
P1	C15	1.832(2)	C25	C26	1.386(3)
P1	C27	1.8353(19)	C27	C32	1.390(3)
P1	C3	1.8369(19)	C27	C28	1.399(3)
O1	C1	1.140(3)	C28	C29	1.382(3)
O2	C2	1.140(3)	C29	C30	1.382(3)
P2	C21	1.8275(19)	C30	C31	1.387(3)
P2	C33	1.8290(19)	C31	C32	1.389(3)
P2	C9	1.8329(19)	C31	C39	1.525(3)
O3	C38	1.389(2)	C33	C38	1.388(3)
O3	C32	1.391(2)	C33	C34	1.399(3)

C3	C4	1.381(3)	C34	C35	1.386(3)
C3	C8	1.393(3)	C35	C36	1.382(3)
C4	C5	1.388(3)	C36	C37	1.394(3)
C5	C6	1.379(4)	C37	C38	1.385(3)
C6	C7	1.370(4)	C37	C39	1.529(3)
C7	C8	1.384(3)	C39	C40	1.531(3)
C9	C10	1.375(3)	C39	C41	1.547(3)
C9	C14	1.384(3)	C42	C47	1.3434(19)
C14	C13	1.382(3)	C42	C43	1.3996(19)
C12	C13	1.359(4)	C43	C44	1.3483(19)
C12	C11	1.361(4)	C44	C45	1.4032(19)
C10	C11	1.389(3)	C45	C46	1.3459(19)
C15	C20	1.385(3)	C46	C47	1.3989(19)
C15	C16	1.388(3)	C48A	C49A	1.349(2)
C16	C17	1.389(3)	C48A	C50A	1.408(2)
C17	C18	1.371(4)	C49A	C50A[1]	1.360(9)
C19	C18	1.366(4)	C48B	C49B	1.349(2)
C19	C20	1.394(3)	C48B	C50B[1]	1.376(13)
C21	C26	1.383(3)	C49B	C50B	1.410(2)

[1]-X,2-Y,1-Z

Table 5 - Bond Angles for XantphosNiCO2.

Atom	Atom	Atom	Angle/°	Atom	Atom	Atom	Angle/°
C1	Ni01	C2	111.81(10)	C23	C22	C21	120.7(2)
C1	Ni01	P2	103.83(8)	C24	C23	C22	120.6(2)
C2	Ni01	P2	114.00(7)	C23	C24	C25	119.5(2)
C1	Ni01	P1	112.89(7)	C24	C25	C26	120.2(2)
C2	Ni01	P1	106.37(8)	C21	C26	C25	120.7(2)
P2	Ni01	P1	108.03(2)	C32	C27	C28	116.31(18)
C15	P1	C27	104.05(9)	C32	C27	P1	117.81(13)
C15	P1	C3	101.62(9)	C28	C27	P1	125.46(15)
C27	P1	C3	101.34(9)	C29	C28	C27	120.3(2)
C15	P1	Ni01	115.94(7)	C28	C29	C30	121.28(19)
C27	P1	Ni01	117.75(6)	C29	C30	C31	120.6(2)
C3	P1	Ni01	113.91(7)	C30	C31	C32	116.56(18)
O1	C1	Ni01	175.5(2)	C30	C31	C39	125.94(18)
C21	P2	C33	102.88(8)	C32	C31	C39	117.50(17)
C21	P2	C9	101.23(8)	C31	C32	O3	119.00(16)
C33	P2	C9	101.84(9)	C31	C32	C27	124.86(17)

C21	P2	Ni01	120.05(6)	O3	C32	C27	116.13(16)
C33	P2	Ni01	112.18(6)	C38	C33	C34	116.48(18)
C9	P2	Ni01	116.26(7)	C38	C33	P2	117.02(13)
O2	C2	Ni01	175.0(2)	C34	C33	P2	126.21(15)
C38	O3	C32	112.76(13)	C35	C34	C33	120.03(19)
C4	C3	C8	118.86(18)	C36	C35	C34	121.39(19)
C4	C3	P1	118.47(15)	C35	C36	C37	120.51(19)
C8	C3	P1	122.65(16)	C38	C37	C36	116.41(18)
C3	C4	C5	120.3(2)	C38	C37	C39	117.14(17)
C6	C5	C4	120.4(2)	C36	C37	C39	126.45(18)
C7	C6	C5	119.6(2)	C37	C38	C33	125.14(17)
C6	C7	C8	120.5(2)	C37	C38	O3	119.46(16)
C7	C8	C3	120.3(2)	C33	C38	O3	115.39(16)
C10	C9	C14	117.98(19)	C31	C39	C37	105.81(15)
C10	C9	P2	118.98(16)	C31	C39	C40	112.35(18)
C14	C9	P2	123.03(15)	C37	C39	C40	112.62(18)
C13	C14	C9	120.9(2)	C31	C39	C41	109.01(17)
C13	C12	C11	119.7(2)	C37	C39	C41	108.29(17)
C9	C10	C11	120.5(2)	C40	C39	C41	108.63(18)
C12	C11	C10	120.5(3)	C47	C42	C43	120.2(3)
C12	C13	C14	120.3(2)	C42	C43	C44	120.2(3)
C20	C15	C16	118.7(2)	C43	C44	C45	119.6(3)
C20	C15	P1	123.47(16)	C46	C45	C44	119.9(3)
C16	C15	P1	117.79(16)	C45	C46	C47	120.4(3)
C15	C16	C17	120.6(2)	C42	C47	C46	119.6(3)
C18	C17	C16	120.3(3)	C49A	C48A	C50A	116.3(7)
C18	C19	C20	121.1(3)	C48A	C49A	C50A[1]	124.0(6)
C19	C18	C17	119.5(2)	C49A[1]	C50A	C48A	119.6(6)
C15	C20	C19	119.8(2)	C49B	C48B	C50B[1]	117.7(10)
C26	C21	C22	118.31(18)	C48B	C49B	C50B	116.3(10)
C26	C21	P2	123.95(15)	C48B[1]	C50B	C49B	126.0(8)
C22	C21	P2	117.74(14)				

[1]-X,2-Y,1-Z

Table 6 - Hydrogen Atom Coordinates (Å×10^4) and Isotropic Displacement Parameters (Å^2×10^3) for XantphosNiCO2.

Atom	*x*	*y*	*z*	U(eq)
H4	8122.28	6158.09	8265.59	62
H5	9301.46	5085.57	8884.56	79
H6	8083.28	4045.68	9443.23	75
H7	5683.41	4069.75	9373.18	74
H8	4487.44	5131.92	8754.64	62
H14	4678.33	10830.26	7429.15	57
H12	8399.58	12594.6	7934.55	80
H10	8366.15	9781.43	7833.5	87
H11	9609.9	11314.87	8030.23	111
H13	5942.7	12360.53	7660.89	66
H16	5344.45	7471.49	9674.63	67
H17	3701	7901.05	10490.71	84
H19	495.79	6874.38	8317.36	89
H18	1278.66	7610.92	9807.92	93
H20	2111.09	6389.85	7489.47	67
H22	4878.88	9375.92	9082.71	59
H23	2980.35	9792.11	9668.58	70
H24	794.69	9810.24	8768.02	68
H25	507.16	9418.33	7263.49	70
H26	2417.86	9033.39	6671.62	58
H28	4698.84	4407.23	6971.69	59
H29	3638.83	3478.21	5538.17	68
H30	2598.92	4188.1	4502.37	63
H34	5650.49	9549.17	5825.38	58
H35	4796.01	8794.52	4330.68	67
H36	3293.71	7305.42	3787.43	61
H40A	1606.03	5936.04	3366.18	92
H40B	1356.93	4949.96	3592.08	92
H40C	2911.06	5404.52	3616.08	92
H41A	365.19	6719.12	4509.11	84
H41B	910.83	6690.14	5478.93	84
H41C	142	5725.78	4726.42	84
H42	1394.53	4198.14	7379.63	118
H43	1647.48	4430.74	8875.25	120
H44	2325.02	3235.06	9480.89	118
H45	2757.09	1773.71	8591.35	115
H46	2404.33	1524.89	7119.26	114
H47	1757.64	2759.78	6507.81	117

H1AA	1078.66	8592.47	4831.24	112
H2AA	-887.3	8706.3	5383.79	112
H0AA	1942.6	9934.13	4399.85	112
H2AB	-1714.45	9403.29	5623.14	132
H1AB	-7.49	8457.1	5230.81	132
H0AB	1683.41	9115.96	4640.23	132

Table 7 - Atomic Occupancy for XantphosNiCO2.

Atom	***Occupancy***	**Atom**	***Occupancy***	**Atom**	***Occupancy***
C48A	0.549(14)	H1AA	0.549(14)	C49A	0.549(14)
H2AA	0.549(14)	C50A	0.549(14)	H0AA	0.549(14)
C48B	0.451(14)	H2AB	0.451(14)	C49B	0.451(14)
H1AB	0.451(14)	C50B	0.451(14)	H0AB	0.451(14)

4.11 NMR Spectra

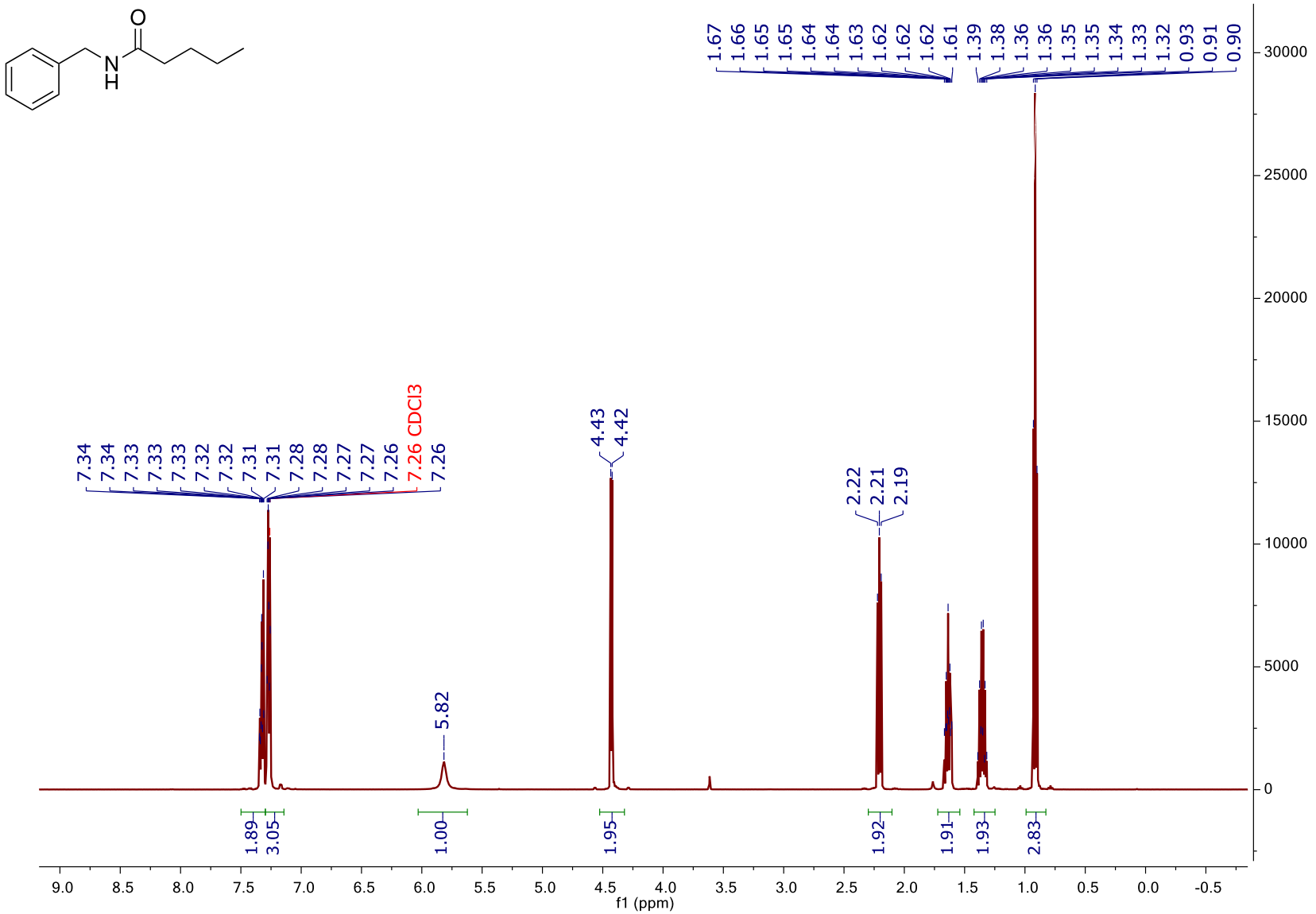

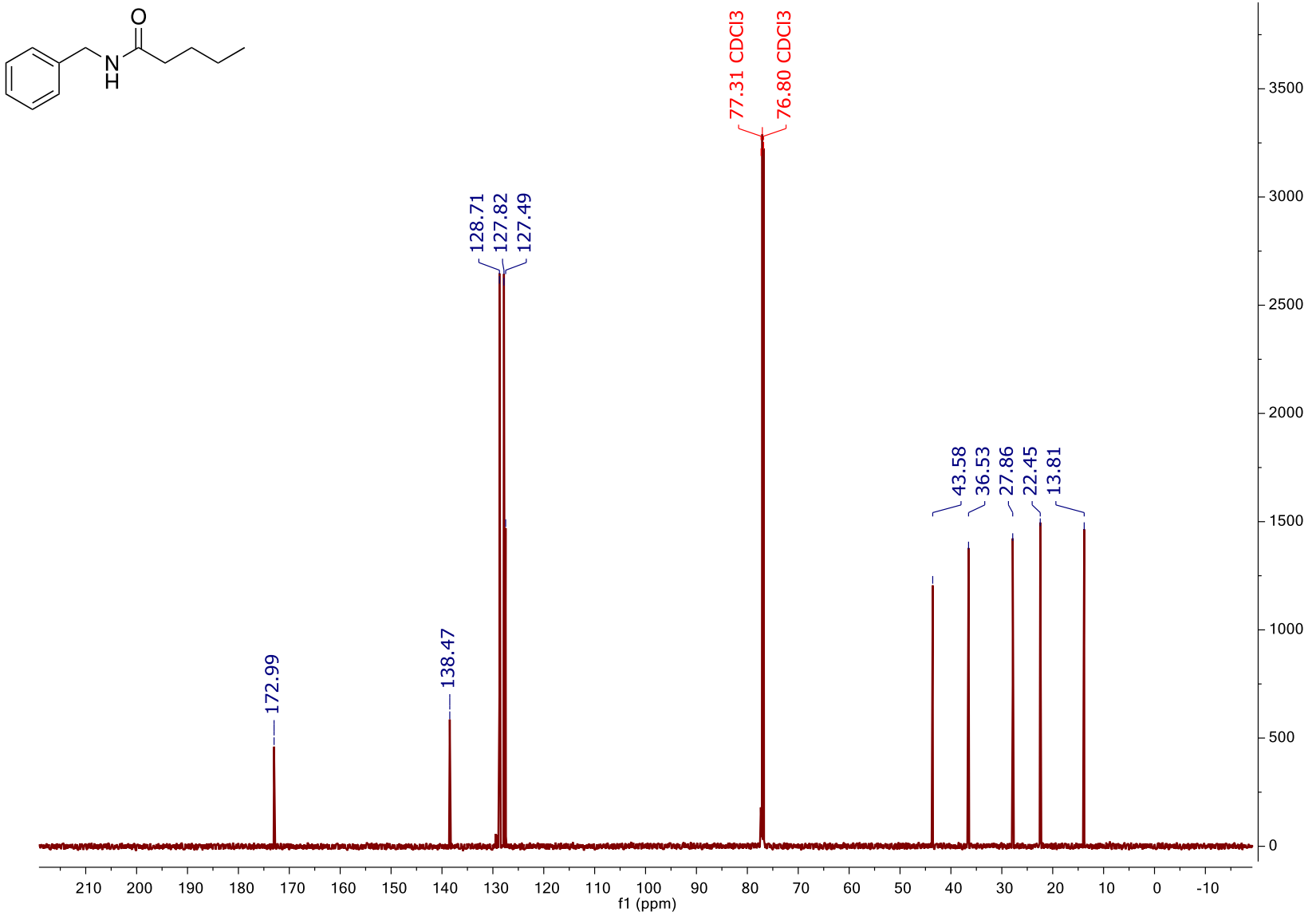
O
N
H
77.31 CDCl3
76.80 CDCl3
128.71
127.82
127.49
43.58
36.53
27.86
22.45
13.81
172.99
138.47
3500
3000
2500
2000
1500
1000
500
0
210 200 190 180 170 160 150 140 130 120 110 100 90 80 70 60 50 40 30 20 10 0 -10
f1 (ppm)

In situ

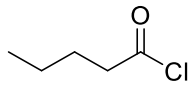
O
Cl

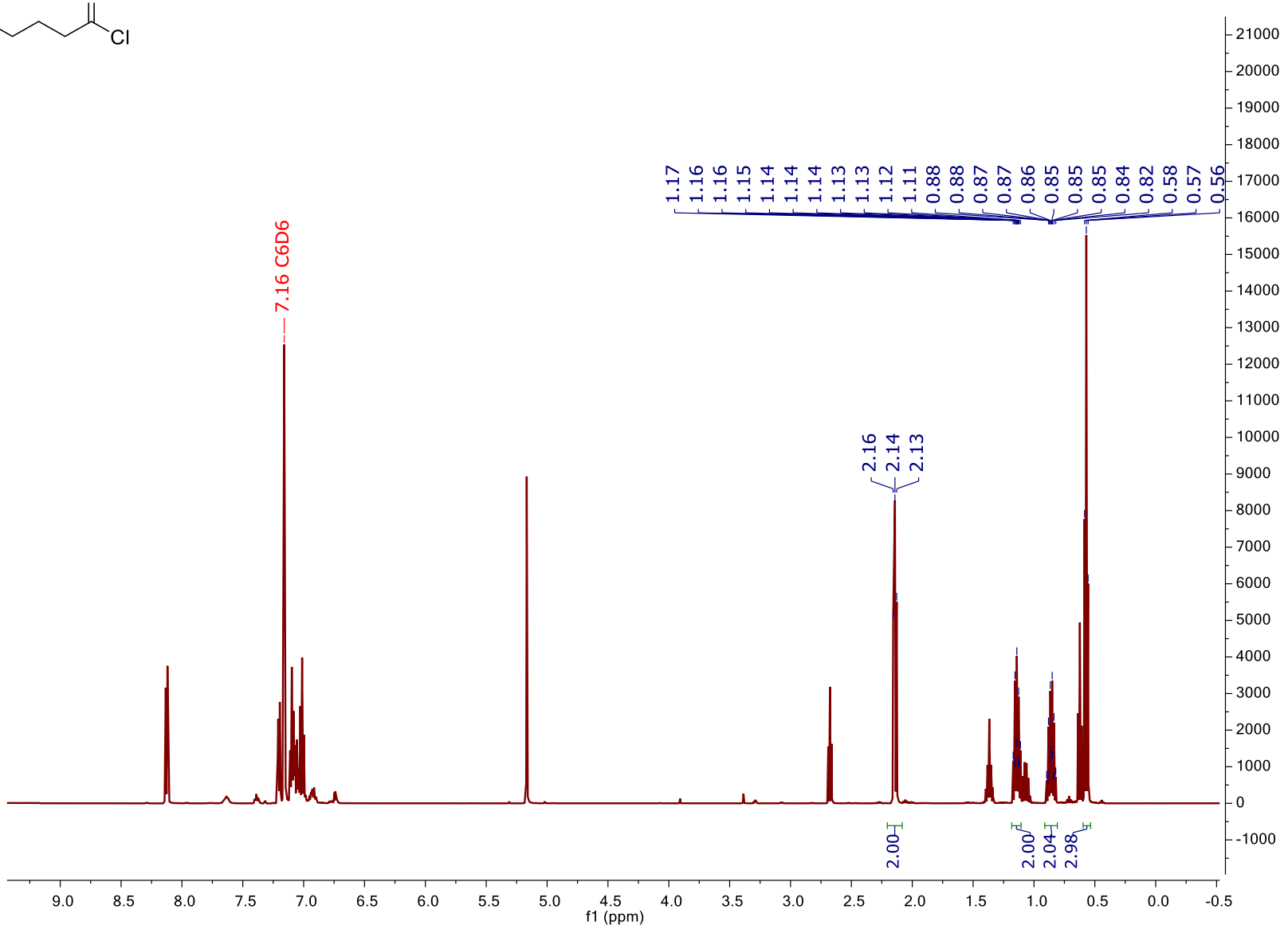
7.16 C6D6
1.17
1.16
1.16
1.15
1.14
1.14
1.14
1.13
1.13
1.12
1.11
0.88
0.88
0.87
0.87
0.86
0.85
0.85
0.85
0.84
0.82
0.58
0.57
0.56
2.16
2.14
2.13
2.00
2.00
2.04
2.98
f1 (ppm)

In situ

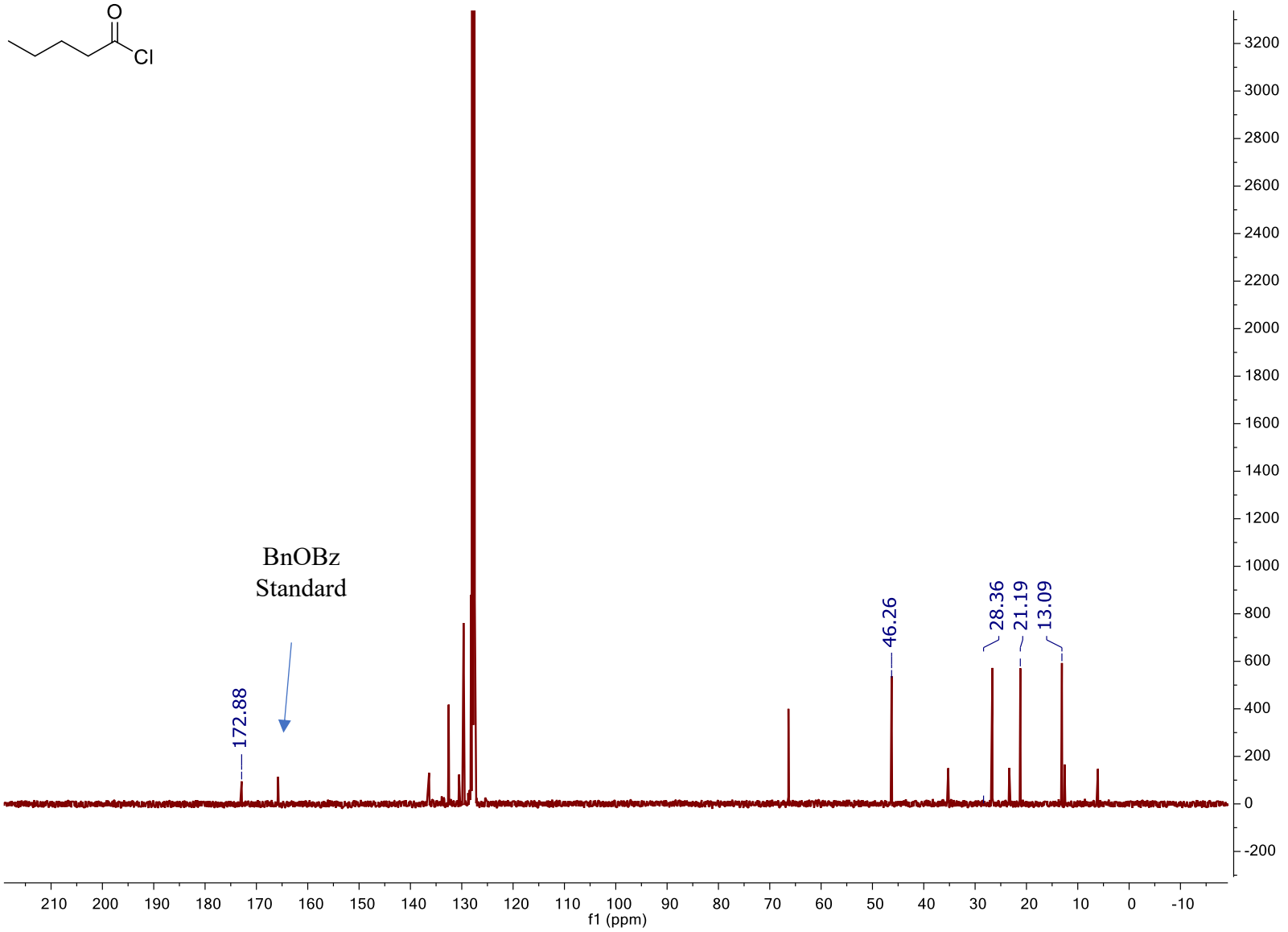

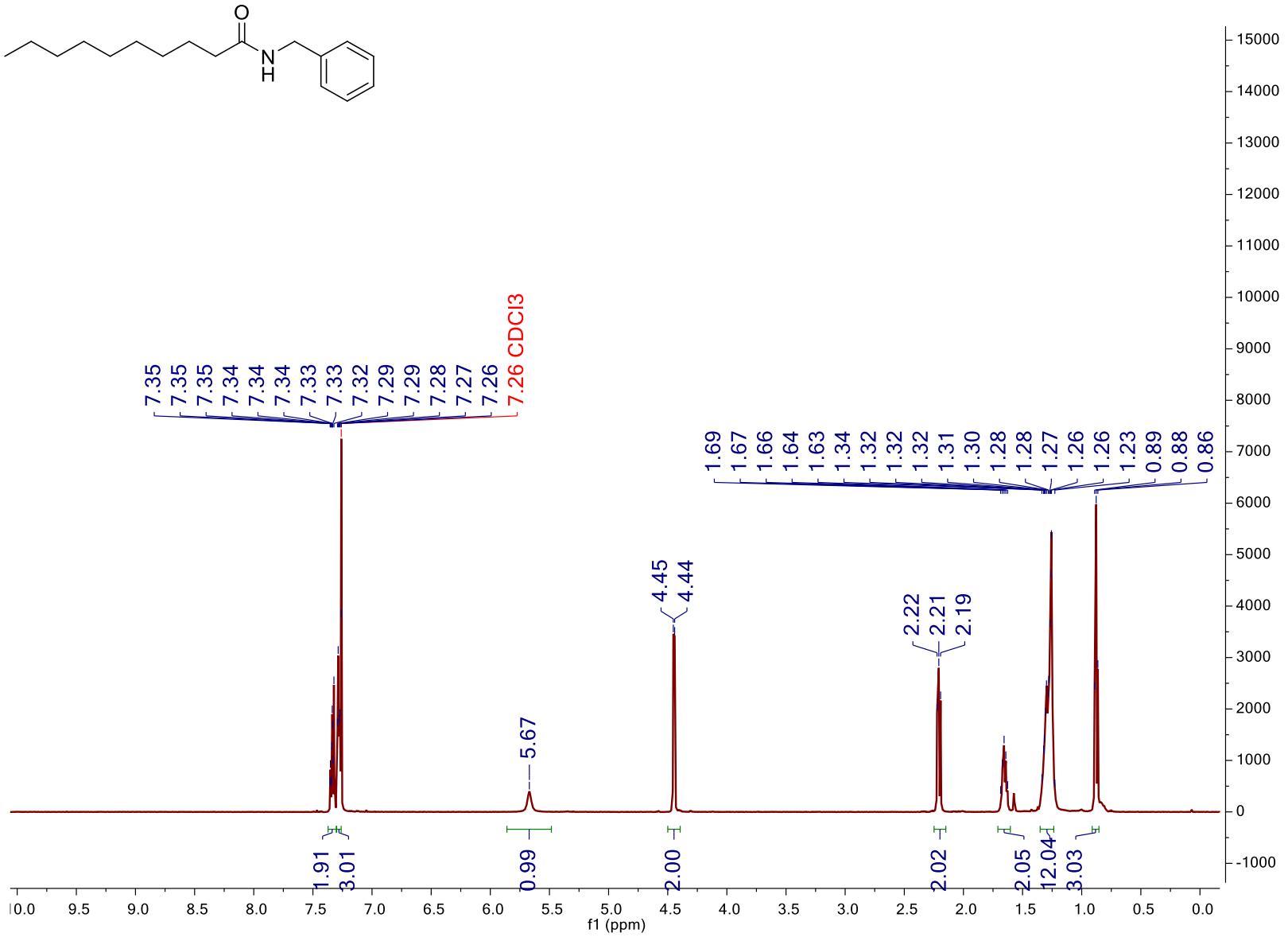
O
N
H
7.35
7.35
7.35
7.34
7.34
7.34
7.33
7.33
7.32
7.29
7.29
7.28
7.27
7.26
7.26 CDCl3
1.69
1.67
1.66
1.64
1.63
1.34
1.32
1.32
1.32
1.31
1.30
1.28
1.28
1.27
1.26
1.26
1.23
0.89
0.88
0.86
4.45
4.44
2.22
2.21
2.19
5.67
1.91
3.01
0.99
2.00
2.02
2.05
12.04
3.03
f1 (ppm)

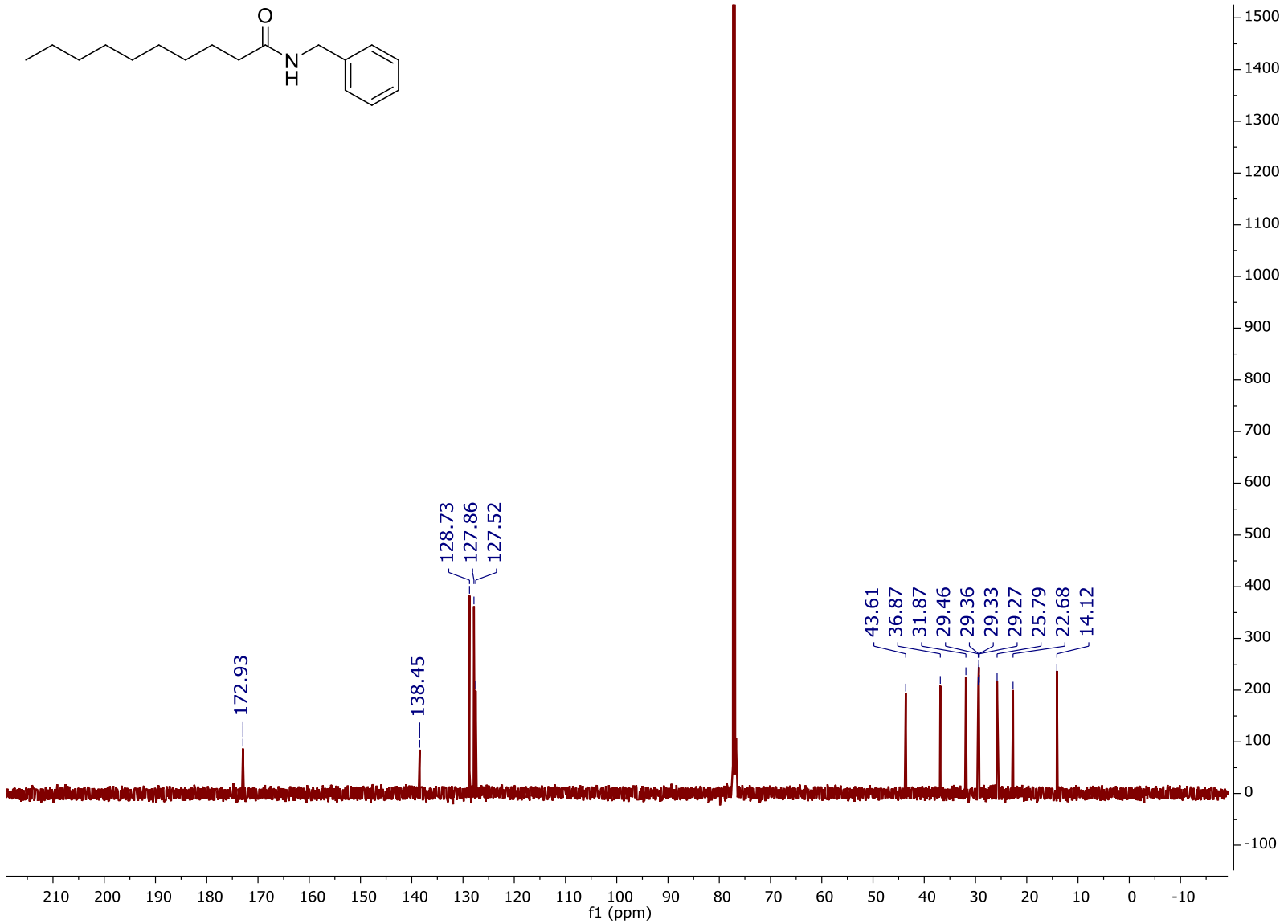
O
N
H
172.93
138.45
128.73
127.86
127.52
43.61
36.87
31.87
29.46
29.36
29.33
29.27
25.79
22.68
14.12
f1 (ppm)

In situ

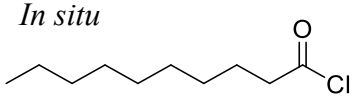

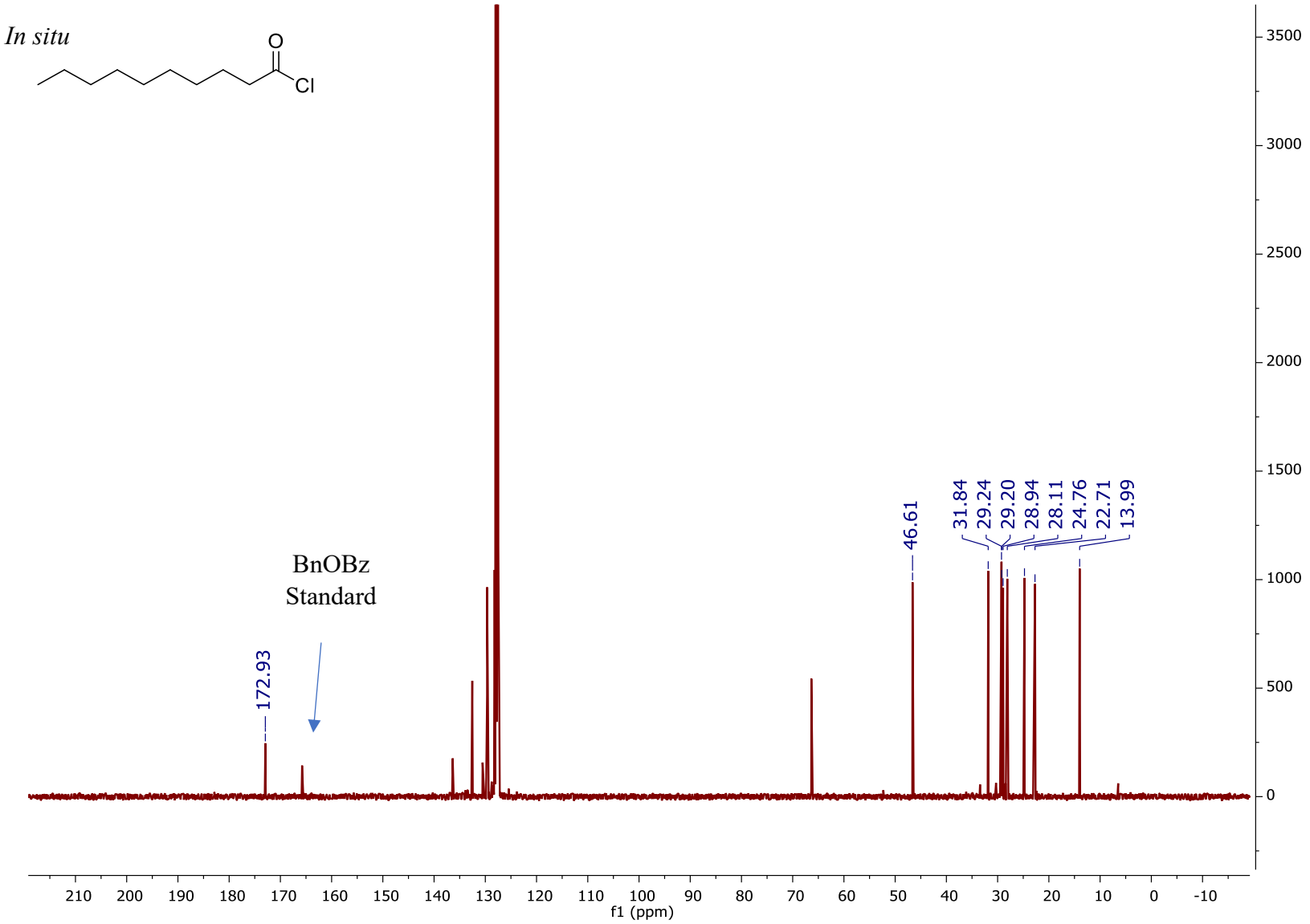
In situ
O
Cl
BnOBz
Standard
172.93
46.61
31.84
29.24
29.20
28.94
28.11
24.76
22.71
13.99
3500
3000
2500
2000
1500
1000
500
0
210 200 190 180 170 160 150 140 130 120 110 100 90 80 70 60 50 40 30 20 10 0 -10
f1 (ppm)

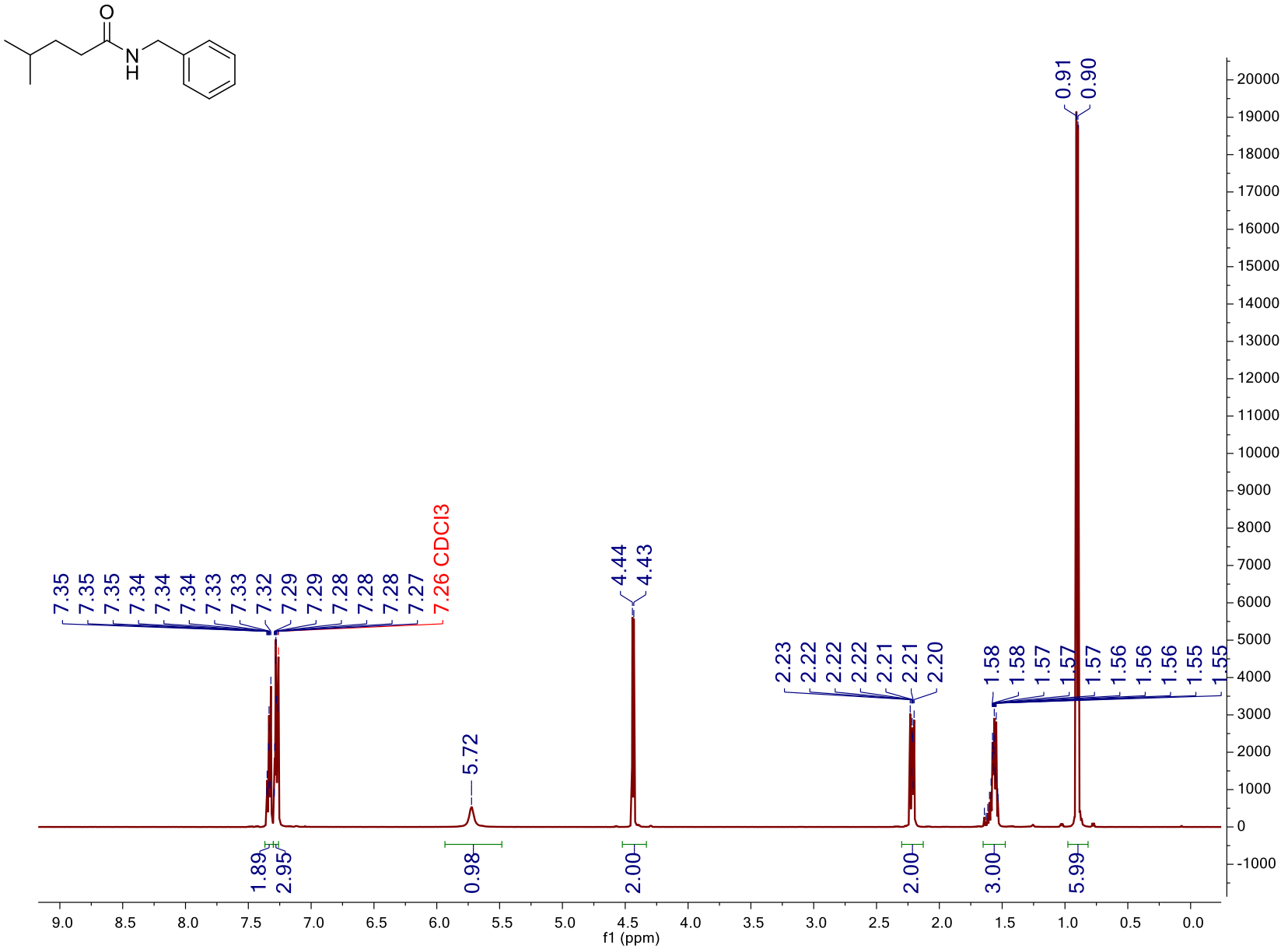
O
N
H
7.35
7.35
7.35
7.34
7.34
7.34
7.33
7.33
7.32
7.29
7.29
7.28
7.28
7.28
7.27
7.26 CDCl3
5.72
4.44
4.43
2.23
2.22
2.22
2.22
2.21
2.21
2.20
1.58
1.58
1.57
1.57
1.57
1.56
1.56
1.56
1.55
1.55
0.91
0.90
1.89
2.95
0.98
2.00
2.00
3.00
5.99
f1 (ppm)

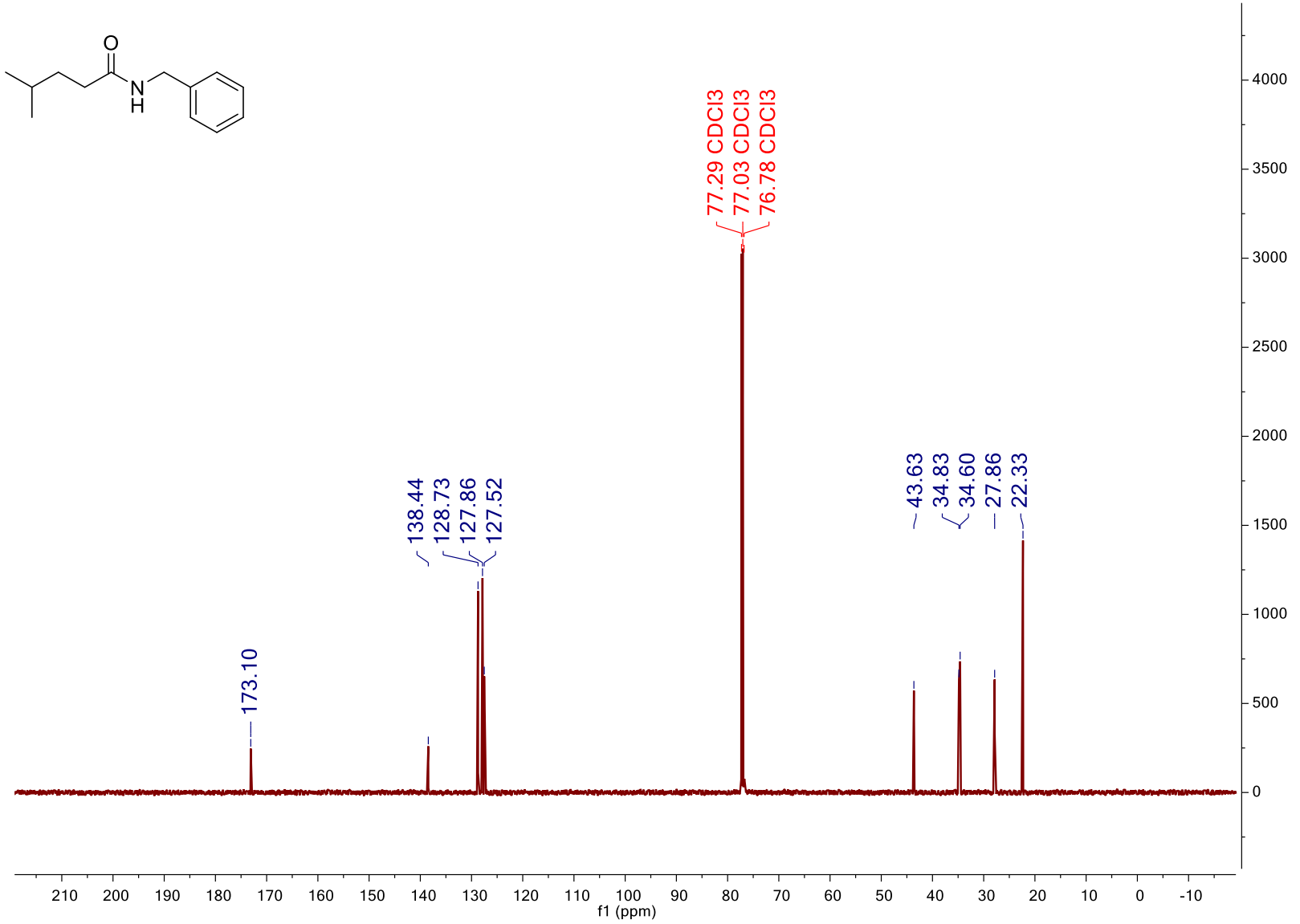
O
N
H
77.29 CDCl3
77.03 CDCl3
76.78 CDCl3
138.44
128.73
127.86
127.52
43.63
34.83
34.60
27.86
22.33
173.10
4000
3500
3000
2500
2000
1500
1000
500
0
210 200 190 180 170 160 150 140 130 120 110 100 90 80 70 60 50 40 30 20 10 0 -10
f1 (ppm)

In situ

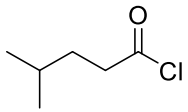

In situ

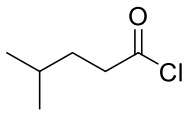
O
Cl

BnOBz
Standard
173.05
44.85
33.22
26.80
21.53
4500
4000
3500
3000
2500
2000
1500
1000
500
0
210 200 190 180 170 160 150 140 130 120 110 100 90 80 70 60 50 40 30 20 10 0 -10
f1 (ppm)

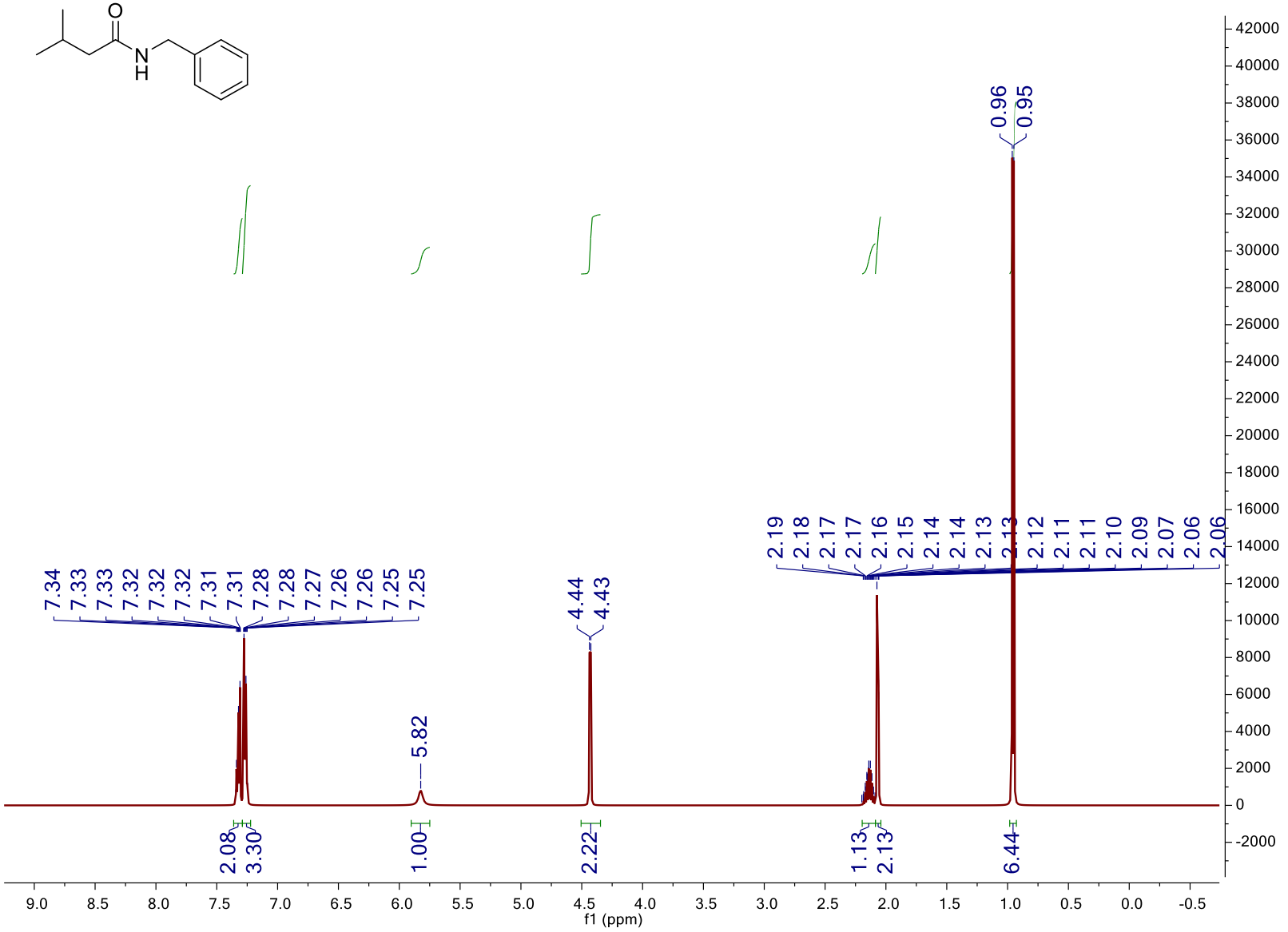
O
N
H
7.34
7.33
7.33
7.32
7.32
7.32
7.31
7.31
7.28
7.28
7.27
7.26
7.26
7.25
7.25
5.82
4.44
4.43
2.19
2.18
2.17
2.17
2.16
2.15
2.14
2.14
2.13
2.13
2.12
2.11
2.11
2.10
2.09
2.07
2.06
2.06
0.96
0.95
2.08
3.30
1.00
2.22
1.13
2.13
6.44
f1 (ppm)

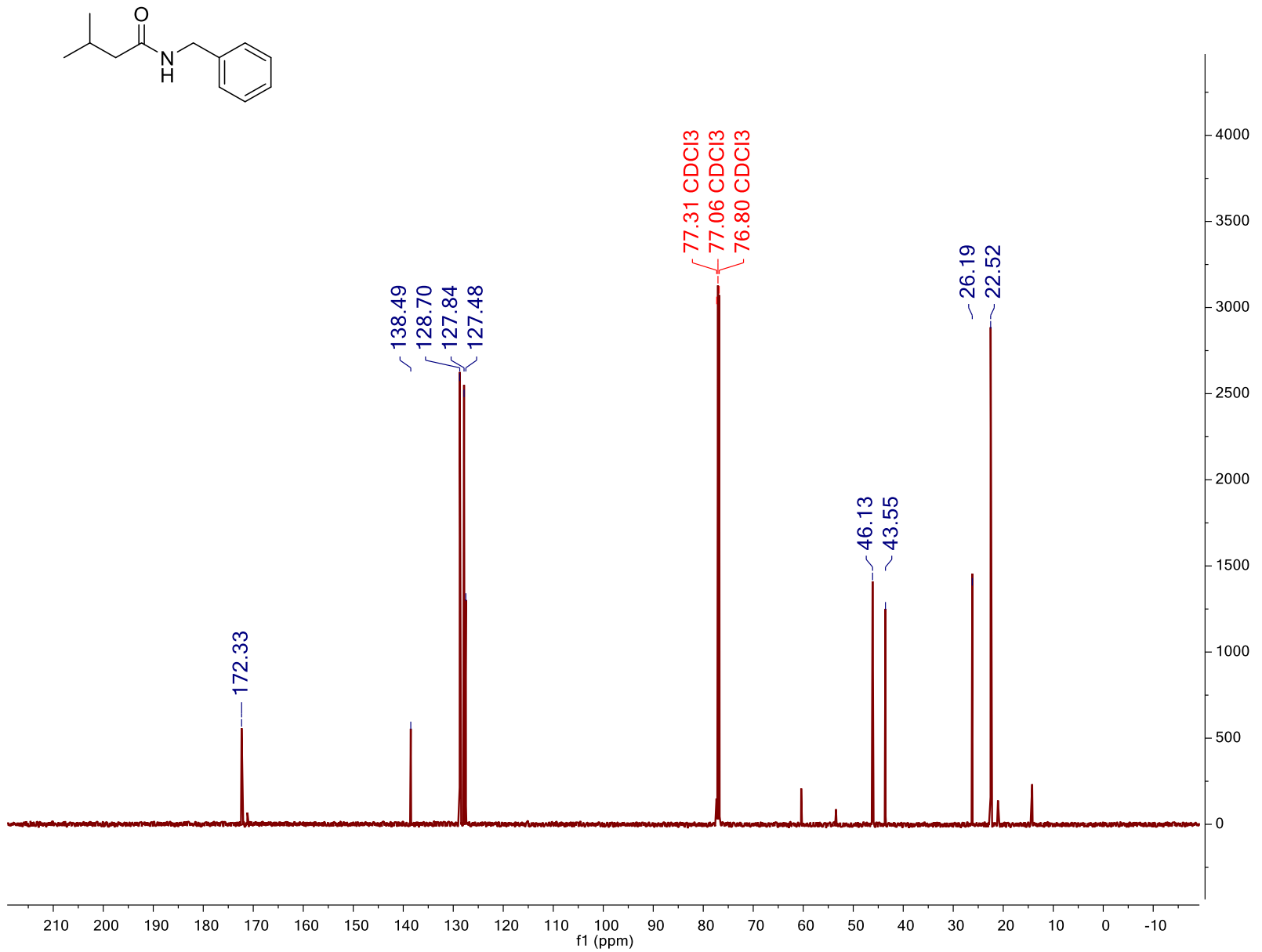
O
N
H
172.33
138.49
128.70
127.84
127.48
77.31 CDCl3
77.06 CDCl3
76.80 CDCl3
46.13
43.55
26.19
22.52
4000
3500
3000
2500
2000
1500
1000
500
0
210 200 190 180 170 160 150 140 130 120 110 100 90 80 70 60 50 40 30 20 10 0 -10
f1 (ppm)

In situ

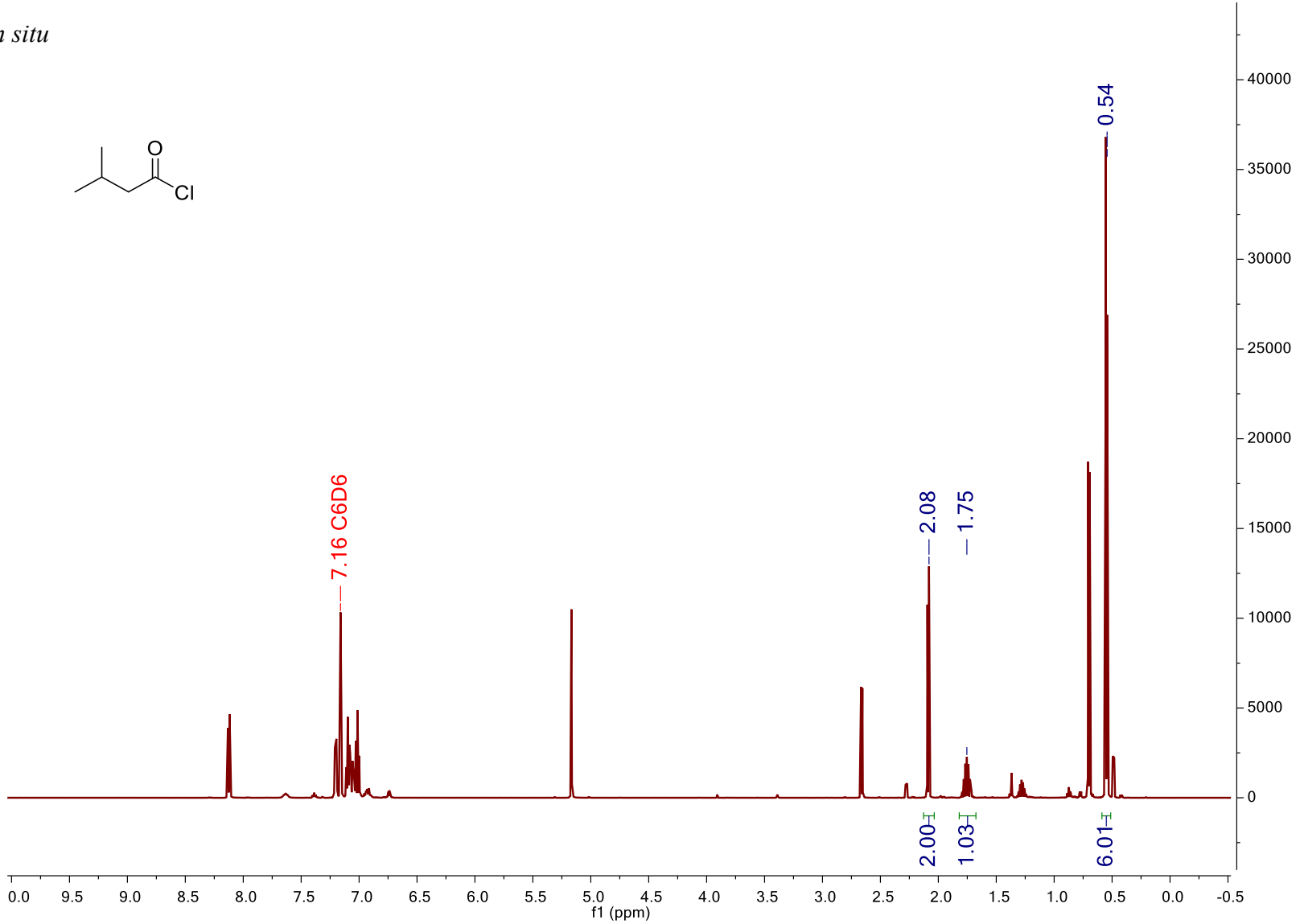

In situ

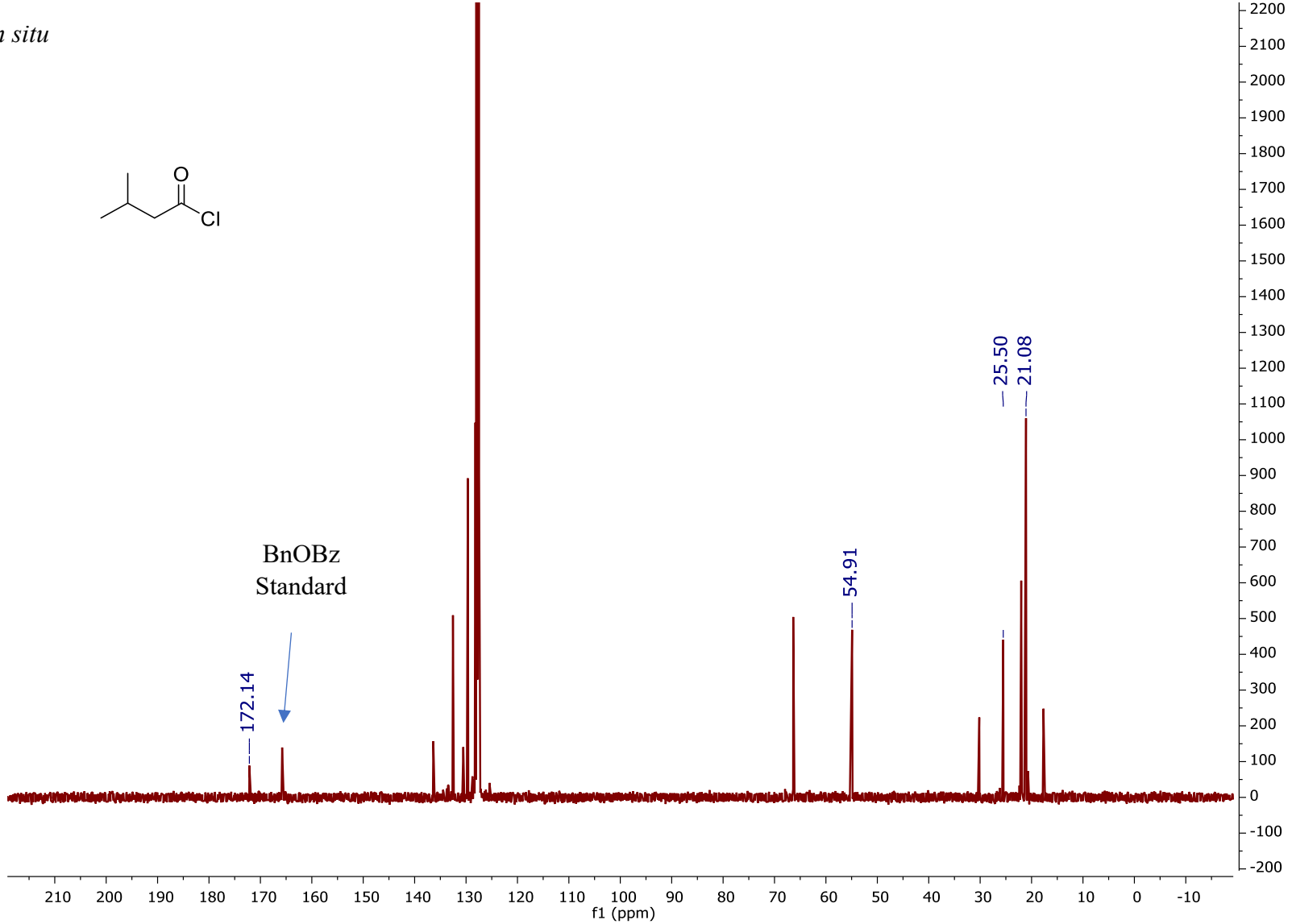

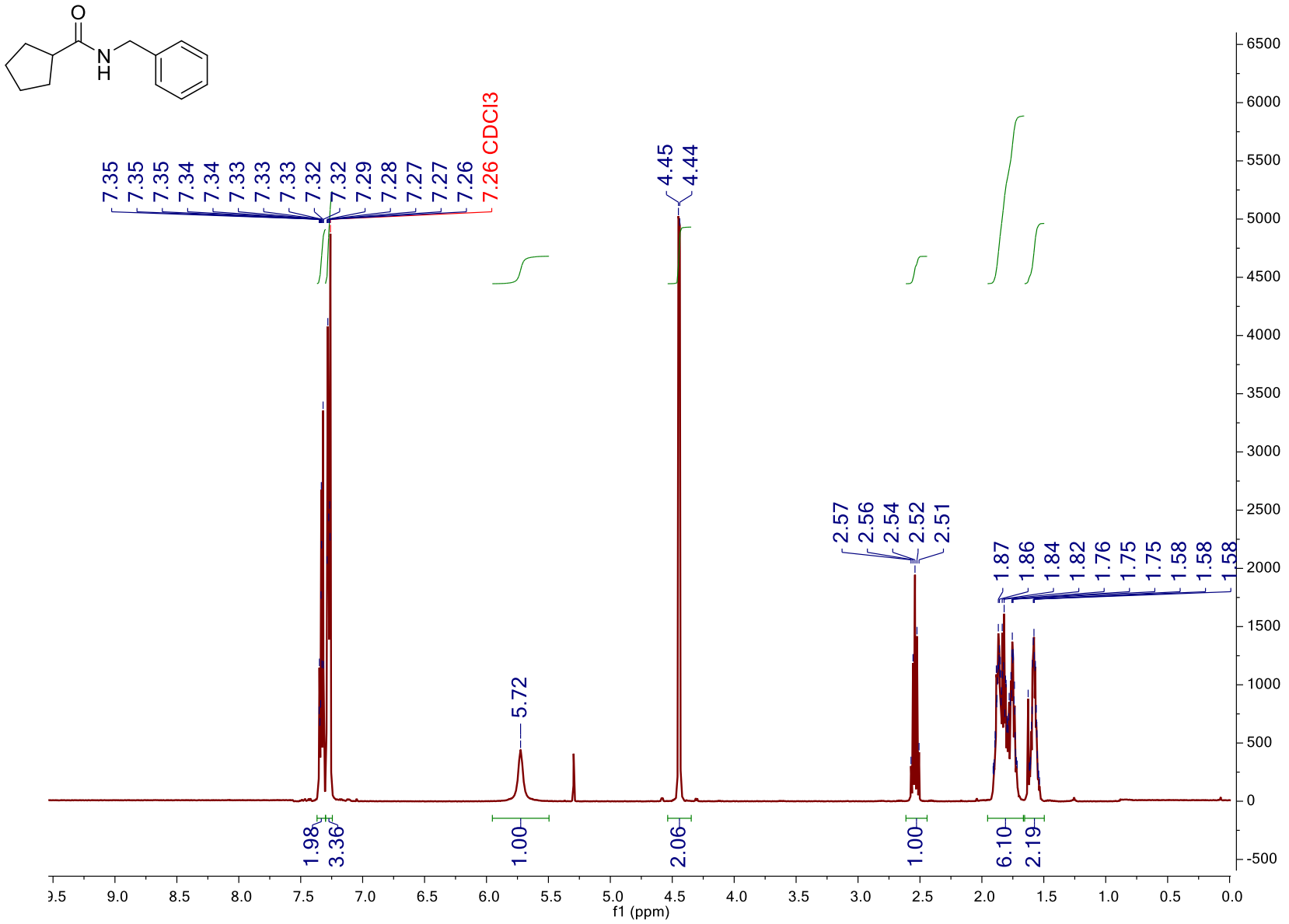
O
N
H
7.35
7.35
7.35
7.34
7.34
7.33
7.33
7.33
7.32
7.32
7.29
7.28
7.27
7.27
7.26
7.26 CDCl3
4.45
4.44
5.72
2.57
2.56
2.54
2.52
2.51
1.87
1.86
1.84
1.82
1.76
1.75
1.75
1.58
1.58
1.58
1.98
3.36
1.00
2.06
1.00
6.10
2.19
f1 (ppm)

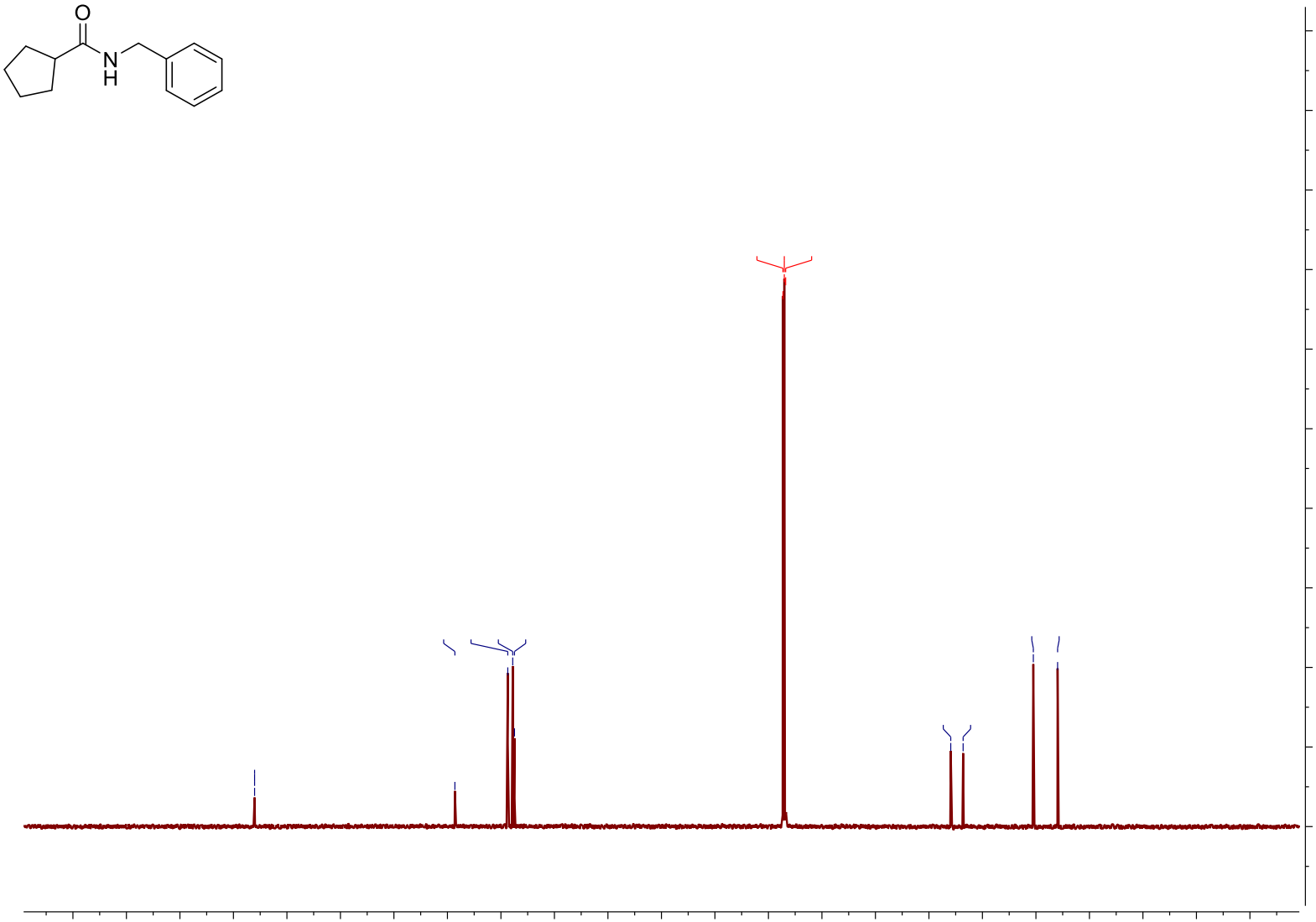
O
N
H

In situ

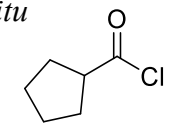

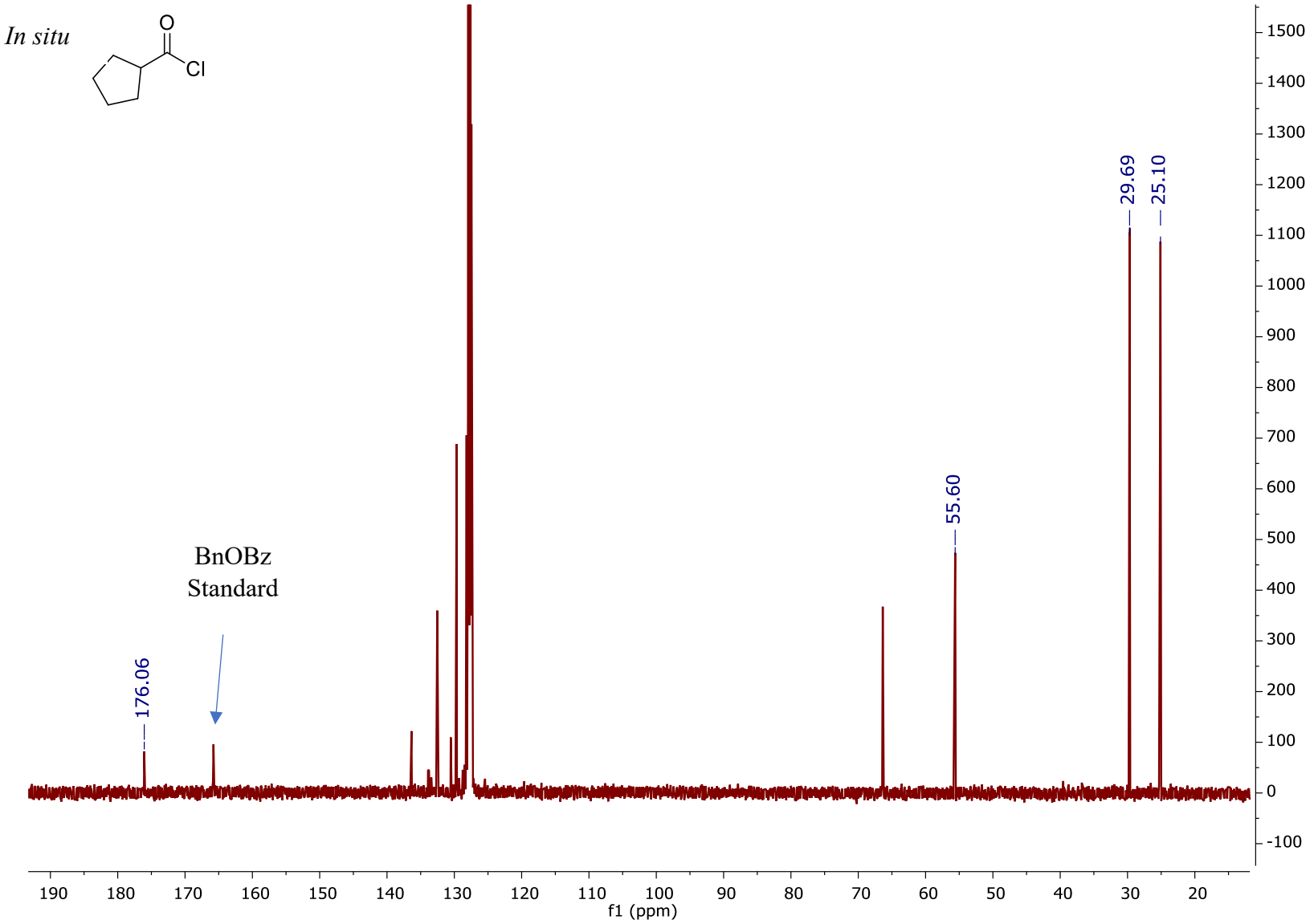
In situ
O
Cl
BnOBz
Standard
176.06
55.60
29.69
25.10
1500
1400
1300
1200
1100
1000
900
800
700
600
500
400
300
200
100
0
-100
190
180
170
160
150
140
130
120
110
100
90
80
70
60
50
40
30
20
f1 (ppm)

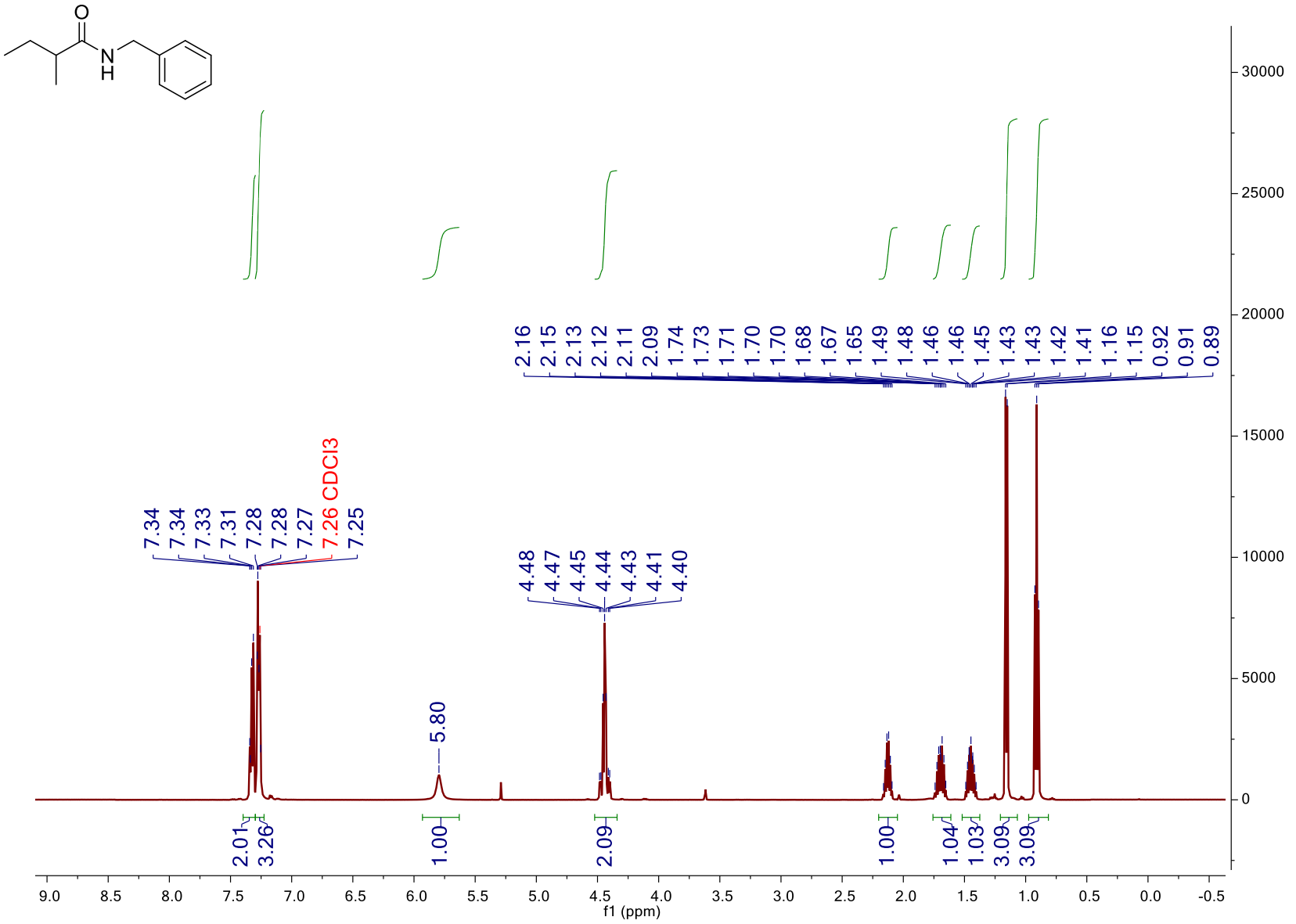
O
N
H
7.34
7.34
7.33
7.31
7.28
7.28
7.27
7.26 CDCl3
7.25
5.80
4.48
4.47
4.45
4.44
4.43
4.41
4.40
2.16
2.15
2.13
2.12
2.11
2.09
1.74
1.73
1.71
1.70
1.70
1.68
1.67
1.65
1.49
1.48
1.46
1.46
1.45
1.43
1.43
1.42
1.41
1.16
1.15
0.92
0.91
0.89
2.01
3.26
1.00
2.09
1.00
1.04
1.03
3.09
3.09
f1 (ppm)

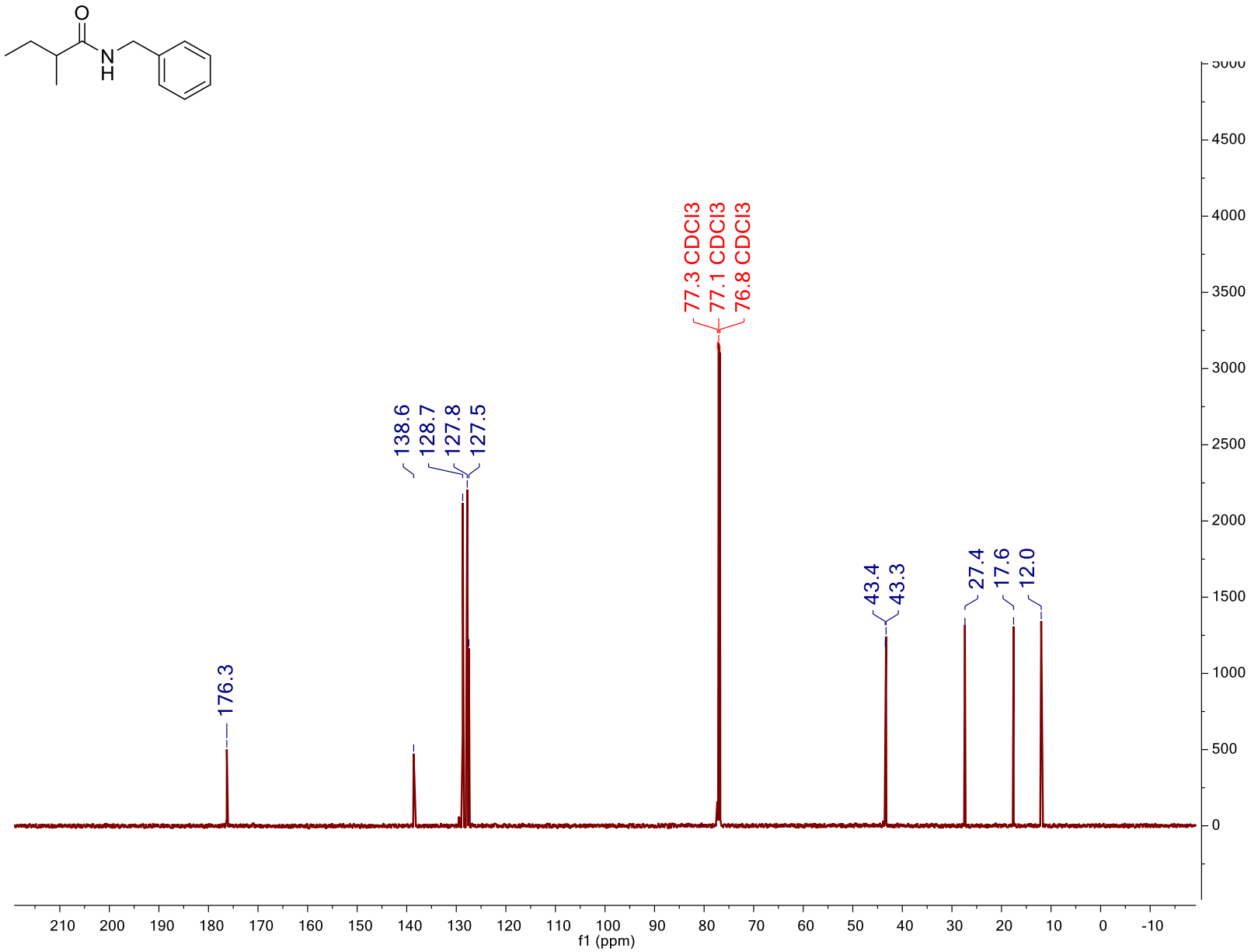
O
N
H
176.3
138.6
128.7
127.8
127.5
77.3 CDCl3
77.1 CDCl3
76.8 CDCl3
43.4
43.3
27.4
17.6
12.0
f1 (ppm)

In situ

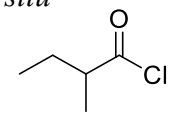
O
Cl

1.42
1.41
1.39
1.38
1.38
1.37
1.37
1.35
1.13
1.12
1.12
1.10
1.10
1.09
1.09
1.09
1.09
1.08
1.07
1.06
1.06
1.05
0.78
0.77
0.59
0.57
0.56
7.16 C6D6
2.27
2.26
2.25
2.23
2.23
2.22
2.20
1.00
1.31
1.07
3.12
3.16
f1 (ppm)

In situ

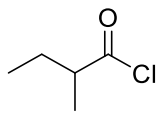

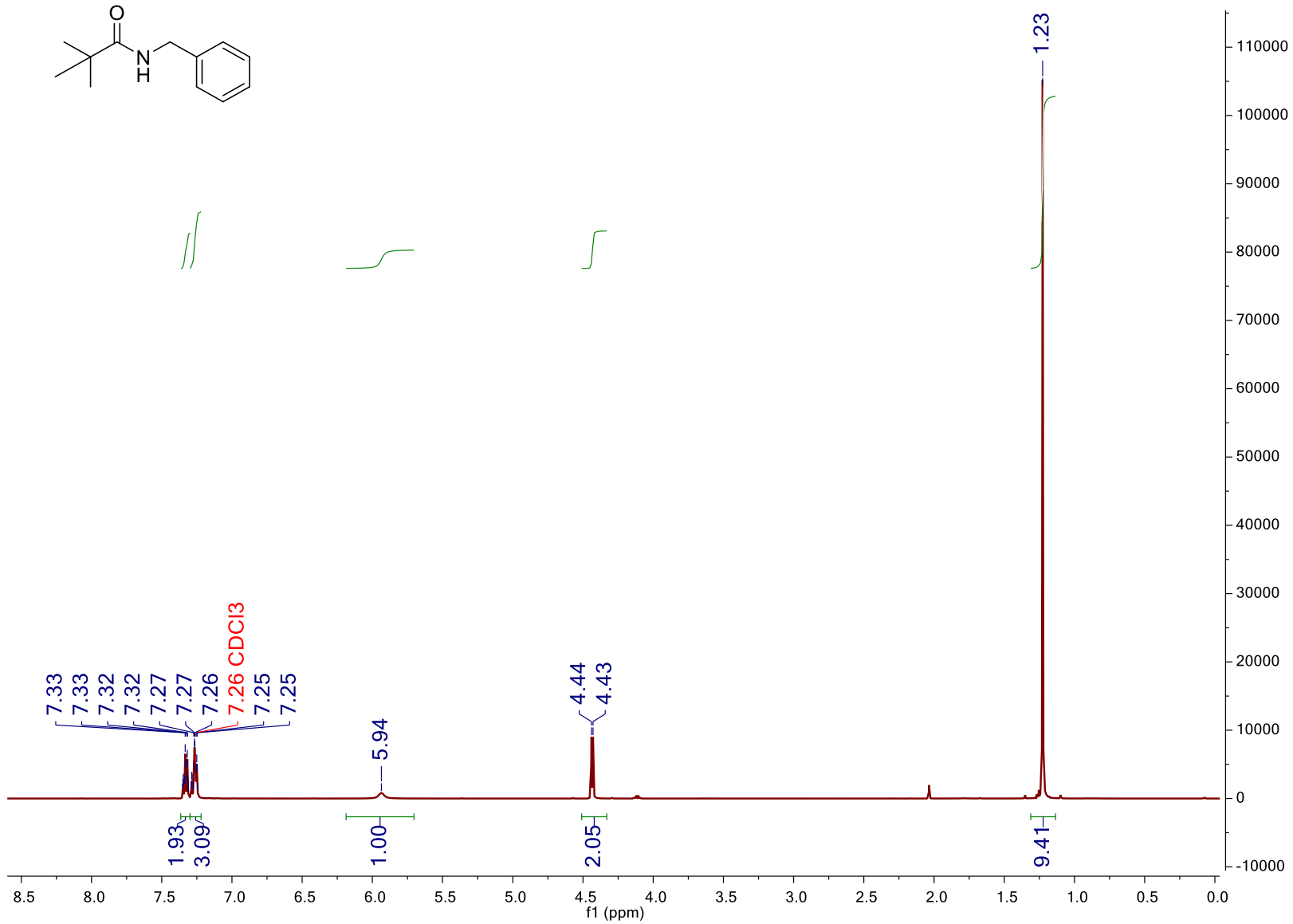
O
N
H
1.23
7.33
7.33
7.32
7.32
7.27
7.27
7.26
7.26 CDCl3
7.25
7.25
5.94
4.44
4.43
1.93
3.09
1.00
2.05
9.41
f1 (ppm)

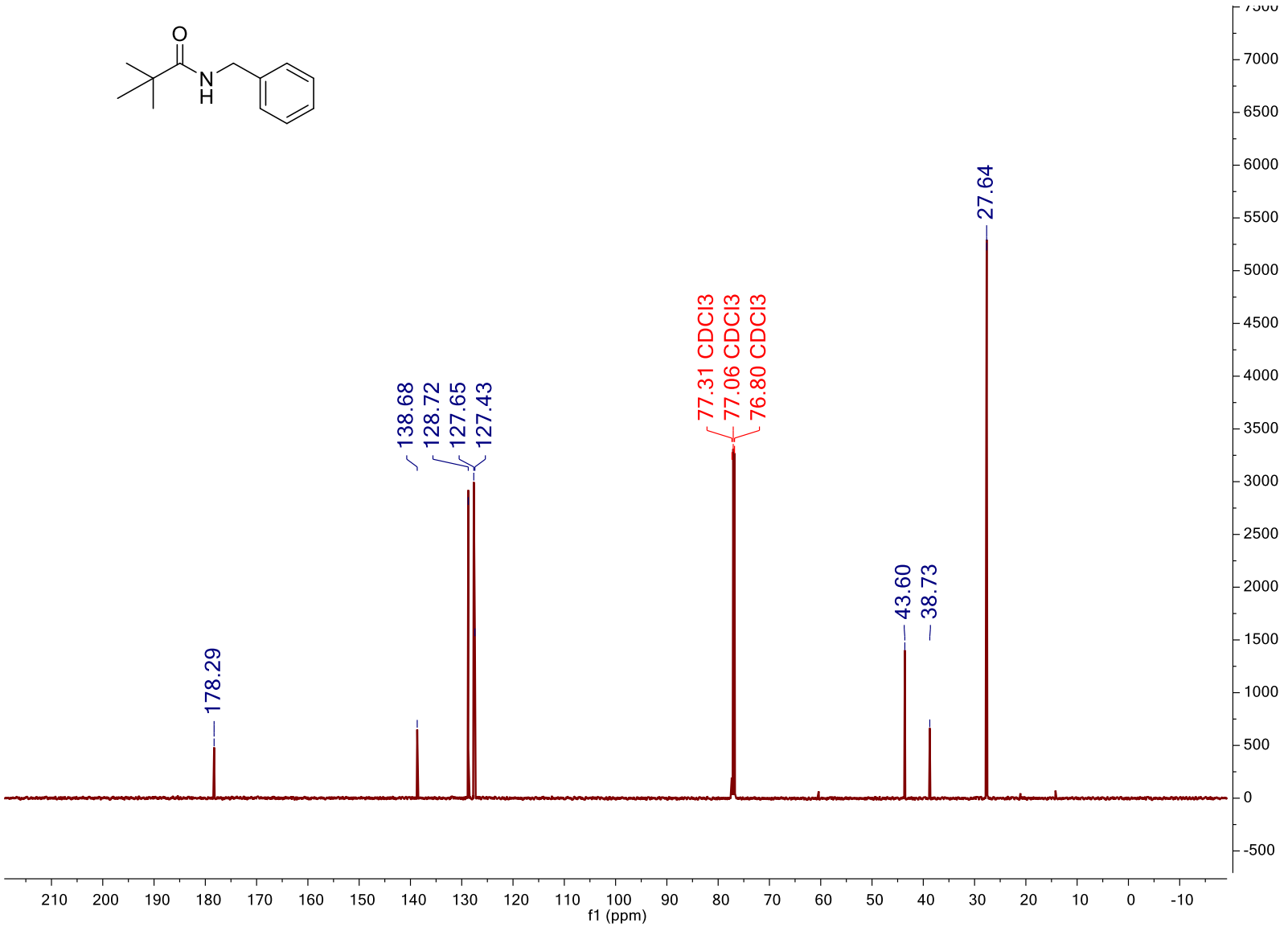
O
N
H
178.29
138.68
128.72
127.65
127.43
77.31 CDCl3
77.06 CDCl3
76.80 CDCl3
43.60
38.73
27.64
f1 (ppm)

In situ

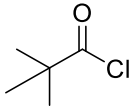
O
Cl

0.89
7.16 C6D6
9.00
75000
70000
65000
60000
55000
50000
45000
40000
35000
30000
25000
20000
15000
10000
5000
0
-5000
8.5
8.0
7.5
7.0
6.5
6.0
5.5
5.0
4.5
4.0
3.5
3.0
2.5
2.0
1.5
1.0
0.5
0.0
f1 (ppm)

In situ

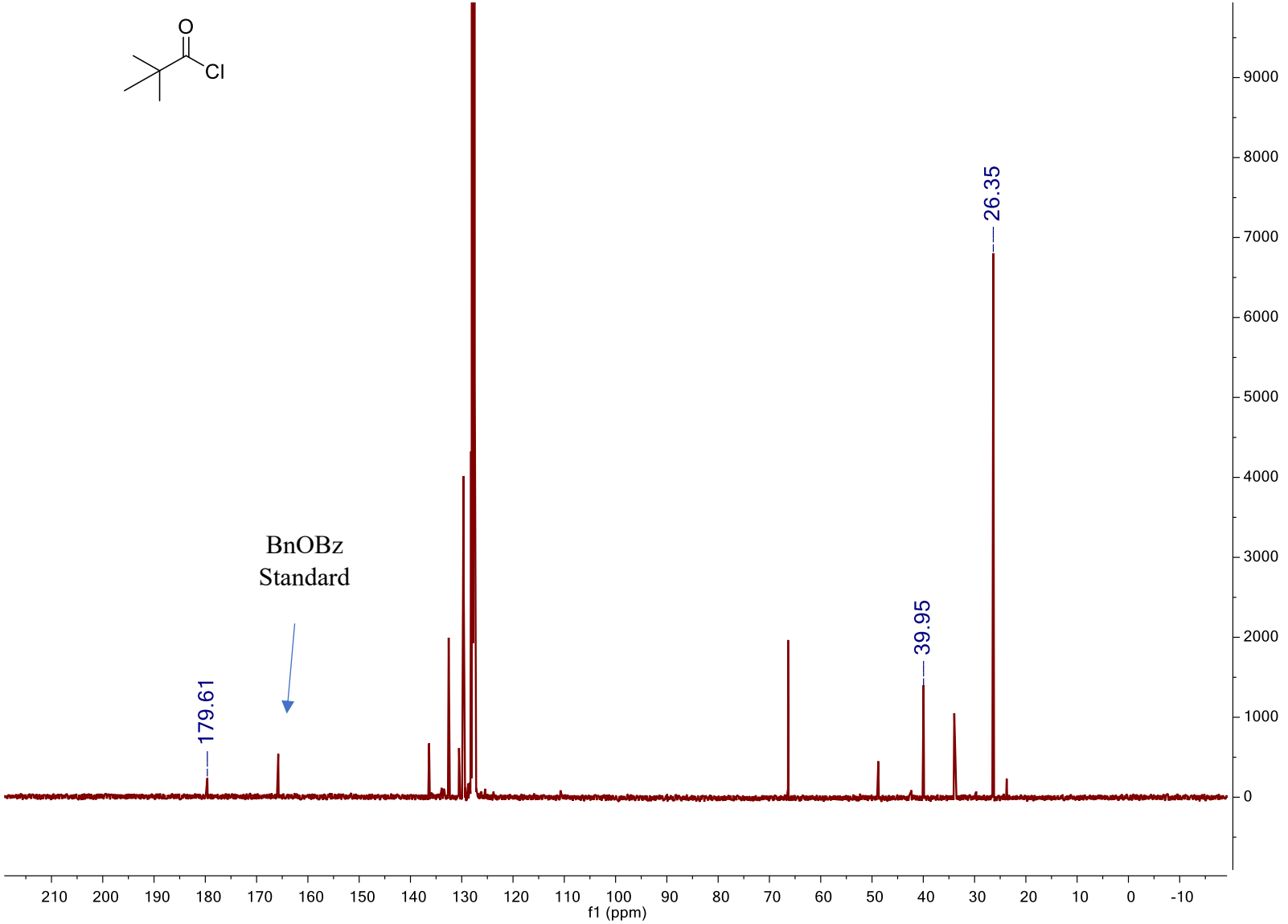
O
Cl
BnOBz
Standard
179.61
39.95
26.35
9000
8000
7000
6000
5000
4000
3000
2000
1000
0
210 200 190 180 170 160 150 140 130 120 110 100 90 80 70 60 50 40 30 20 10 0 -10
f1 (ppm)

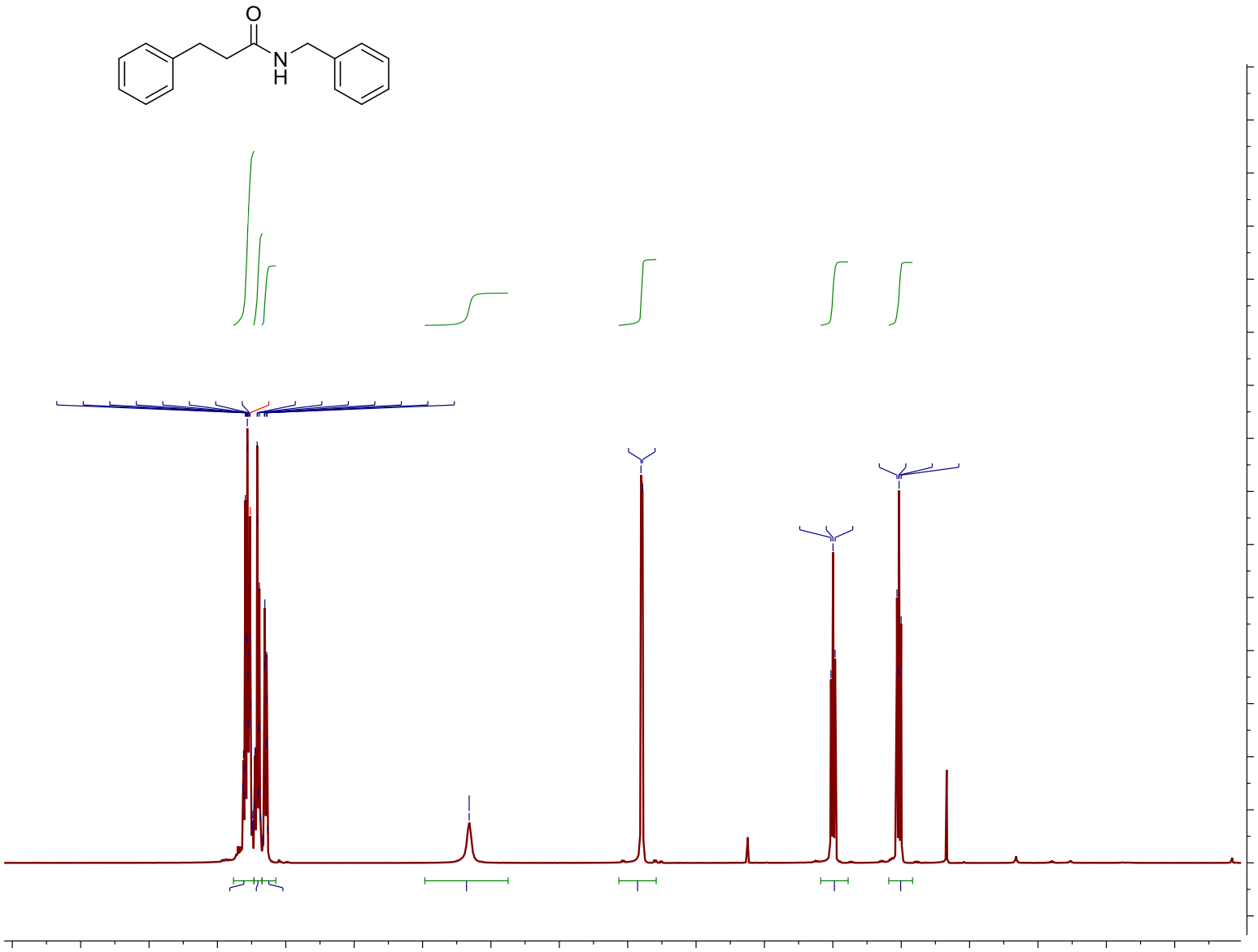
O
N
H

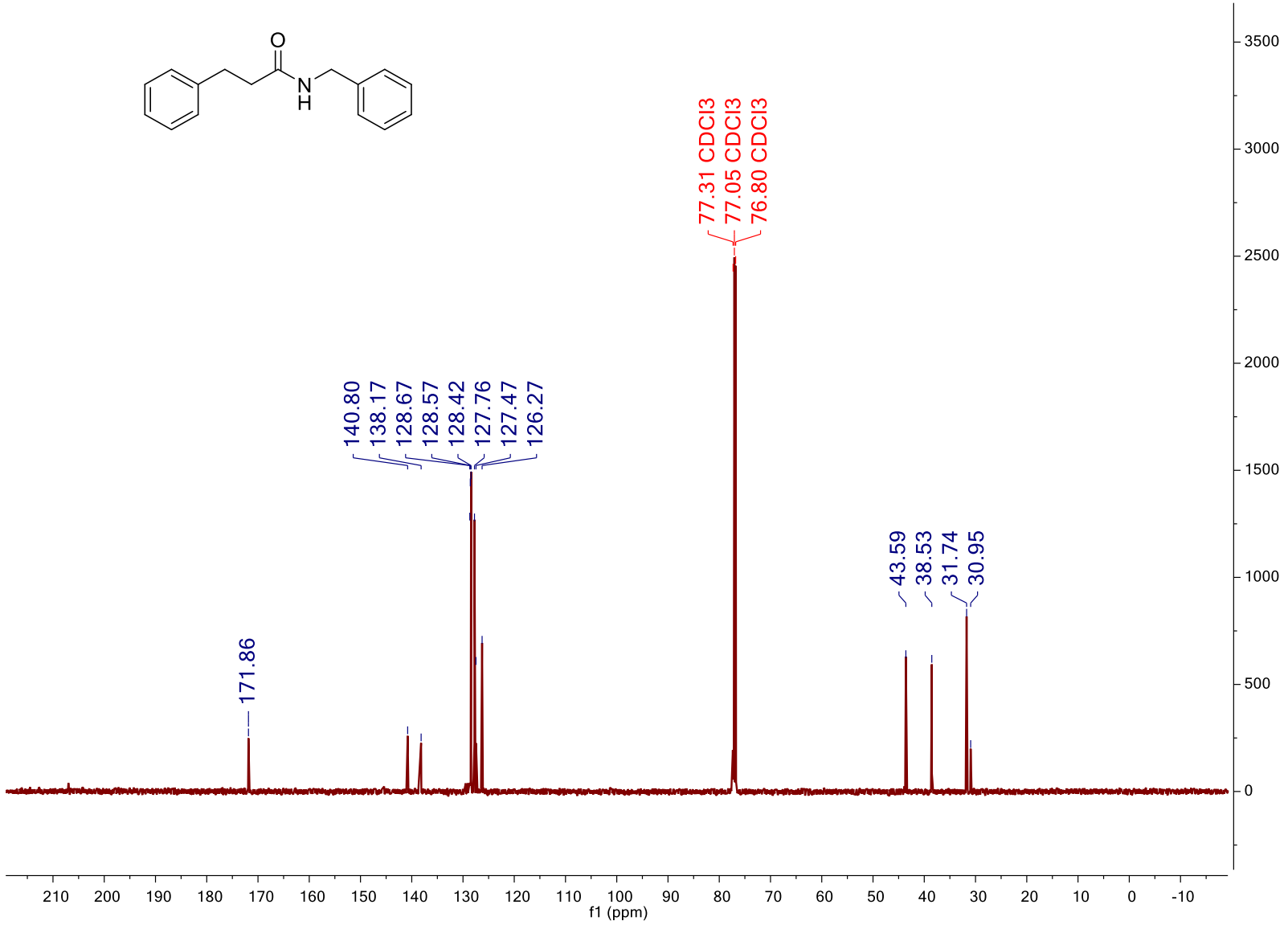
O
N
H
77.31 CDCl3
77.05 CDCl3
76.80 CDCl3
140.80
138.17
128.67
128.57
128.42
127.76
127.47
126.27
171.86
43.59
38.53
31.74
30.95
f1 (ppm)

In situ

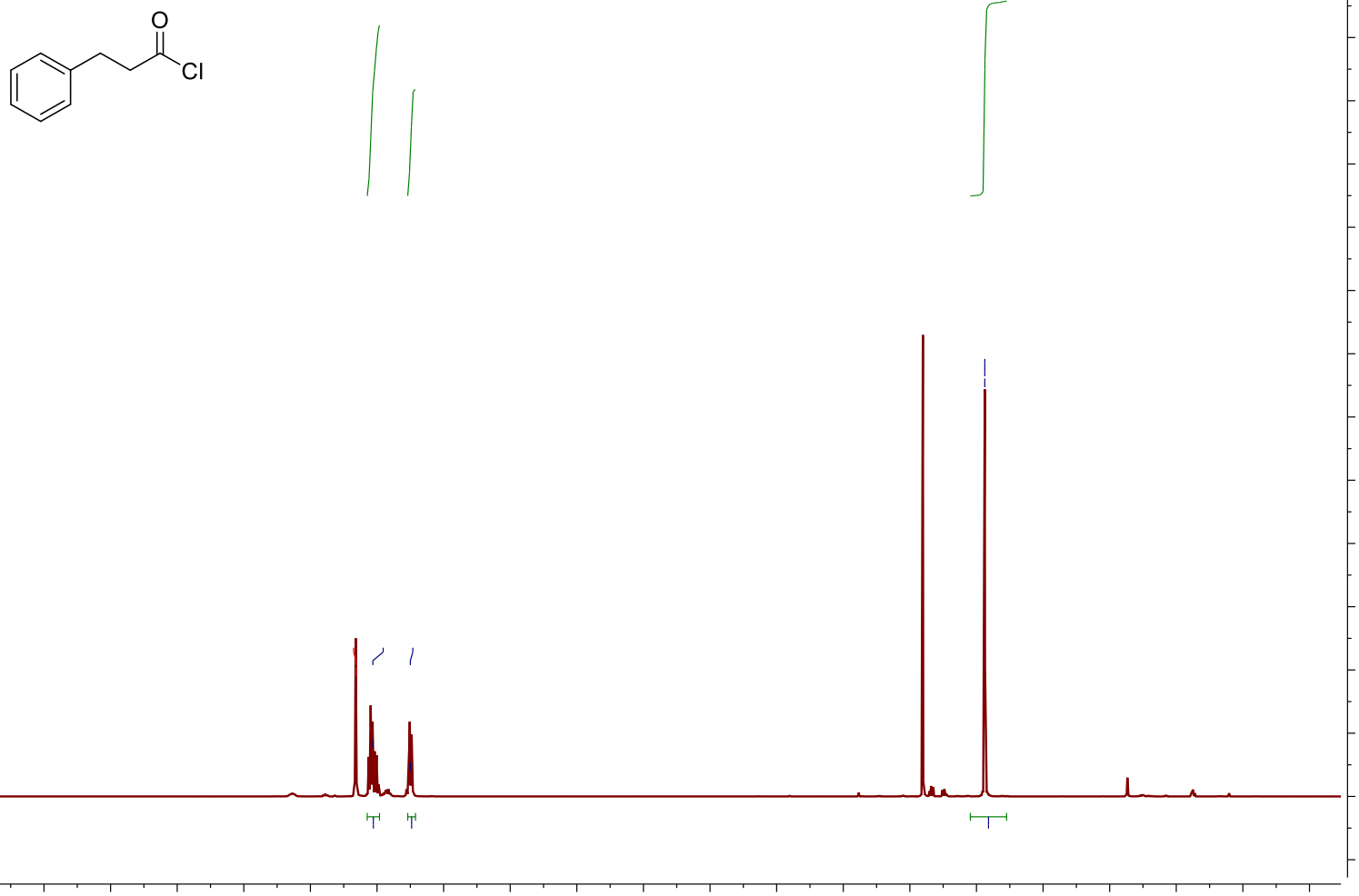

In situ

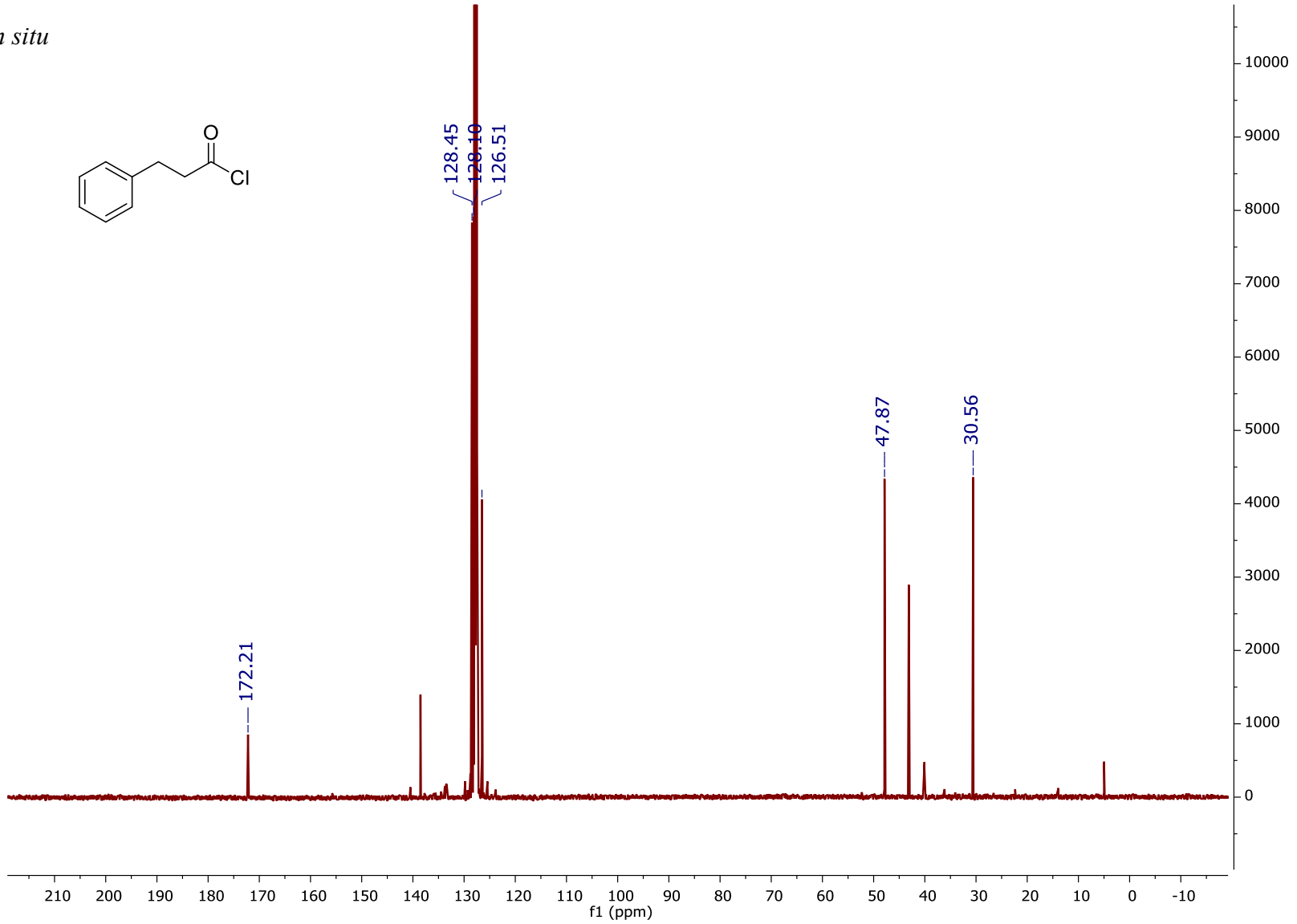
O
Cl
128.45
128.10
126.51
172.21
47.87
30.56
10000
9000
8000
7000
6000
5000
4000
3000
2000
1000
0
210 200 190 180 170 160 150 140 130 120 110 100 90 80 70 60 50 40 30 20 10 0 -10
f1 (ppm)

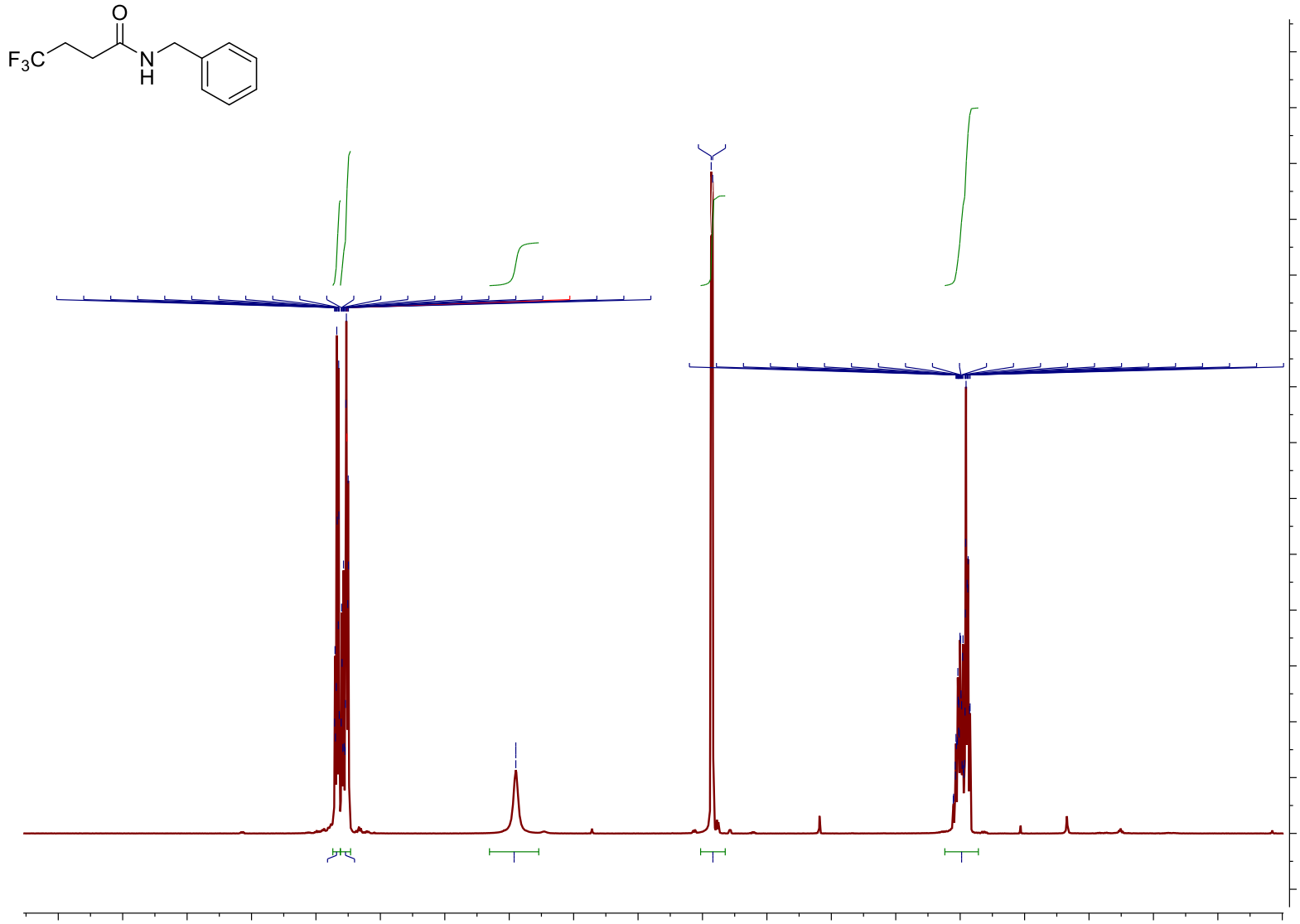
O
F3C
N
H

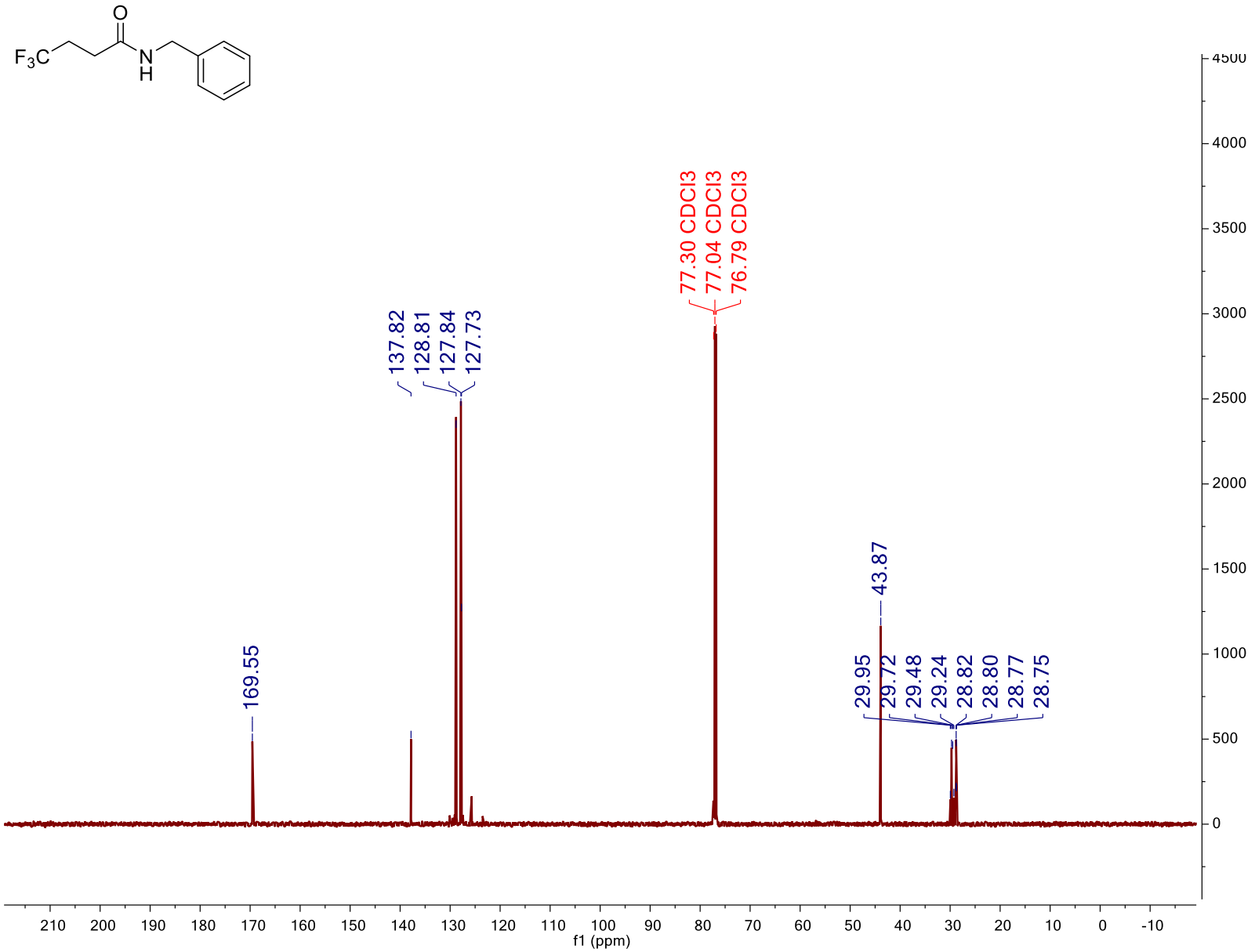
O
F3C
N
H
169.55
137.82
128.81
127.84
127.73
77.30 CDCl3
77.04 CDCl3
76.79 CDCl3
43.87
29.95
29.72
29.48
29.24
28.82
28.80
28.77
28.75
f1 (ppm)

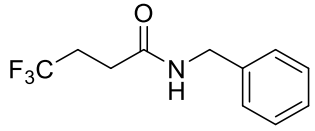

^{19}F NMR

In situ

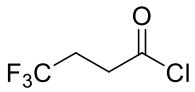
O
F3C
Cl

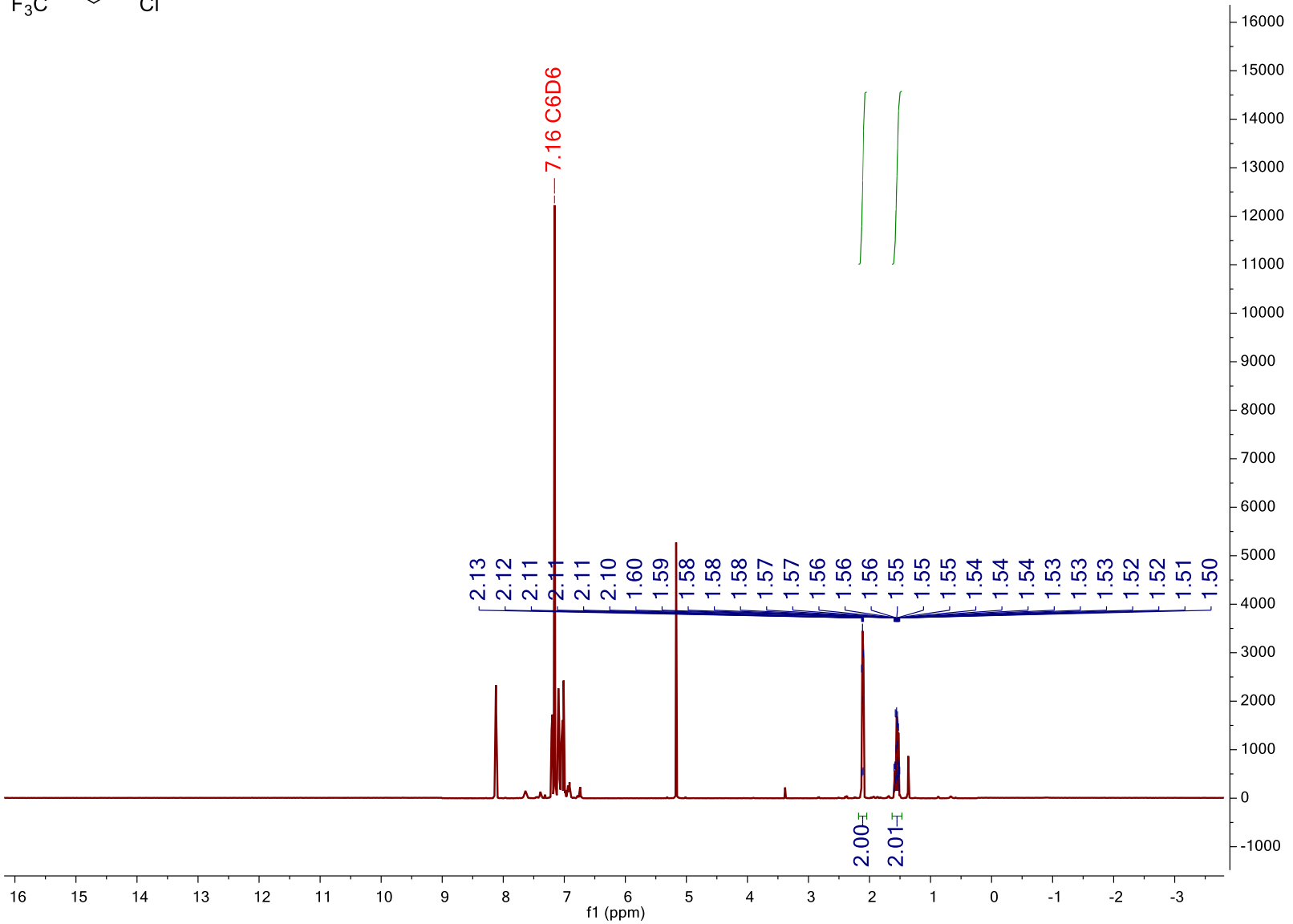
7.16 C6D6
2.13
2.12
2.11
2.11
2.11
2.10
1.60
1.59
1.58
1.58
1.58
1.57
1.57
1.56
1.56
1.56
1.55
1.55
1.55
1.54
1.54
1.54
1.53
1.53
1.53
1.52
1.52
1.51
1.50
2.00
2.01
f1 (ppm)

In situ

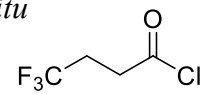
O
F3C
Cl

BnOBz
Standard
170.71
38.75
38.73
38.70
28.87
28.63
28.39
28.15
550
500
450
400
350
300
250
200
150
100
50
0
-50
210
200
190
180
170
160
150
140
130
120
110
100
90
80
70
60
50
40
30
20
10
0
-10
f1 (ppm)

In situ

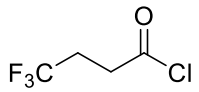

^{19}F NMR

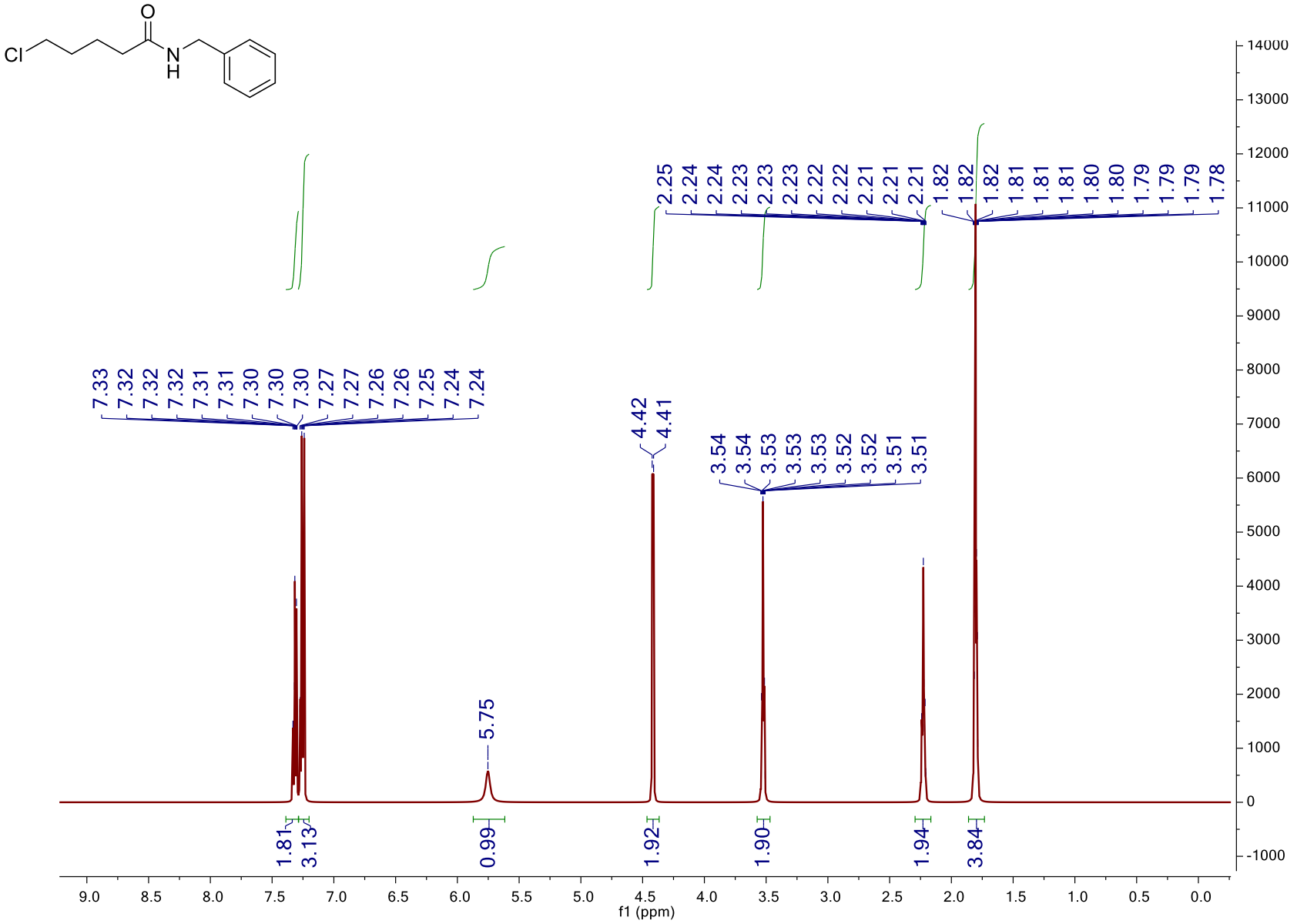
Cl
O
N
H
7.33
7.32
7.32
7.32
7.31
7.31
7.30
7.30
7.30
7.27
7.27
7.26
7.26
7.25
7.24
7.24
5.75
4.42
4.41
3.54
3.54
3.53
3.53
3.53
3.52
3.52
3.51
3.51
2.25
2.24
2.24
2.23
2.23
2.23
2.22
2.22
2.21
2.21
2.21
1.82
1.82
1.82
1.81
1.81
1.81
1.80
1.80
1.79
1.79
1.79
1.78
1.81
3.13
0.99
1.92
1.90
1.94
3.84
f1 (ppm)

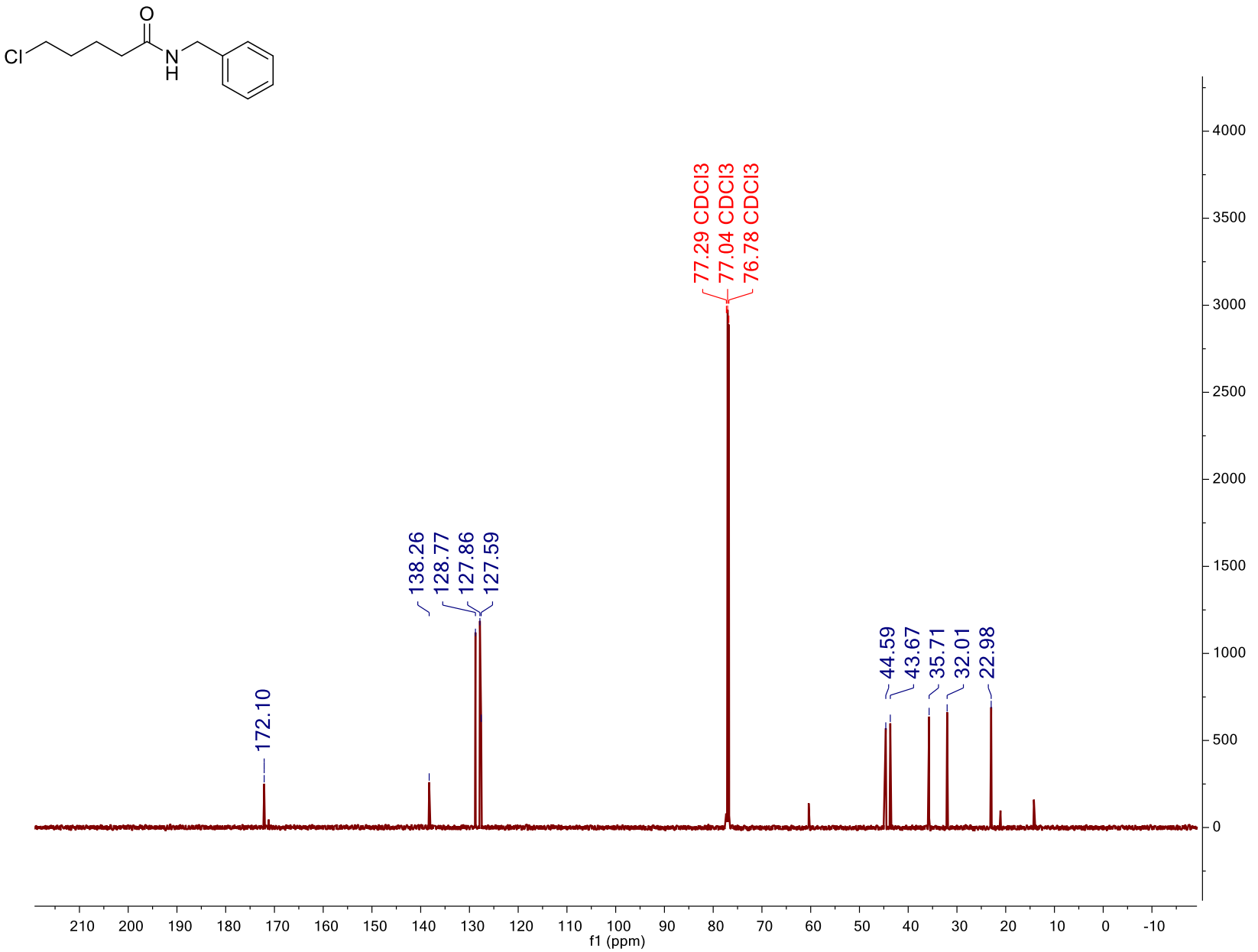
O
Cl
N
H
77.29 CDCl3
77.04 CDCl3
76.78 CDCl3
138.26
128.77
127.86
127.59
172.10
44.59
43.67
35.71
32.01
22.98
4000
3500
3000
2500
2000
1500
1000
500
0
210 200 190 180 170 160 150 140 130 120 110 100 90 80 70 60 50 40 30 20 10 0 -10
f1 (ppm)

In situ

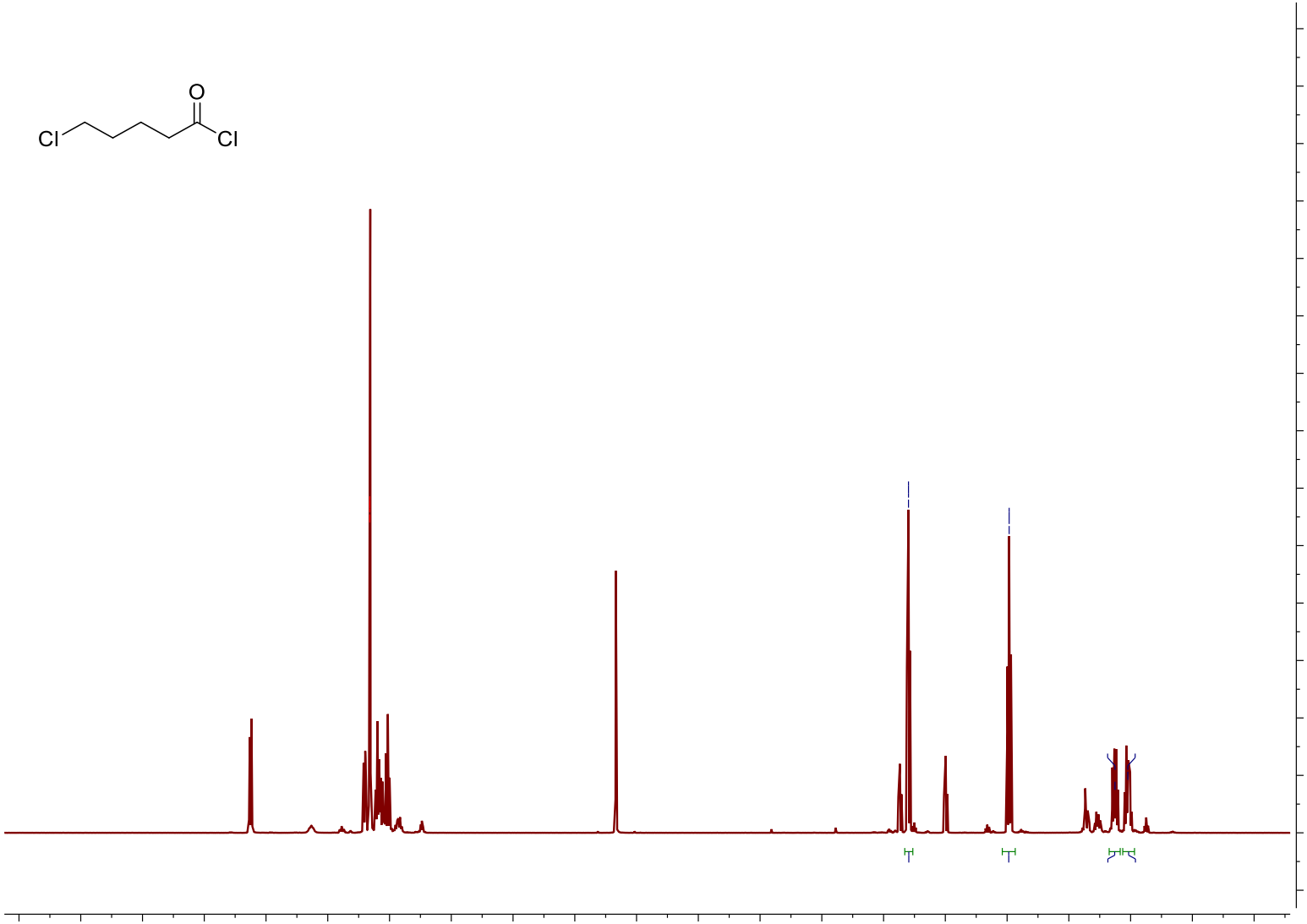

In situ

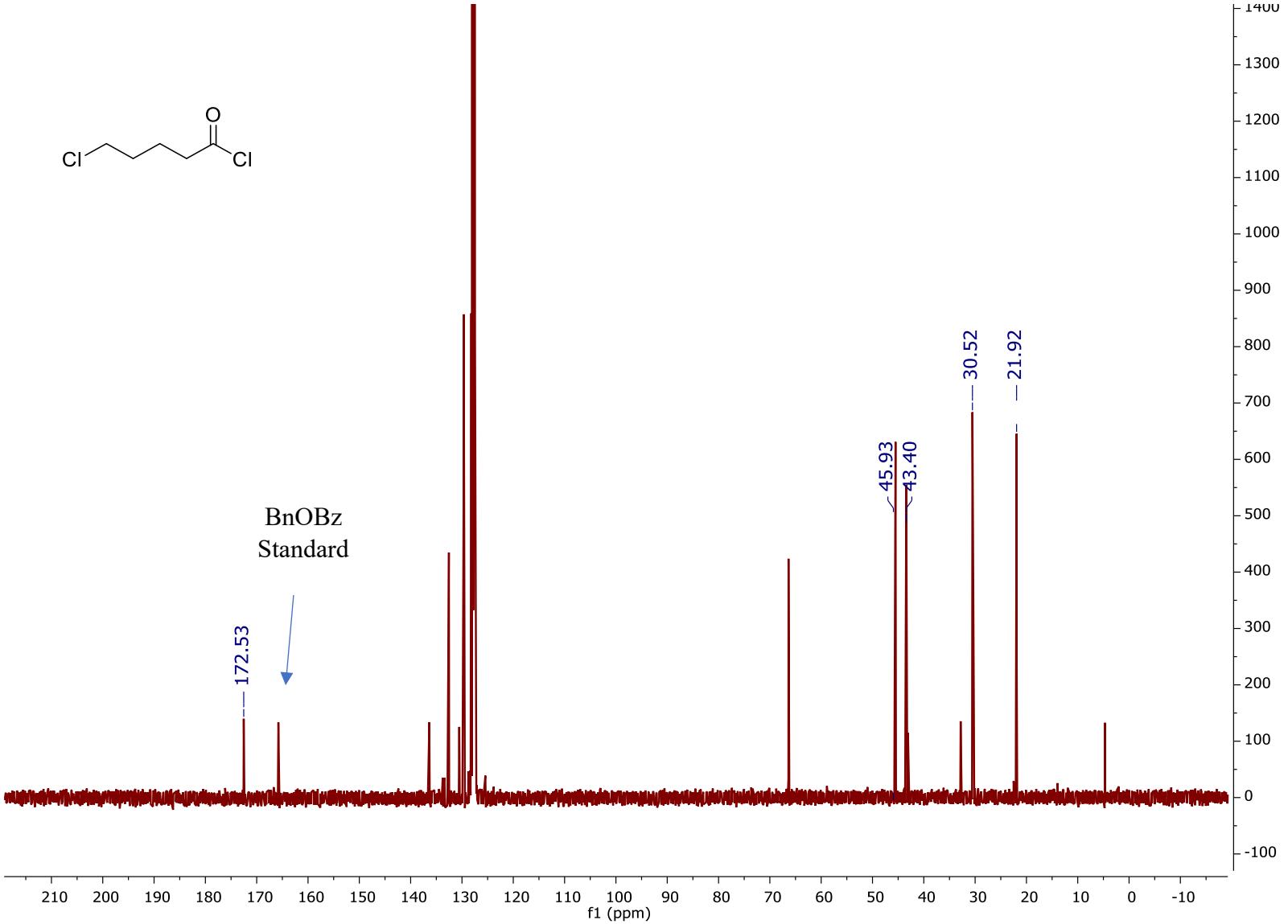

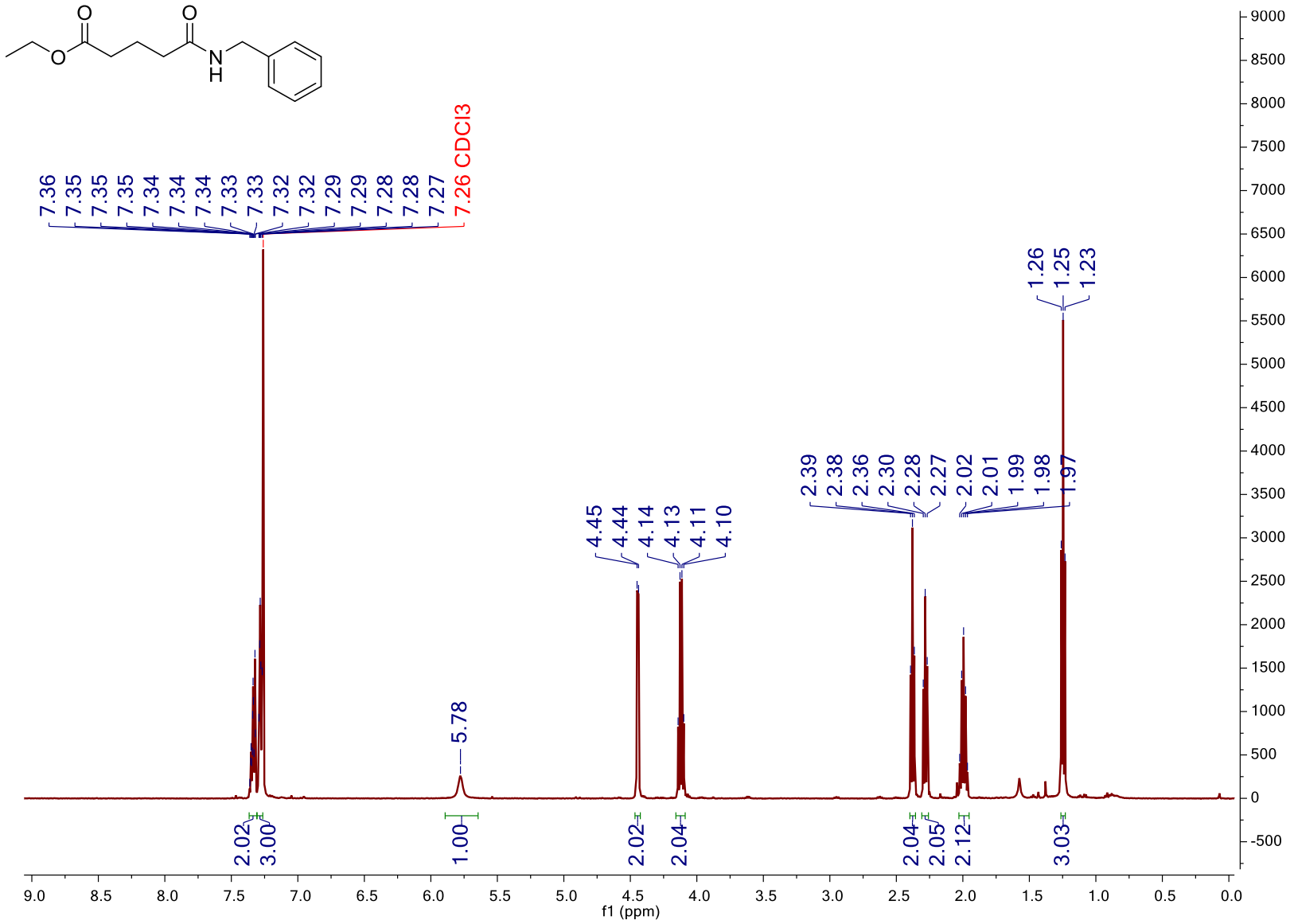
O
O
O
N
H
7.36
7.35
7.35
7.35
7.34
7.34
7.34
7.33
7.33
7.32
7.32
7.29
7.29
7.28
7.28
7.27
7.26 CDCl3
5.78
4.45
4.44
4.14
4.13
4.11
4.10
2.39
2.38
2.36
2.30
2.28
2.27
2.02
2.01
1.99
1.98
1.97
1.26
1.25
1.23
2.02
3.00
1.00
2.02
2.04
2.04
2.05
2.12
3.03
f1 (ppm)

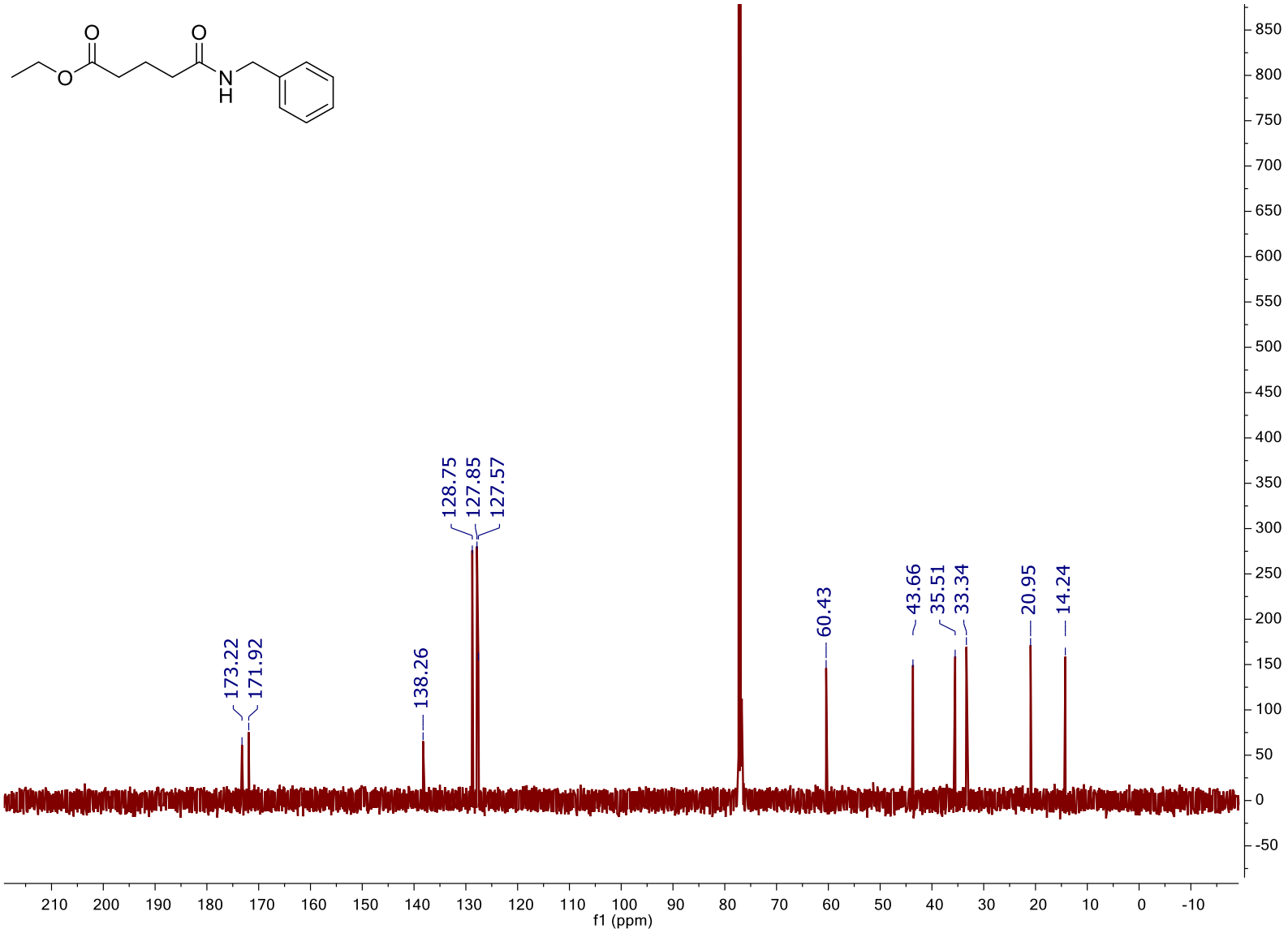
O
O
O
N
H
173.22
171.92
138.26
128.75
127.85
127.57
60.43
43.66
35.51
33.34
20.95
14.24
f1 (ppm)

In situ

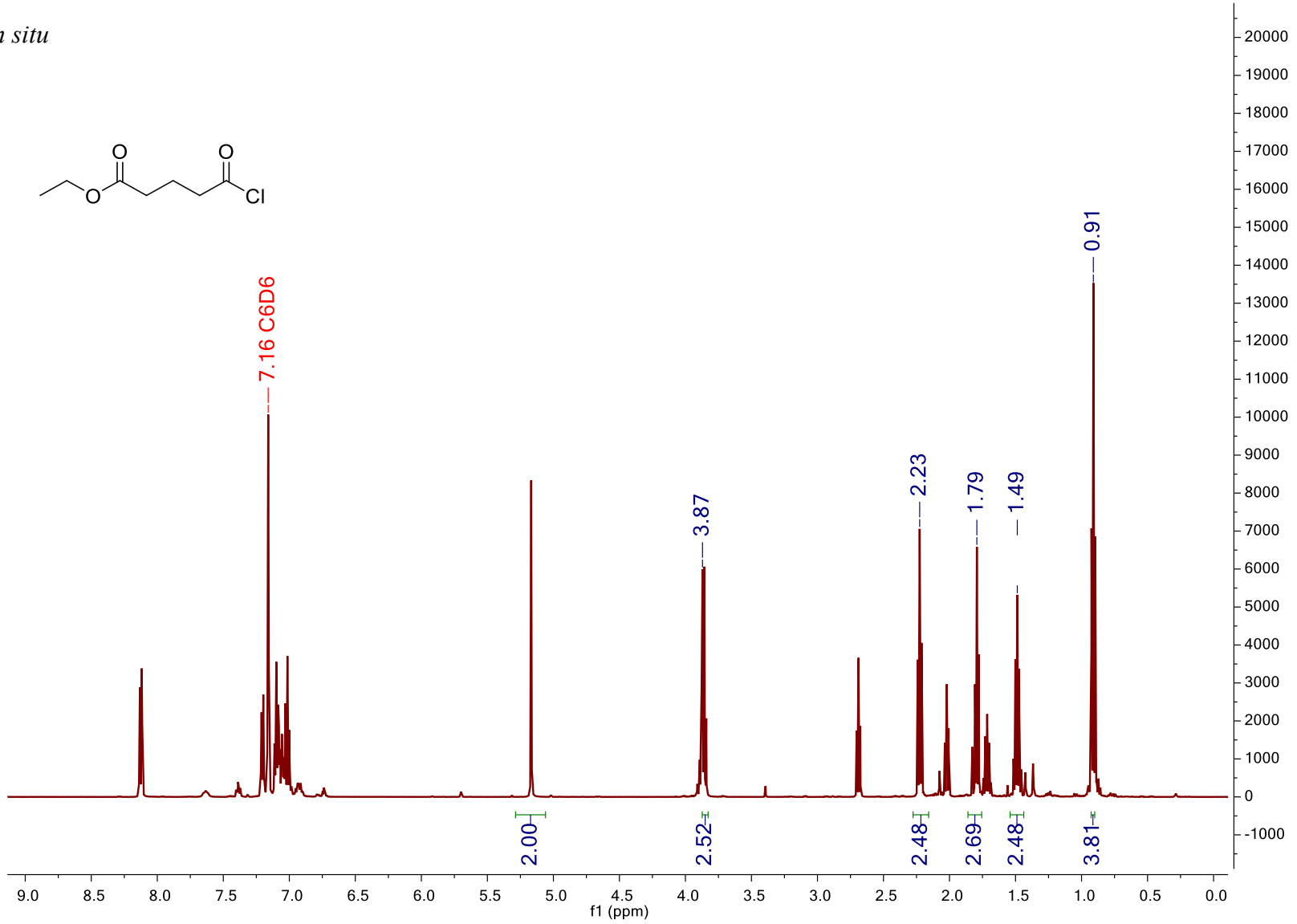
O
O
O
Cl
7.16 C6D6
0.91
3.87
2.23
1.79
1.49
2.00
2.52
2.48
2.69
2.48
3.81
f1 (ppm)

In situ

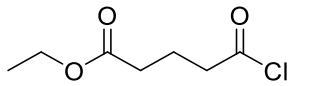
O
O
O
Cl

BnOBz
Standard
172.64
171.28
59.94
45.47
31.79
19.94
13.82
9000
8500
8000
7500
7000
6500
6000
5500
5000
4500
4000
3500
3000
2500
2000
1500
1000
500
0
-500
210
200
190
180
170
160
150
140
130
120
110
100
90
80
70
60
50
40
30
20
10
0
-10
f1 (ppm)

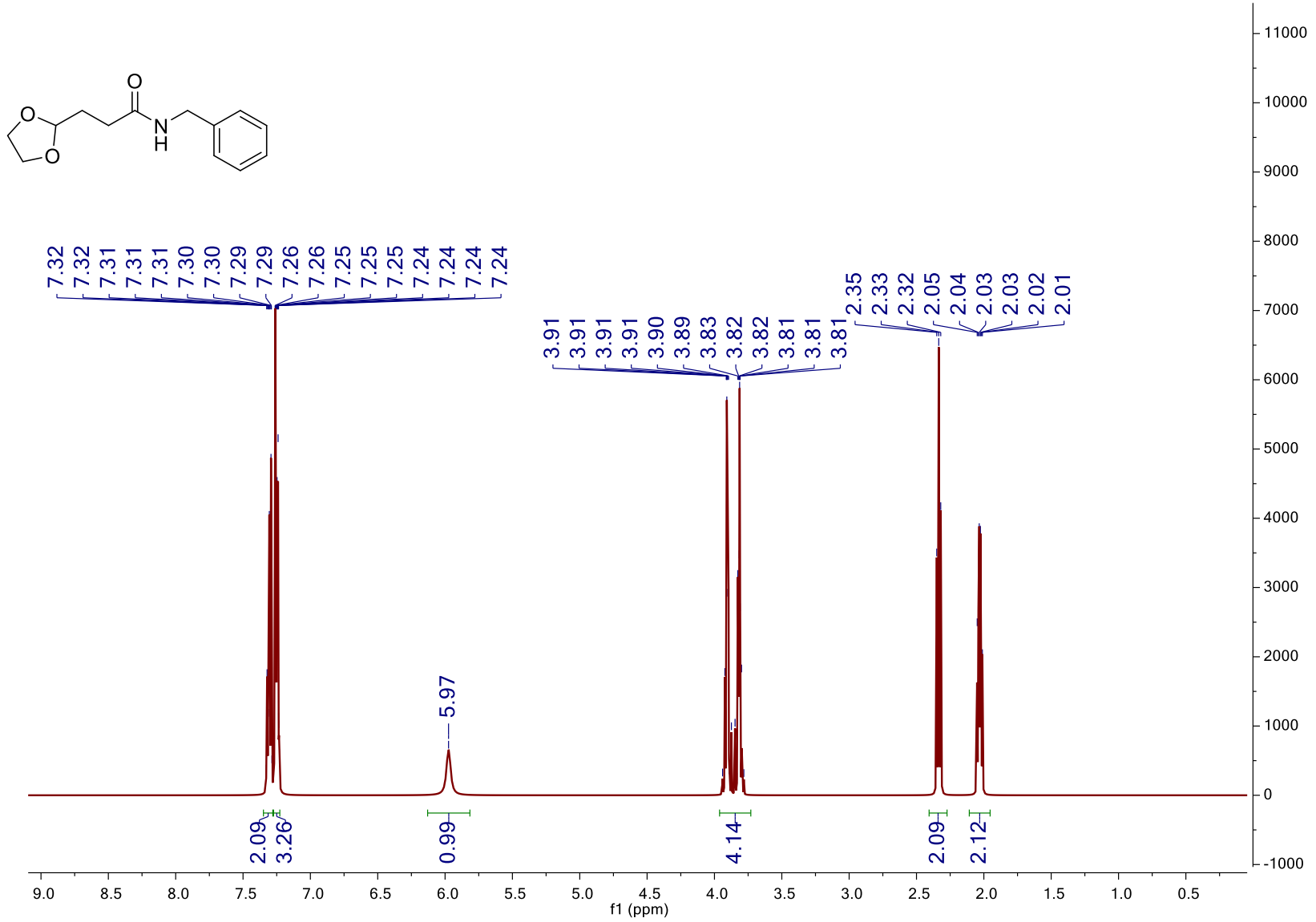
O
O
O
N
H
7.32
7.32
7.31
7.31
7.31
7.30
7.30
7.29
7.29
7.26
7.26
7.25
7.25
7.25
7.24
7.24
7.24
7.24
3.91
3.91
3.91
3.91
3.90
3.89
3.83
3.82
3.82
3.81
3.81
3.81
2.35
2.33
2.32
2.05
2.04
2.03
2.03
2.02
2.01
5.97
2.09
3.26
0.99
4.14
2.09
2.12
f1 (ppm)

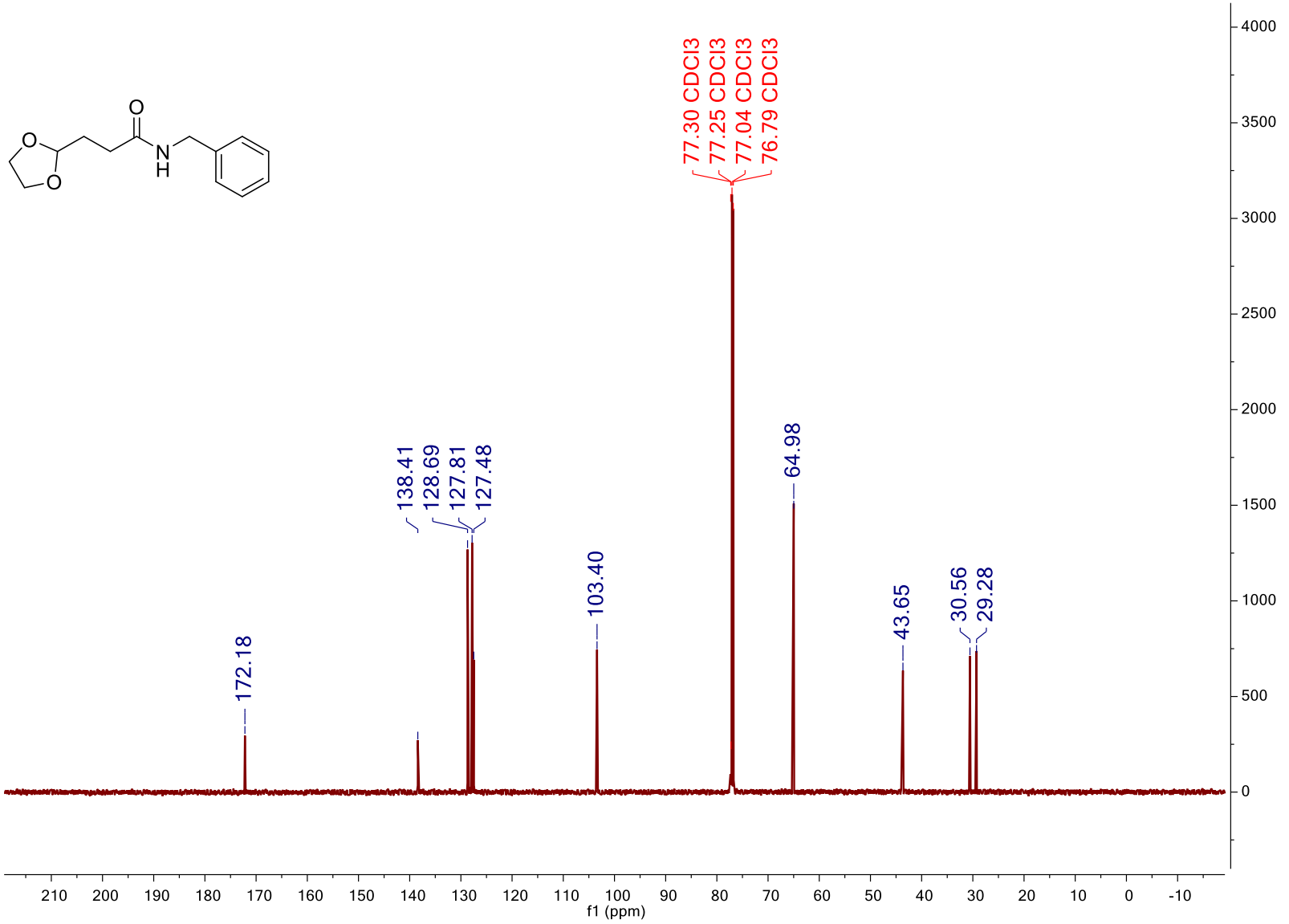
O
O
O
N
H
77.30 CDCl3
77.25 CDCl3
77.04 CDCl3
76.79 CDCl3
138.41
128.69
127.81
127.48
172.18
103.40
64.98
43.65
30.56
29.28
4000
3500
3000
2500
2000
1500
1000
500
0
210 200 190 180 170 160 150 140 130 120 110 100 90 80 70 60 50 40 30 20 10 0 -10
f1 (ppm)

In situ

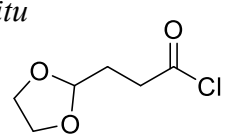

In situ

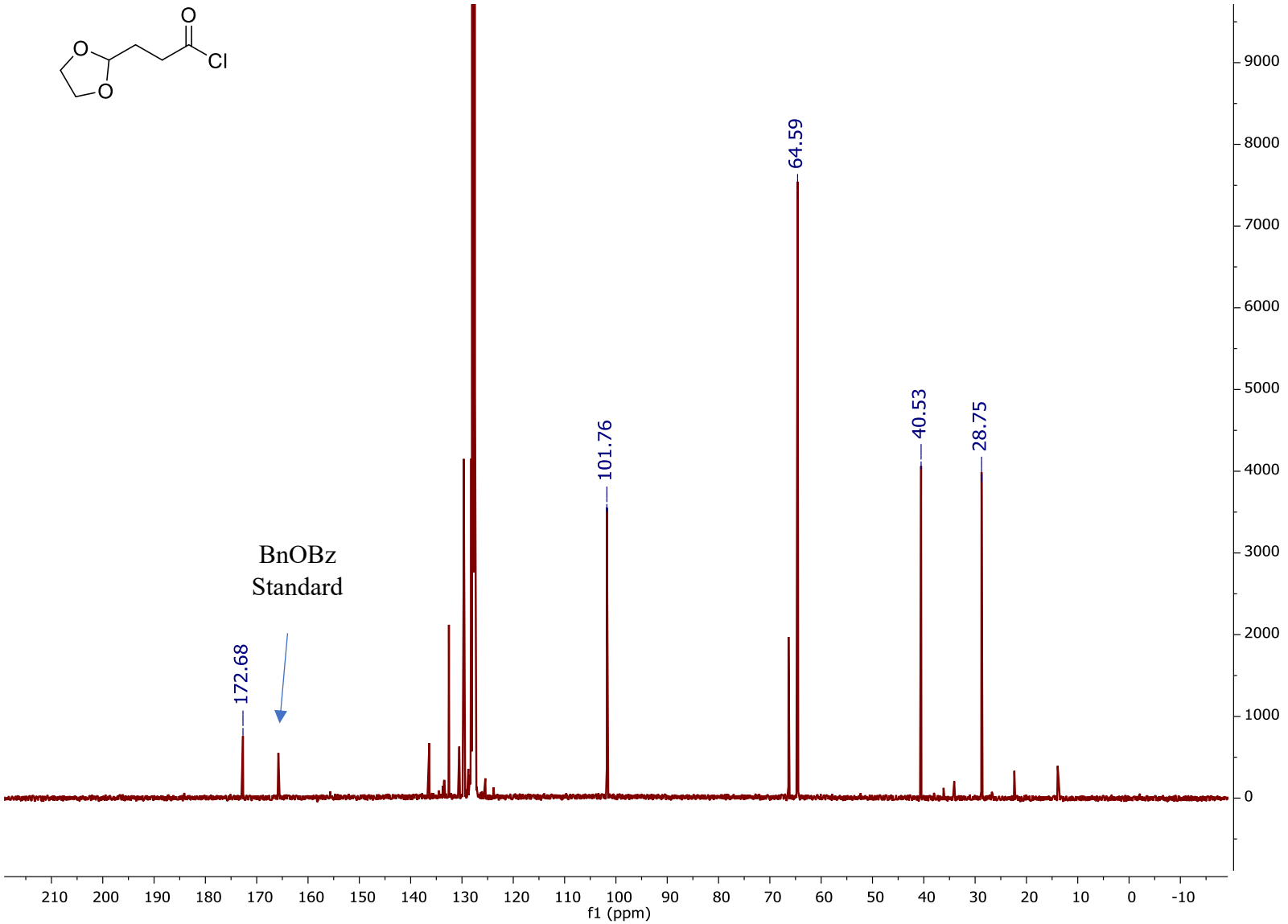
O
O
O
Cl
BnOBz
Standard
172.68
101.76
64.59
40.53
28.75
9000
8000
7000
6000
5000
4000
3000
2000
1000
0
210 200 190 180 170 160 150 140 130 120 110 100 90 80 70 60 50 40 30 20 10 0 -10
f1 (ppm)

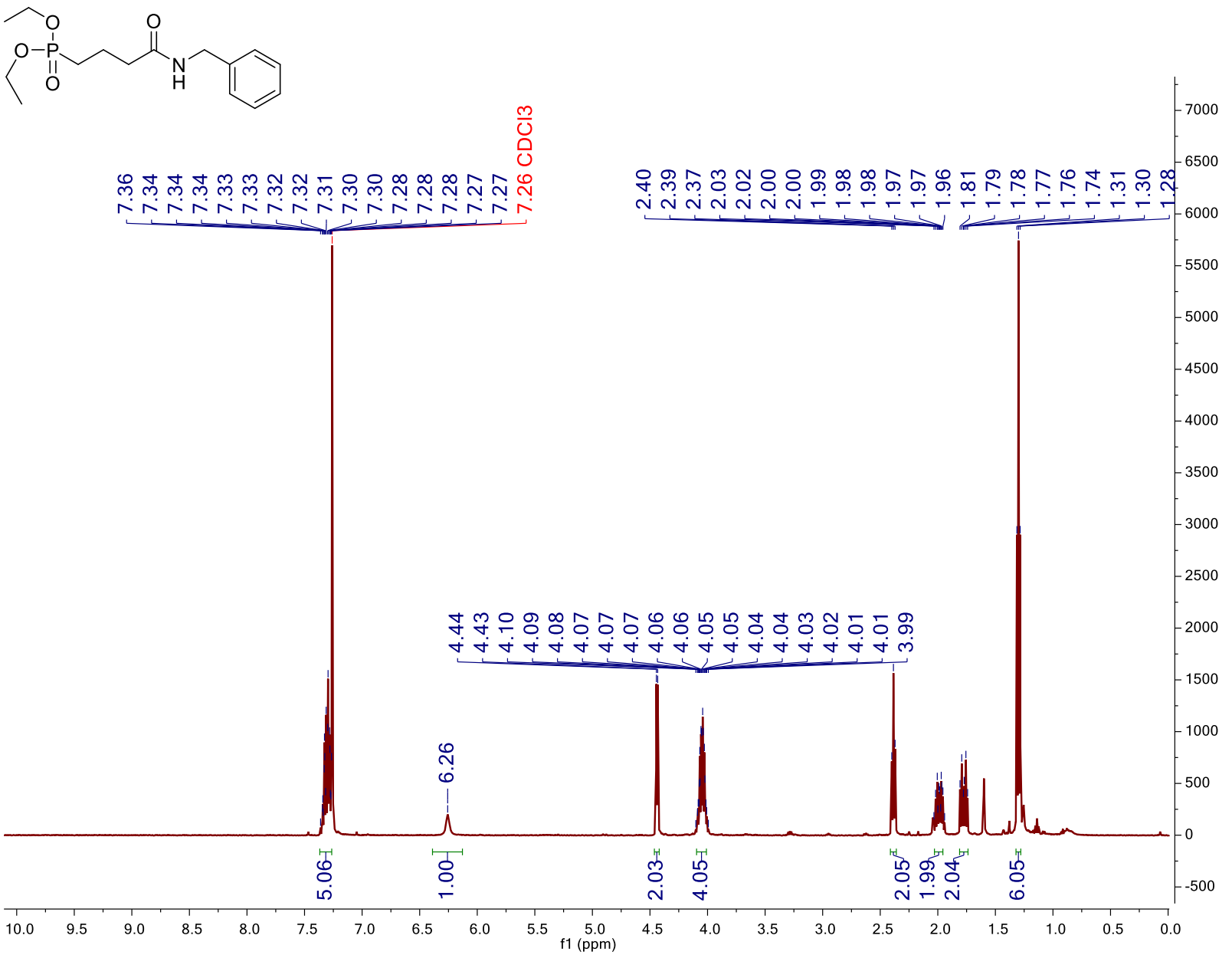
7.36
7.34
7.34
7.34
7.33
7.33
7.32
7.32
7.31
7.30
7.30
7.28
7.28
7.28
7.27
7.27
7.26 CDCl3
2.40
2.39
2.37
2.03
2.02
2.00
2.00
1.99
1.98
1.98
1.97
1.97
1.96
1.81
1.79
1.78
1.77
1.76
1.74
1.31
1.30
1.28
4.44
4.43
4.10
4.09
4.08
4.07
4.07
4.07
4.06
4.06
4.05
4.05
4.04
4.04
4.03
4.02
4.01
4.01
3.99
6.26
5.06
1.00
2.03
4.05
2.05
1.99
2.04
6.05
f1 (ppm)

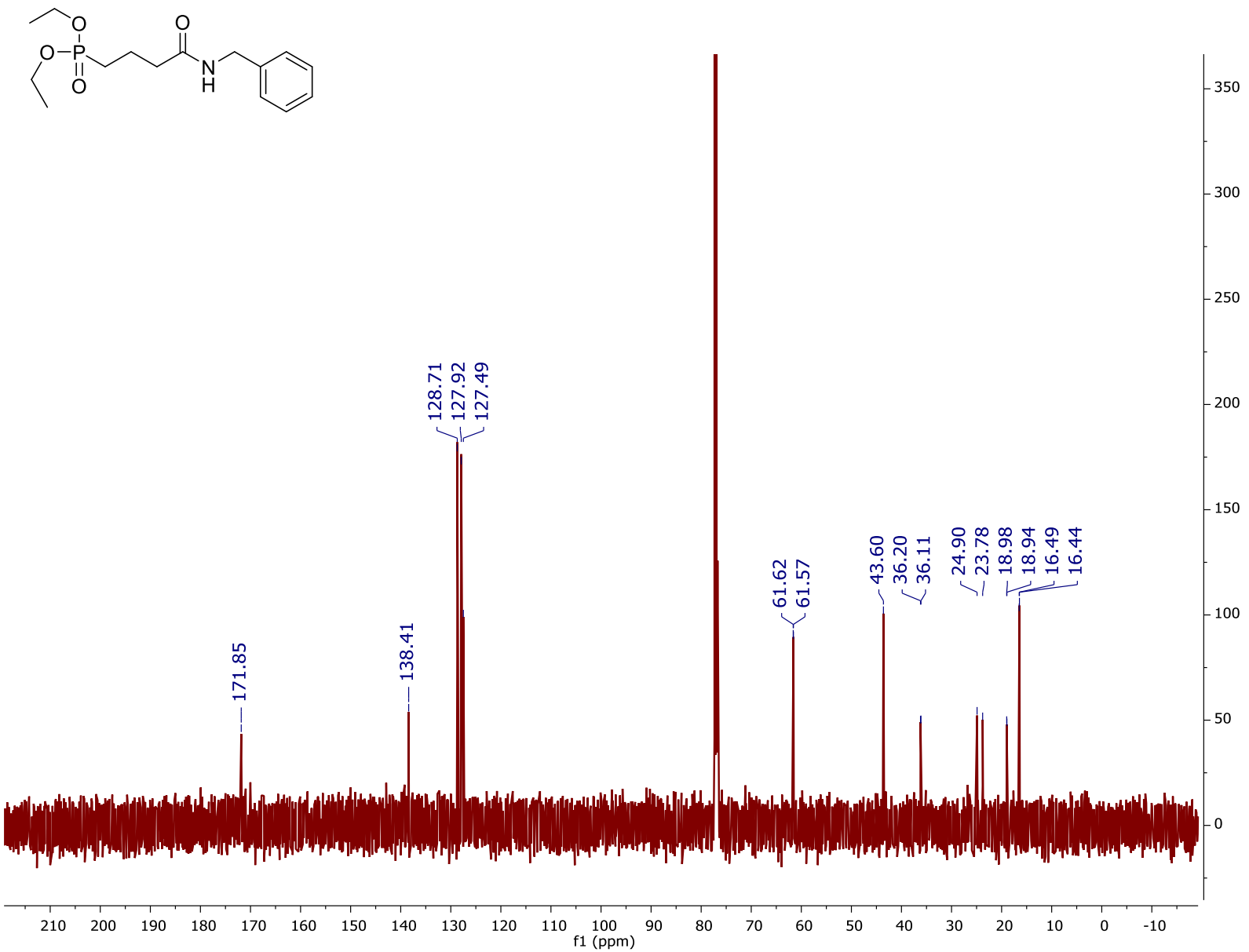
O
O
O
P
O
O
N
H
171.85
138.41
128.71
127.92
127.49
61.62
61.57
43.60
36.20
36.11
24.90
23.78
18.98
18.94
16.49
16.44
350
300
250
200
150
100
50
0
210
200
190
180
170
160
150
140
130
120
110
100
90
80
70
60
50
40
30
20
10
0
-10
f1 (ppm)

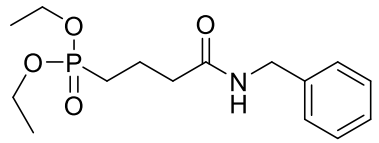

^{31}P NMR

31.41
600
550
500
450
400
350
300
250
200
150
100
50
0
-50
140
120
100
80
60
40
20
0
-20
-40
-60
-80
-100
-120
-140
-160
-180
-200
-220
-240
f1 (ppm)

In situ

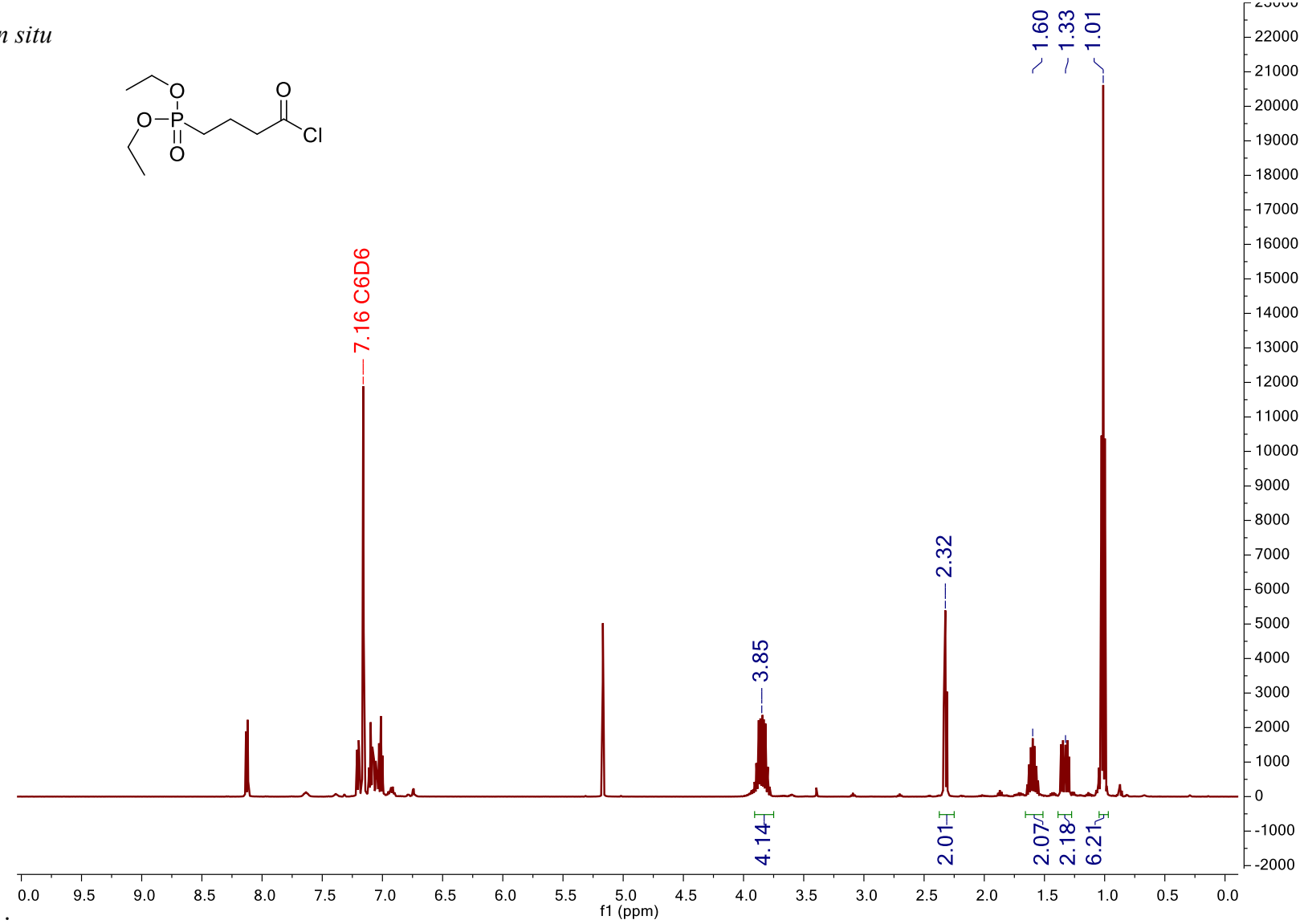

In situ

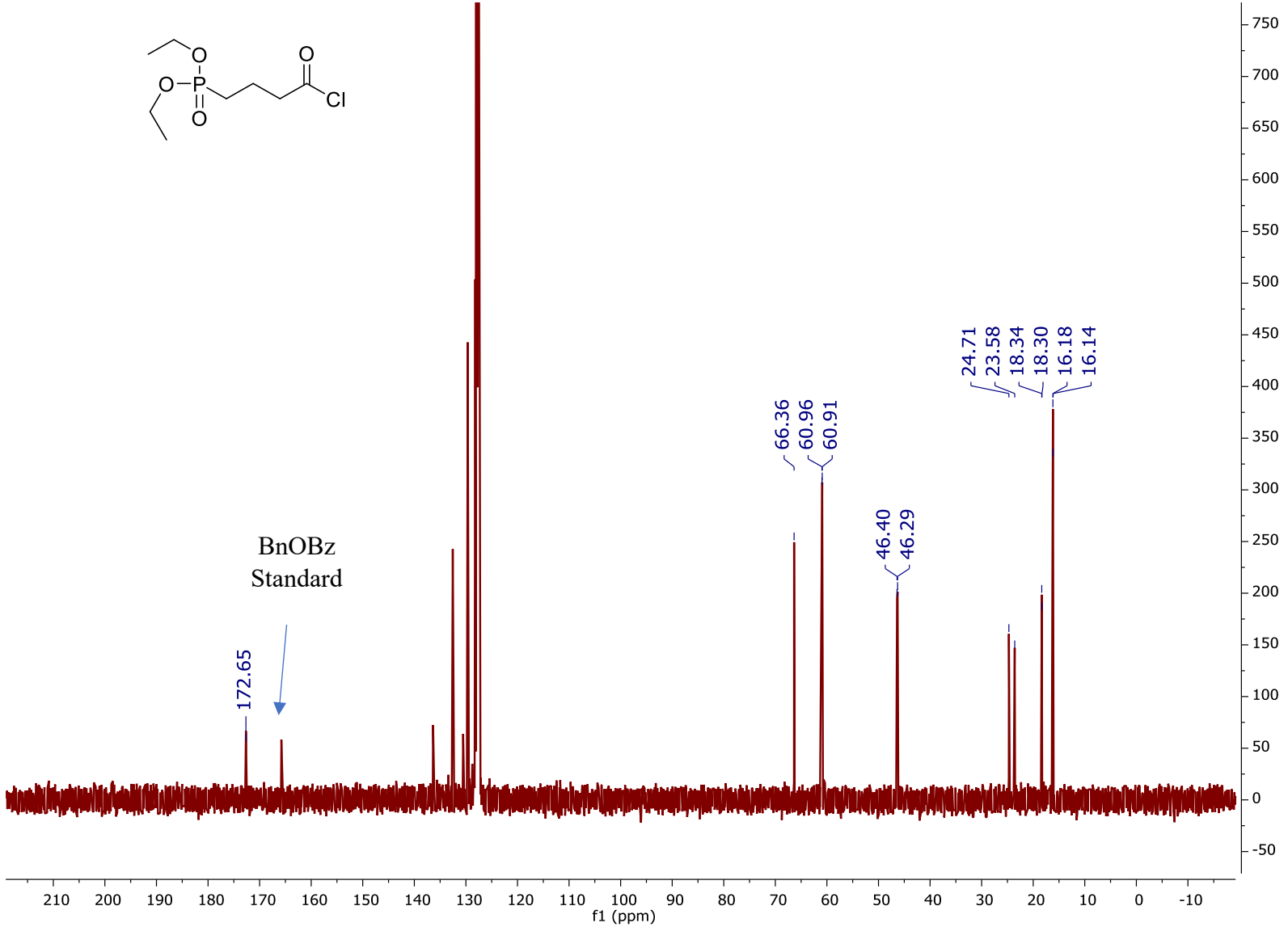
BnOBz
Standard
172.65
66.36
60.96
60.91
46.40
46.29
24.71
23.58
18.34
18.30
16.18
16.14
f1 (ppm)

In situ

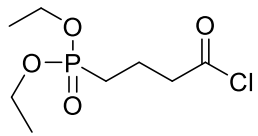

^{31}P NMR

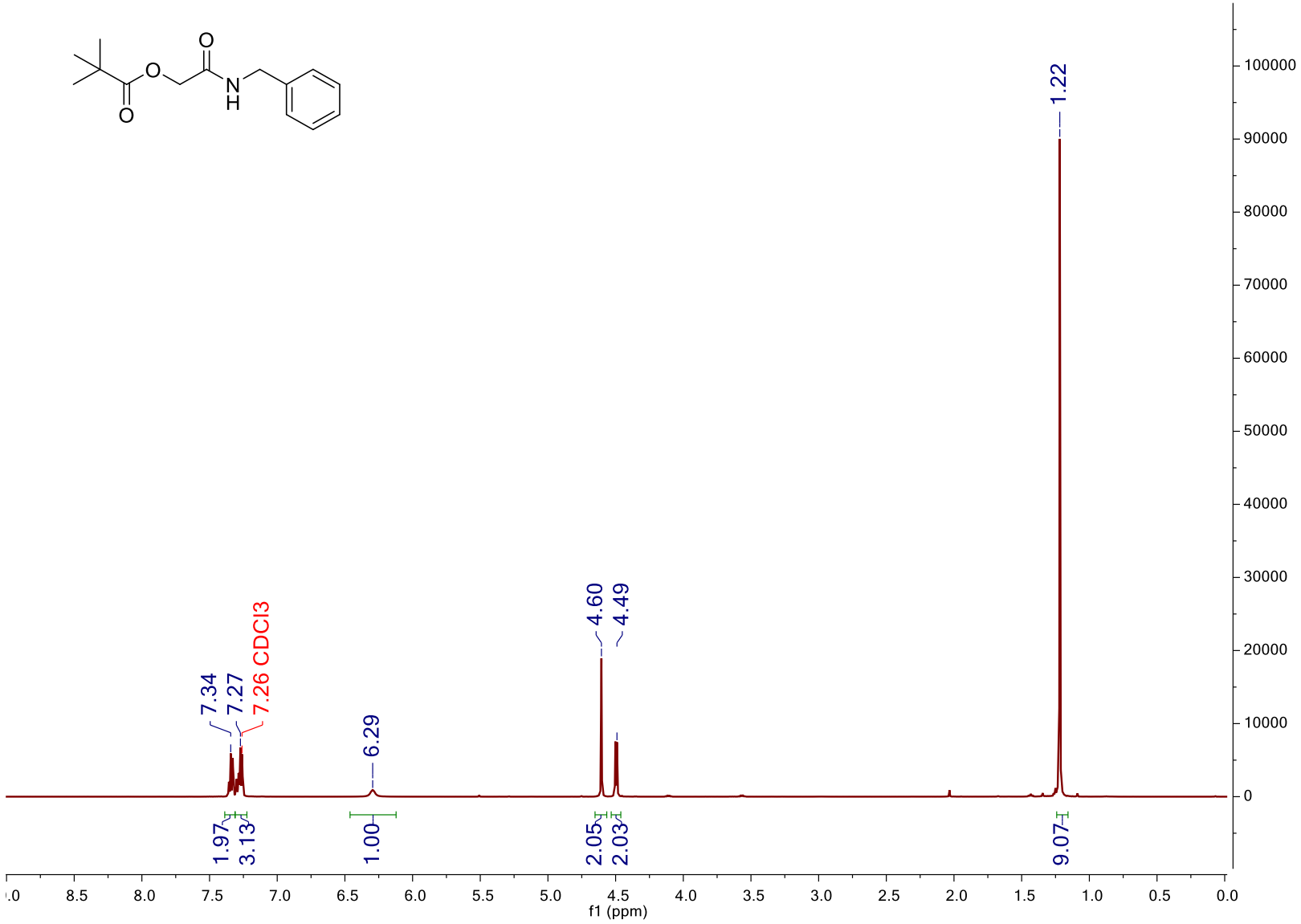
O
O
O
N
H
7.34
7.27
7.26 CDCl3
6.29
4.60
4.49
1.22
1.97
3.13
1.00
2.05
2.03
9.07
f1 (ppm)

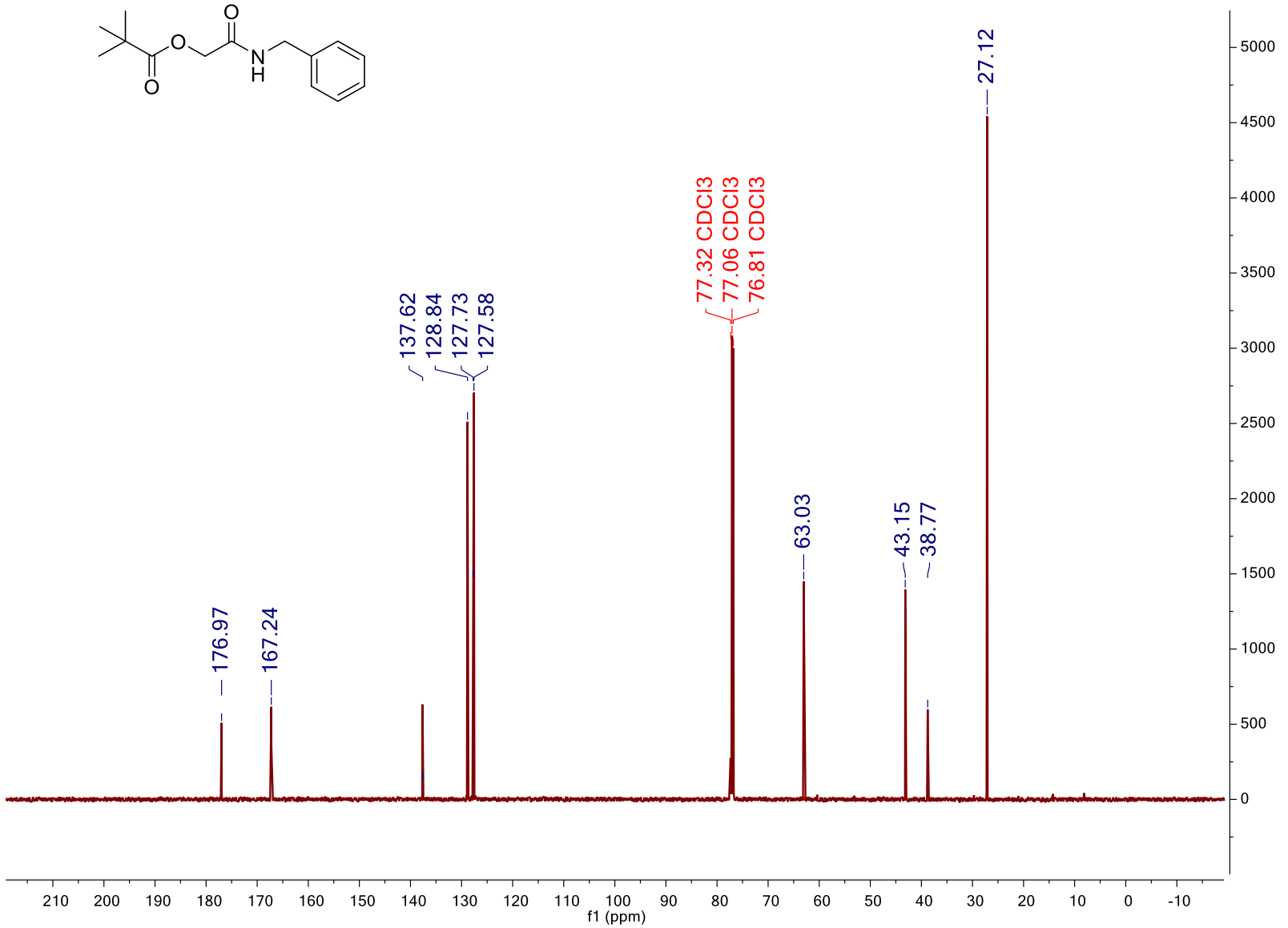
O
O
O
N
H
176.97
167.24
137.62
128.84
127.73
127.58
77.32 CDCl3
77.06 CDCl3
76.81 CDCl3
63.03
43.15
38.77
27.12
5000
4500
4000
3500
3000
2500
2000
1500
1000
500
0
210 200 190 180 170 160 150 140 130 120 110 100 90 80 70 60 50 40 30 20 10 0 -10
f1 (ppm)

In situ

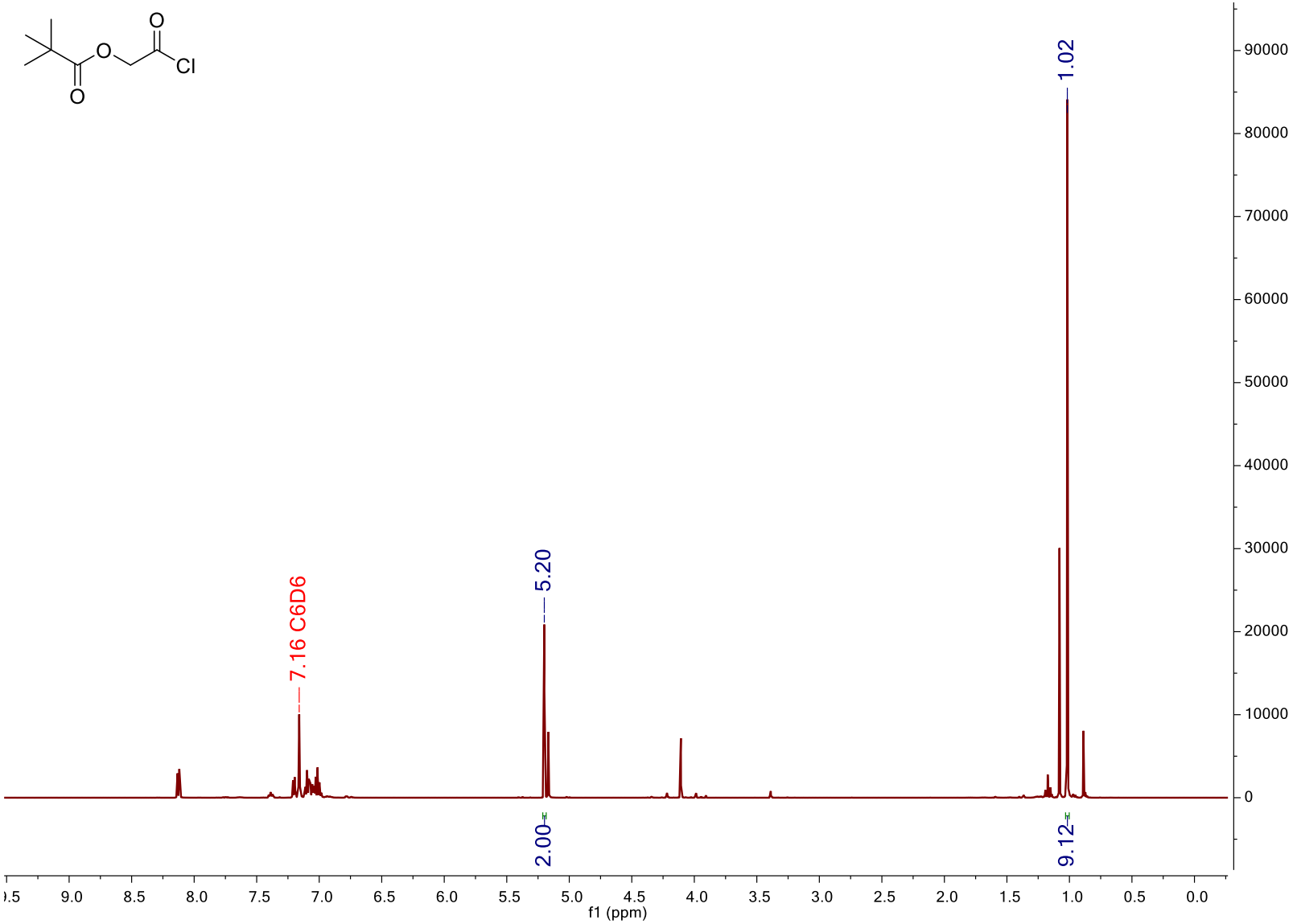

In situ

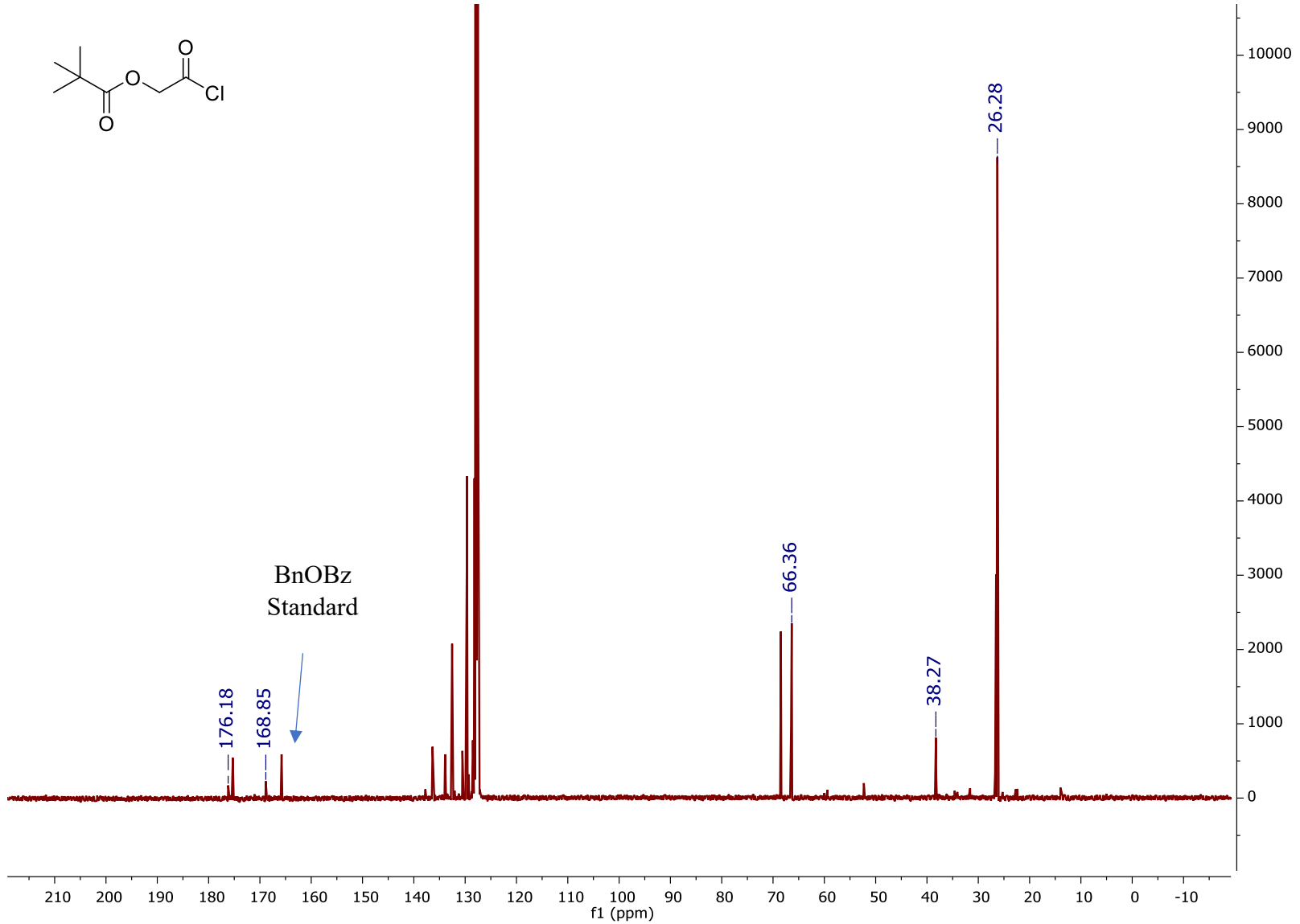
O
O
O
Cl
BnOBz
Standard
176.18
168.85
66.36
38.27
26.28
10000
9000
8000
7000
6000
5000
4000
3000
2000
1000
0
210 200 190 180 170 160 150 140 130 120 110 100 90 80 70 60 50 40 30 20 10 0 -10
f1 (ppm)

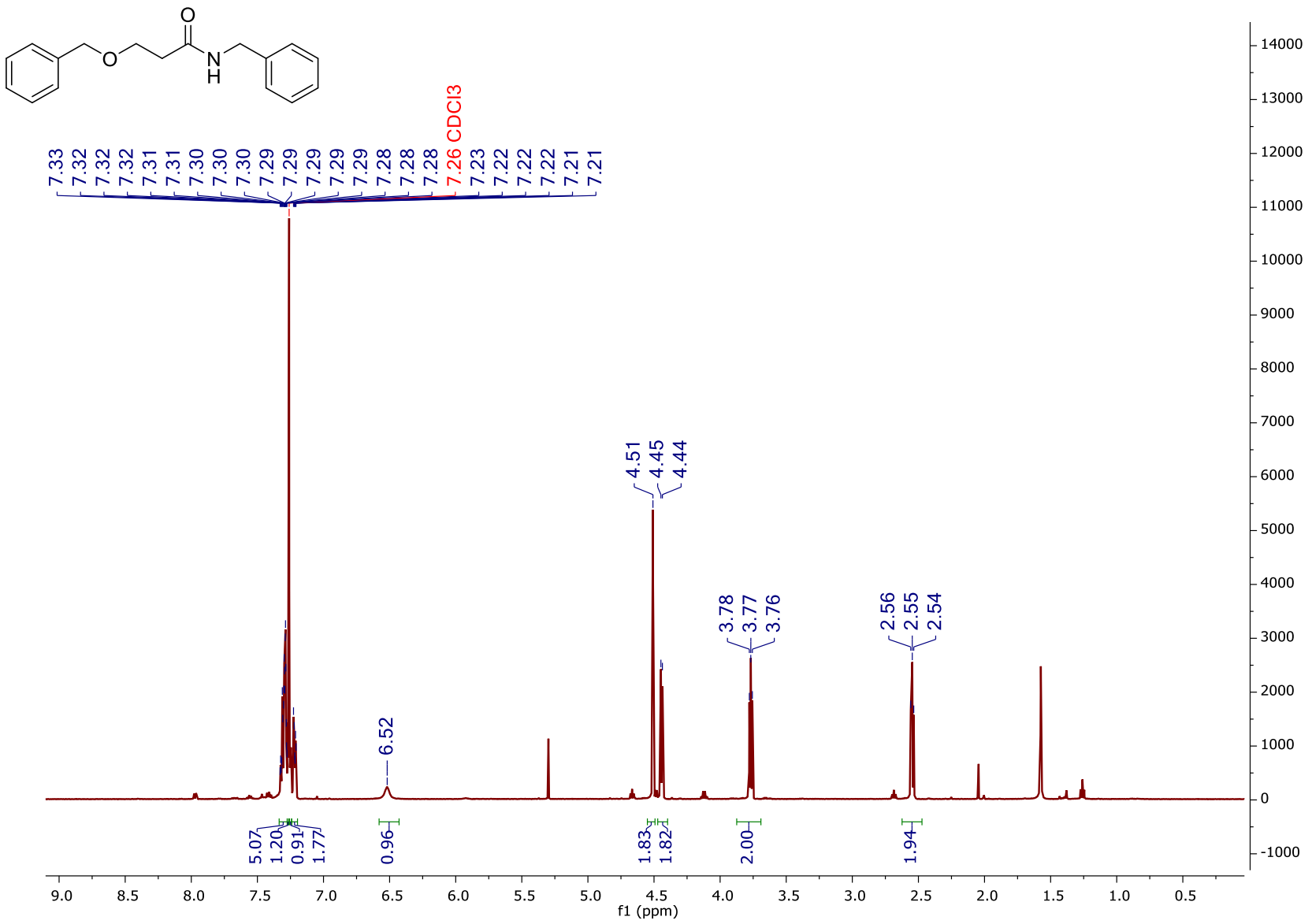
O
O
N
H
7.33
7.32
7.32
7.32
7.31
7.31
7.30
7.30
7.30
7.29
7.29
7.29
7.29
7.29
7.28
7.28
7.28
7.26 CDCl3
7.23
7.22
7.22
7.22
7.21
7.21
4.51
4.45
4.44
6.52
3.78
3.77
3.76
2.56
2.55
2.54
5.07
1.20
0.91
1.77
0.96
1.83
1.82
2.00
1.94
f1 (ppm)

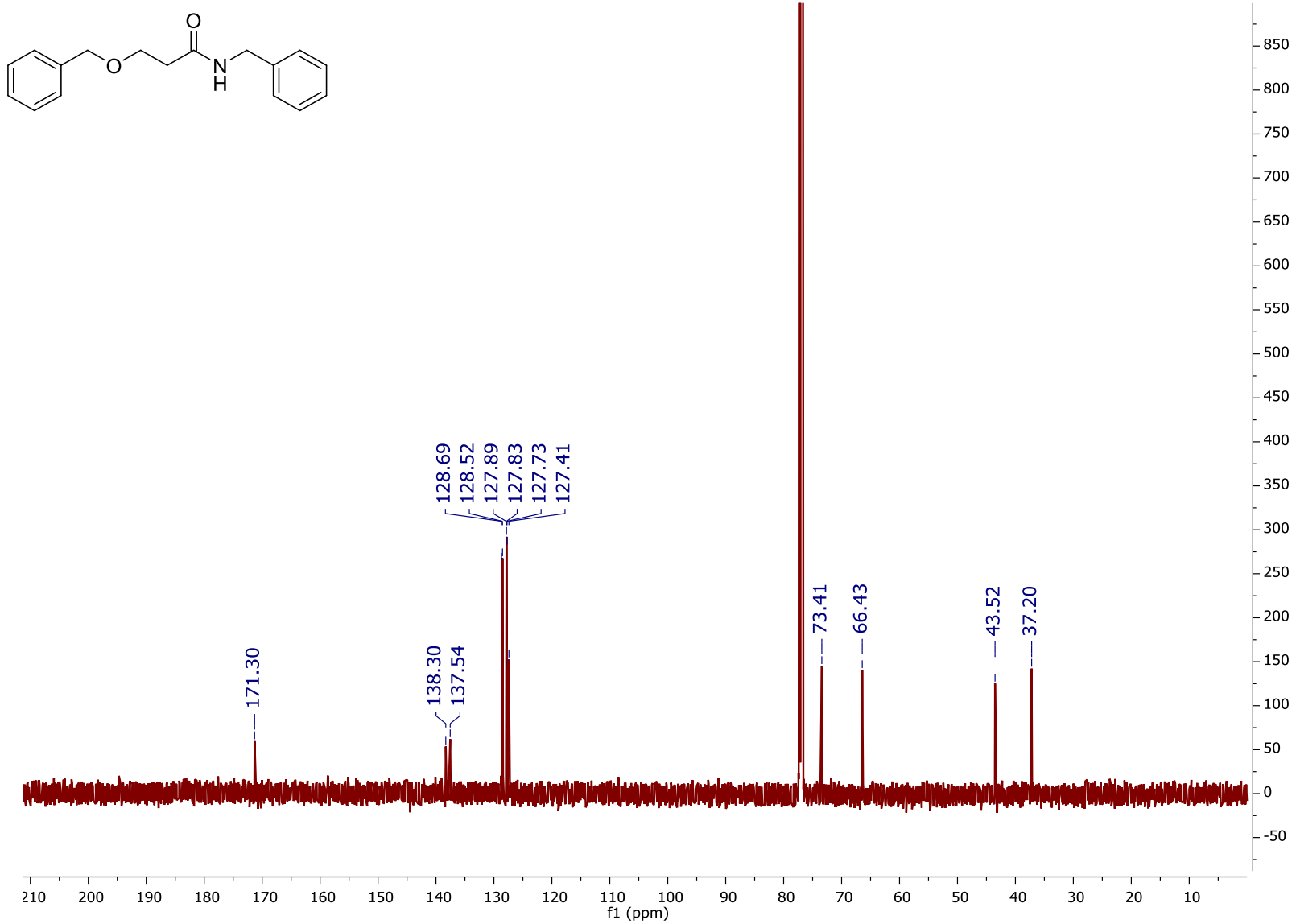
O
O
N
H
171.30
138.30
137.54
128.69
128.52
127.89
127.83
127.73
127.41
73.41
66.43
43.52
37.20
f1 (ppm)

In situ

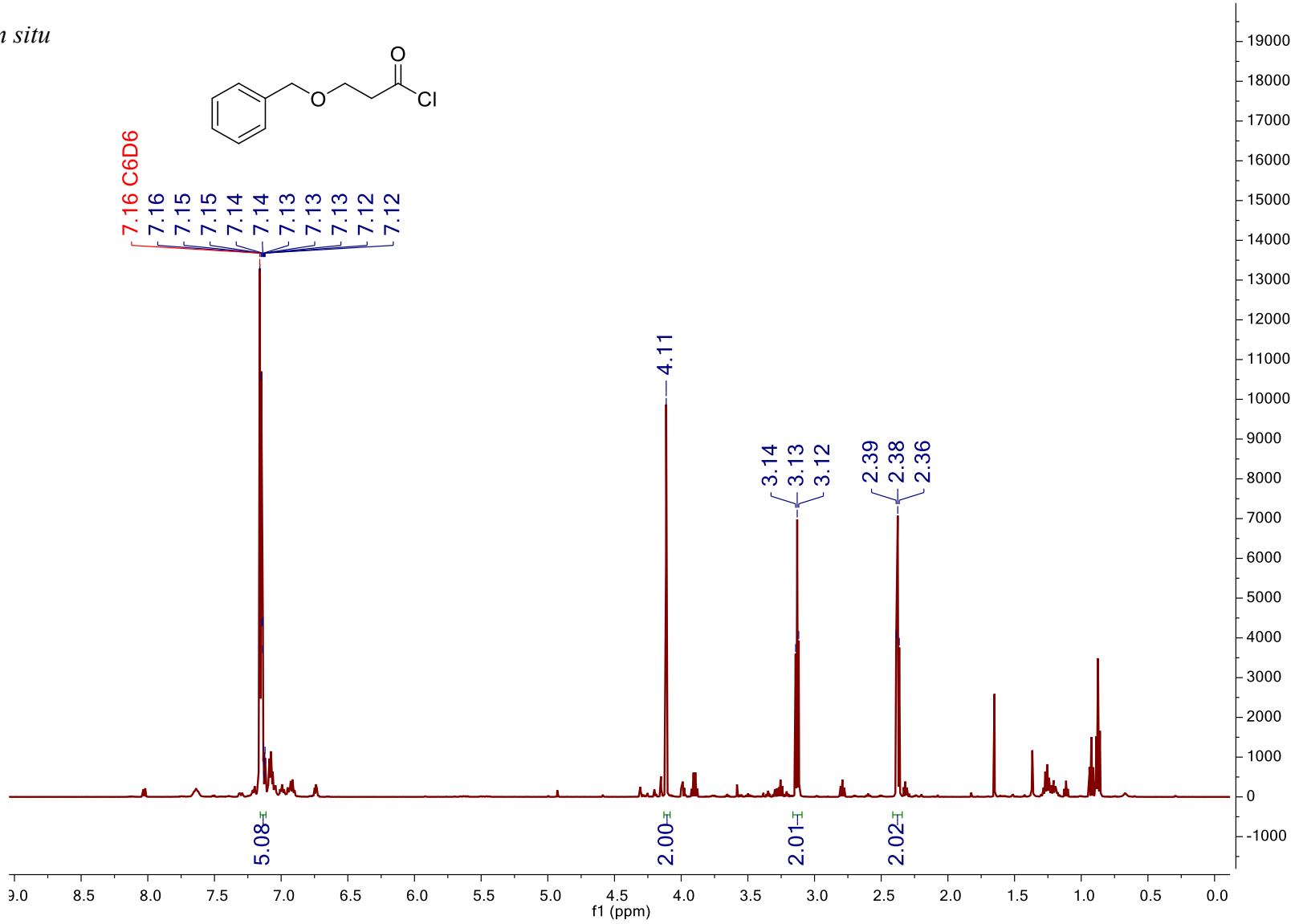
O
O
Cl
7.16 C6D6
7.16
7.15
7.15
7.14
7.14
7.13
7.13
7.13
7.12
7.12
4.11
3.14
3.13
3.12
2.39
2.38
2.36
5.08
2.00
2.01
2.02
f1 (ppm)

In situ

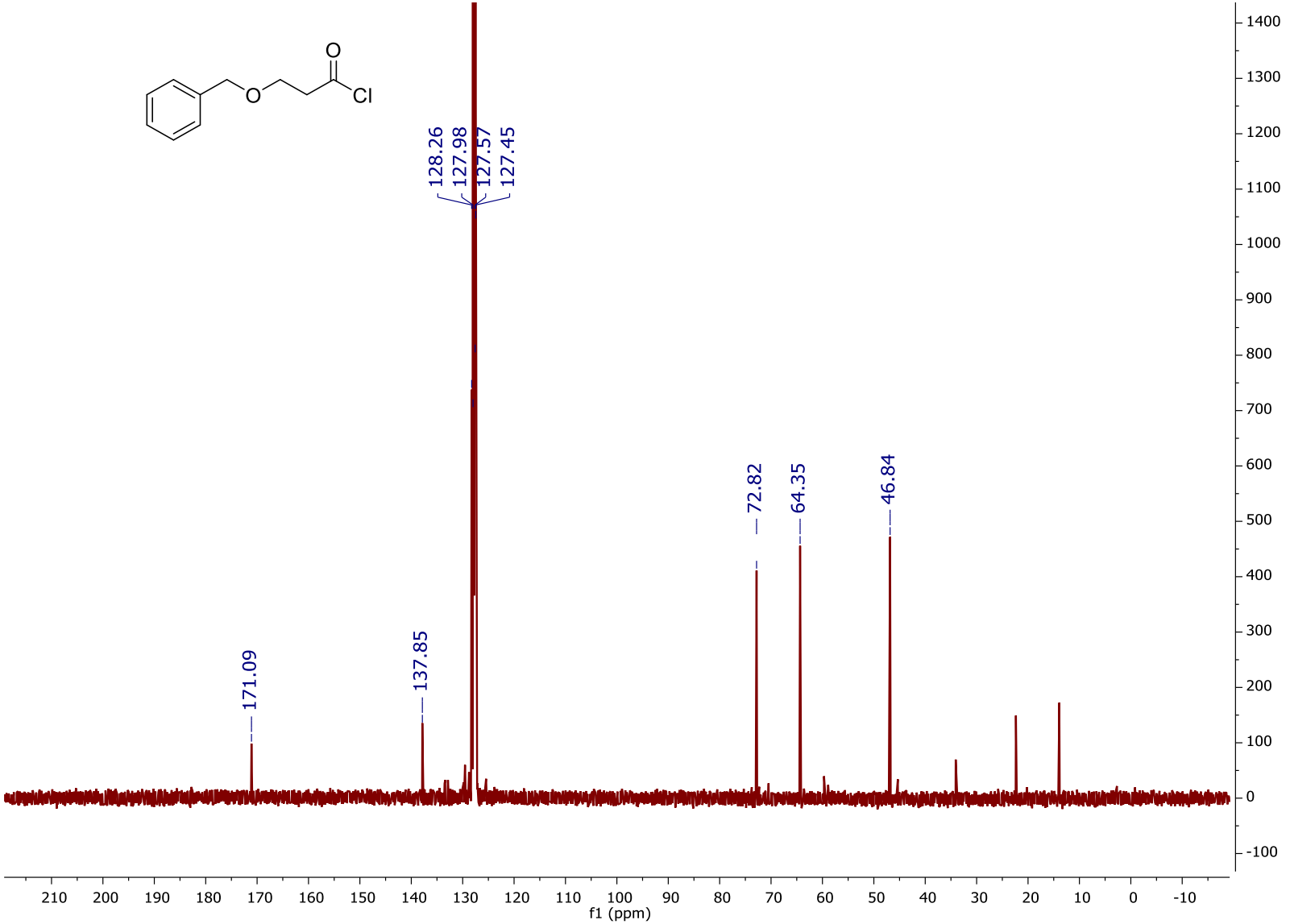
O
O
Cl
128.26
127.98
127.57
127.45
171.09
137.85
72.82
64.35
46.84
f1 (ppm)

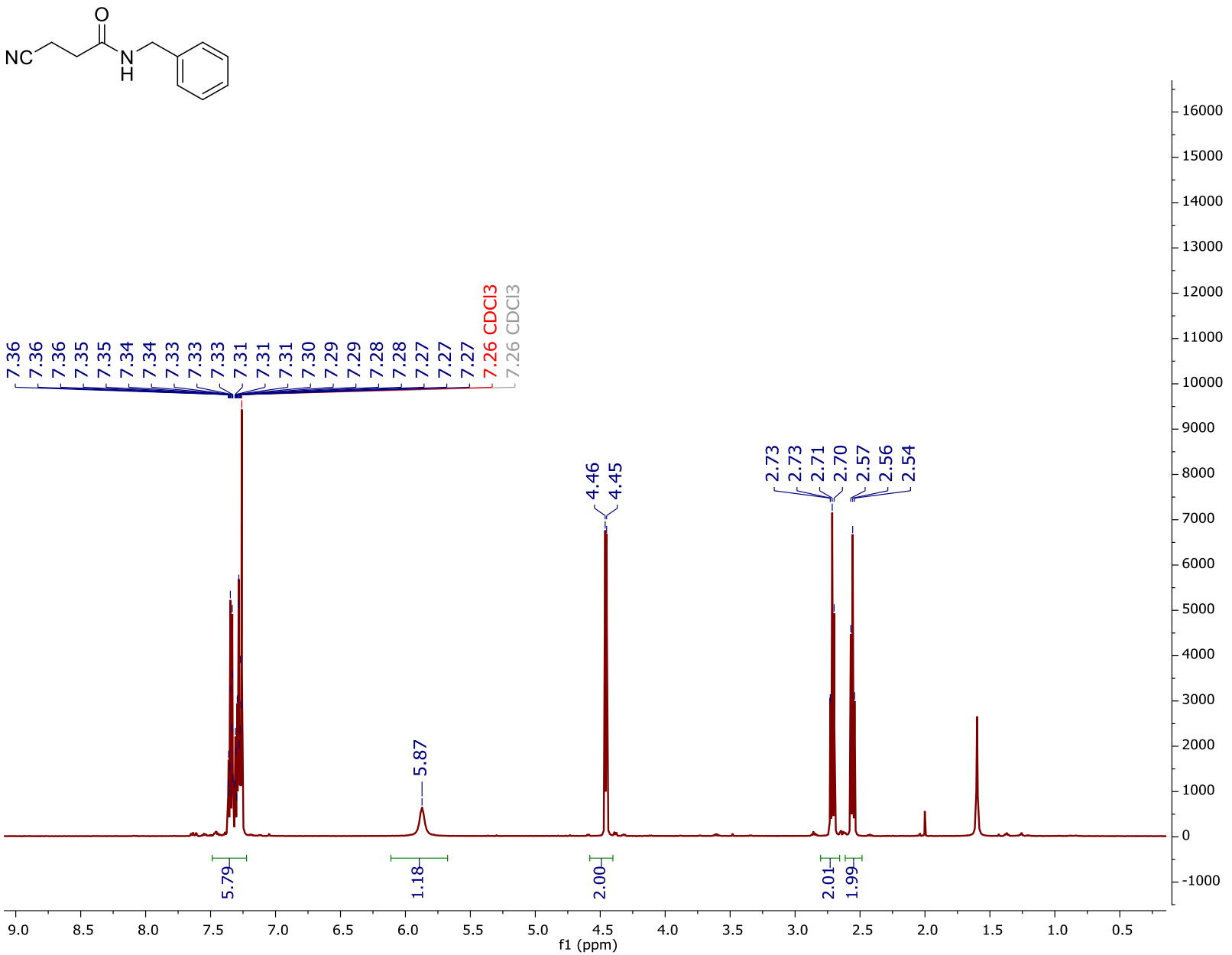
NC
O
N
H
7.36
7.36
7.36
7.35
7.35
7.34
7.34
7.33
7.33
7.33
7.31
7.31
7.31
7.30
7.29
7.29
7.28
7.28
7.27
7.27
7.27
7.26 CDCl3
7.26 CDCl3
4.46
4.45
2.73
2.73
2.71
2.70
2.57
2.56
2.54
5.87
5.79
1.18
2.00
2.01
1.99
f1 (ppm)

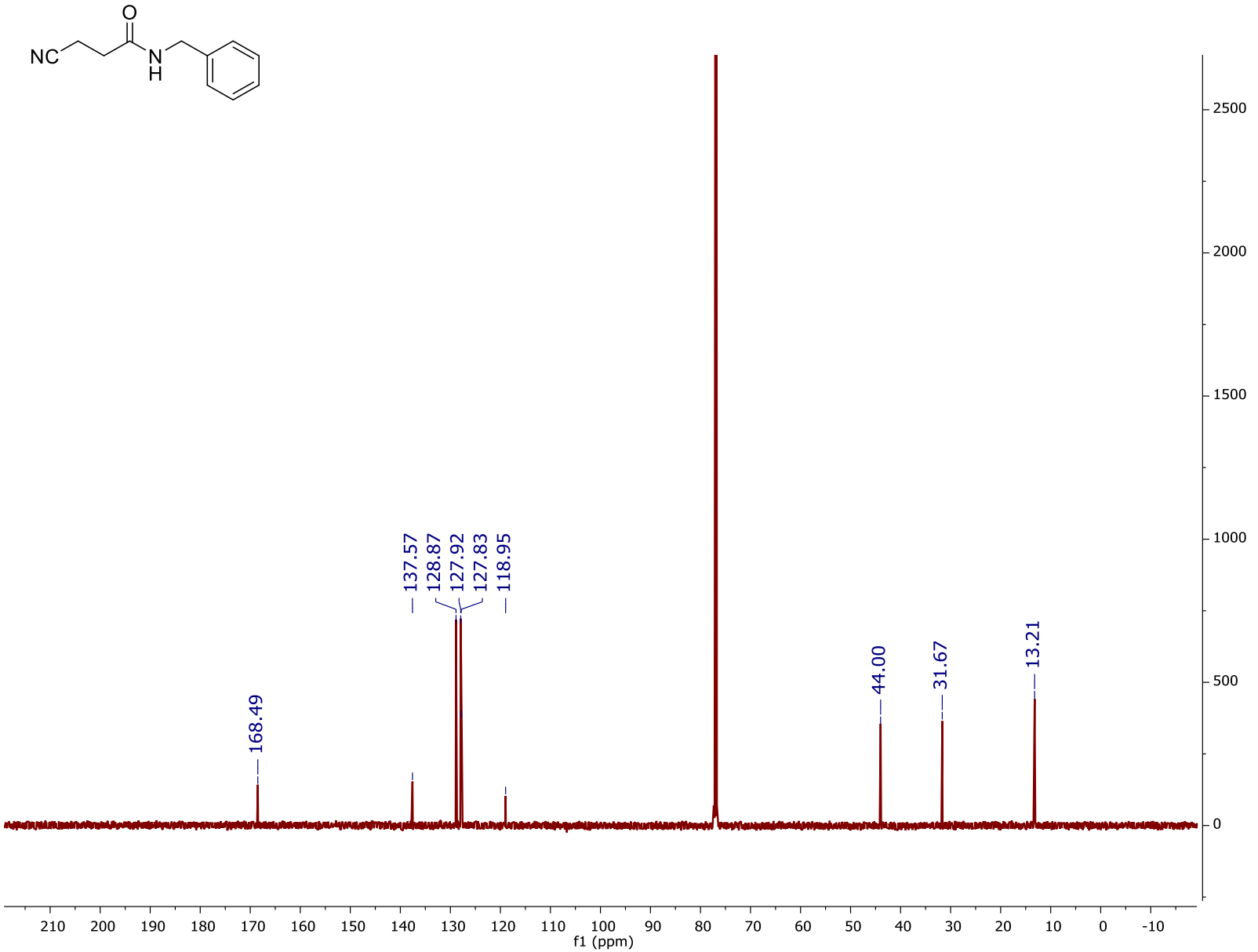
O
NC
N
H
168.49
137.57
128.87
127.92
127.83
118.95
44.00
31.67
13.21
2500
2000
1500
1000
500
0
210
200
190
180
170
160
150
140
130
120
110
100
90
80
70
60
50
40
30
20
10
0
-10
f1 (ppm)

In situ

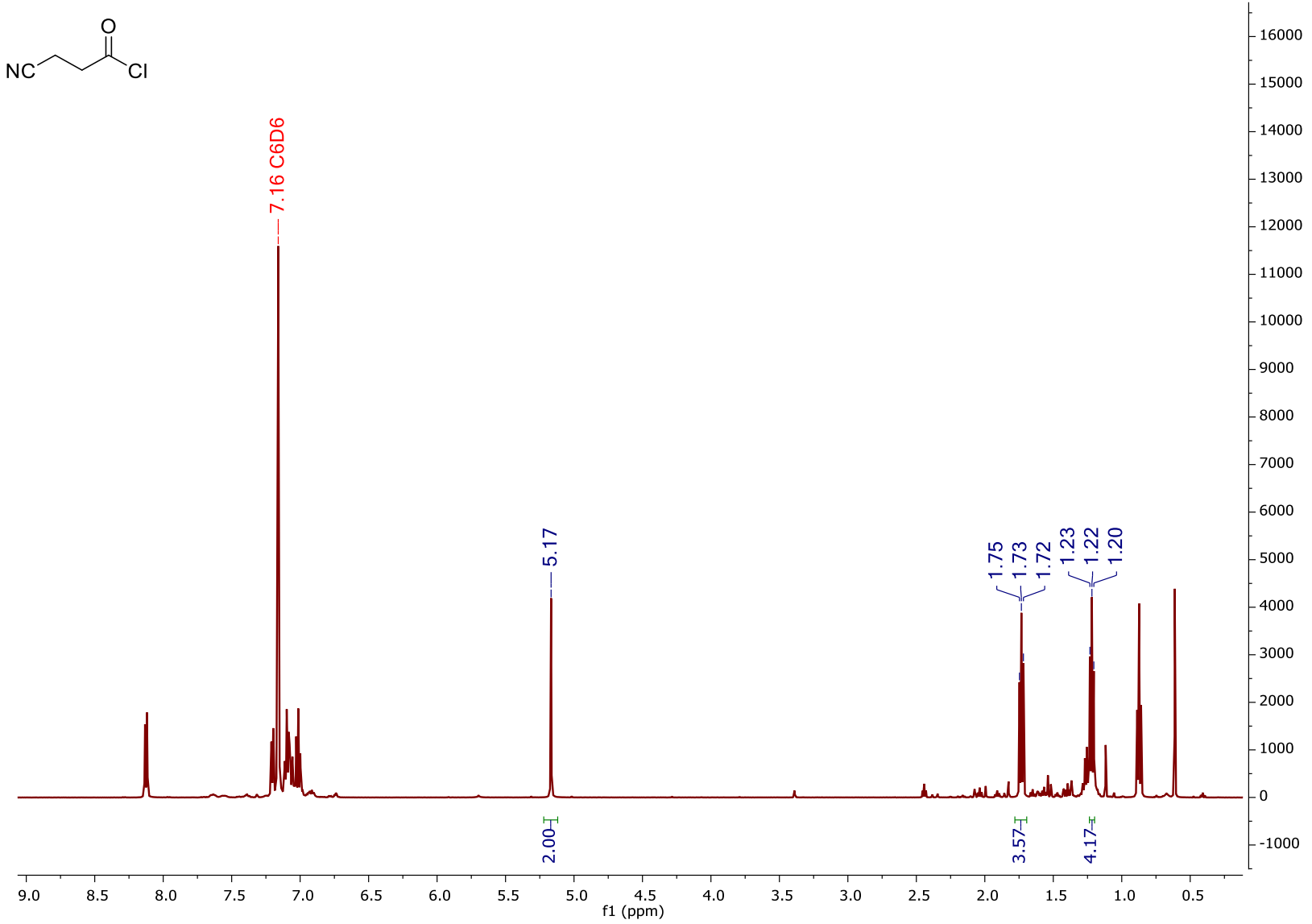

In situ

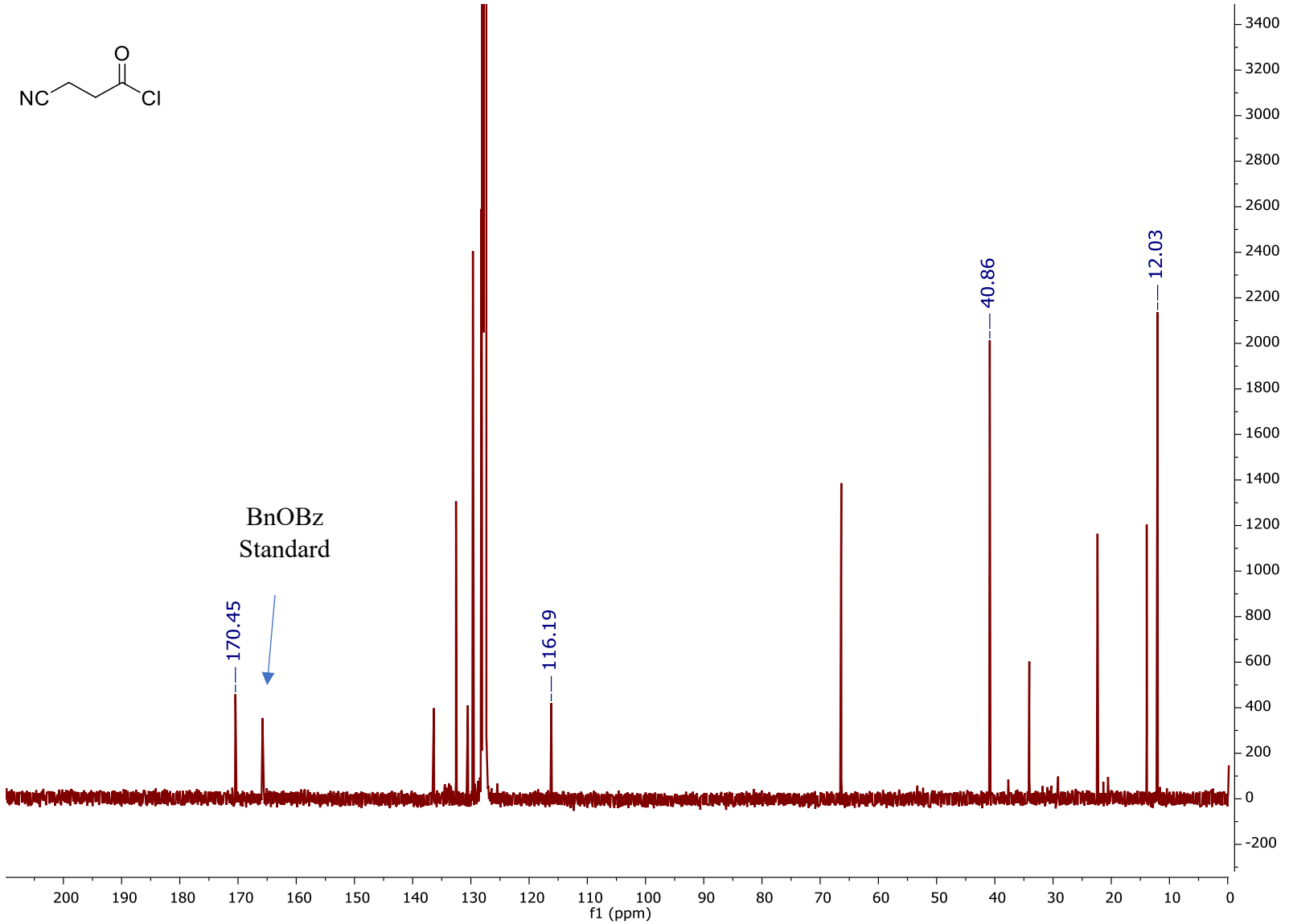
O
NC
Cl
BnOBz
Standard
170.45
116.19
40.86
12.03
3400
3200
3000
2800
2600
2400
2200
2000
1800
1600
1400
1200
1000
800
600
400
200
0
-200
200
190
180
170
160
150
140
130
120
110
100
90
80
70
60
50
40
30
20
10
0
f1 (ppm)

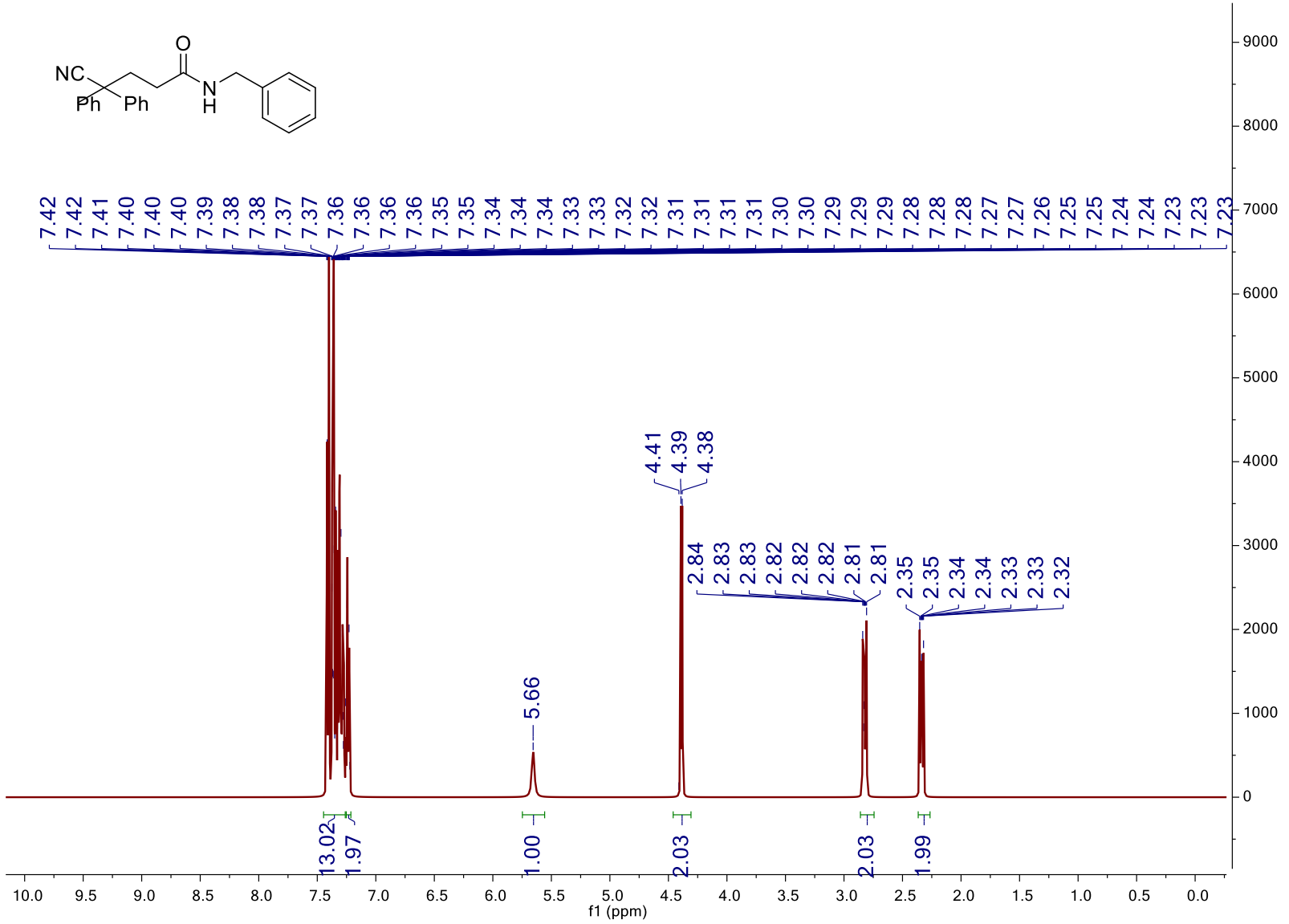
NC
Ph
Ph
O
N
H
7.42 7.42 7.41 7.40 7.40 7.40 7.39 7.38 7.38 7.37 7.37 7.36 7.36 7.36 7.36 7.35 7.35 7.34 7.34 7.34 7.33 7.33 7.32 7.32 7.31 7.31 7.31 7.31 7.30 7.30 7.29 7.29 7.29 7.28 7.28 7.28 7.27 7.27 7.26 7.25 7.25 7.24 7.24 7.23 7.23 7.23
4.41 4.39 4.38
2.84 2.83 2.83 2.82 2.82 2.82 2.81 2.81
2.35 2.35 2.34 2.34 2.33 2.33 2.32
5.66
13.02 1.97 1.00 2.03 2.03 1.99
9000 8000 7000 6000 5000 4000 3000 2000 1000 0
10.0 9.5 9.0 8.5 8.0 7.5 7.0 6.5 6.0 5.5 5.0 4.5 4.0 3.5 3.0 2.5 2.0 1.5 1.0 0.5 0.0
f1 (ppm)

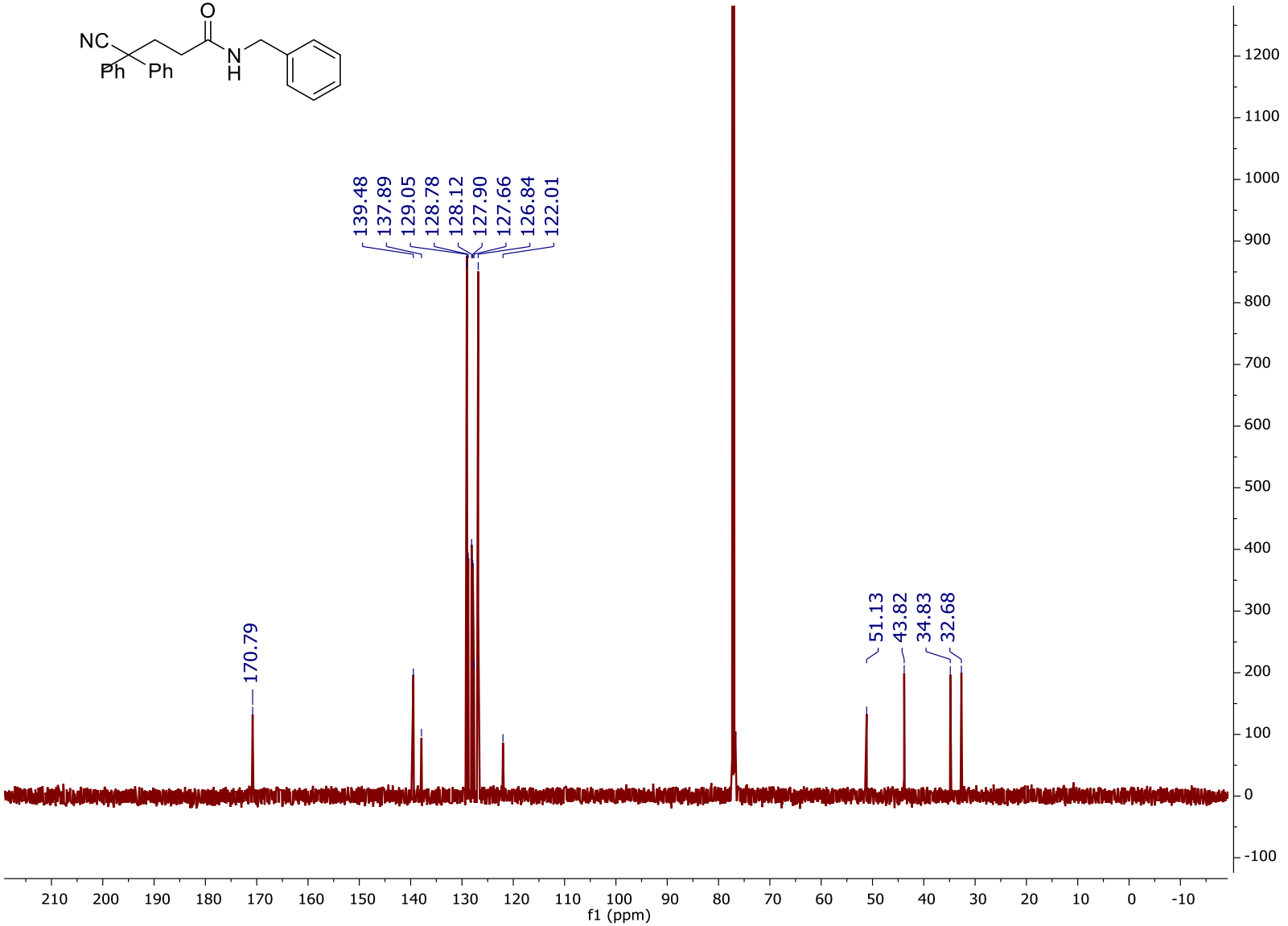
NC
Ph
Ph
O
N
H
139.48
137.89
129.05
128.78
128.12
127.90
127.66
126.84
122.01
170.79
51.13
43.82
34.83
32.68
f1 (ppm)

In situ

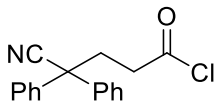

In situ

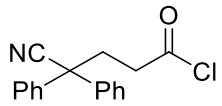
NC
Ph
Ph
O
Cl

172.02
138.98
127.97
120.92
50.22
43.23 DCE
43.16
33.96
f1 (ppm)

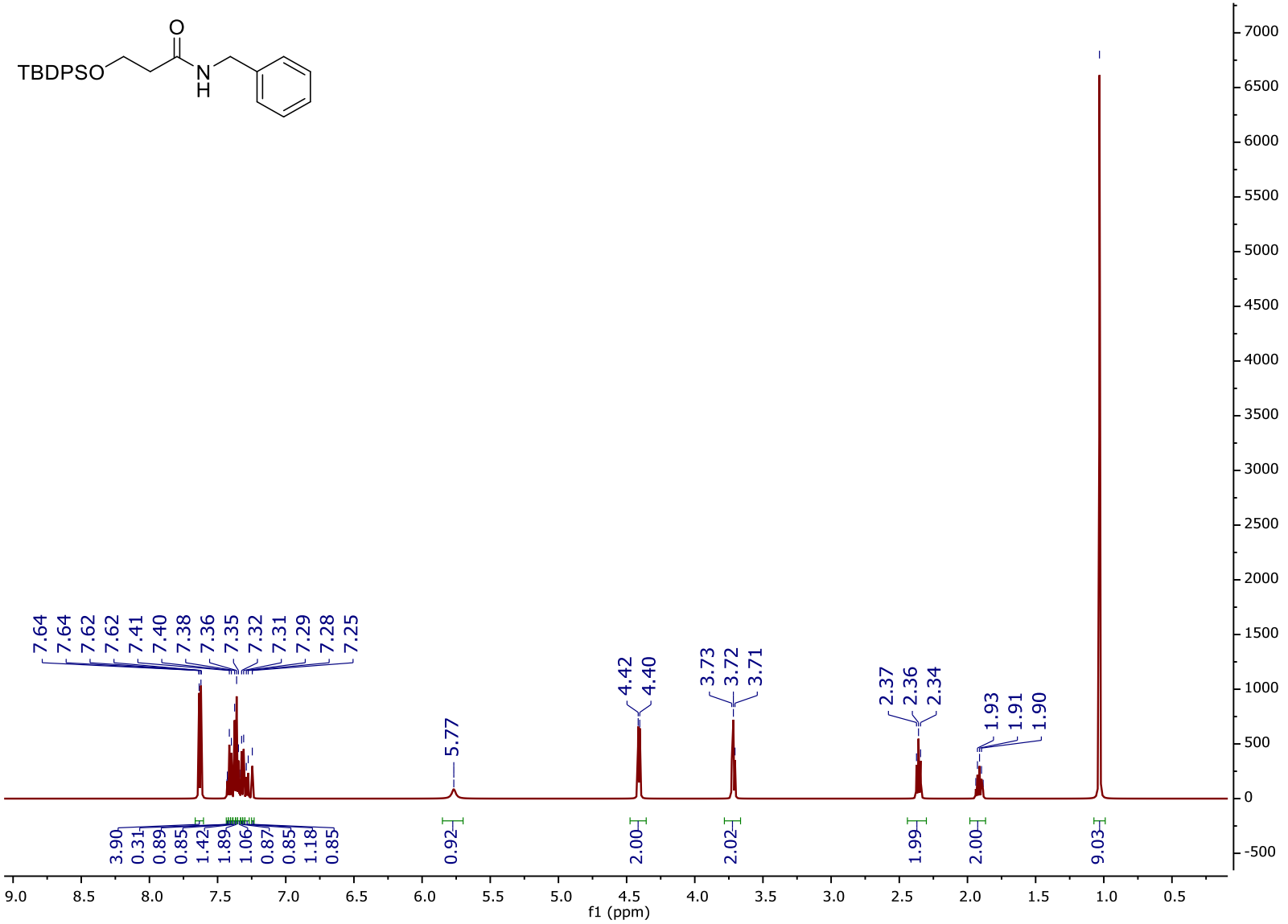
TBDPSO
O
N
H
7.64
7.64
7.62
7.62
7.41
7.40
7.38
7.36
7.35
7.32
7.31
7.29
7.28
7.25
5.77
4.42
4.40
3.73
3.72
3.71
2.37
2.36
2.34
1.93
1.91
1.90
3.90
0.31
0.89
0.85
1.42
1.89
1.06
0.87
0.85
1.18
0.85
0.92
2.00
2.02
1.99
2.00
9.03
f1 (ppm)

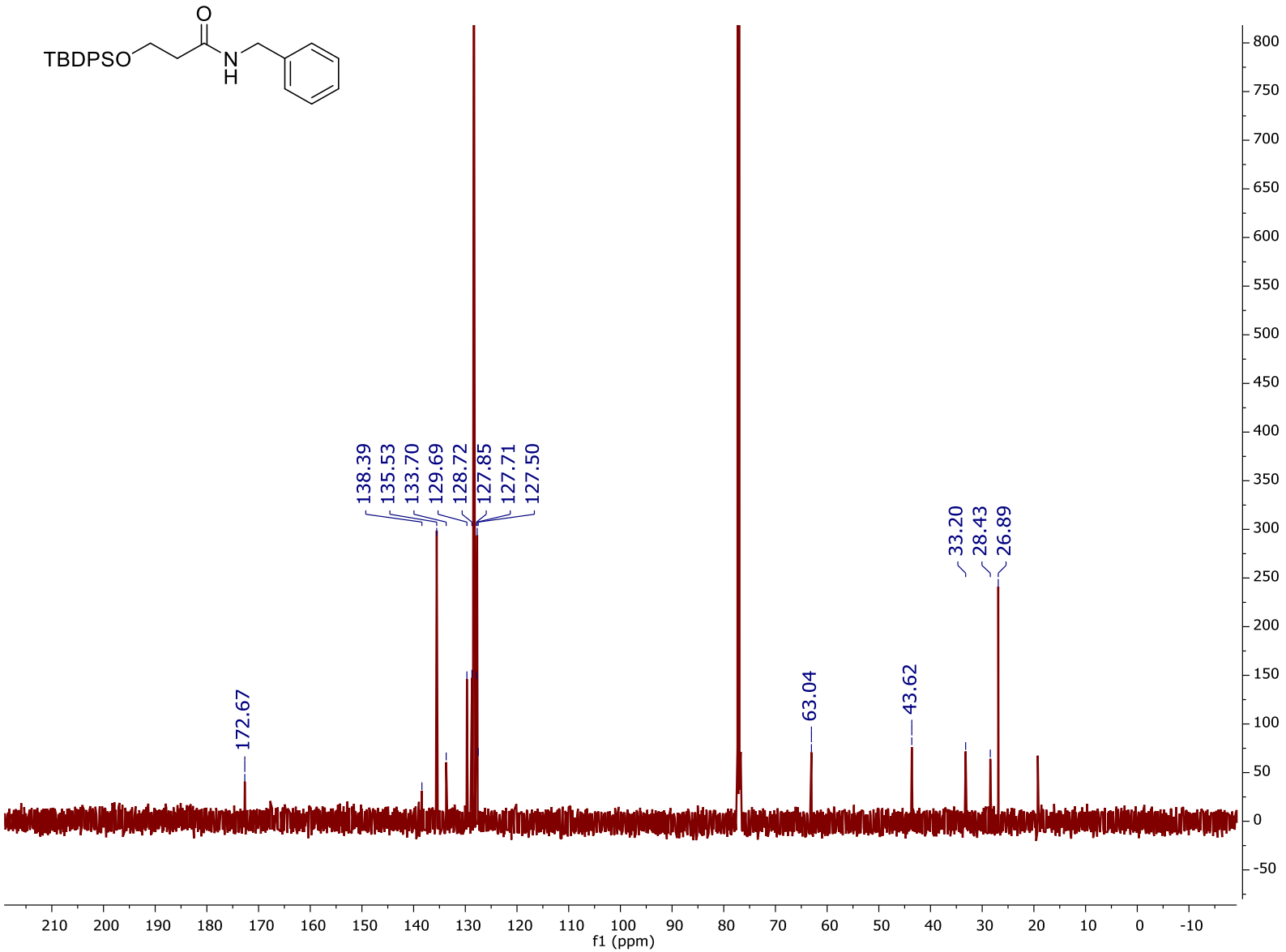
TBDPSO
O
N
H
172.67
138.39
135.53
133.70
129.69
128.72
127.85
127.71
127.50
63.04
43.62
33.20
28.43
26.89
f1 (ppm)

In situ

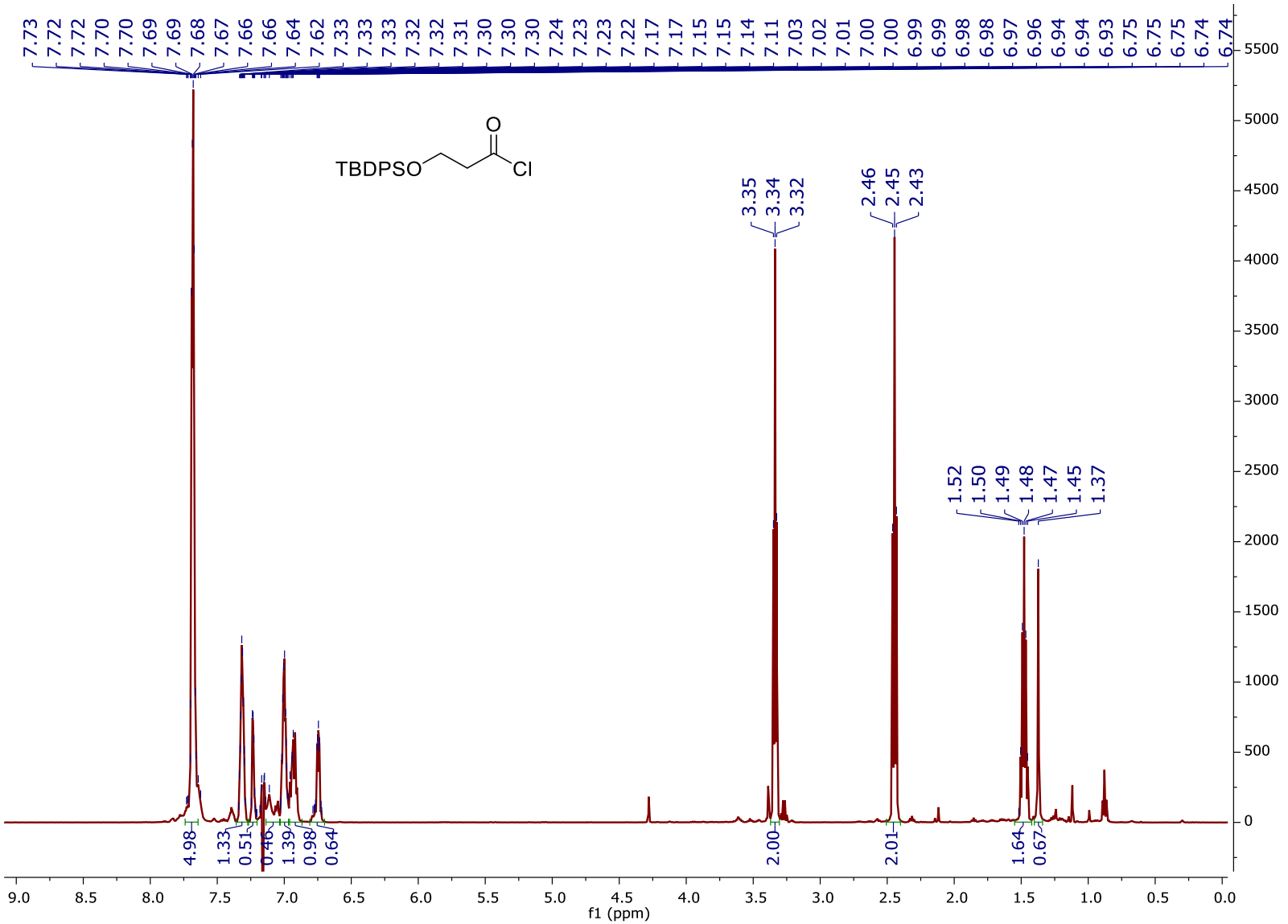
7.73 7.72 7.72 7.70 7.70 7.69 7.69 7.68 7.67 7.66 7.66 7.64 7.62 7.33 7.33 7.33 7.32 7.32 7.31 7.30 7.30 7.30 7.24 7.23 7.23 7.22 7.17 7.17 7.15 7.15 7.14 7.11 7.03 7.02 7.01 7.00 7.00 6.99 6.99 6.98 6.98 6.97 6.96 6.94 6.94 6.93 6.75 6.75 6.75 6.74 6.74
O
TBDPSO
Cl
3.35 3.34 3.32
2.46 2.45 2.43
1.52 1.50 1.49 1.48 1.47 1.45 1.37
4.98 1.33 0.51 0.46 1.39 0.98 0.64 2.00 2.01 1.64 0.67
f1 (ppm)

In situ

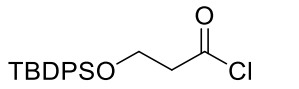
O
TBDPSO
Cl

136.87
135.93
133.89
133.79
27.98
27.02
19.37
62.14
43.72
173.30
f1 (ppm)

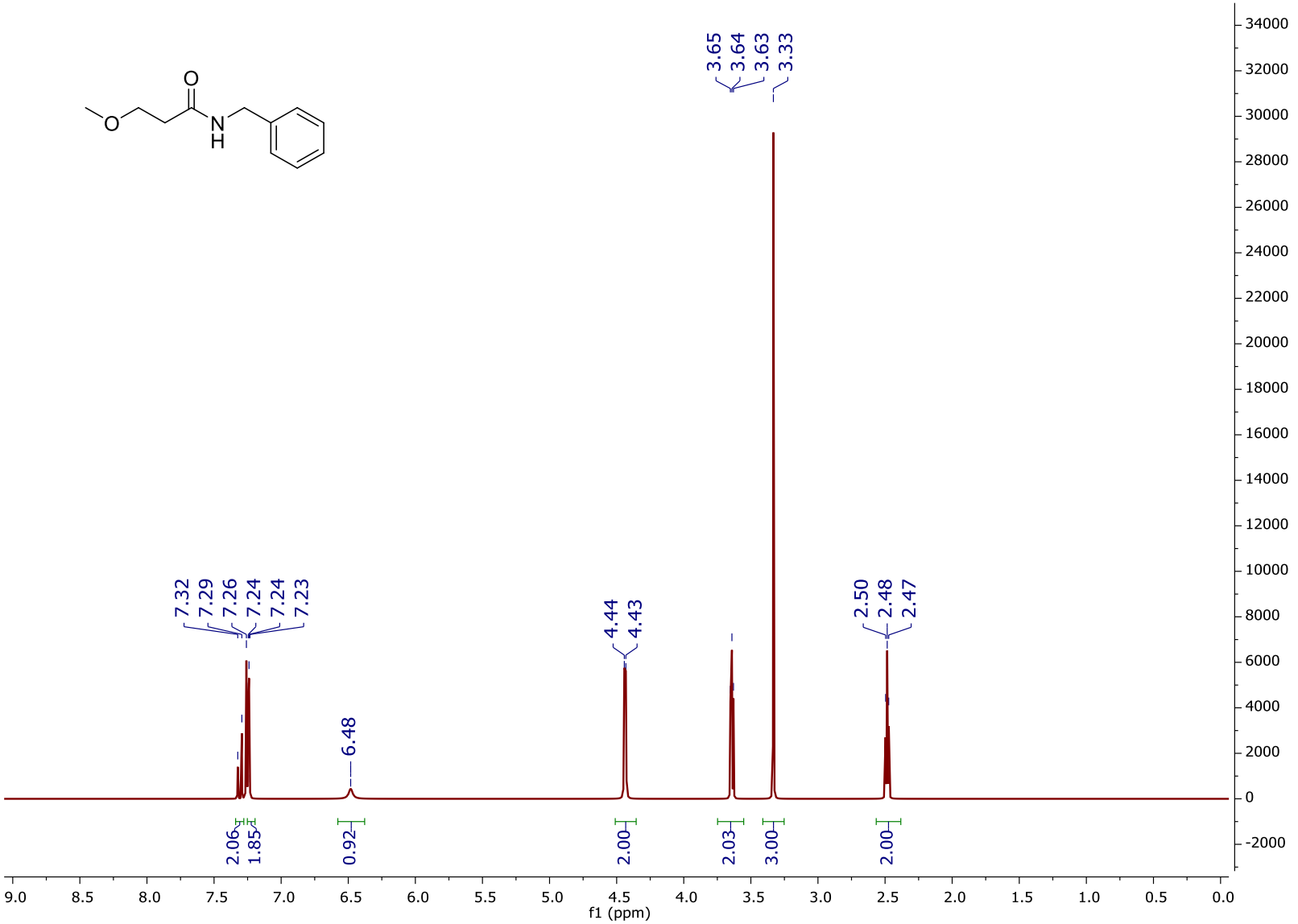
O
O
N
H
3.65
3.64
3.63
3.33
7.32
7.29
7.26
7.24
7.24
7.23
6.48
4.44
4.43
2.50
2.48
2.47
2.06
1.85
0.92
2.00
2.03
3.00
2.00
f1 (ppm)

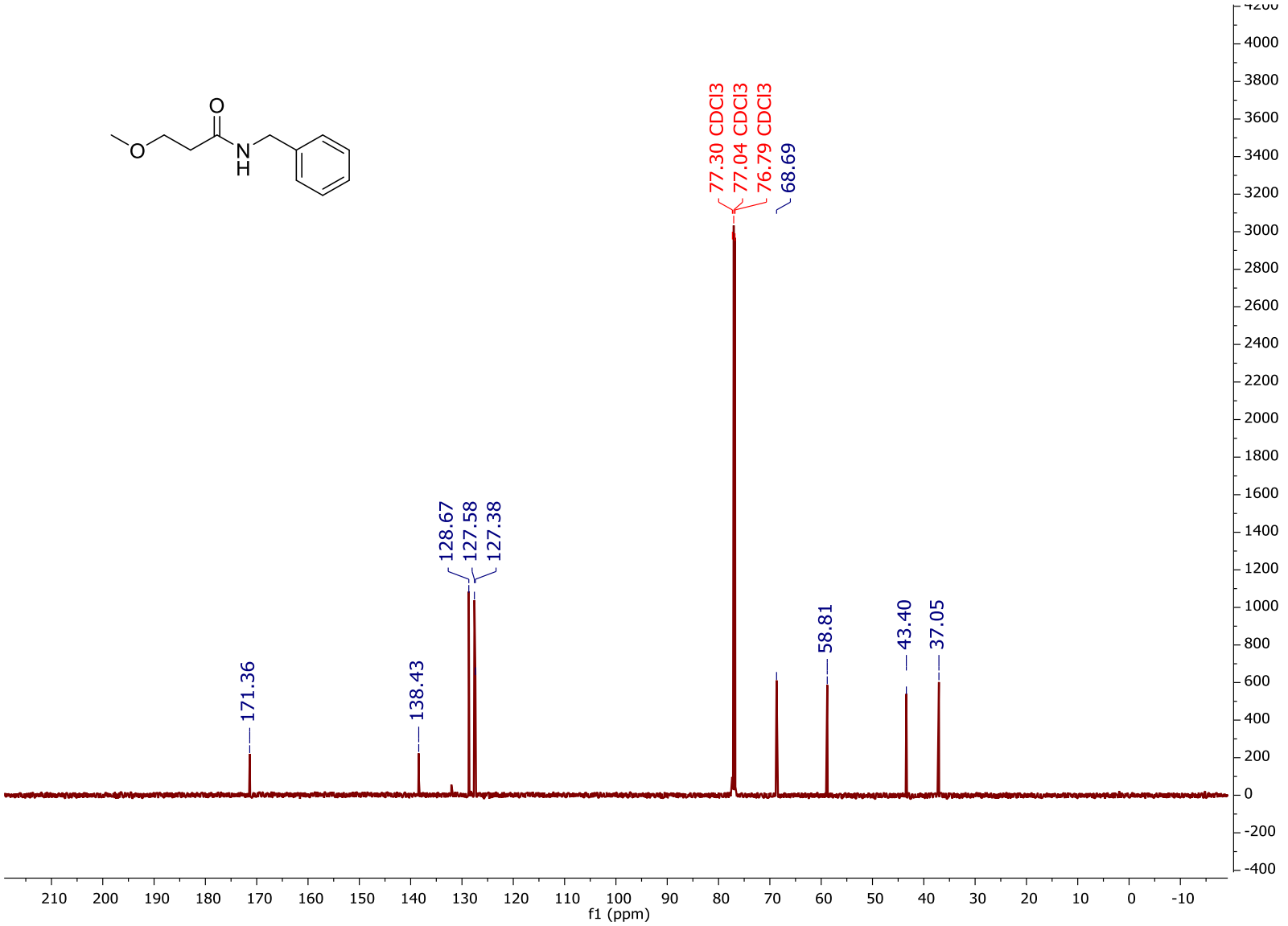
O
O
N
H
77.30 CDCl3
77.04 CDCl3
76.79 CDCl3
68.69
128.67
127.58
127.38
171.36
138.43
58.81
43.40
37.05
f1 (ppm)

In situ

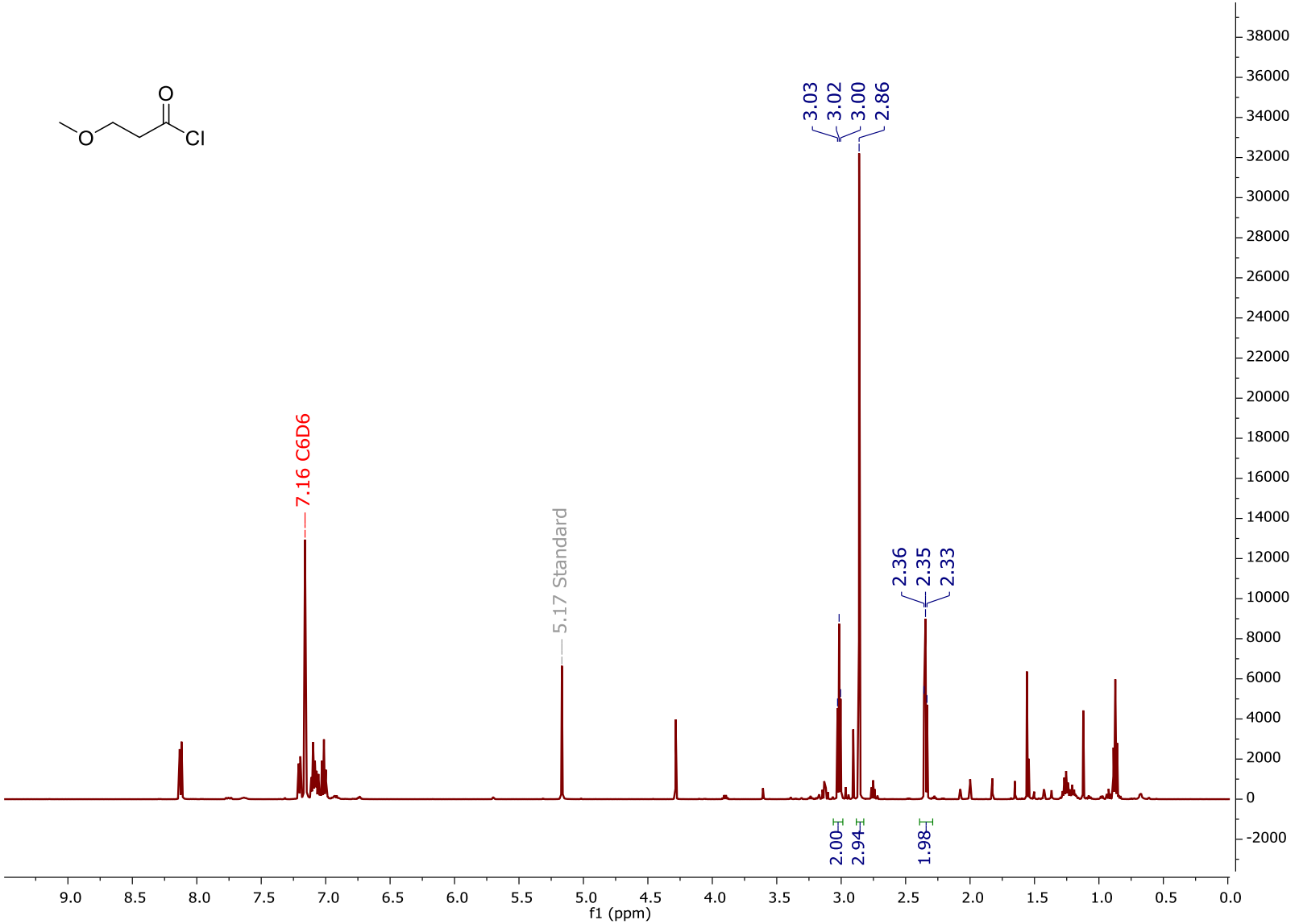
O
O
Cl
7.16 C6D6
5.17 Standard
3.03
3.02
3.00
2.86
2.36
2.35
2.33
2.00
2.94
1.98
f1 (ppm)

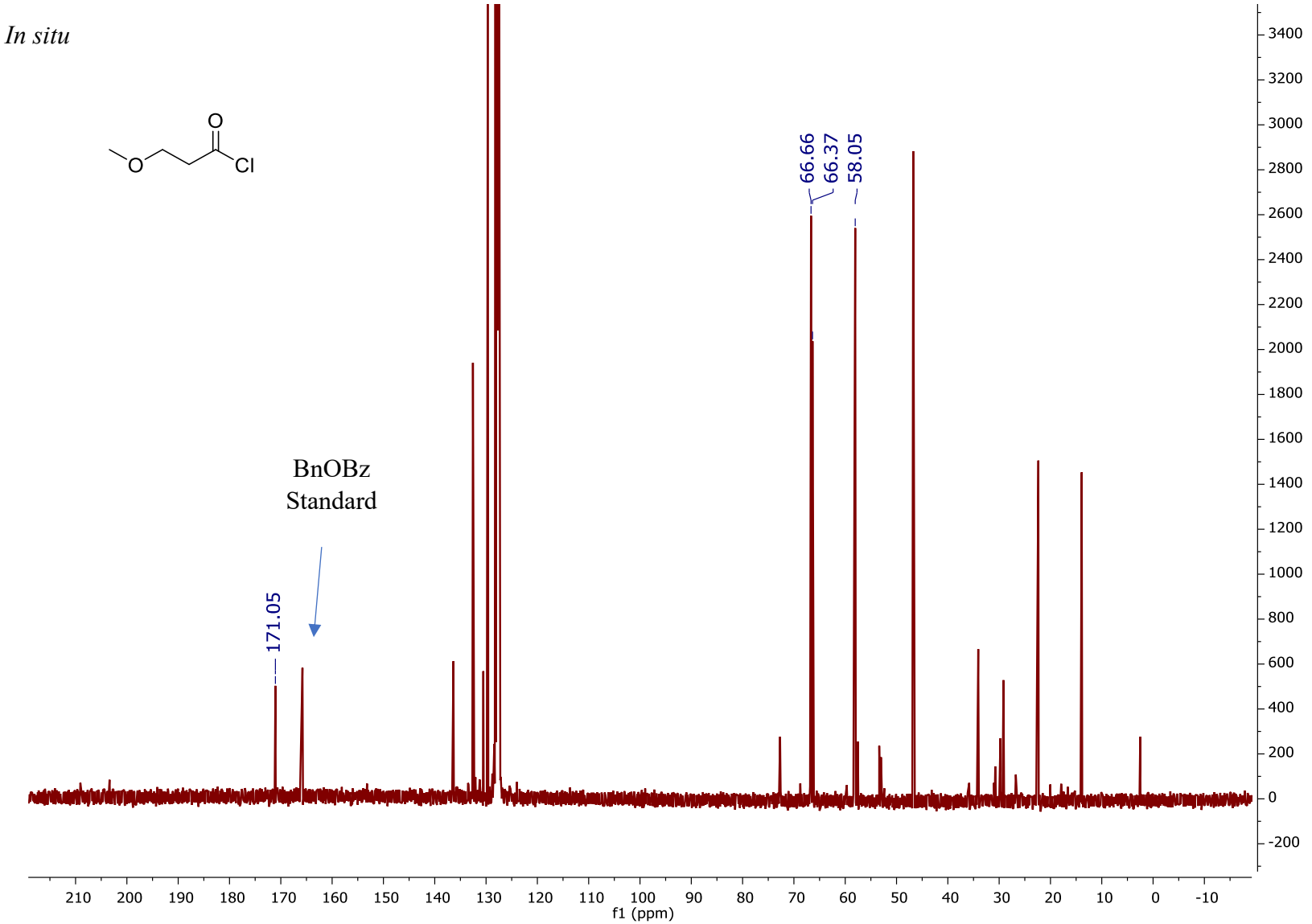
In situ
O
O
Cl
66.66
66.37
58.05
BnOBz
Standard
171.05
3400
3200
3000
2800
2600
2400
2200
2000
1800
1600
1400
1200
1000
800
600
400
200
0
-200
210
200
190
180
170
160
150
140
130
120
110
100
90
80
70
60
50
40
30
20
10
0
-10
f1 (ppm)

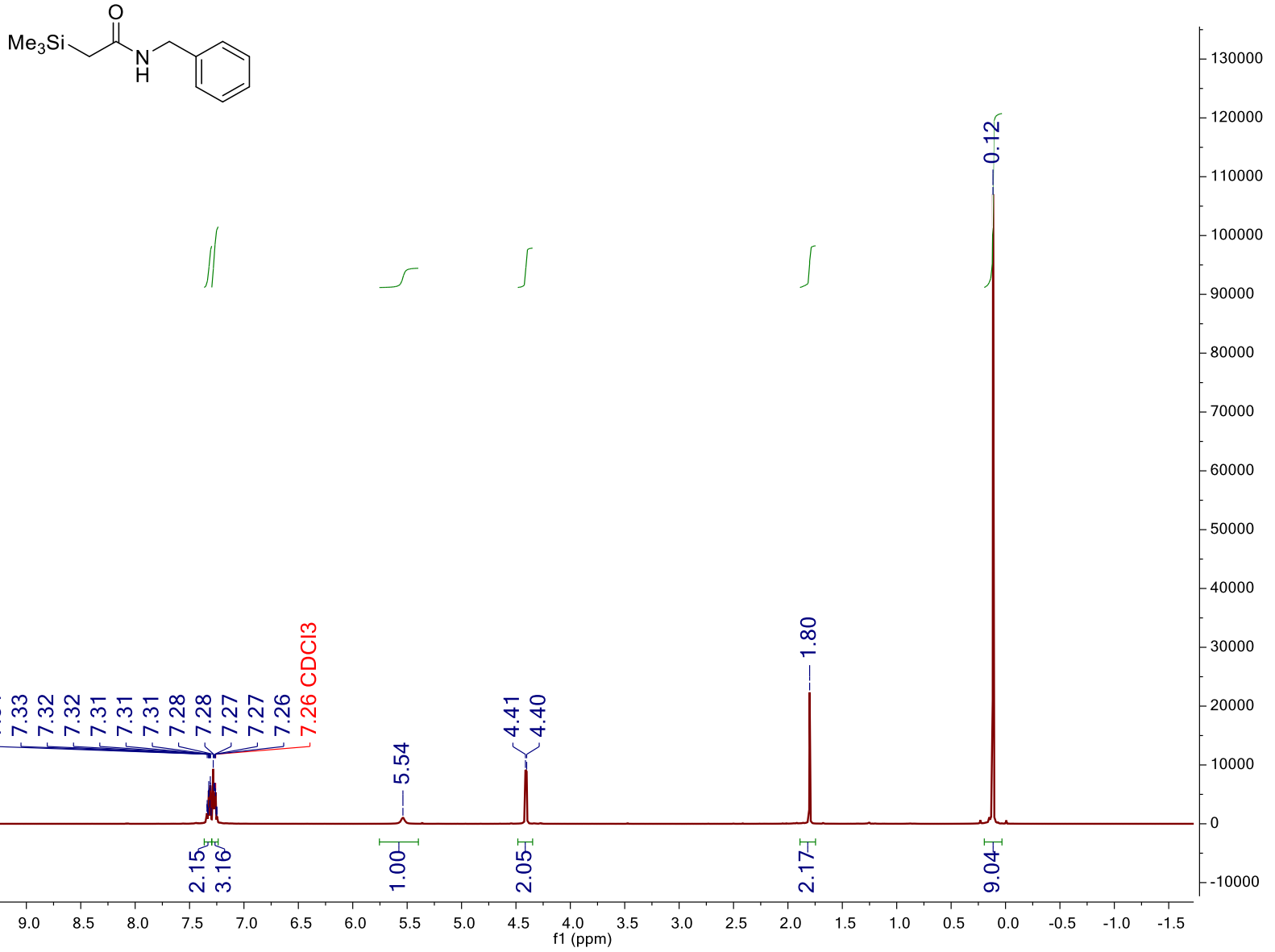
Me3Si
O
N
H
7.34
7.33
7.32
7.32
7.31
7.31
7.31
7.28
7.28
7.27
7.27
7.26
7.26 CDCl3
5.54
4.41
4.40
1.80
0.12
2.15
3.16
1.00
2.05
2.17
9.04
f1 (ppm)

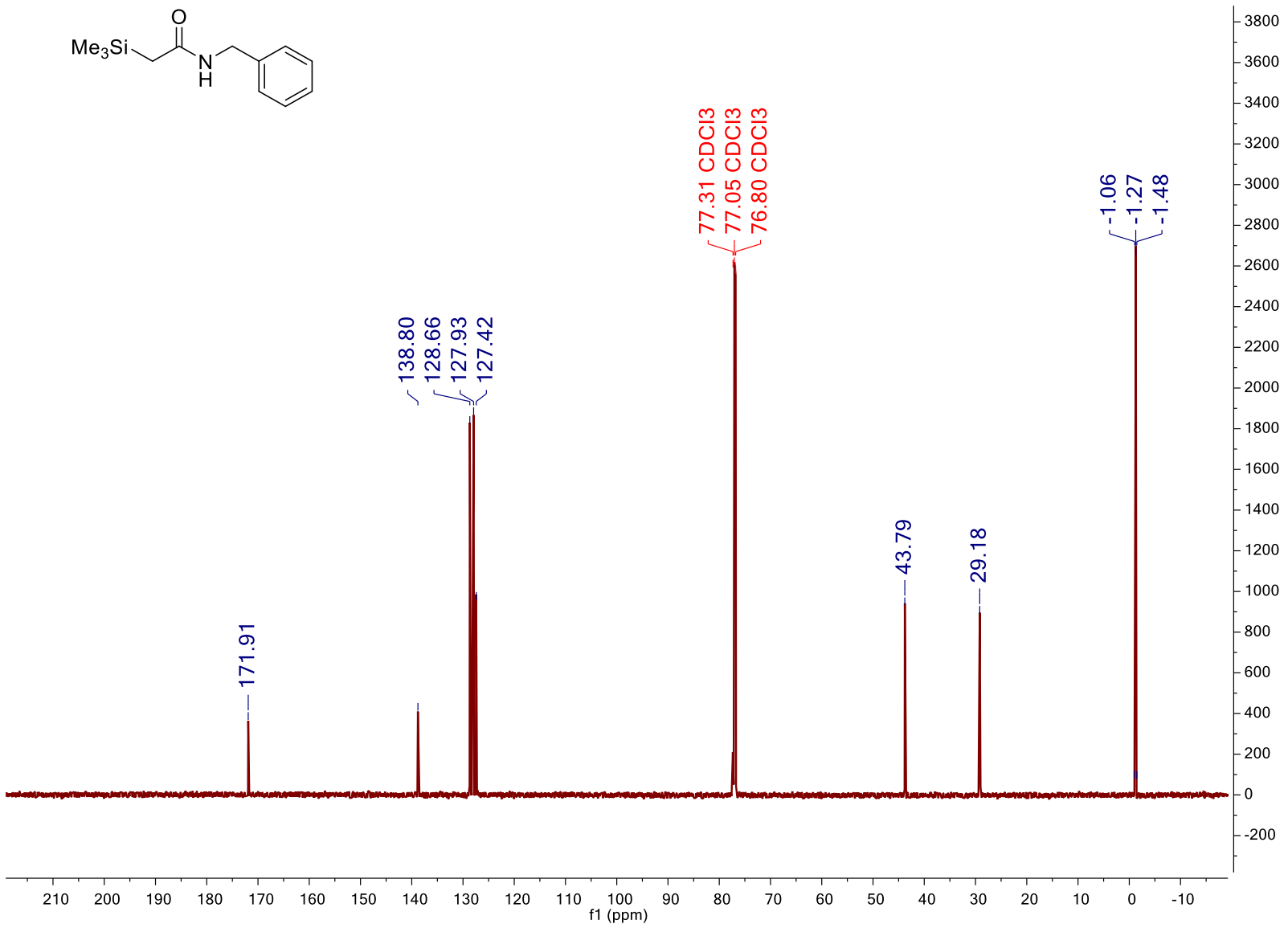
Me3Si
O
N
H
171.91
138.80
128.66
127.93
127.42
77.31 CDCl3
77.05 CDCl3
76.80 CDCl3
43.79
29.18
1.06
1.27
1.48
f1 (ppm)

In situ

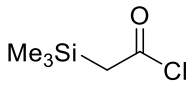

In situ

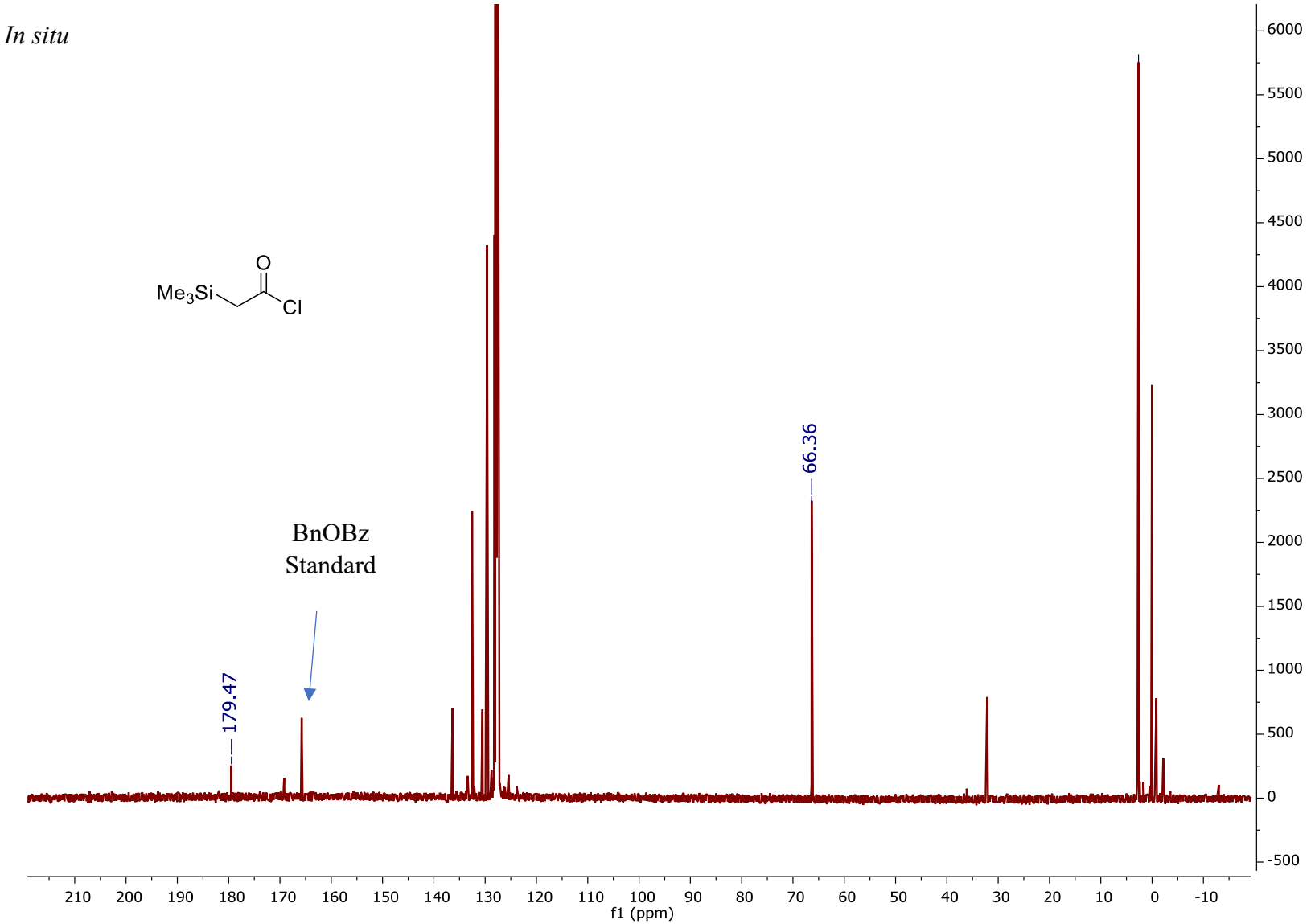
Me3Si
O
Cl
BnOBz
Standard
179.47
66.36
6000
5500
5000
4500
4000
3500
3000
2500
2000
1500
1000
500
0
-500
210 200 190 180 170 160 150 140 130 120 110 100 90 80 70 60 50 40 30 20 10 0 -10
f1 (ppm)

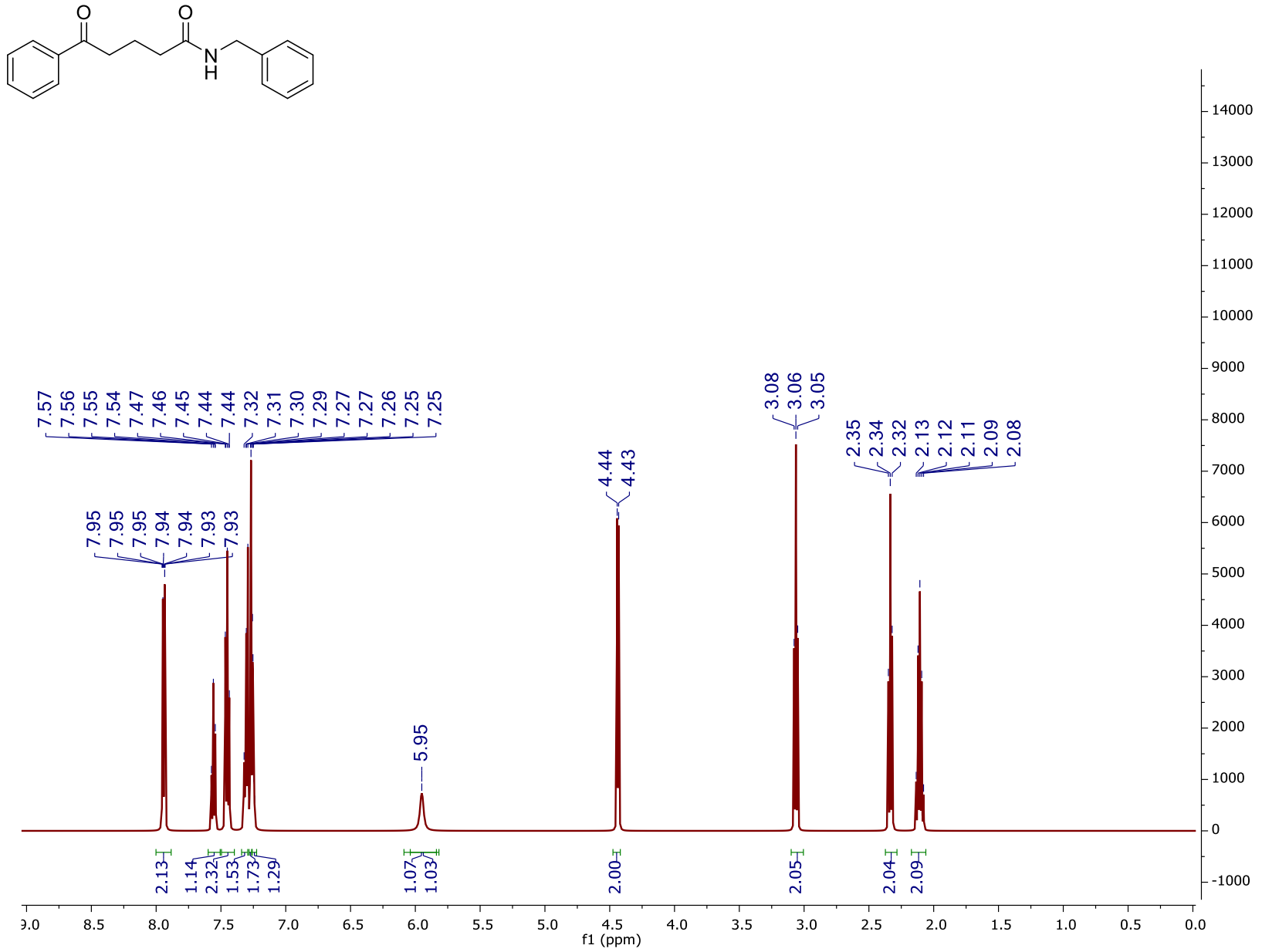
O
O
N
H
7.57
7.56
7.55
7.54
7.47
7.46
7.45
7.44
7.44
7.32
7.31
7.30
7.29
7.27
7.27
7.26
7.25
7.25
7.95
7.95
7.95
7.94
7.94
7.93
7.93
5.95
4.44
4.43
3.08
3.06
3.05
2.35
2.34
2.32
2.13
2.12
2.11
2.09
2.08
2.13
1.14
2.32
1.53
1.73
1.29
1.07
1.03
2.00
2.05
2.04
2.09
f1 (ppm)

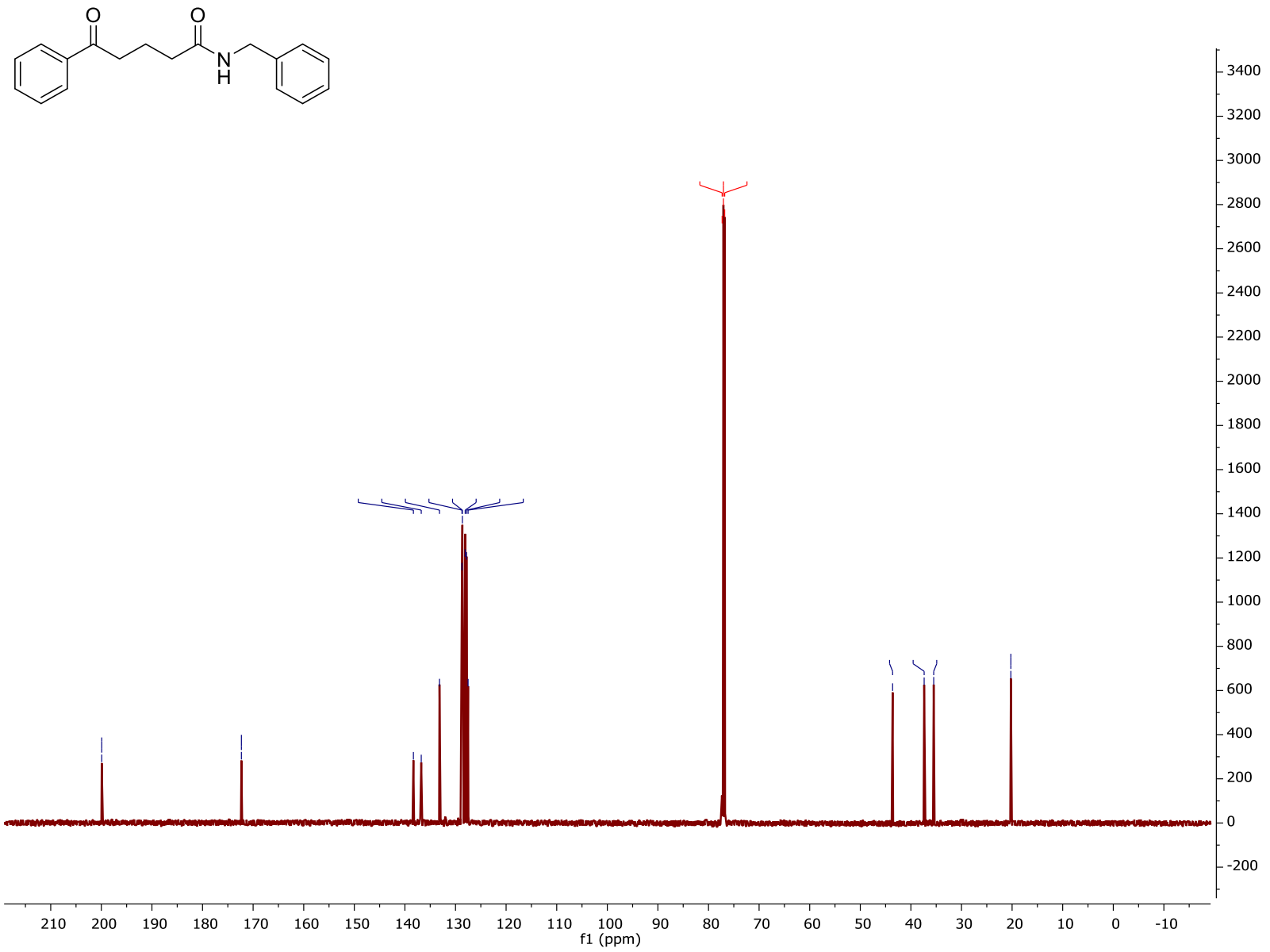
O
O
N
H
3400
3200
3000
2800
2600
2400
2200
2000
1800
1600
1400
1200
1000
800
600
400
200
0
-200
210
200
190
180
170
160
150
140
130
120
110
100
90
80
70
60
50
40
30
20
10
0
-10
f1 (ppm)

In situ

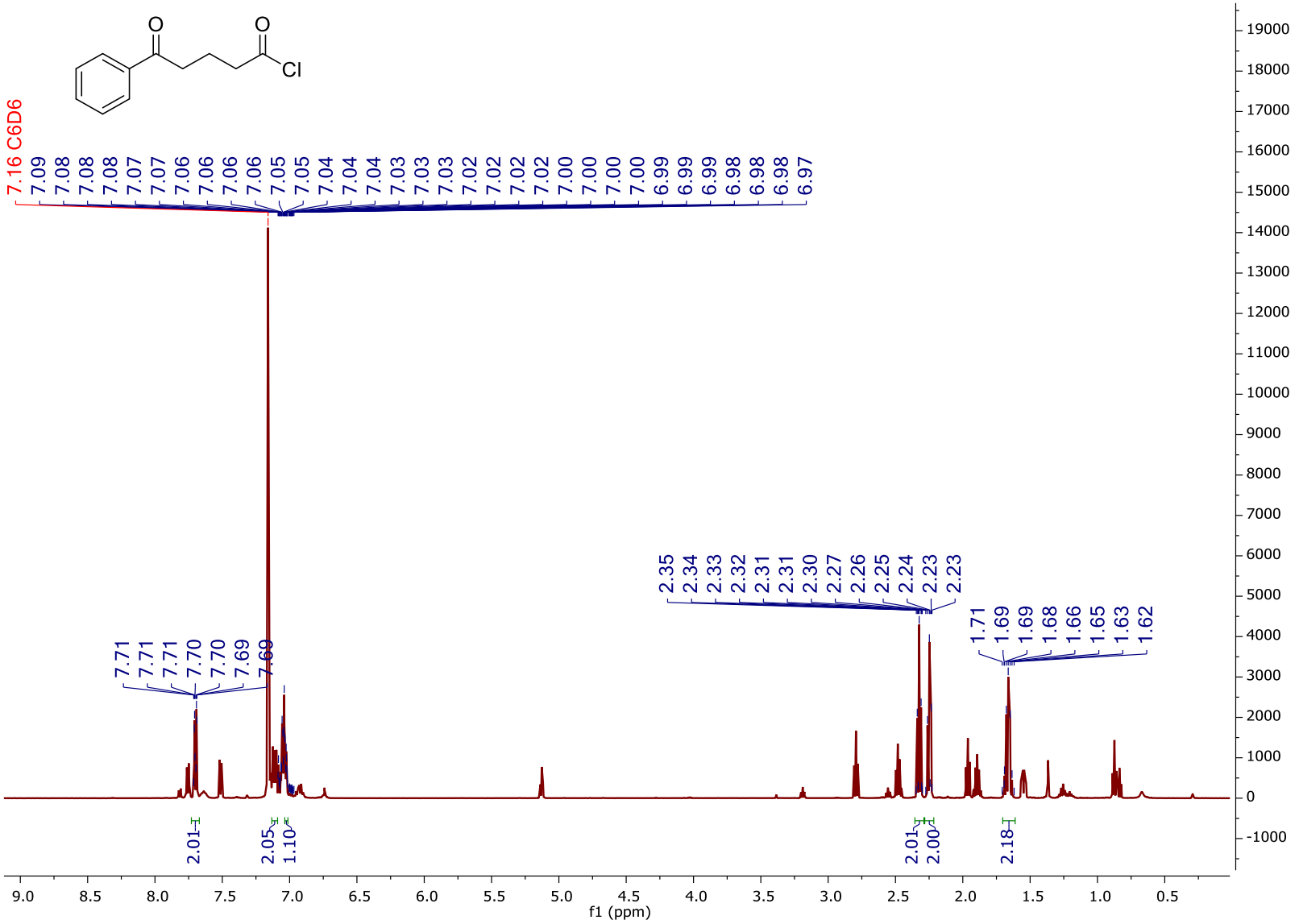
O
O
Cl
7.16 C6D6
7.09 7.08 7.08 7.08 7.07 7.07 7.06 7.06 7.06 7.06 7.05 7.05 7.04 7.04 7.04 7.03 7.03 7.03 7.02 7.02 7.02 7.02 7.00 7.00 7.00 7.00 6.99 6.99 6.99 6.98 6.98 6.98 6.97
7.71 7.71 7.71 7.70 7.70 7.69 7.69
2.35 2.34 2.33 2.32 2.31 2.31 2.30 2.27 2.26 2.25 2.24 2.23 2.23
1.71 1.69 1.69 1.68 1.66 1.65 1.63 1.62
2.01 2.05 1.10 2.01 2.00 2.18
f1 (ppm)

In situ

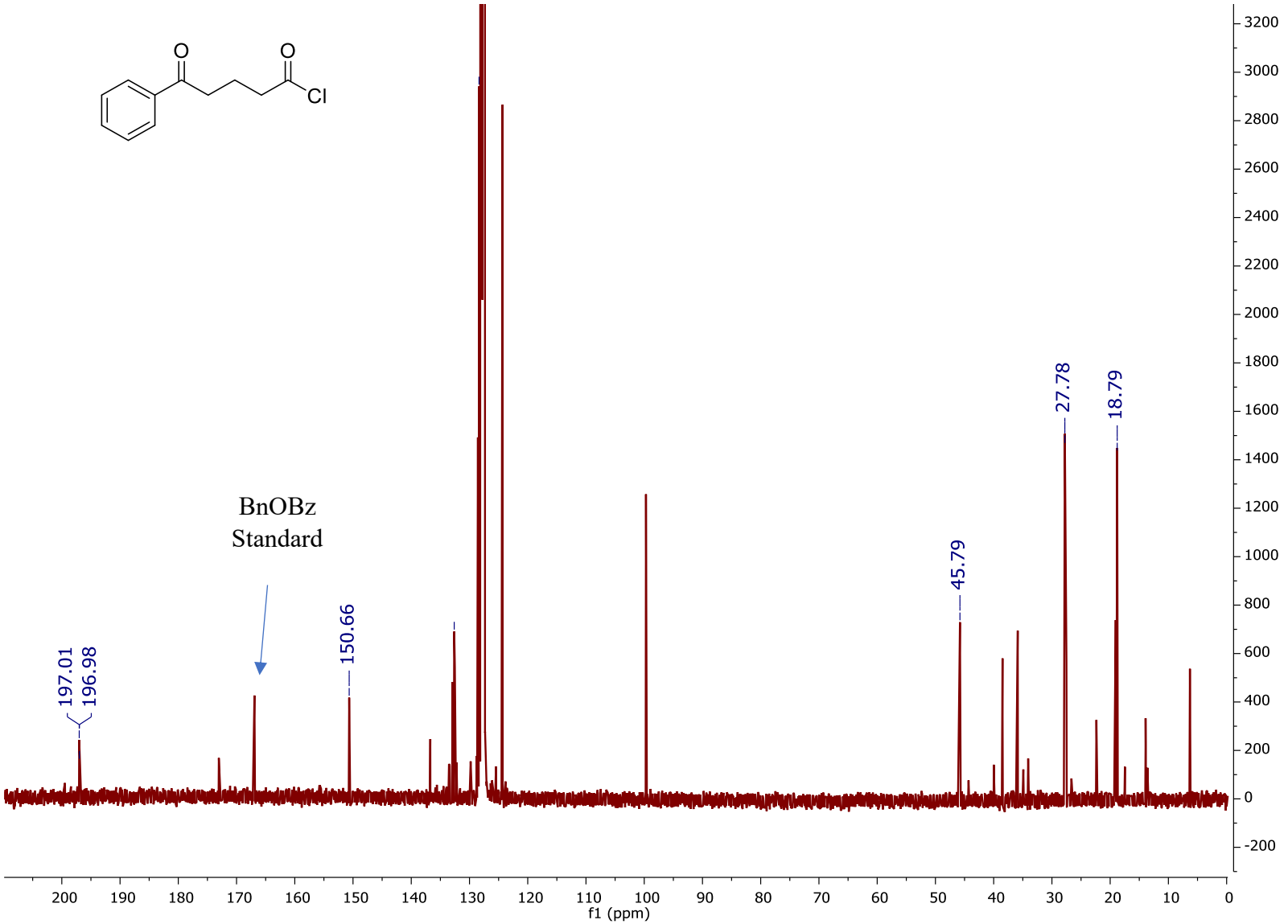

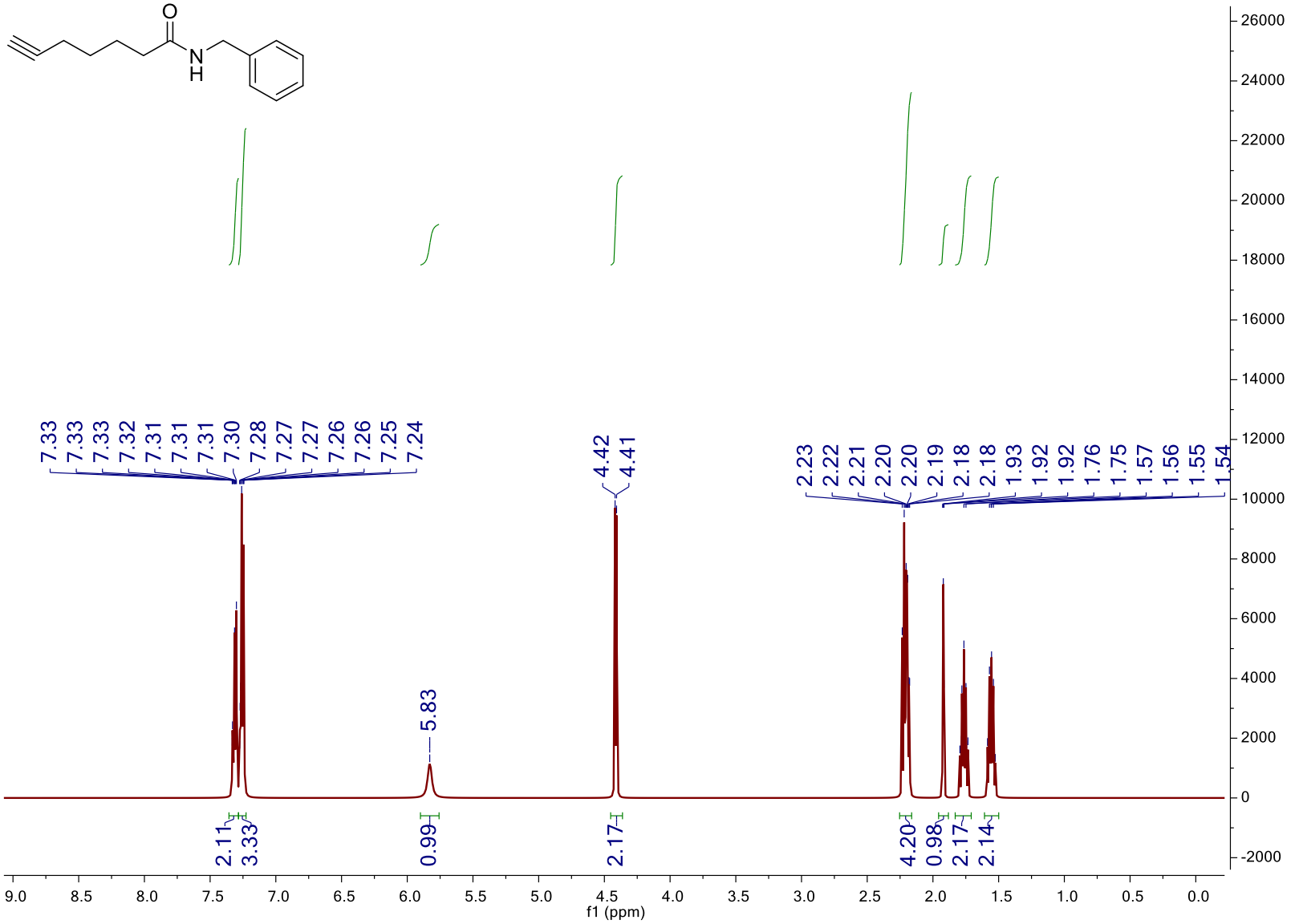
O
N
H
7.33
7.33
7.33
7.32
7.31
7.31
7.31
7.30
7.28
7.27
7.27
7.26
7.26
7.25
7.24
5.83
4.42
4.41
2.23
2.22
2.21
2.20
2.20
2.19
2.18
2.18
1.93
1.92
1.92
1.76
1.75
1.57
1.56
1.55
1.54
2.11
3.33
0.99
2.17
4.20
0.98
2.17
2.14
f1 (ppm)

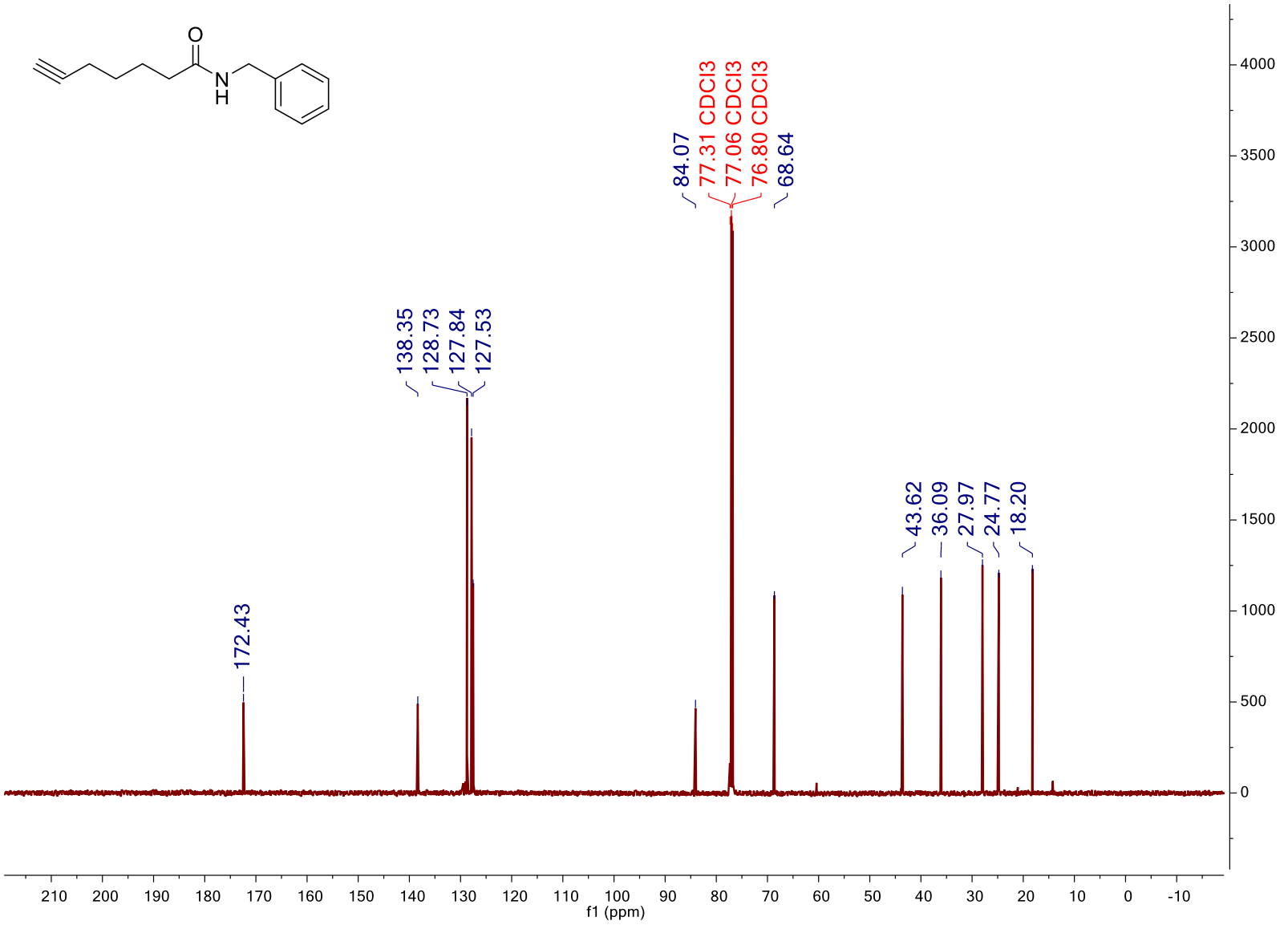
O
N
H
172.43
138.35
128.73
127.84
127.53
84.07
77.31 CDCl3
77.06 CDCl3
76.80 CDCl3
68.64
43.62
36.09
27.97
24.77
18.20
4000
3500
3000
2500
2000
1500
1000
500
0
210 200 190 180 170 160 150 140 130 120 110 100 90 80 70 60 50 40 30 20 10 0 -10
f1 (ppm)

In situ

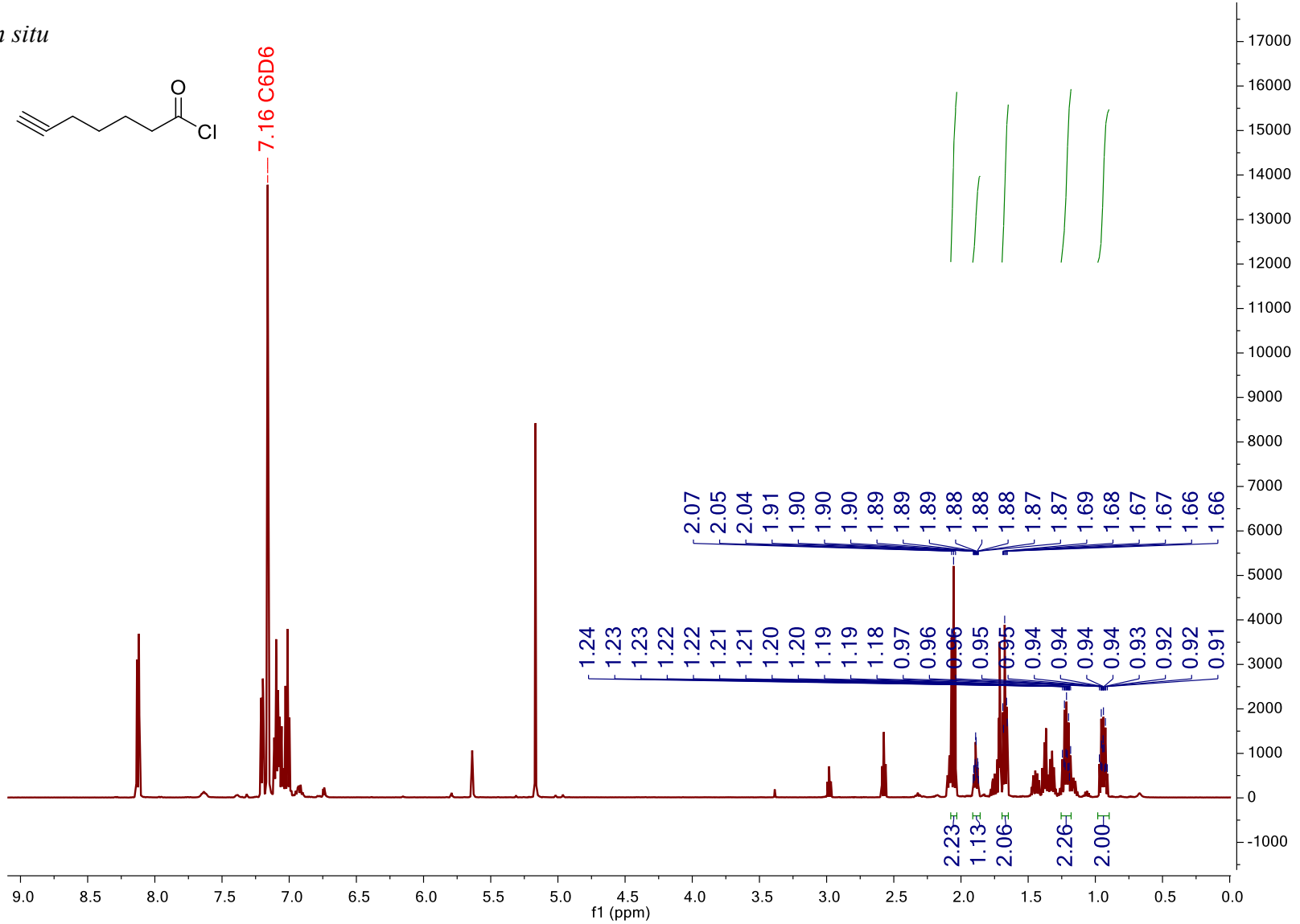
O
Cl
7.16 C6D6
2.07
2.05
2.04
1.91
1.90
1.90
1.90
1.89
1.89
1.89
1.88
1.88
1.88
1.87
1.87
1.69
1.68
1.67
1.67
1.66
1.66
1.24
1.23
1.23
1.22
1.22
1.21
1.21
1.20
1.20
1.19
1.19
1.18
0.97
0.96
0.96
0.95
0.95
0.94
0.94
0.94
0.94
0.93
0.92
0.92
0.91
2.23
1.13
2.06
2.26
2.00
f1 (ppm)

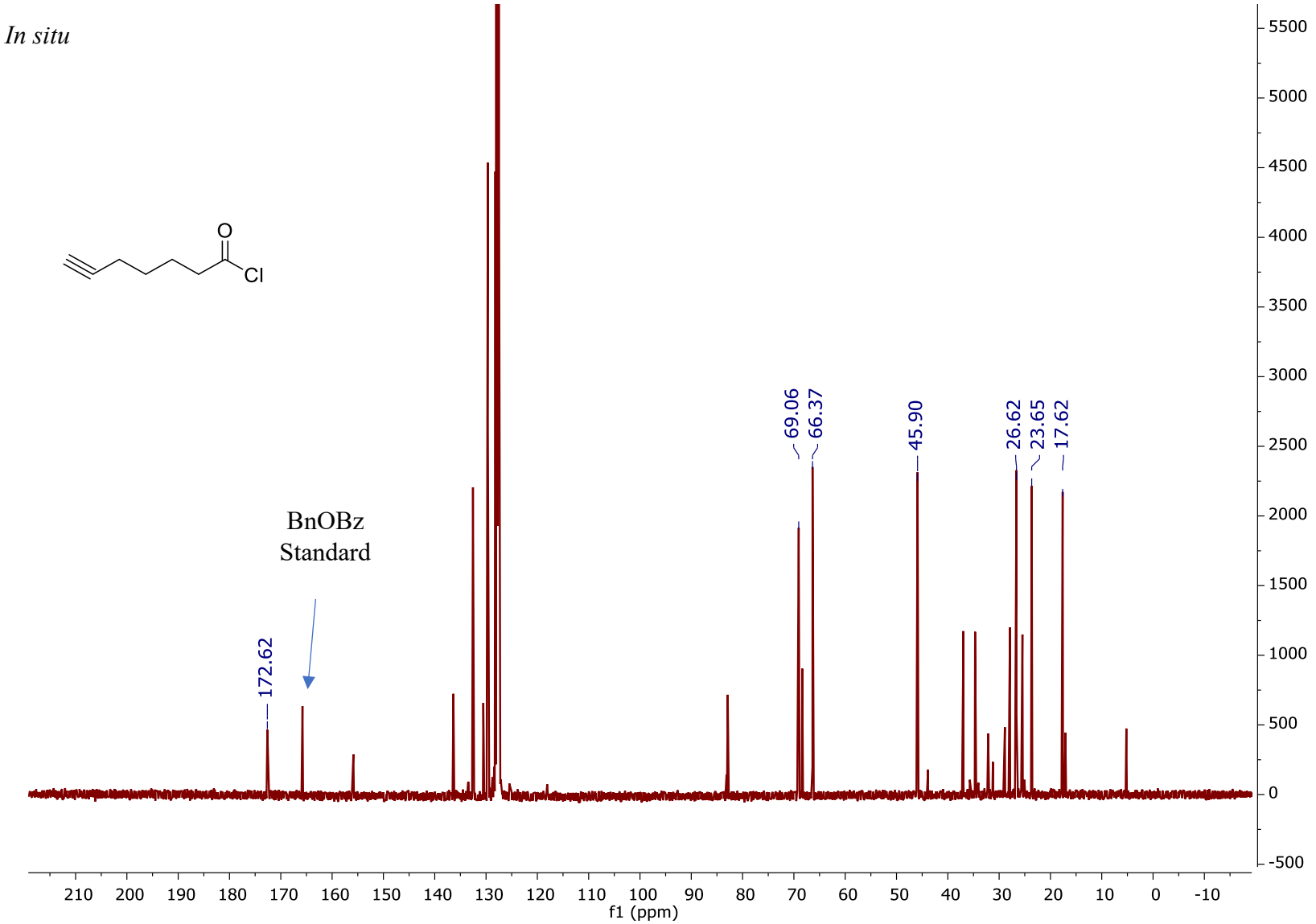
In situ
O
Cl
BnOBz
Standard
172.62
69.06
66.37
45.90
26.62
23.65
17.62
5500
5000
4500
4000
3500
3000
2500
2000
1500
1000
500
0
-500
210 200 190 180 170 160 150 140 130 120 110 100 90 80 70 60 50 40 30 20 10 0 -10
f1 (ppm)

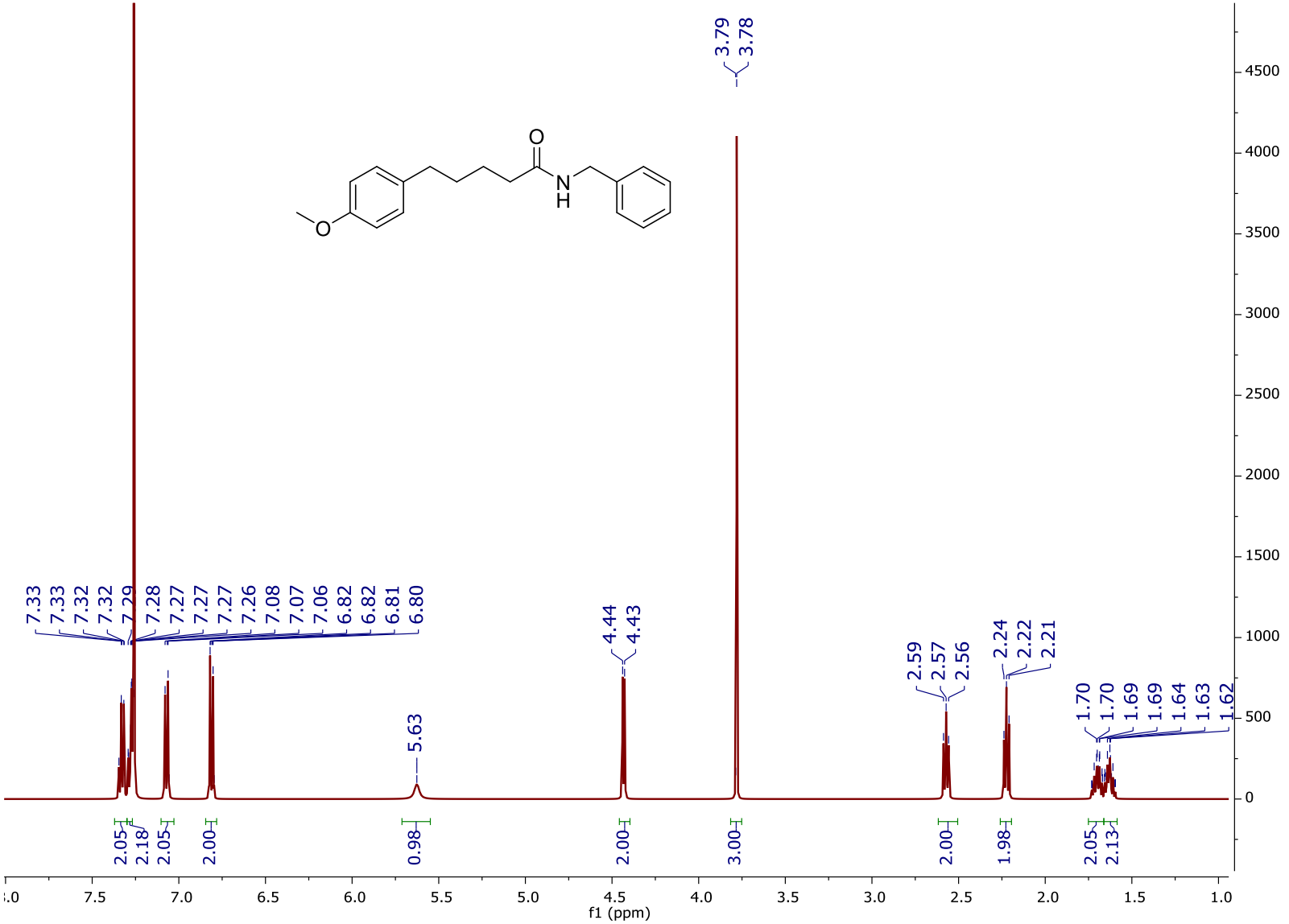
O
N
H
O
3.79
3.78
7.33
7.33
7.32
7.32
7.29
7.28
7.27
7.27
7.27
7.26
7.08
7.07
7.06
6.82
6.82
6.81
6.80
5.63
4.44
4.43
2.59
2.57
2.56
2.24
2.22
2.21
1.70
1.70
1.69
1.69
1.64
1.63
1.62
2.05
2.18
2.05
2.00
0.98
2.00
3.00
2.00
1.98
2.05
2.13
4500
4000
3500
3000
2500
2000
1500
1000
500
0
7.5
7.0
6.5
6.0
5.5
5.0
4.5
4.0
3.5
3.0
2.5
2.0
1.5
1.0
f1 (ppm)

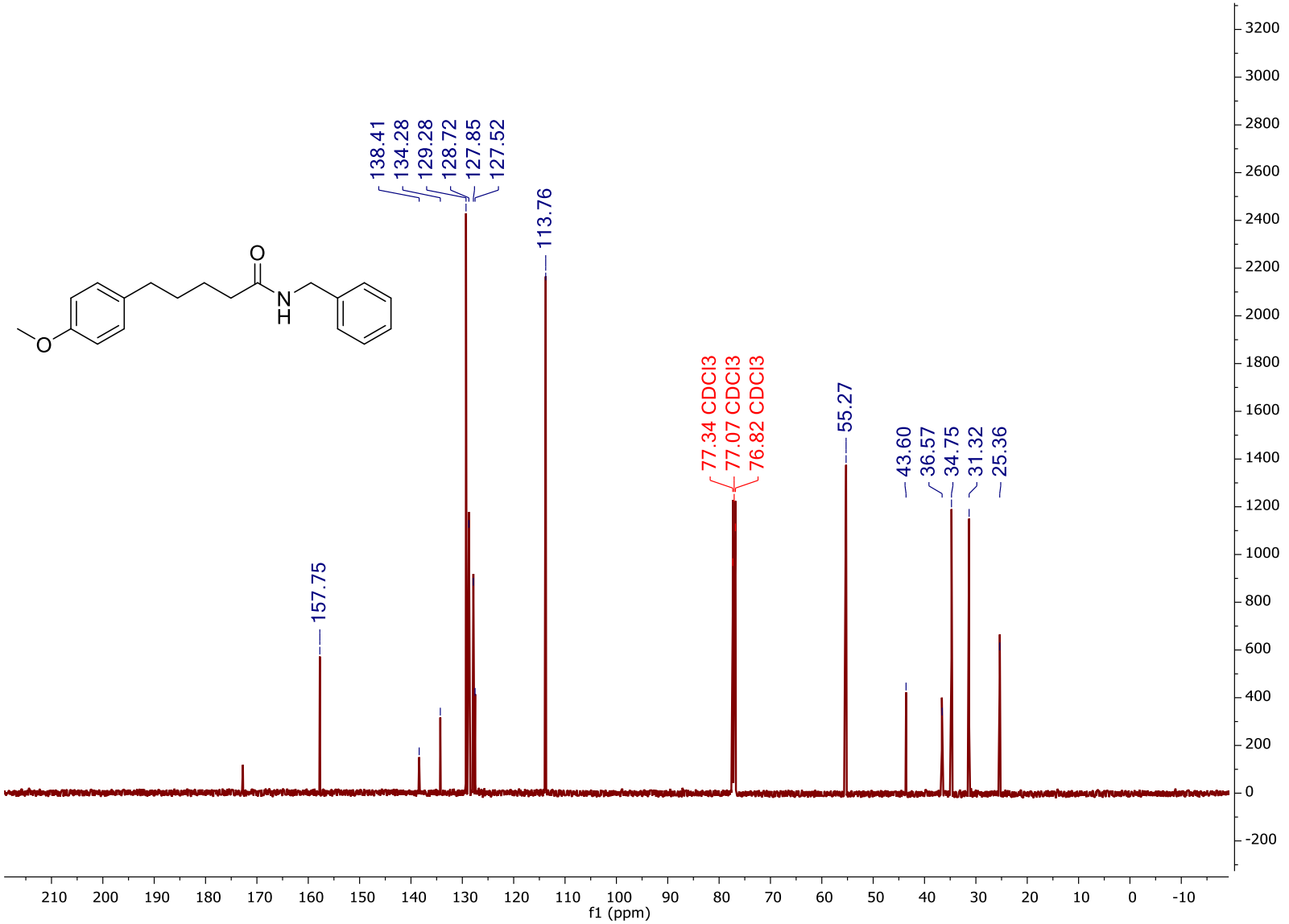
138.41
134.28
129.28
128.72
127.85
127.52
113.76
77.34 CDCl3
77.07 CDCl3
76.82 CDCl3
55.27
43.60
36.57
34.75
31.32
25.36
157.75
O
N
H
O
f1 (ppm)

In situ

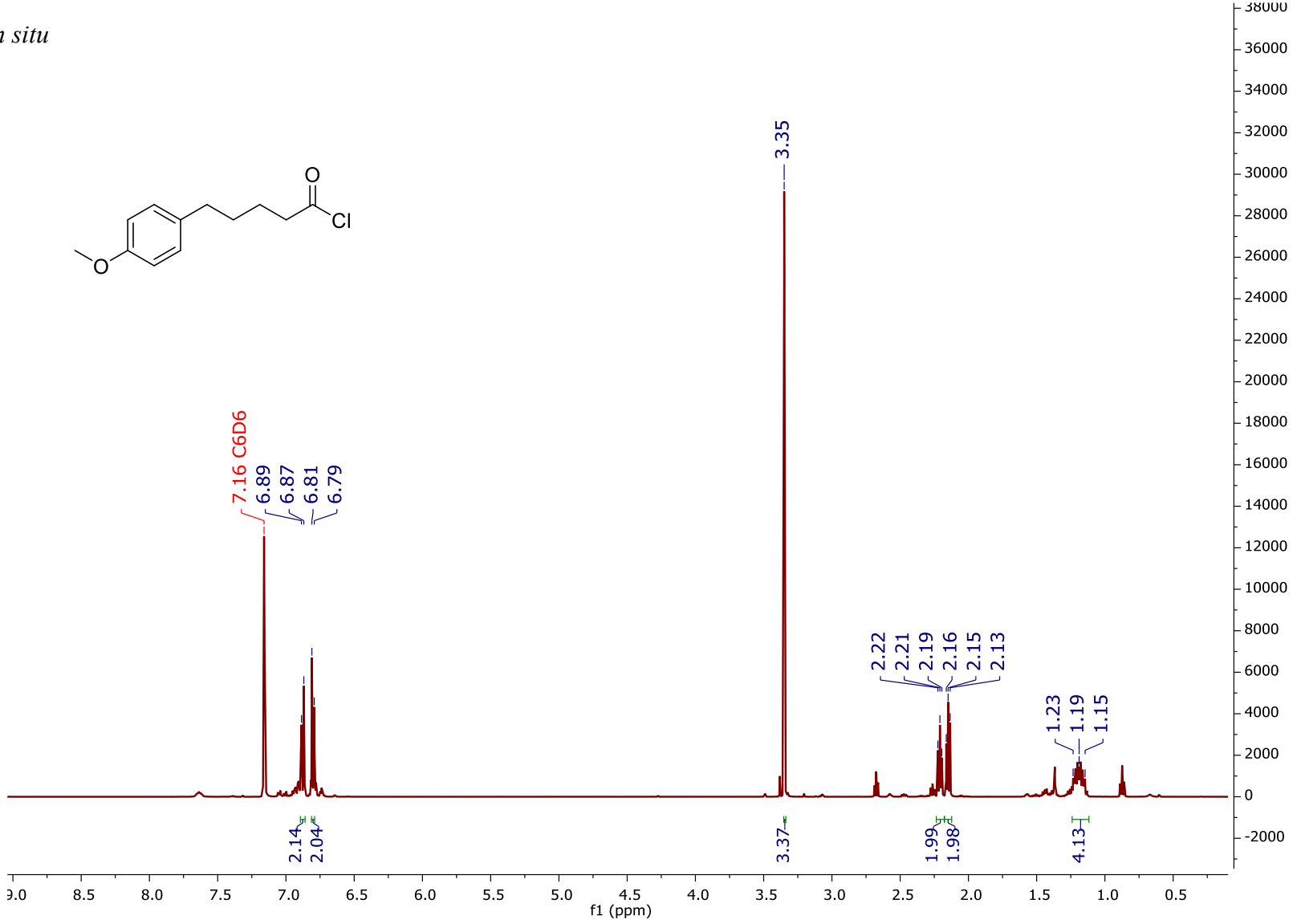
O
Cl
O
7.16 C6D6
6.89
6.87
6.81
6.79
3.35
2.22
2.21
2.19
2.16
2.15
2.13
1.23
1.19
1.15
2.14
2.04
3.37
1.99
1.98
4.13
f1 (ppm)

In situ

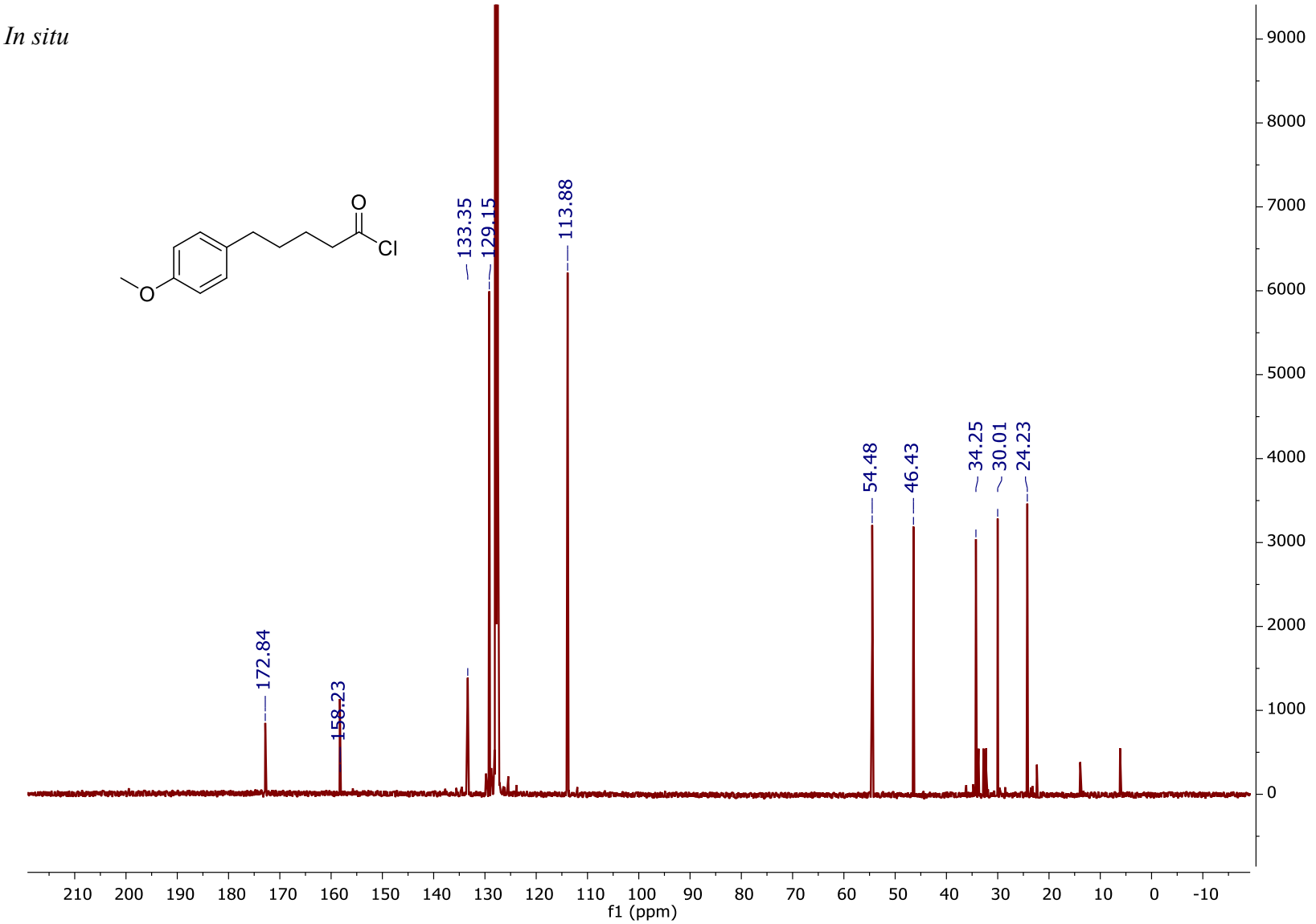
O
Cl
O
133.35
129.15
113.88
54.48
46.43
34.25
30.01
24.23
172.84
158.23
9000
8000
7000
6000
5000
4000
3000
2000
1000
0
210 200 190 180 170 160 150 140 130 120 110 100 90 80 70 60 50 40 30 20 10 0 -10
f1 (ppm)

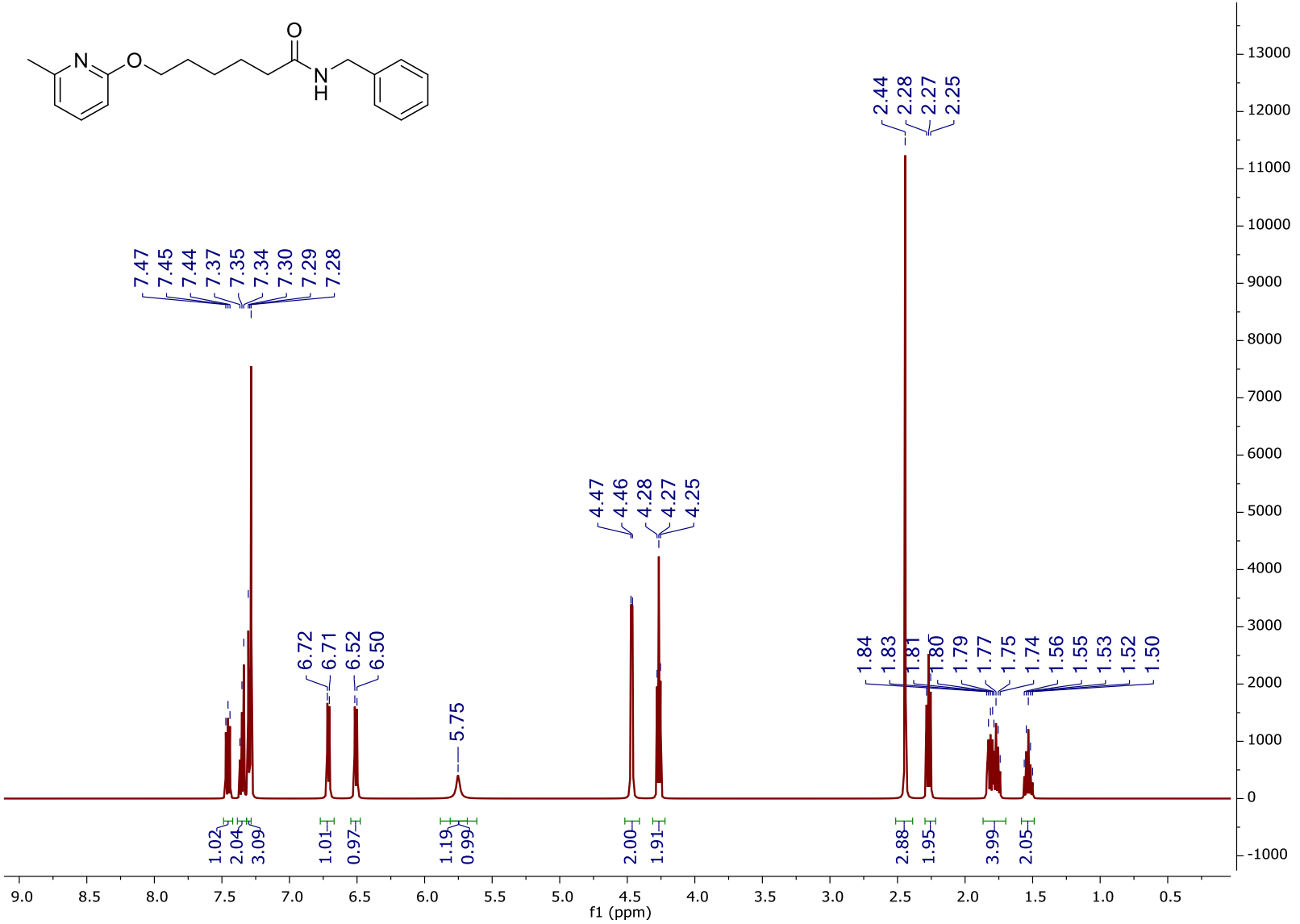
O
N
O
N
H
7.47
7.45
7.44
7.37
7.35
7.34
7.30
7.29
7.28
6.72
6.71
6.52
6.50
5.75
4.47
4.46
4.28
4.27
4.25
2.44
2.28
2.27
2.25
1.84
1.83
1.81
1.80
1.79
1.77
1.75
1.74
1.56
1.55
1.53
1.52
1.50
1.02
2.04
3.09
1.01
0.97
1.19
0.99
2.00
1.91
2.88
1.95
3.99
2.05
f1 (ppm)

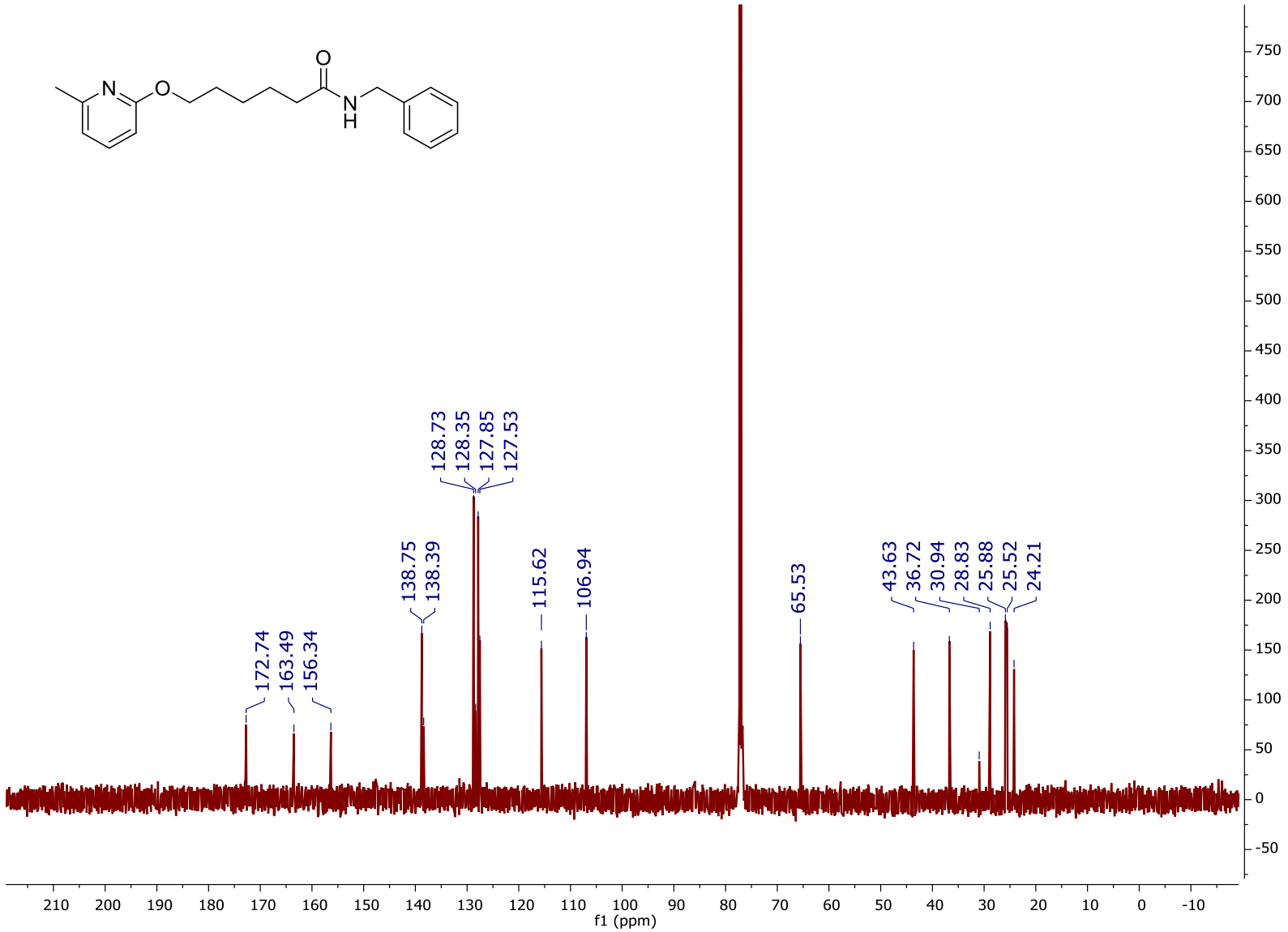
O
N
O
N
H
172.74
163.49
156.34
138.75
138.39
128.73
128.35
127.85
127.53
115.62
106.94
65.53
43.63
36.72
30.94
28.83
25.88
25.52
24.21
f1 (ppm)

In situ

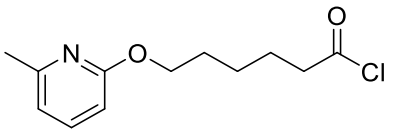
N
O
O
Cl

7.16
16000
15000
14000
13000
12000
11000
10000
9000
8000
7000
6000
5000
4000
3000
2000
1000
0
-1000
9.0
8.5
8.0
7.5
7.0
6.5
6.0
5.5
5.0
4.5
4.0
3.5
3.0
2.5
2.0
1.5
1.0
0.5
f1 (ppm)

In situ

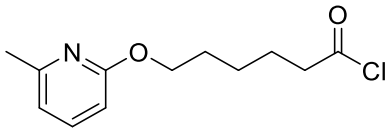
N
O
O
Cl

172.78
163.50
155.99
138.62
115.33
107.63
65.12
46.46
28.38
24.69
24.42
6.04
f1 (ppm)

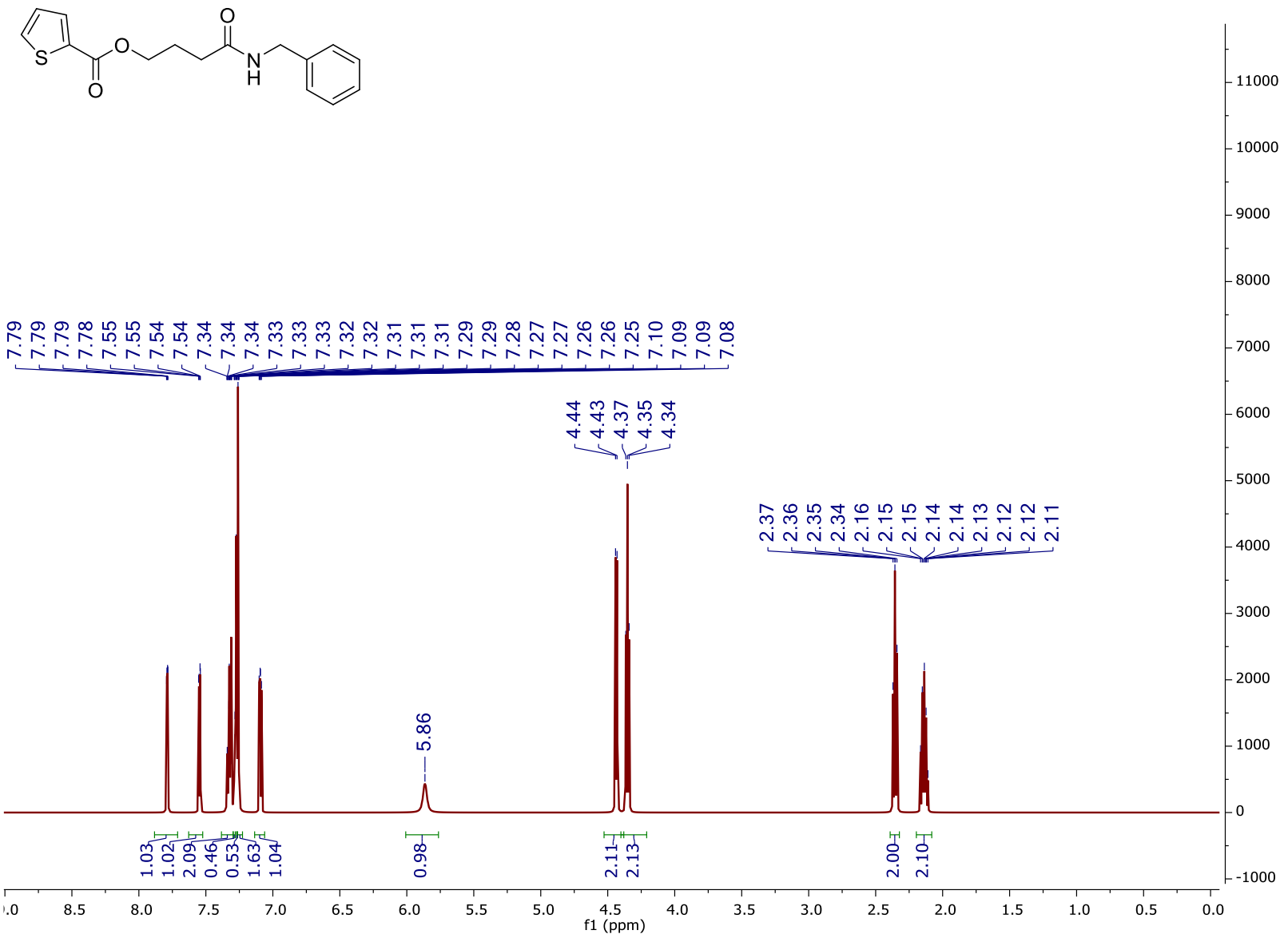
O
S
O
O
N
H
7.79
7.79
7.79
7.78
7.55
7.55
7.54
7.54
7.34
7.34
7.34
7.33
7.33
7.33
7.32
7.32
7.31
7.31
7.31
7.29
7.29
7.28
7.27
7.27
7.26
7.26
7.25
7.10
7.09
7.09
7.08
4.44
4.43
4.37
4.35
4.34
2.37
2.36
2.35
2.34
2.16
2.15
2.15
2.14
2.14
2.13
2.12
2.12
2.11
5.86
1.03
1.02
2.09
0.46
0.53
1.63
1.04
0.98
2.11
2.13
2.00
2.10
11000
10000
9000
8000
7000
6000
5000
4000
3000
2000
1000
0
-1000
8.5
8.0
7.5
7.0
6.5
6.0
5.5
5.0
4.5
4.0
3.5
3.0
2.5
2.0
1.5
1.0
0.5
0.0
f1 (ppm)

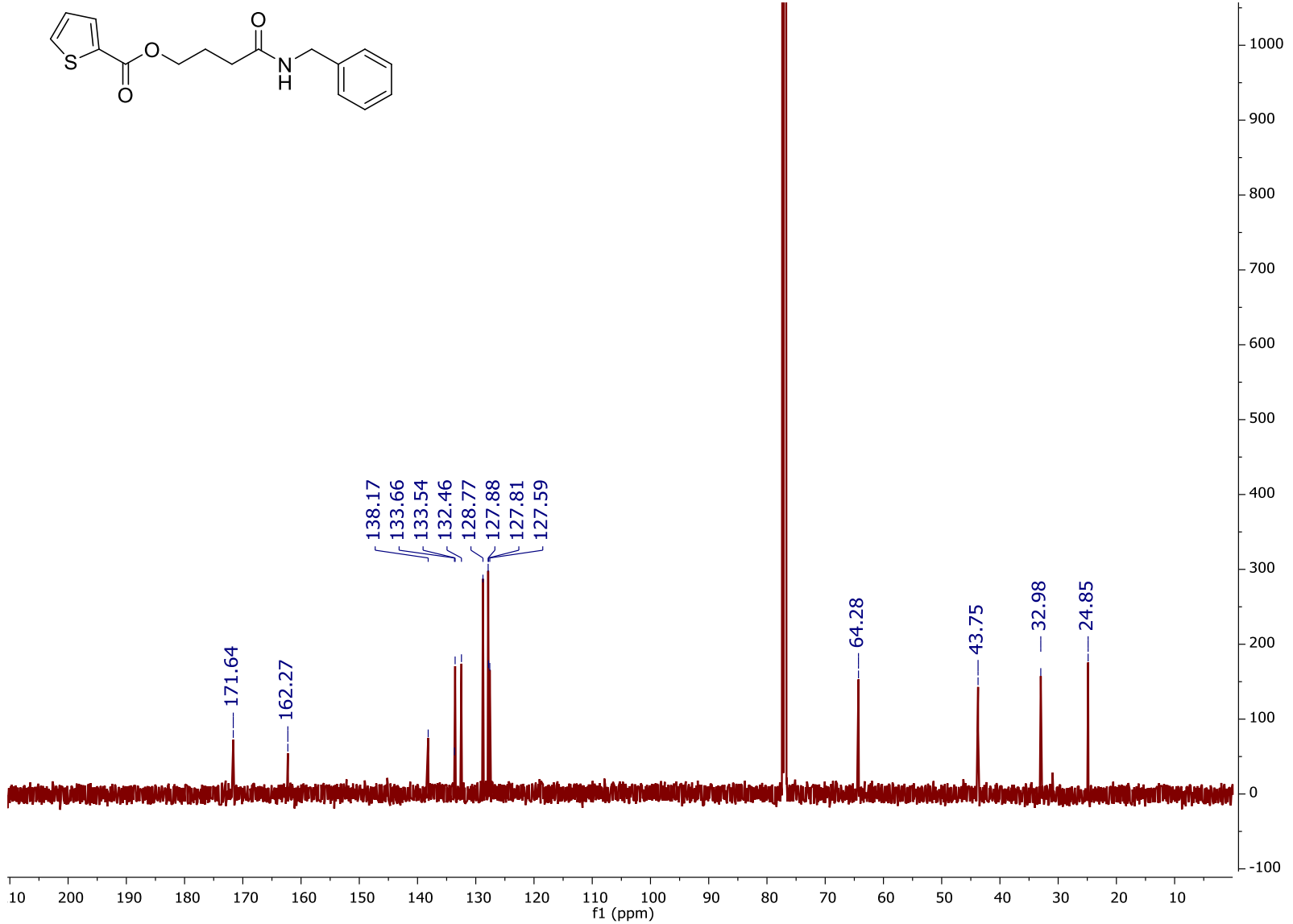
O
O
S
O
N
H
138.17
133.66
133.54
132.46
128.77
127.88
127.81
127.59
171.64
162.27
64.28
43.75
32.98
24.85
1000
900
800
700
600
500
400
300
200
100
0
-100
10
200
190
180
170
160
150
140
130
120
110
100
90
80
70
60
50
40
30
20
10
f1 (ppm)

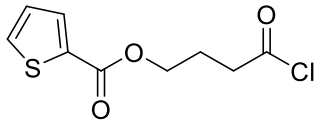
O
S
O
O
Cl

In situ

7.16 C6D6
6.81
6.81
6.80
6.80
6.54
6.53
6.53
6.52
7.68
7.68
7.67
7.67
3.76
3.75
3.74
2.18
2.17
2.15
1.40
1.39
1.38
1.36
1.35
0.97
1.15
1.15
2.00
2.02
2.43
f1 (ppm)

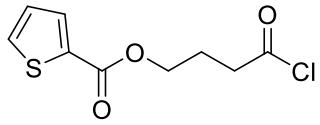
S
O
O
O
Cl

In situ

172.43
161.28
133.68
133.34
132.14
128.22
62.64
43.20
23.92
5500
5000
4500
4000
3500
3000
2500
2000
1500
1000
500
0
-500
200
190
180
170
160
150
140
130
120
110
100
90
80
70
60
50
40
30
20
10
0
f1 (ppm)

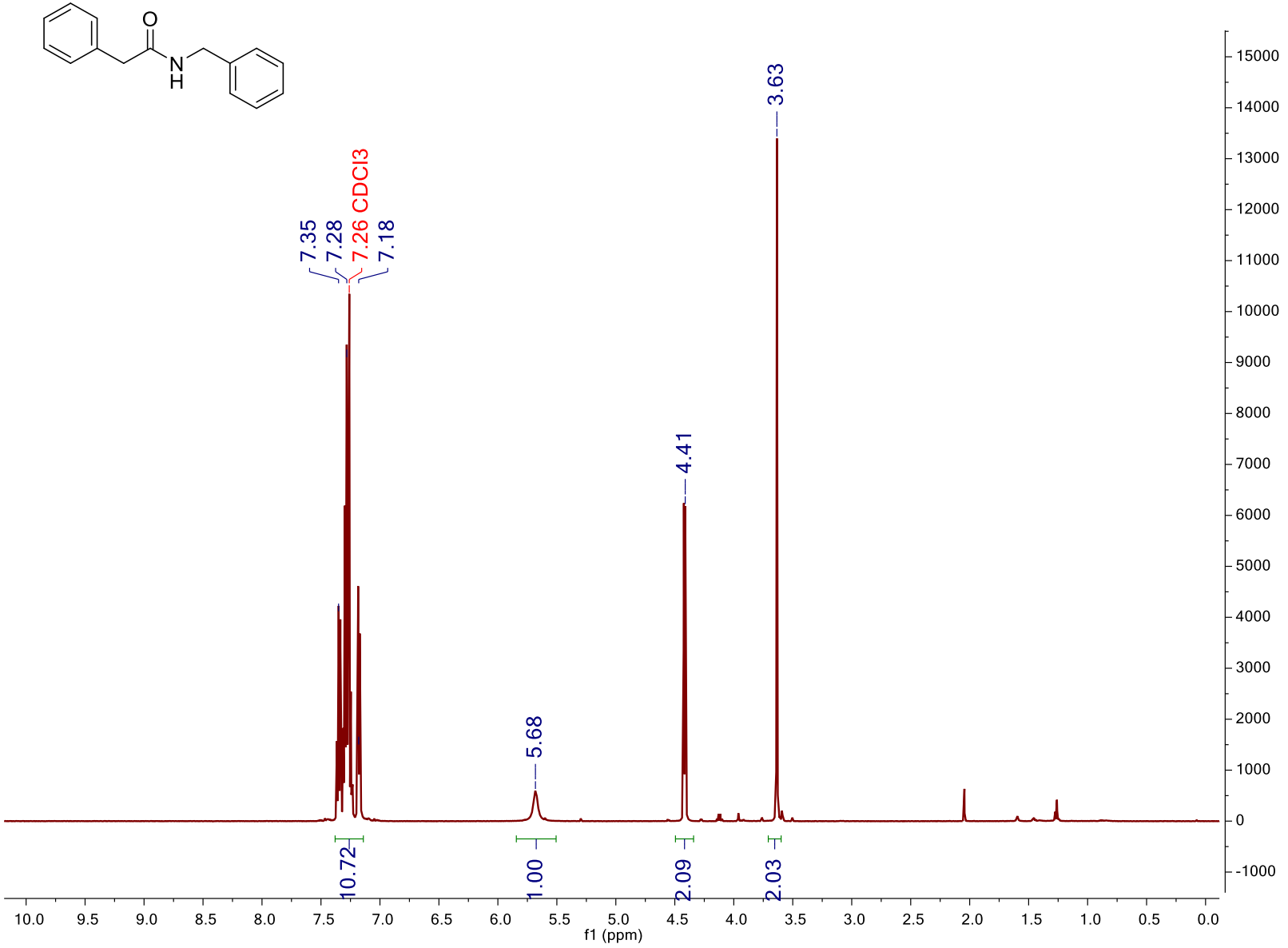
O
N
H
7.35
7.28
7.26 CDCl3
7.18
5.68
4.41
3.63
10.72
1.00
2.09
2.03
f1 (ppm)

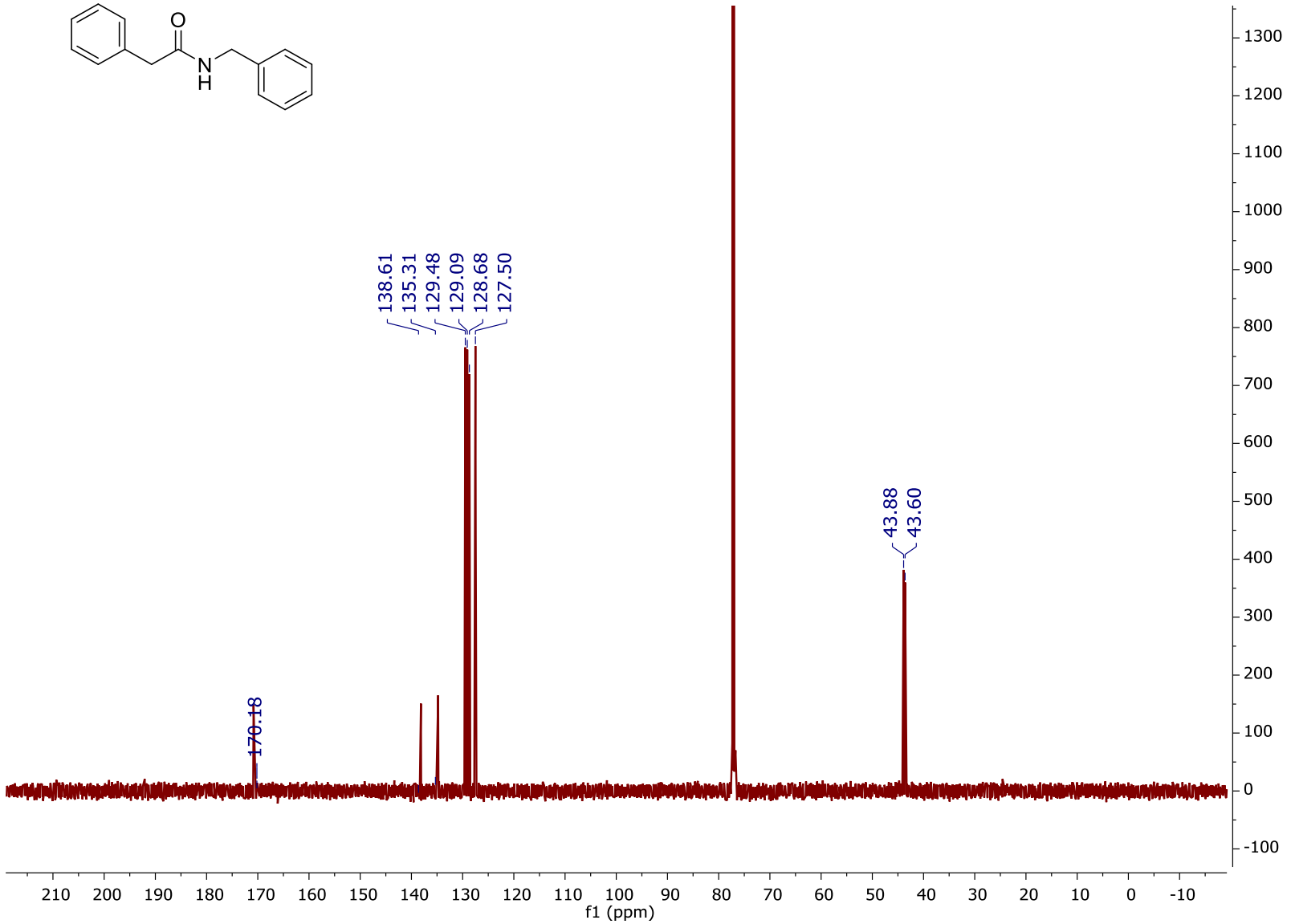
O
N
H
138.61
135.31
129.48
129.09
128.68
127.50
170.18
43.88
43.60
1300
1200
1100
1000
900
800
700
600
500
400
300
200
100
0
-100
210 200 190 180 170 160 150 140 130 120 110 100 90 80 70 60 50 40 30 20 10 0 -10
f1 (ppm)

In situ

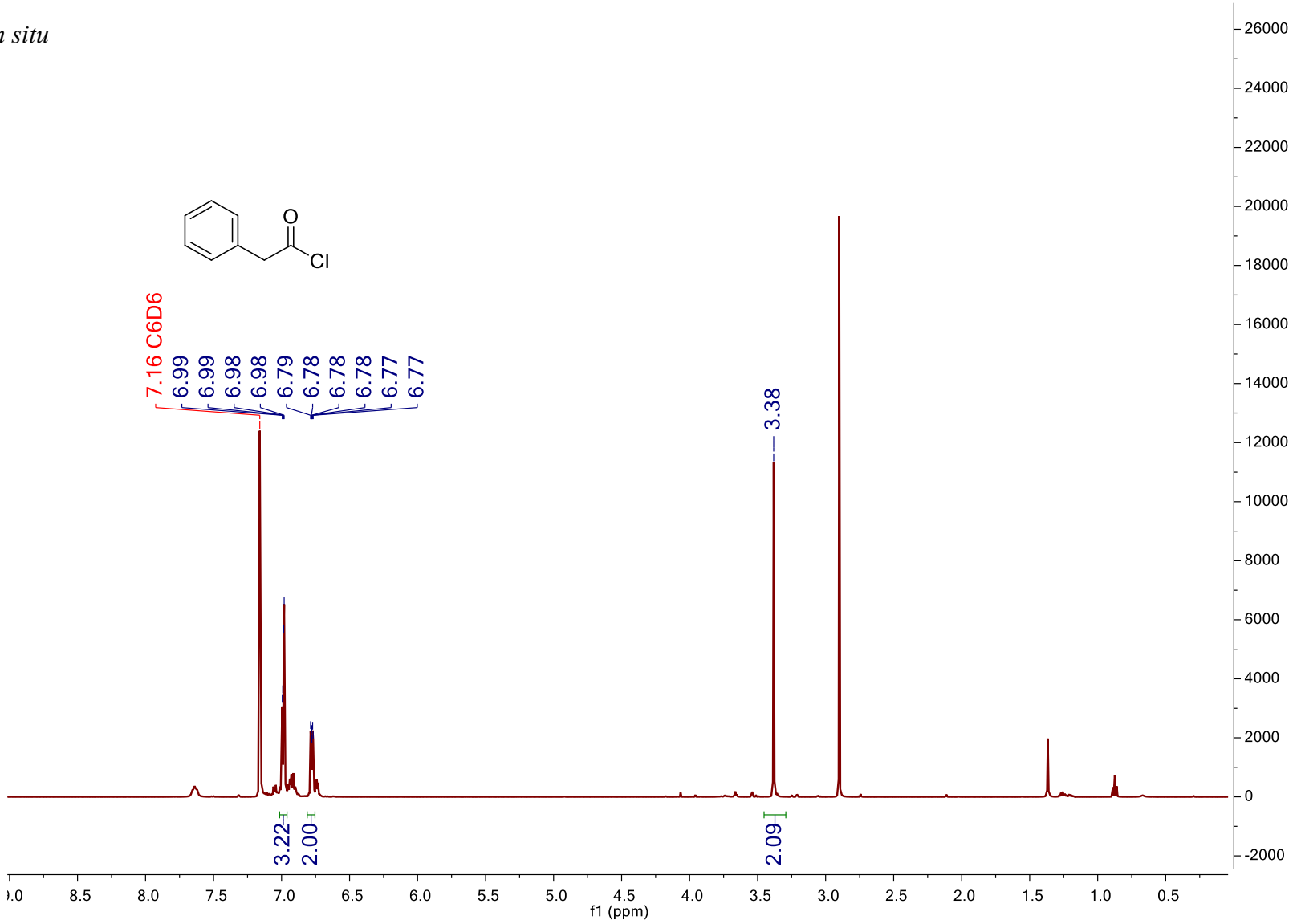
O
Cl
7.16 C6D6
6.99
6.99
6.98
6.98
6.79
6.78
6.78
6.78
6.77
6.77
3.38
3.22
2.00
2.09
f1 (ppm)

In situ

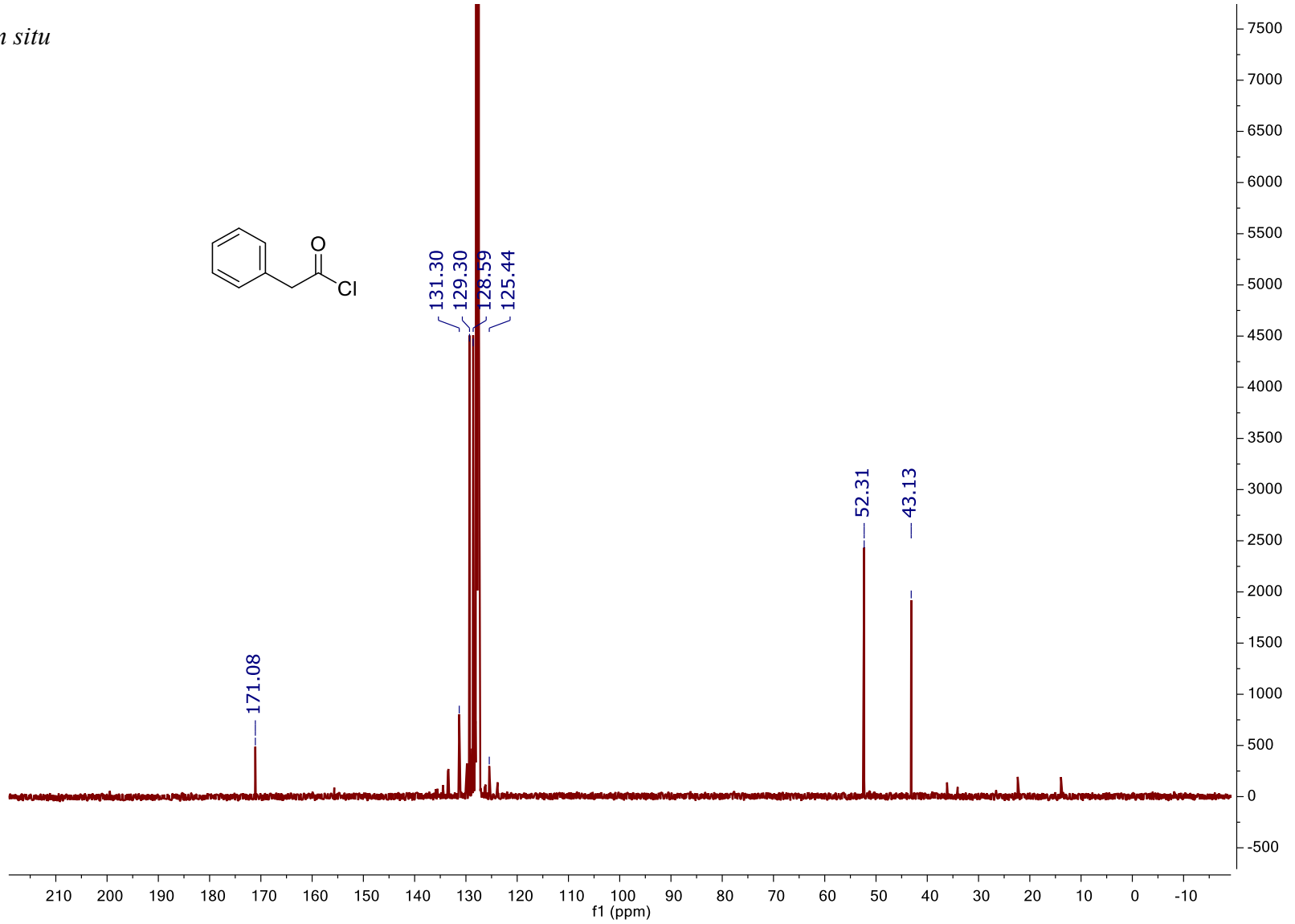

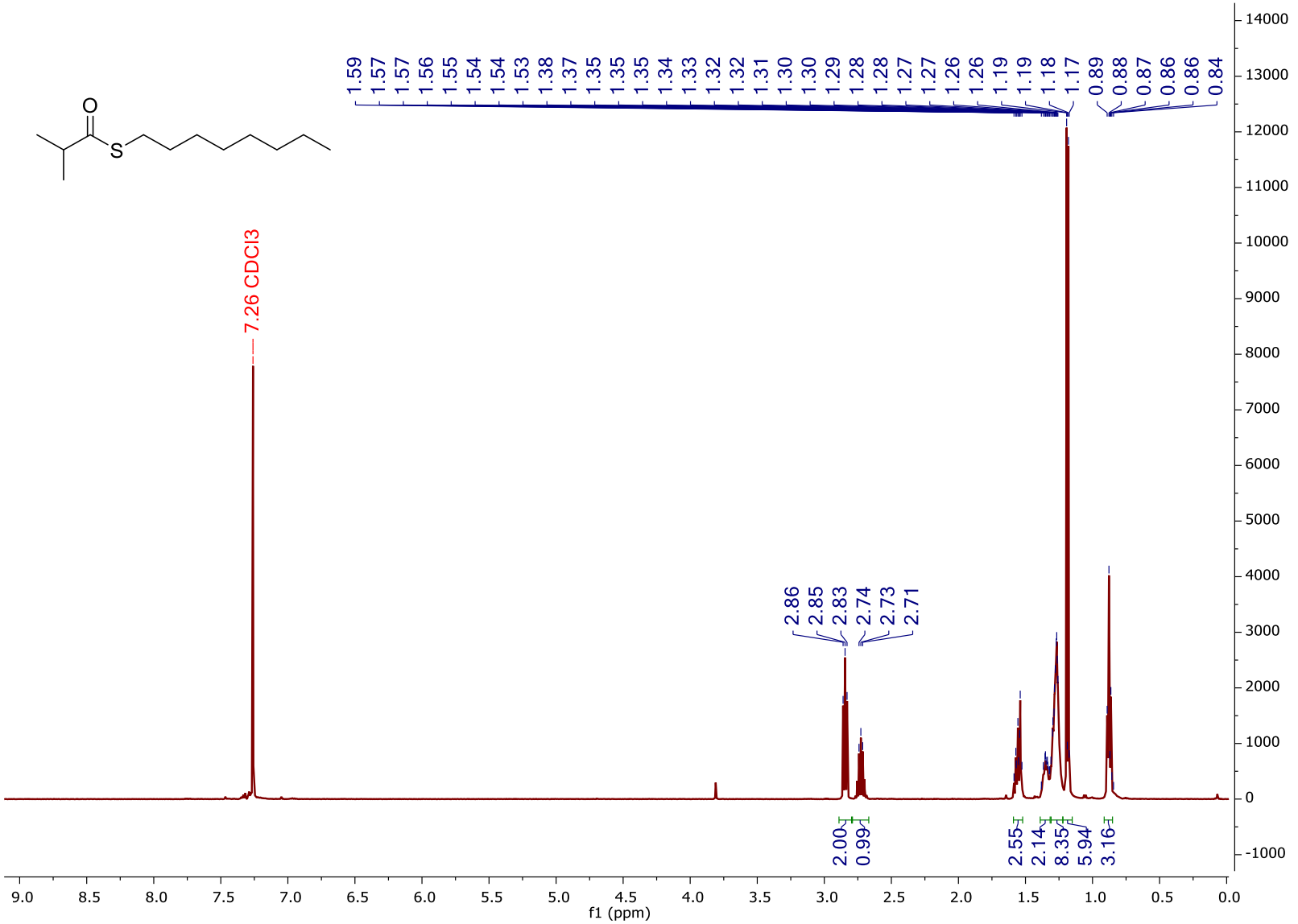
O
S
7.26 CDCl3
1.59 1.57 1.57 1.56 1.55 1.54 1.54 1.53 1.38 1.37 1.35 1.35 1.35 1.34 1.33 1.32 1.32 1.31 1.30 1.30 1.29 1.28 1.28 1.27 1.27 1.26 1.26 1.19 1.19 1.18 1.17 0.89 0.88 0.87 0.86 0.86 0.84
2.86 2.85 2.83 2.74 2.73 2.71
2.00 0.99 2.55 2.14 8.35 5.94 3.16
f1 (ppm)

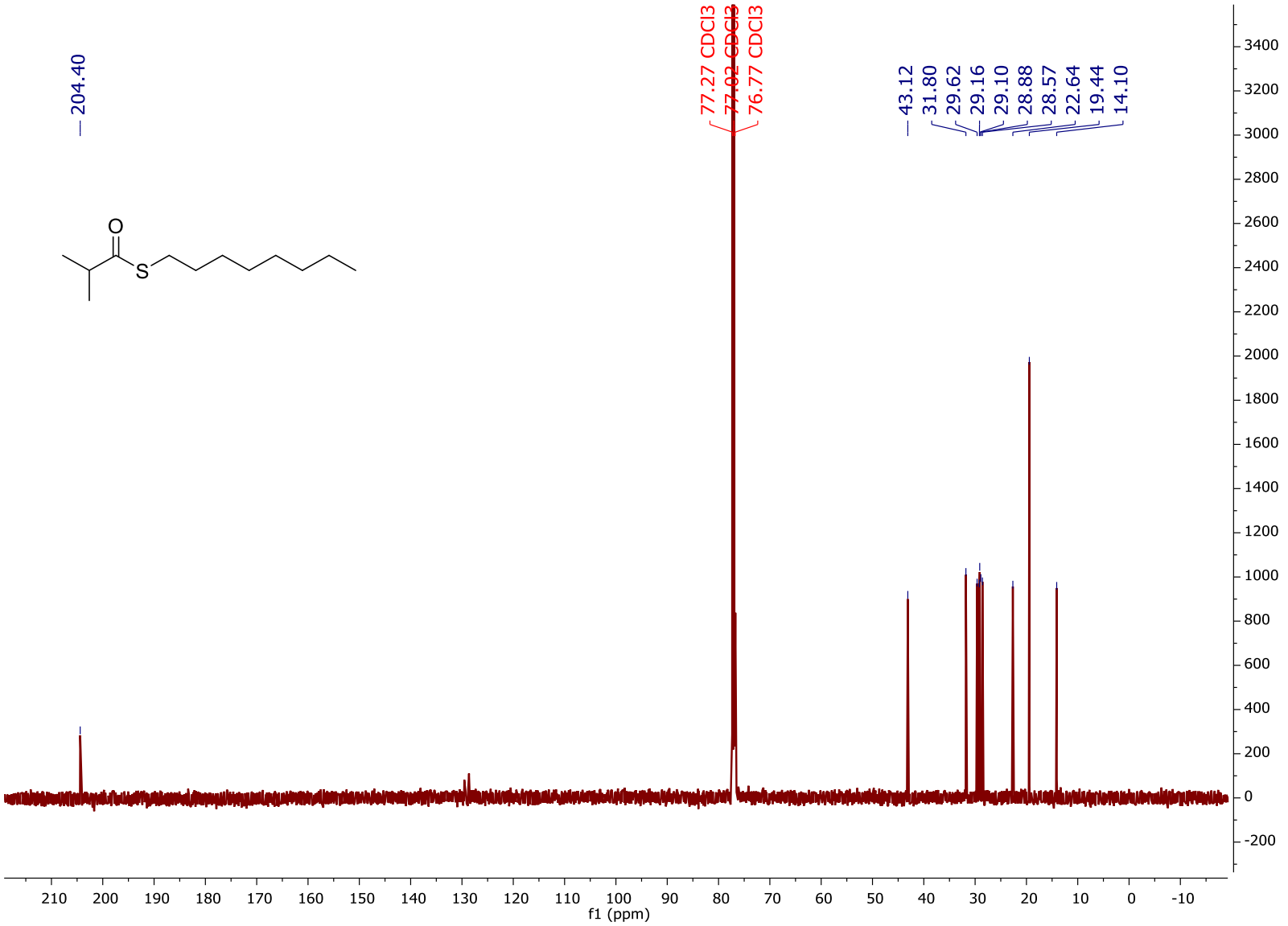
204.40
77.27 CDCl3
77.02 CDCl3
76.77 CDCl3
43.12
31.80
29.62
29.16
29.10
28.88
28.57
22.64
19.44
14.10
O
S
f1 (ppm)

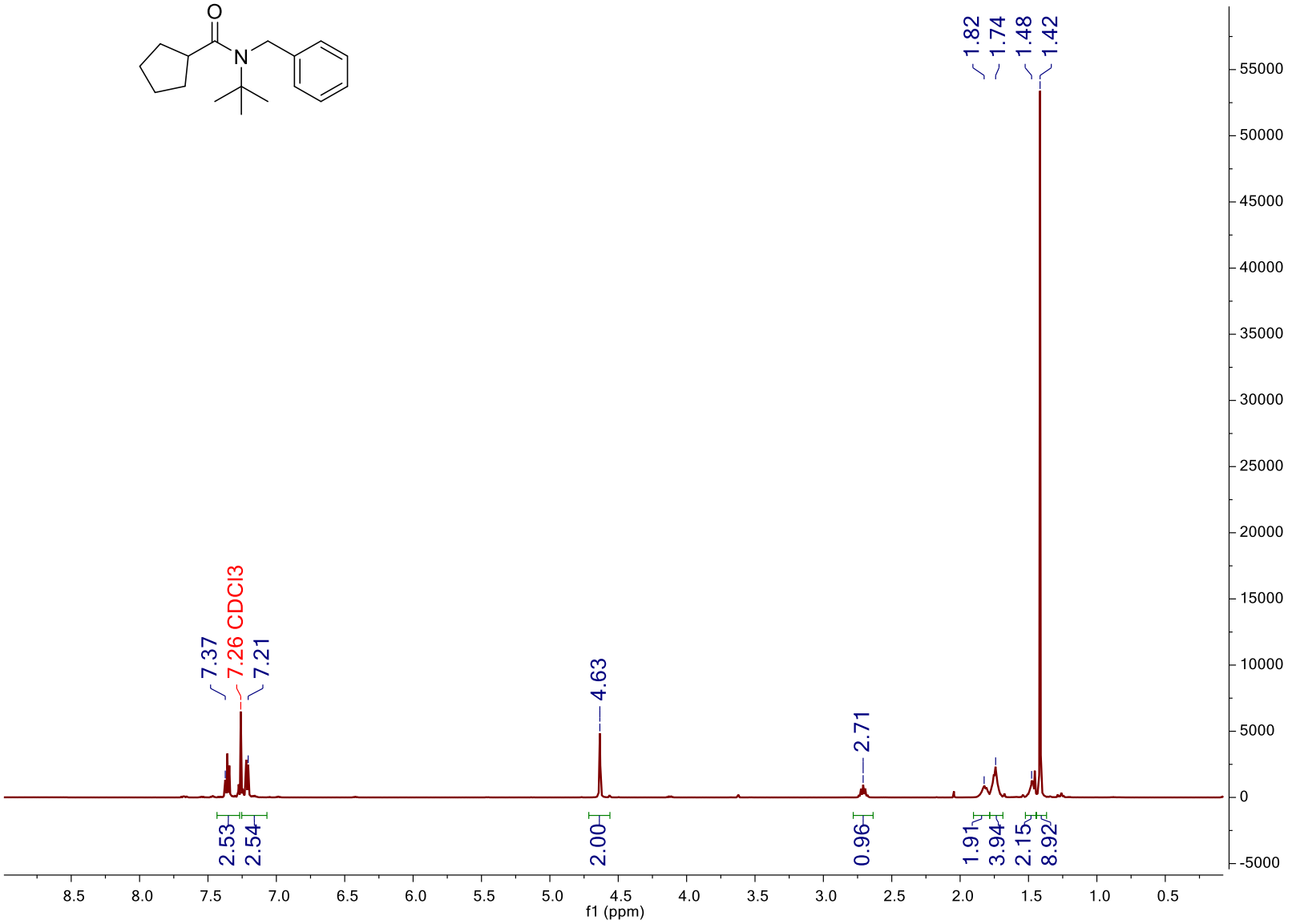
O
N
7.37
7.26 CDCl3
7.21
4.63
2.71
1.82
1.74
1.48
1.42
2.53
2.54
2.00
0.96
1.91
3.94
2.15
8.92
f1 (ppm)

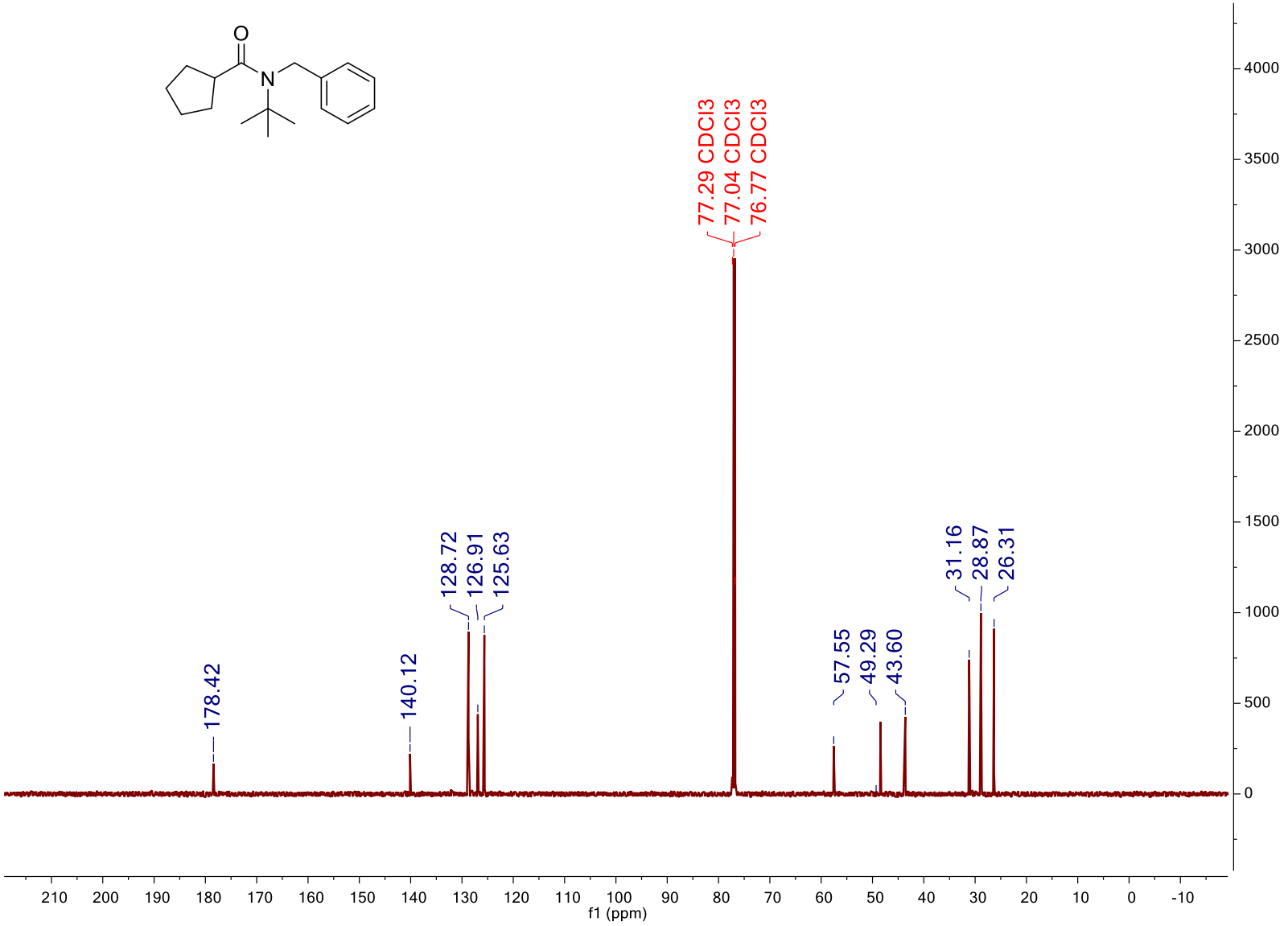
O
N
178.42
140.12
128.72
126.91
125.63
77.29 CDCl3
77.04 CDCl3
76.77 CDCl3
57.55
49.29
43.60
31.16
28.87
26.31
f1 (ppm)

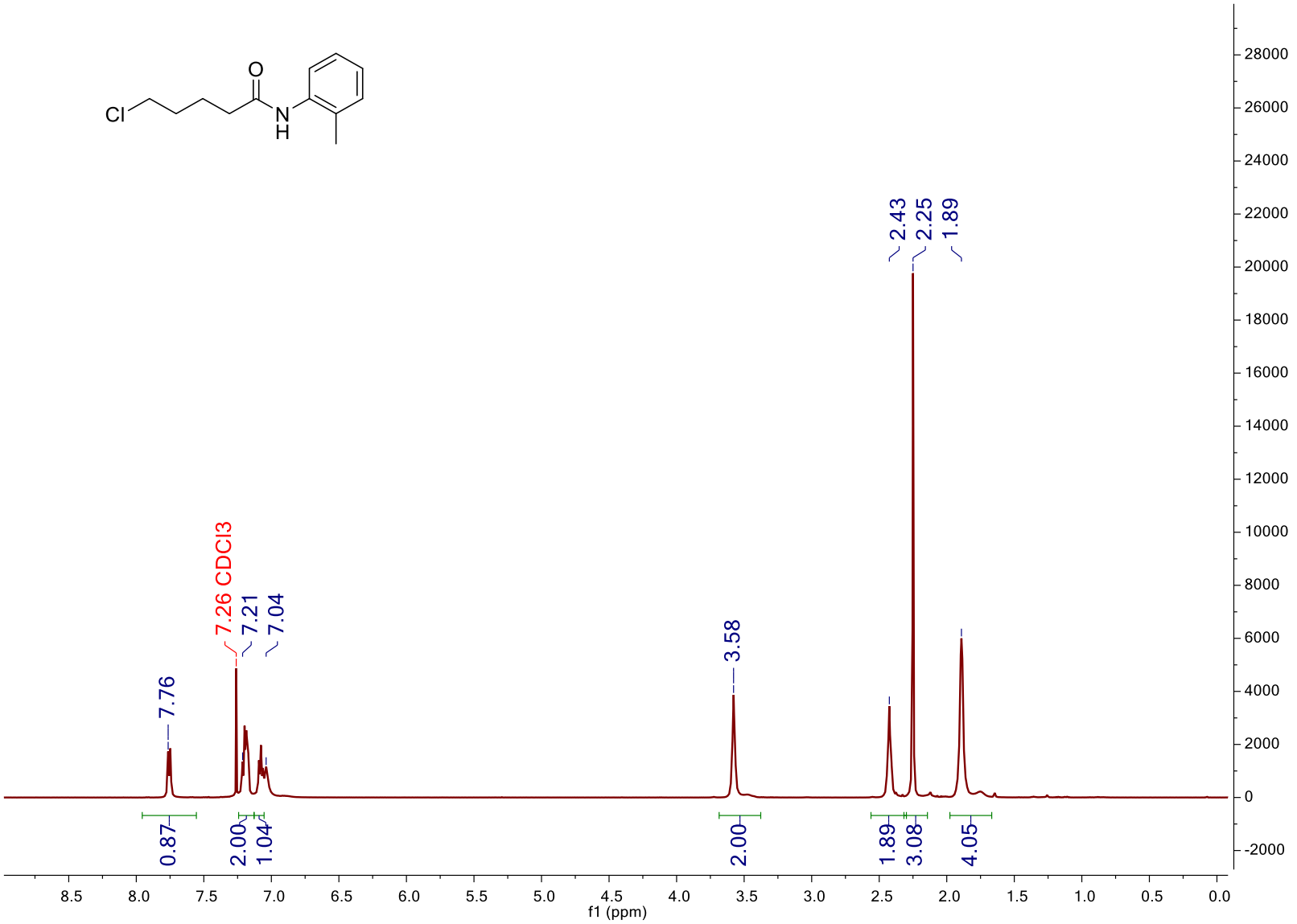
Cl
O
N
H
7.76
7.26 CDCl3
7.21
7.04
3.58
2.43
2.25
1.89
0.87
2.00
1.04
2.00
1.89
3.08
4.05
f1 (ppm)

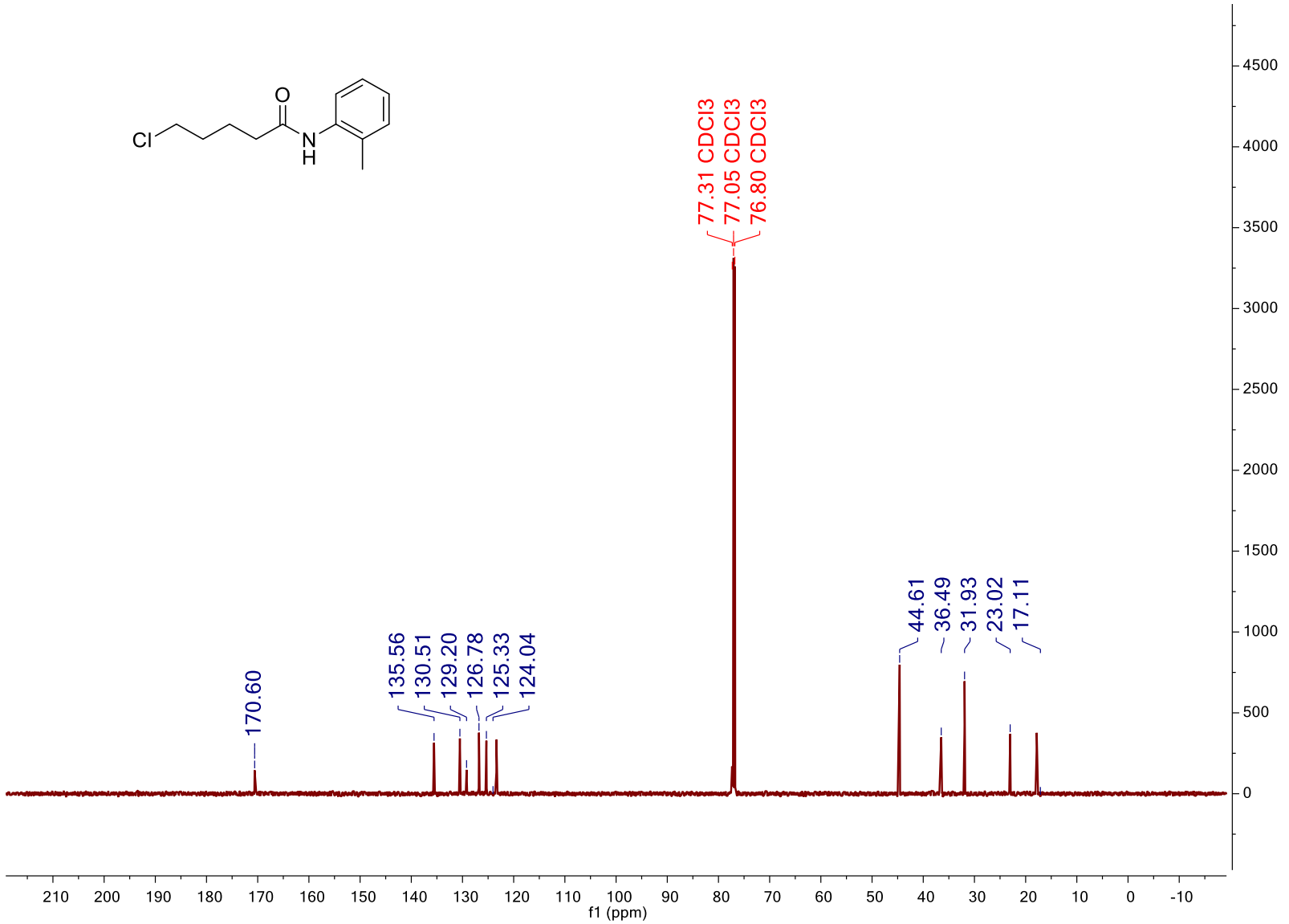
Cl
O
N
H
77.31 CDCl3
77.05 CDCl3
76.80 CDCl3
170.60
135.56
130.51
129.20
126.78
125.33
124.04
44.61
36.49
31.93
23.02
17.11
4500
4000
3500
3000
2500
2000
1500
1000
500
0
210 200 190 180 170 160 150 140 130 120 110 100 90 80 70 60 50 40 30 20 10 0 -10
f1 (ppm)

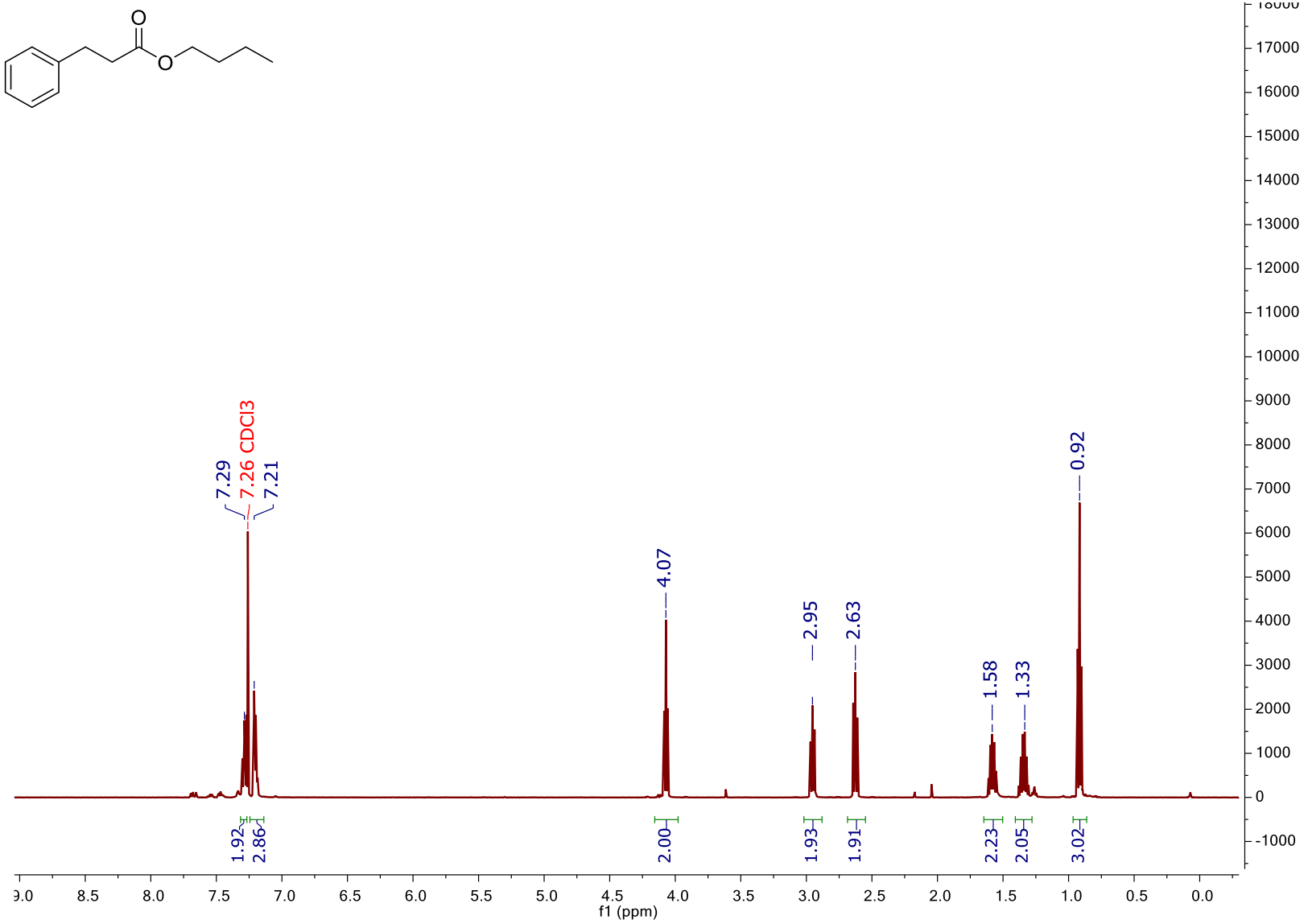
O
O
7.29
7.26 CDCl3
7.21
4.07
2.95
2.63
1.58
1.33
0.92
1.92
2.86
2.00
1.93
1.91
2.23
2.05
3.02
f1 (ppm)

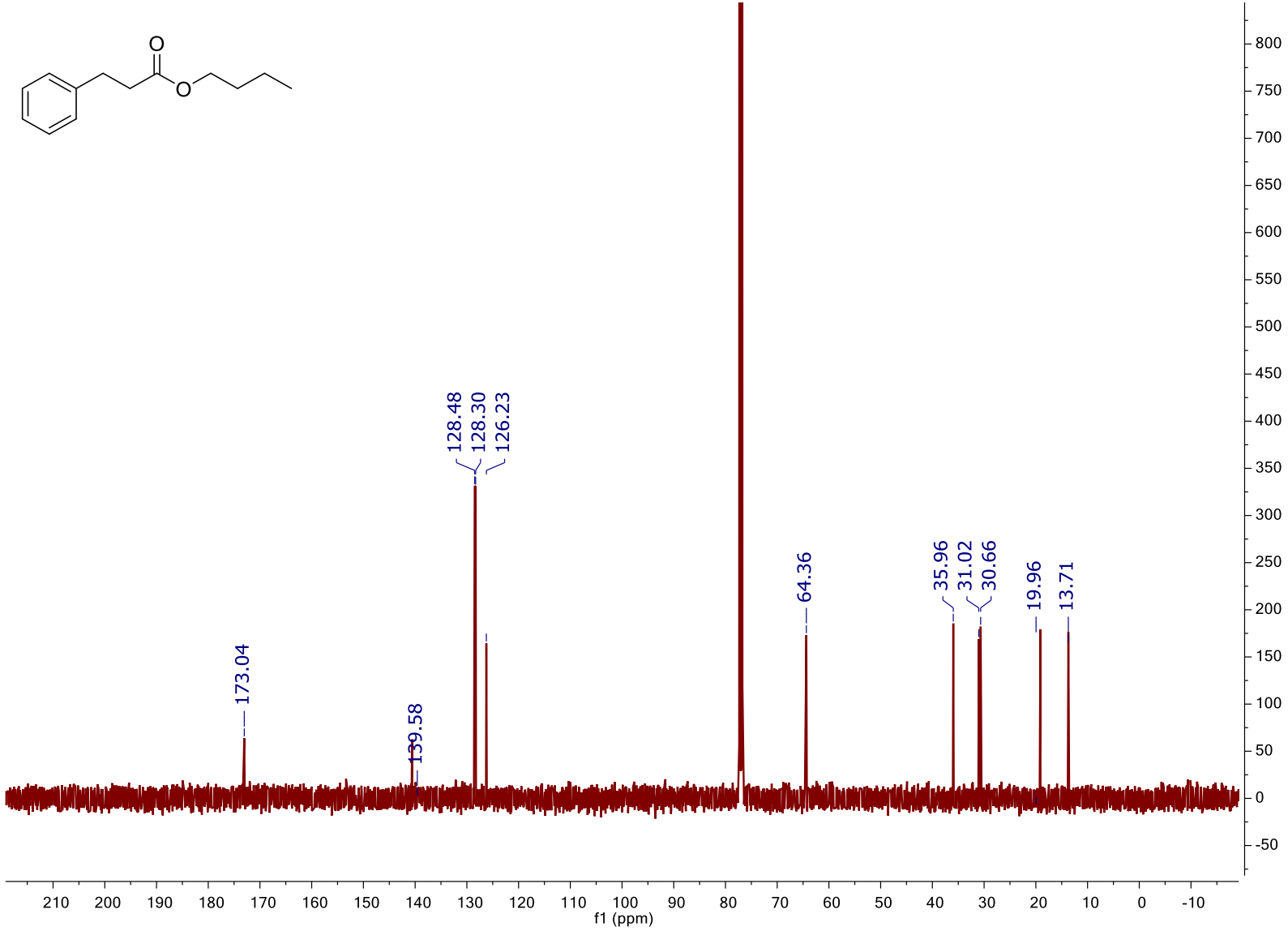
O
O
173.04
139.58
128.48
128.30
126.23
64.36
35.96
31.02
30.66
19.96
13.71
f1 (ppm)

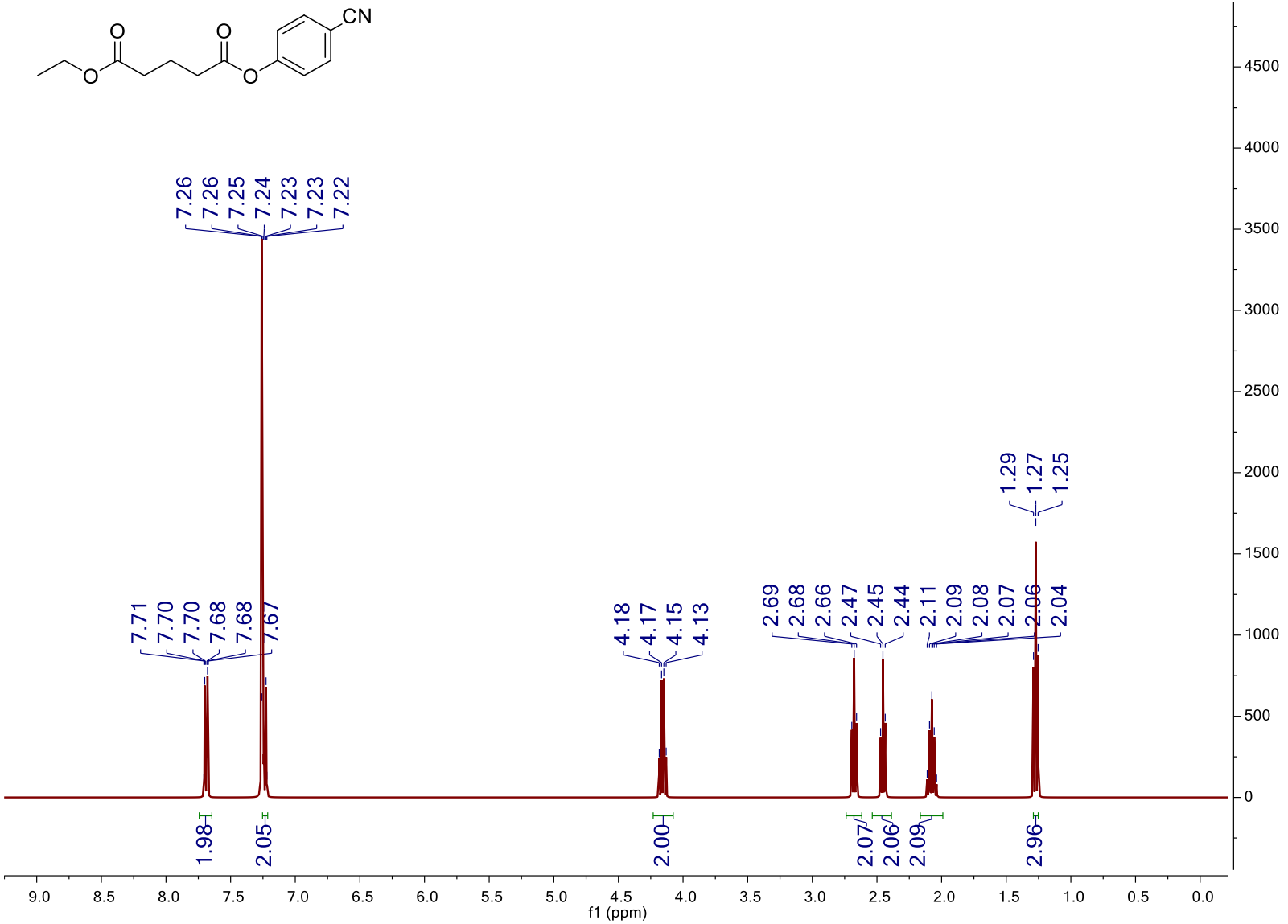
CN
O
O
O
O
7.26
7.26
7.25
7.24
7.23
7.23
7.22
7.71
7.70
7.70
7.68
7.68
7.67
4.18
4.17
4.15
4.13
2.69
2.68
2.66
2.47
2.45
2.44
2.11
2.09
2.08
2.07
2.06
2.04
1.29
1.27
1.25
1.98
2.05
2.00
2.07
2.06
2.09
2.96
f1 (ppm)

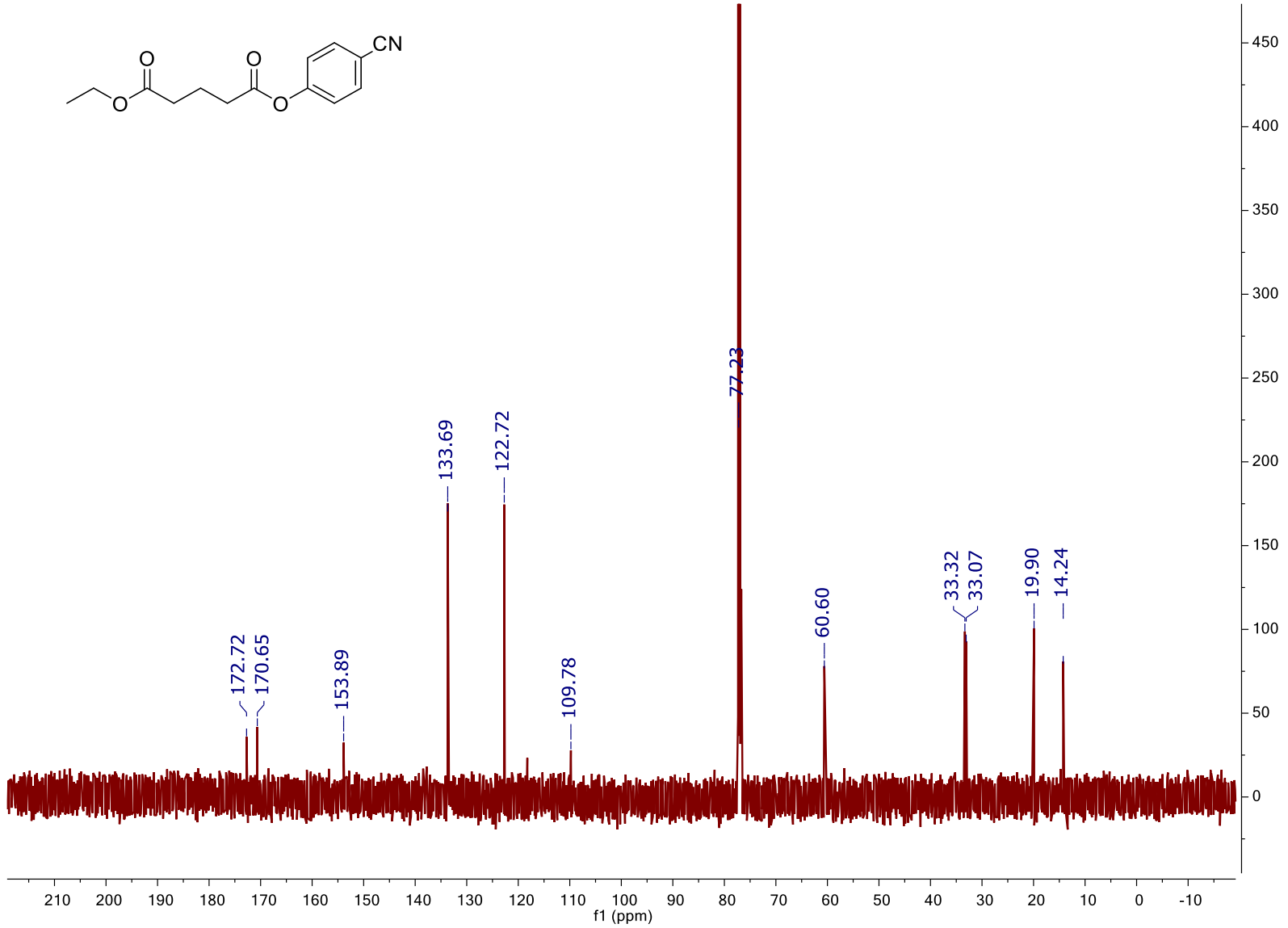
CN
O
O
O
O
172.72
170.65
153.89
133.69
122.72
109.78
77.23
60.60
33.32
33.07
19.90
14.24
450
400
350
300
250
200
150
100
50
0
210
200
190
180
170
160
150
140
130
120
110
100
90
80
70
60
50
40
30
20
10
0
-10
f1 (ppm)

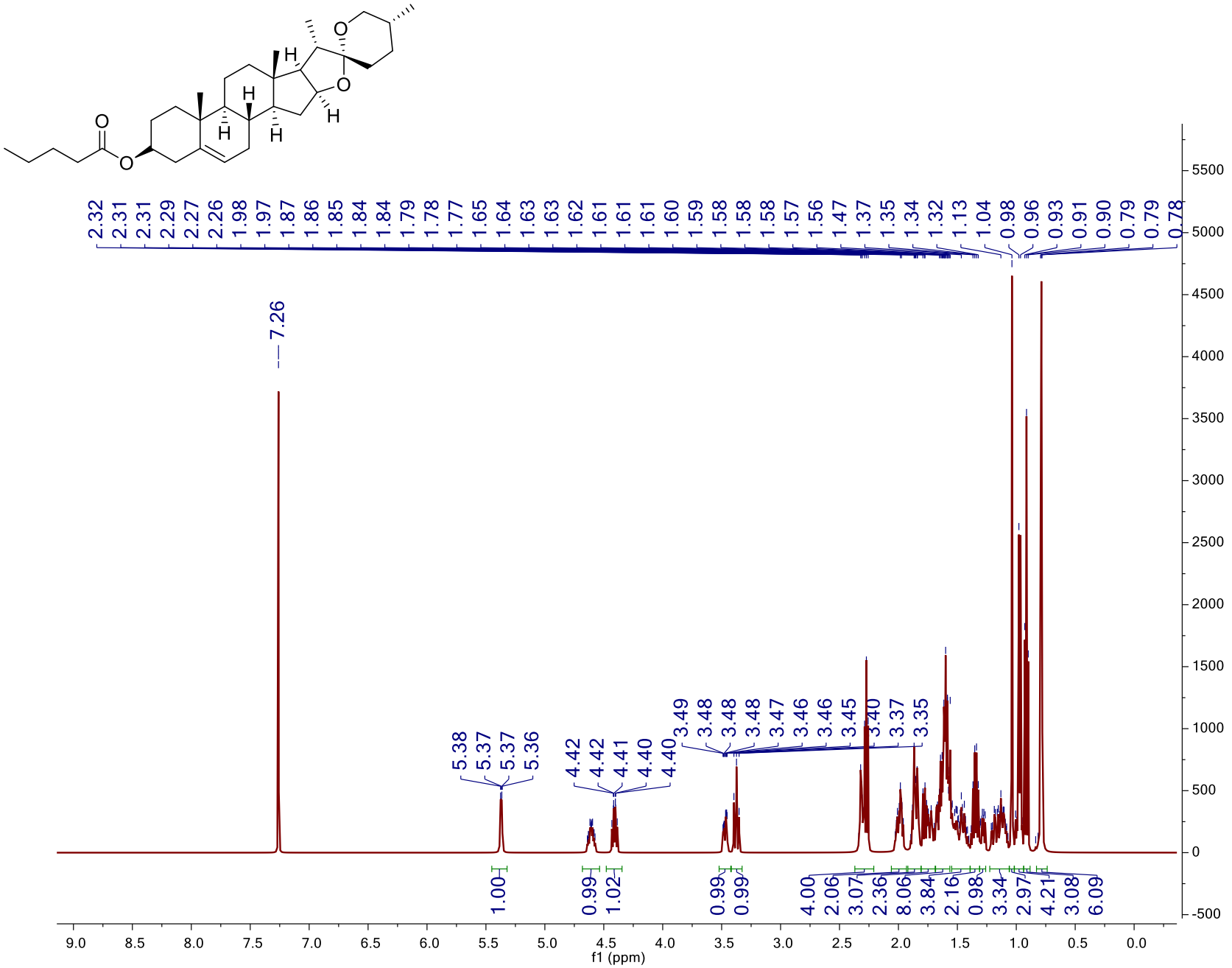
O
O
H
H
H
H
O
O
H
2.32 2.31 2.31 2.29 2.27 2.26 1.98 1.97 1.87 1.86 1.85 1.84 1.84 1.79 1.78 1.77 1.65 1.64 1.63 1.63 1.62 1.61 1.61 1.61 1.60 1.59 1.58 1.58 1.58 1.57 1.56 1.47 1.37 1.35 1.34 1.32 1.13 1.04 0.98 0.96 0.93 0.91 0.90 0.79 0.79 0.78
7.26
5.38 5.37 5.37 5.36
4.42 4.42 4.41 4.40 4.40
3.49 3.48 3.48 3.48 3.47 3.46 3.46 3.45 3.40 3.37 3.35
1.00 0.99 1.02 0.99 0.99 4.00 2.06 3.07 2.36 8.06 3.84 2.16 0.98 3.34 2.97 4.21 3.08 6.09
f1 (ppm)

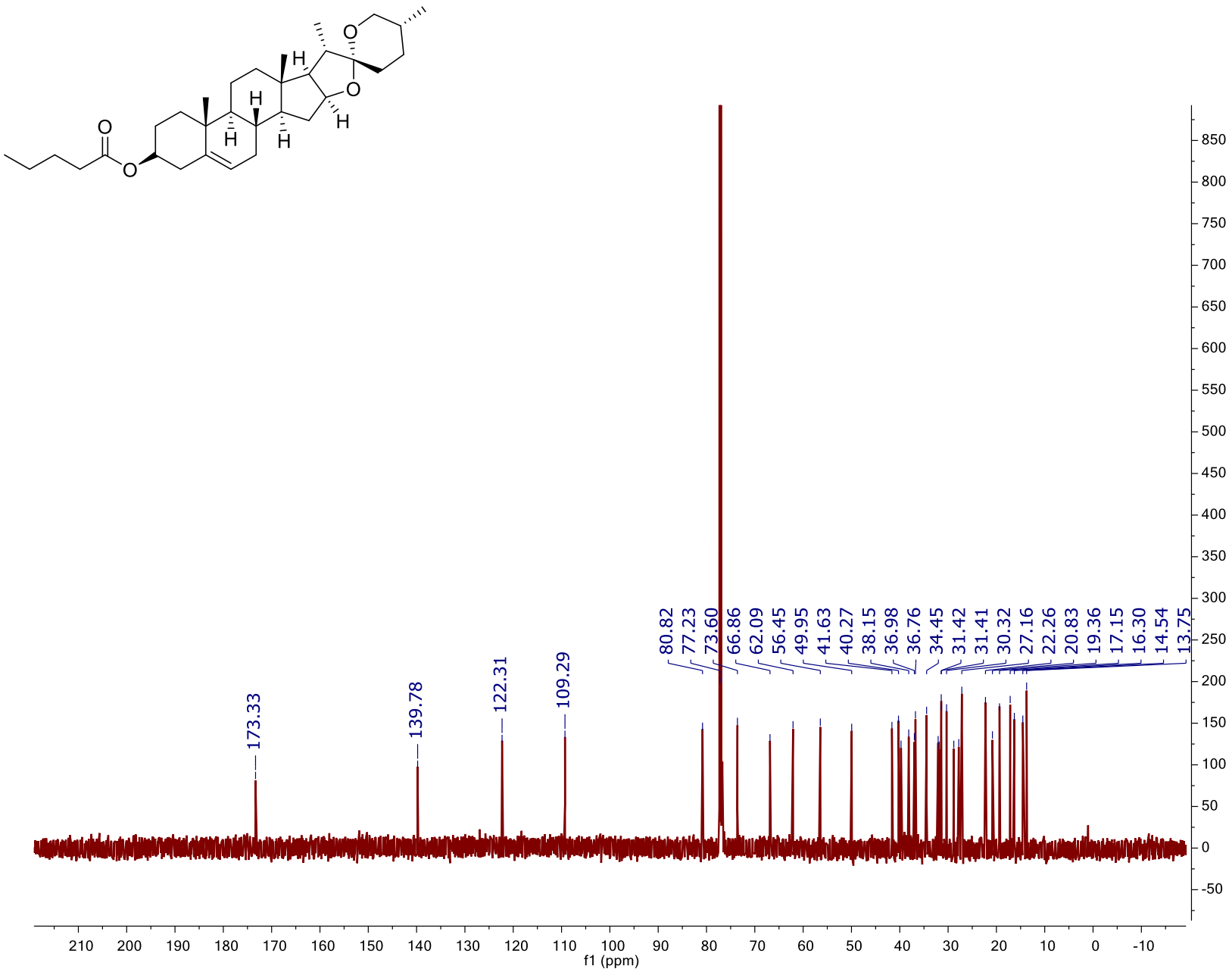
O
O
H
H
H
H
O
O
H
80.82
77.23
73.60
66.86
62.09
56.45
49.95
41.63
40.27
38.15
36.98
36.76
34.45
31.42
31.41
30.32
27.16
22.26
20.83
19.36
17.15
16.30
14.54
13.75
173.33
139.78
122.31
109.29
850
800
750
700
650
600
550
500
450
400
350
300
250
200
150
100
50
0
-50
210
200
190
180
170
160
150
140
130
120
110
100
90
80
70
60
50
40
30
20
10
0
-10
f1 (ppm)

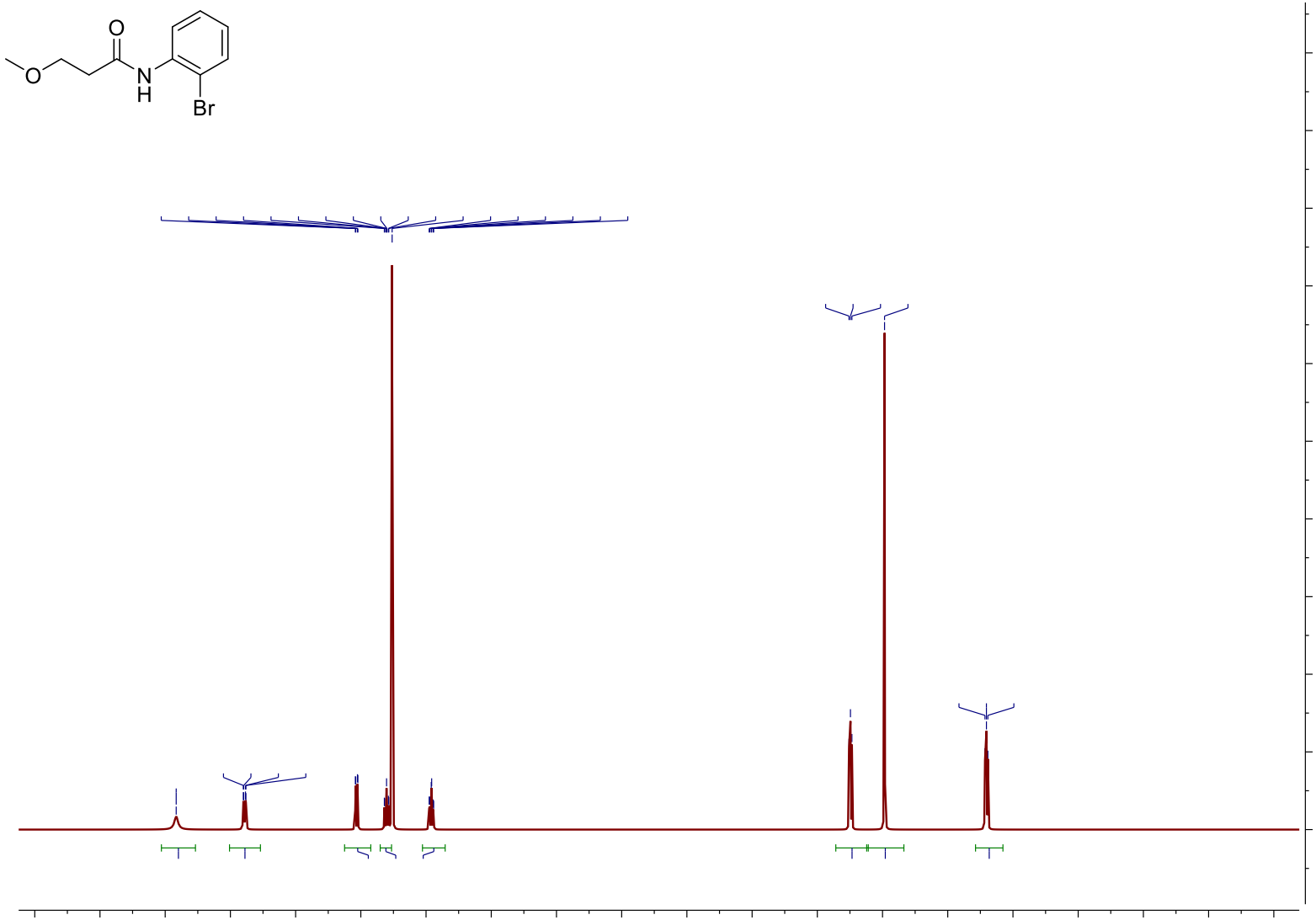
O
O
N
H
Br

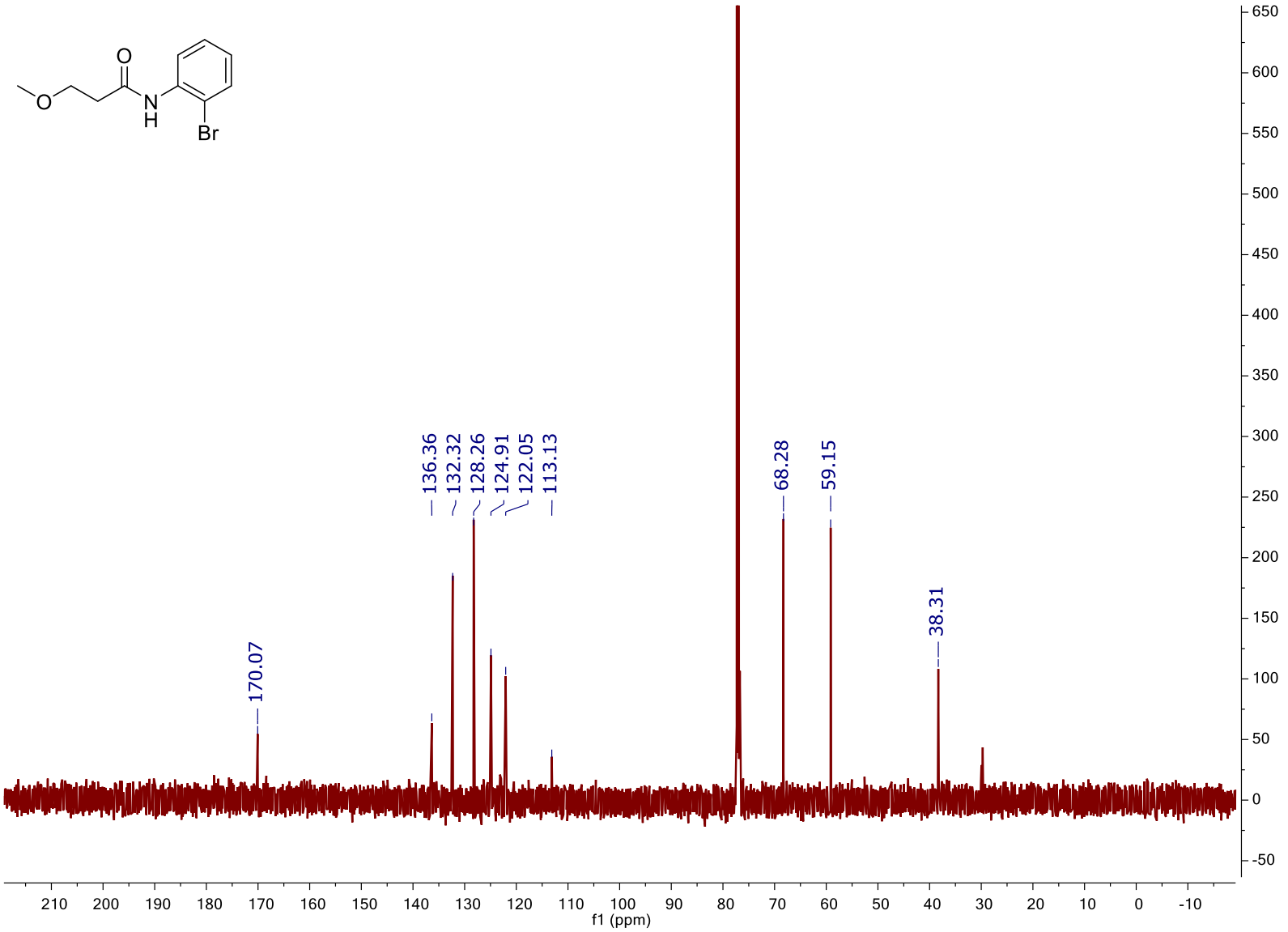
O
O
N
H
Br
170.07
136.36
132.32
128.26
124.91
122.05
113.13
68.28
59.15
38.31
650
600
550
500
450
400
350
300
250
200
150
100
50
0
-50
210
200
190
180
170
160
150
140
130
120
110
100
90
80
70
60
50
40
30
20
10
0
-10
f1 (ppm)

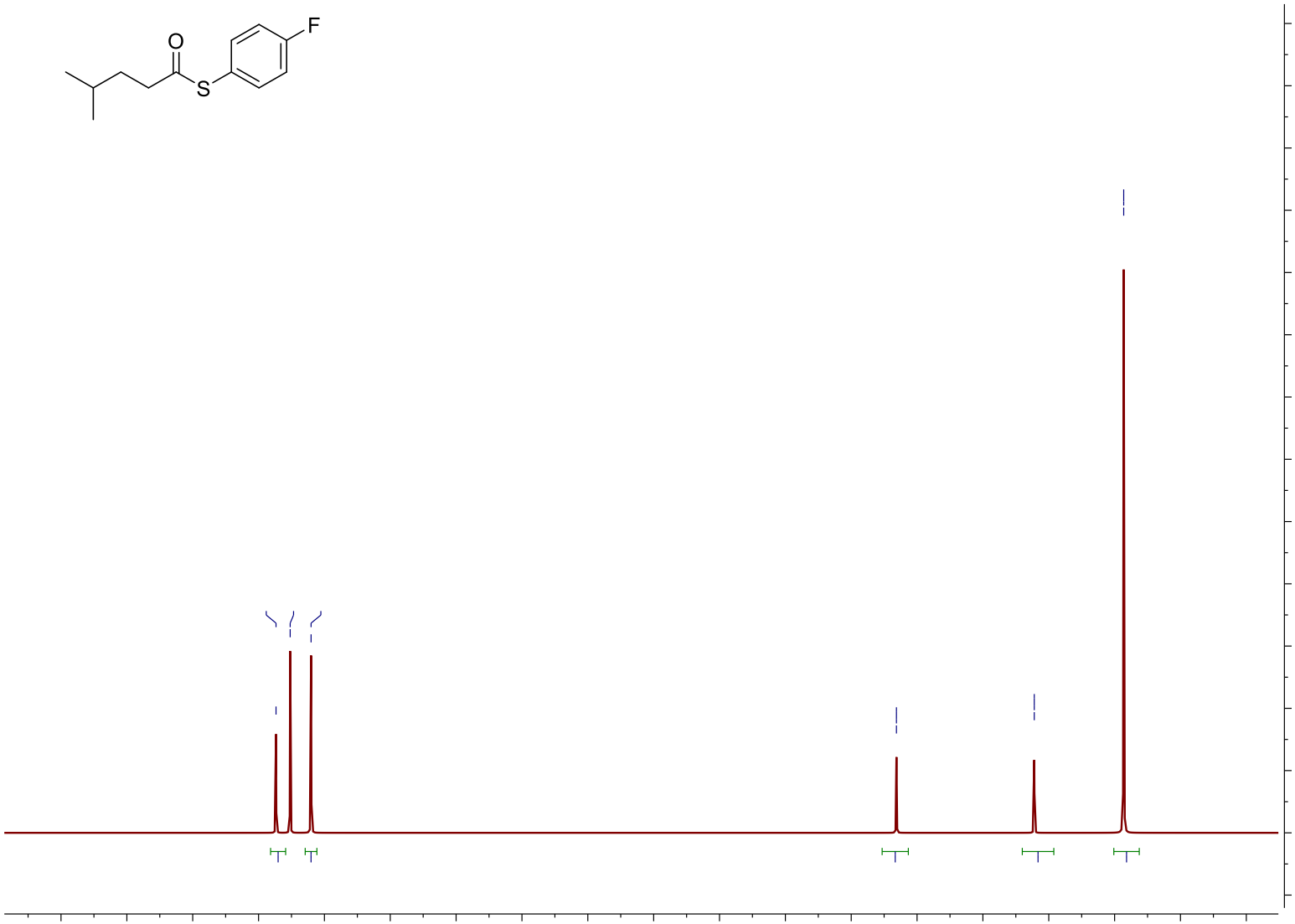
O
S
F

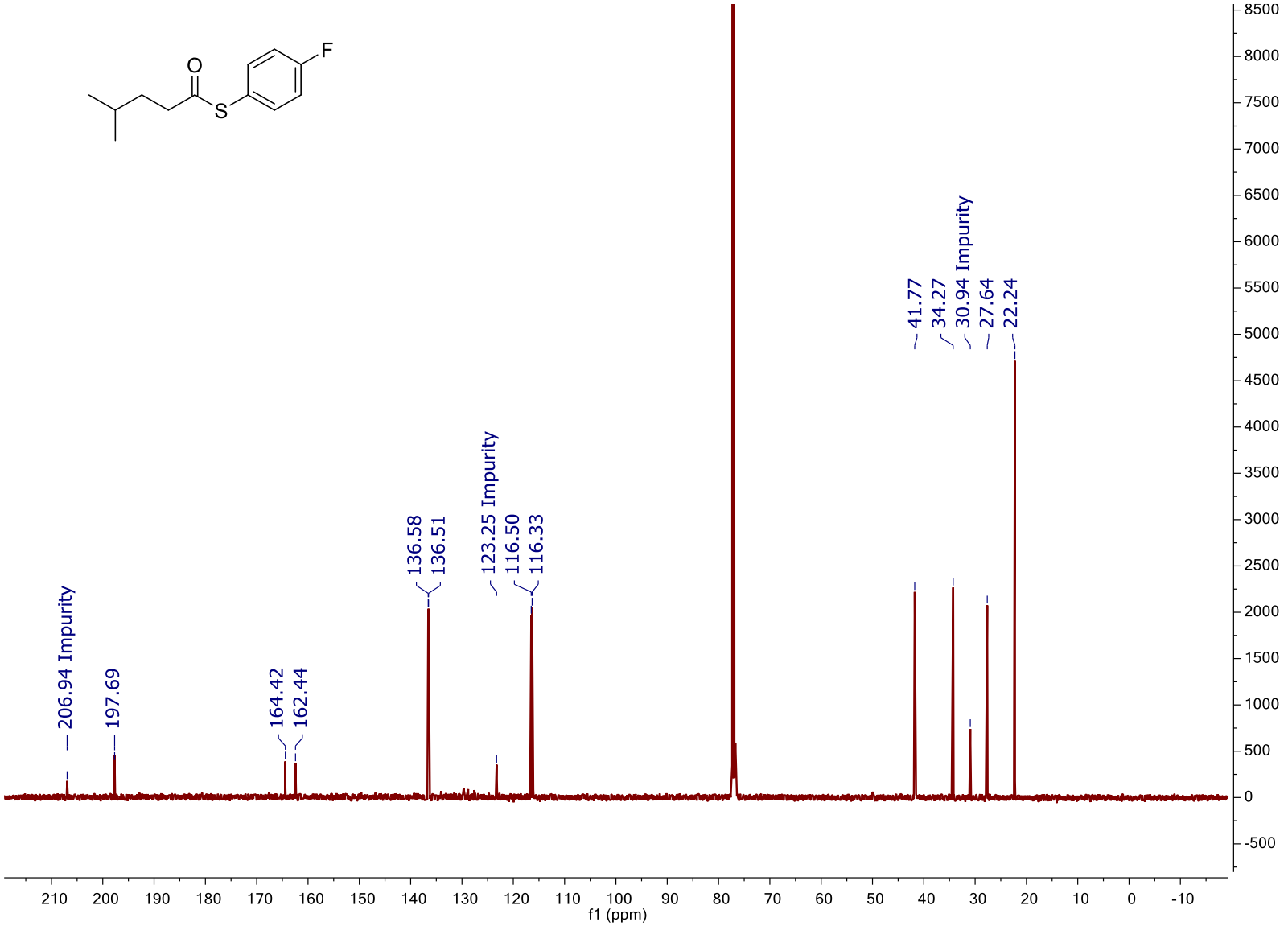
O
S
F
206.94 Impurity
197.69
164.42
162.44
136.58
136.51
123.25 Impurity
116.50
116.33
41.77
34.27
30.94 Impurity
27.64
22.24
f1 (ppm)

^{19}F NMR

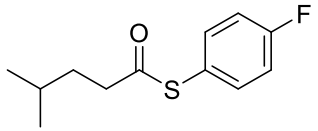
O
S
F

-111.40
2400
2200
2000
1800
1600
1400
1200
1000
800
600
400
200
0
-200
-98 -99 -100 -101 -102 -103 -104 -105 -106 -107 -108 -109 -110 -111 -112 -113 -114 -115 -116 -117 -118 -119 -120 -121 -122 -123 -124
f1 (ppm)

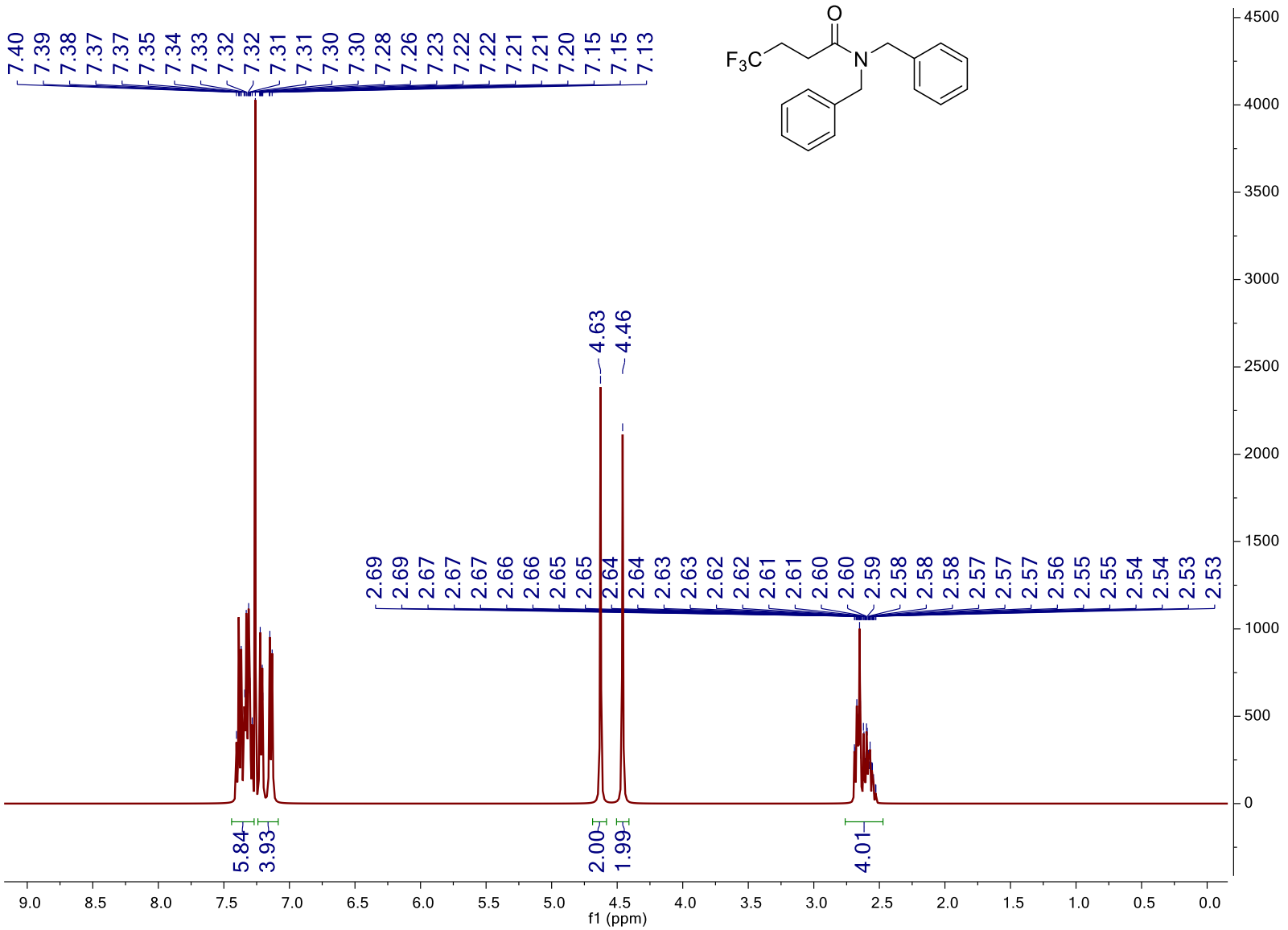
7.40 7.39 7.38 7.37 7.37 7.35 7.34 7.33 7.32 7.32 7.31 7.31 7.30 7.30 7.28 7.26 7.23 7.22 7.22 7.21 7.21 7.20 7.15 7.15 7.13
4.63 4.46
2.69 2.69 2.67 2.67 2.67 2.66 2.66 2.65 2.65 2.64 2.64 2.63 2.63 2.62 2.62 2.61 2.61 2.60 2.60 2.59 2.58 2.58 2.58 2.57 2.57 2.57 2.56 2.55 2.55 2.54 2.54 2.53 2.53
5.84 3.93 2.00 1.99 4.01
O
F3C
N
f1 (ppm)

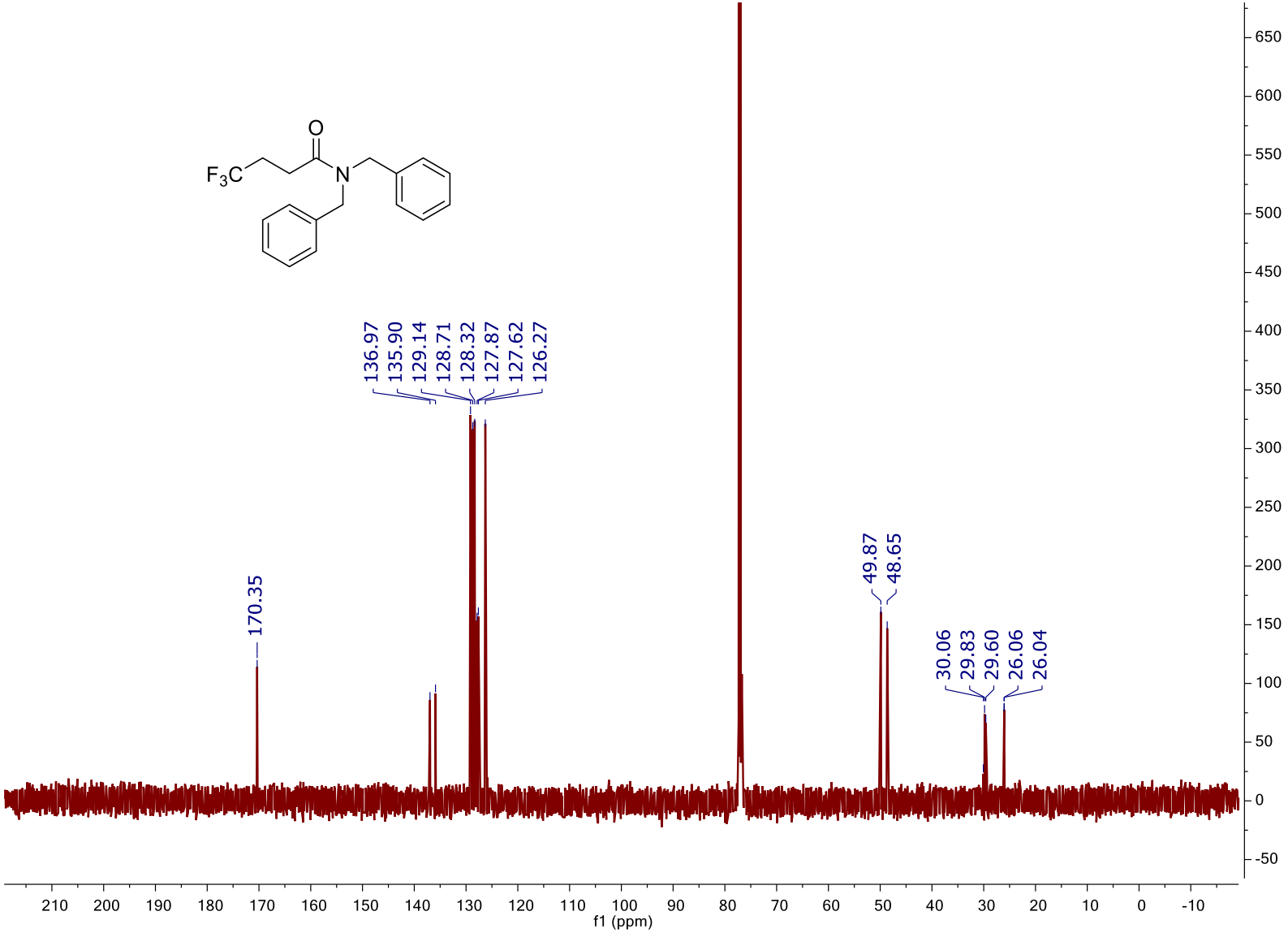
O
F3C
N
136.97
135.90
129.14
128.71
128.32
127.87
127.62
126.27
170.35
49.87
48.65
30.06
29.83
29.60
26.06
26.04
650
600
550
500
450
400
350
300
250
200
150
100
50
0
-50
210
200
190
180
170
160
150
140
130
120
110
100
90
80
70
60
50
40
30
20
10
0
-10
f1 (ppm)

^{19}F NMR


-66.50
-66.53
-66.56
O
F3C
N
500
450
400
350
300
250
200
150
100
50
0
-50
10
0
-10
-20
-30
-40
-50
-60
-70
-80
-90
-100
-110
-120
-130
-140
-150
-160
-170
-180
-190
-200
-210
f1 (ppm)

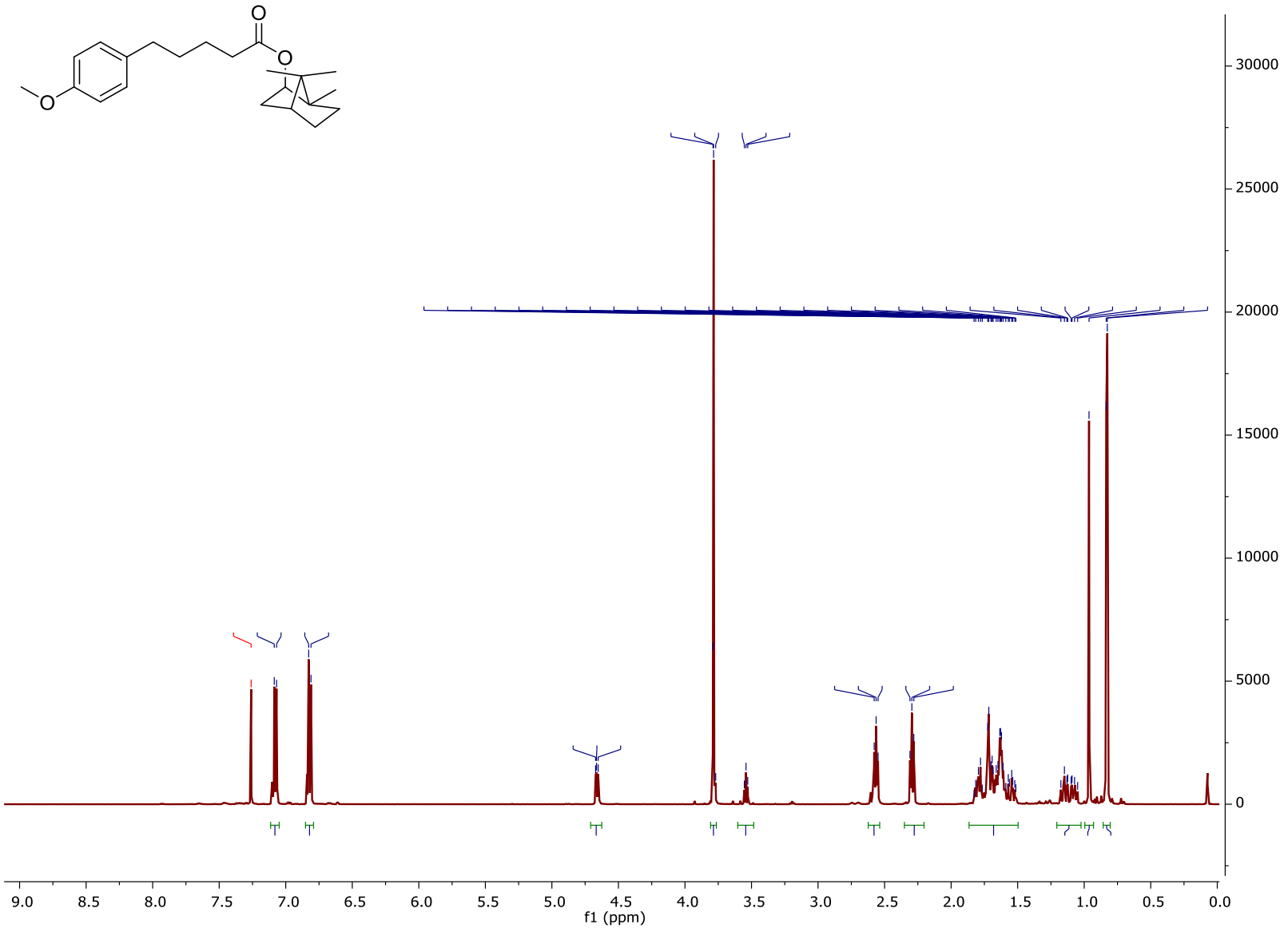
O
O
O
30000
25000
20000
15000
10000
5000
0
9.0
8.5
8.0
7.5
7.0
6.5
6.0
5.5
5.0
4.5
4.0
3.5
3.0
2.5
2.0
1.5
1.0
0.5
0.0
f1 (ppm)

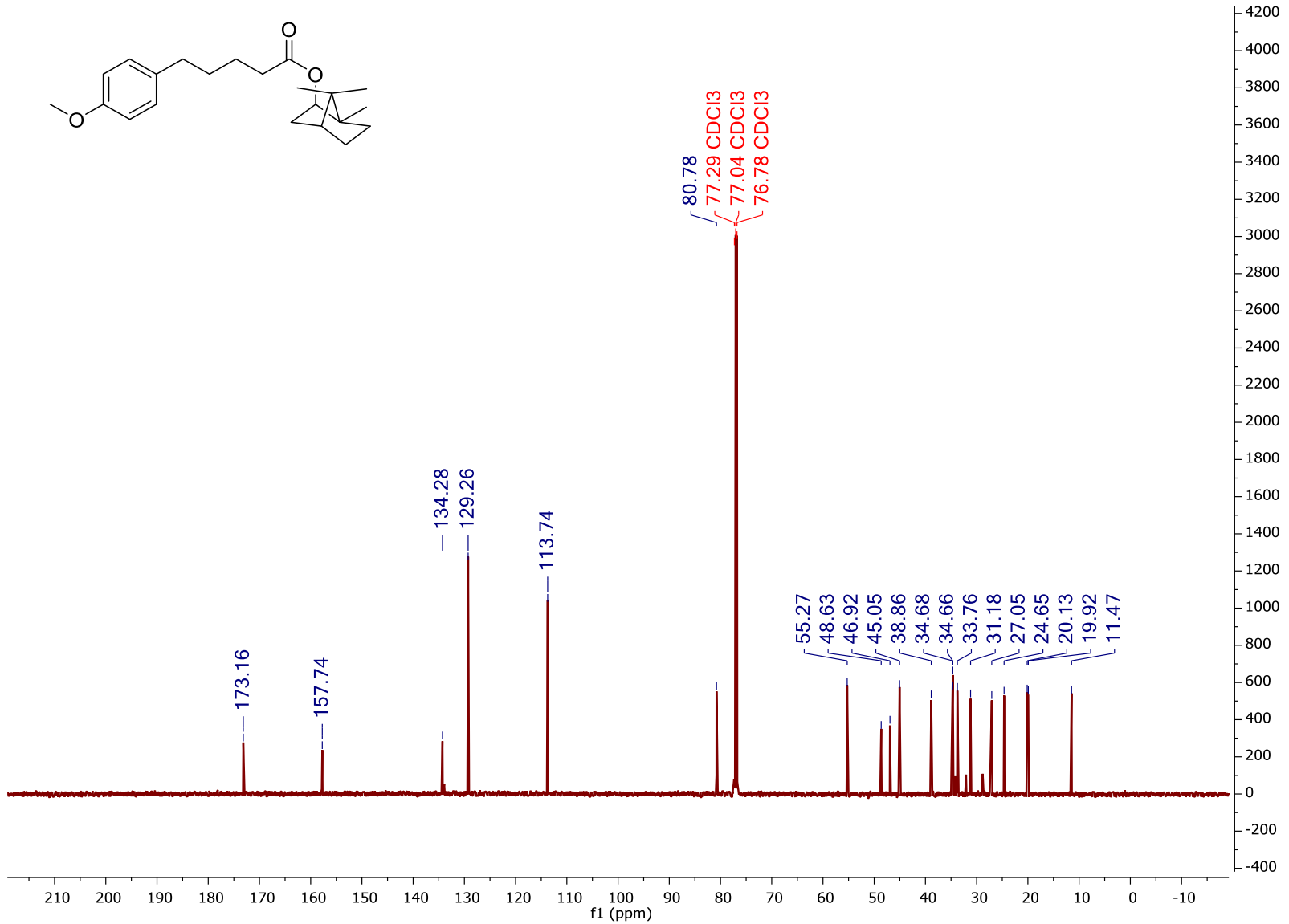
O
O
O
80.78
77.29 CDCl3
77.04 CDCl3
76.78 CDCl3
134.28
129.26
113.74
173.16
157.74
55.27
48.63
46.92
45.05
38.86
34.68
34.66
33.76
31.18
27.05
24.65
20.13
19.92
11.47
f1 (ppm)

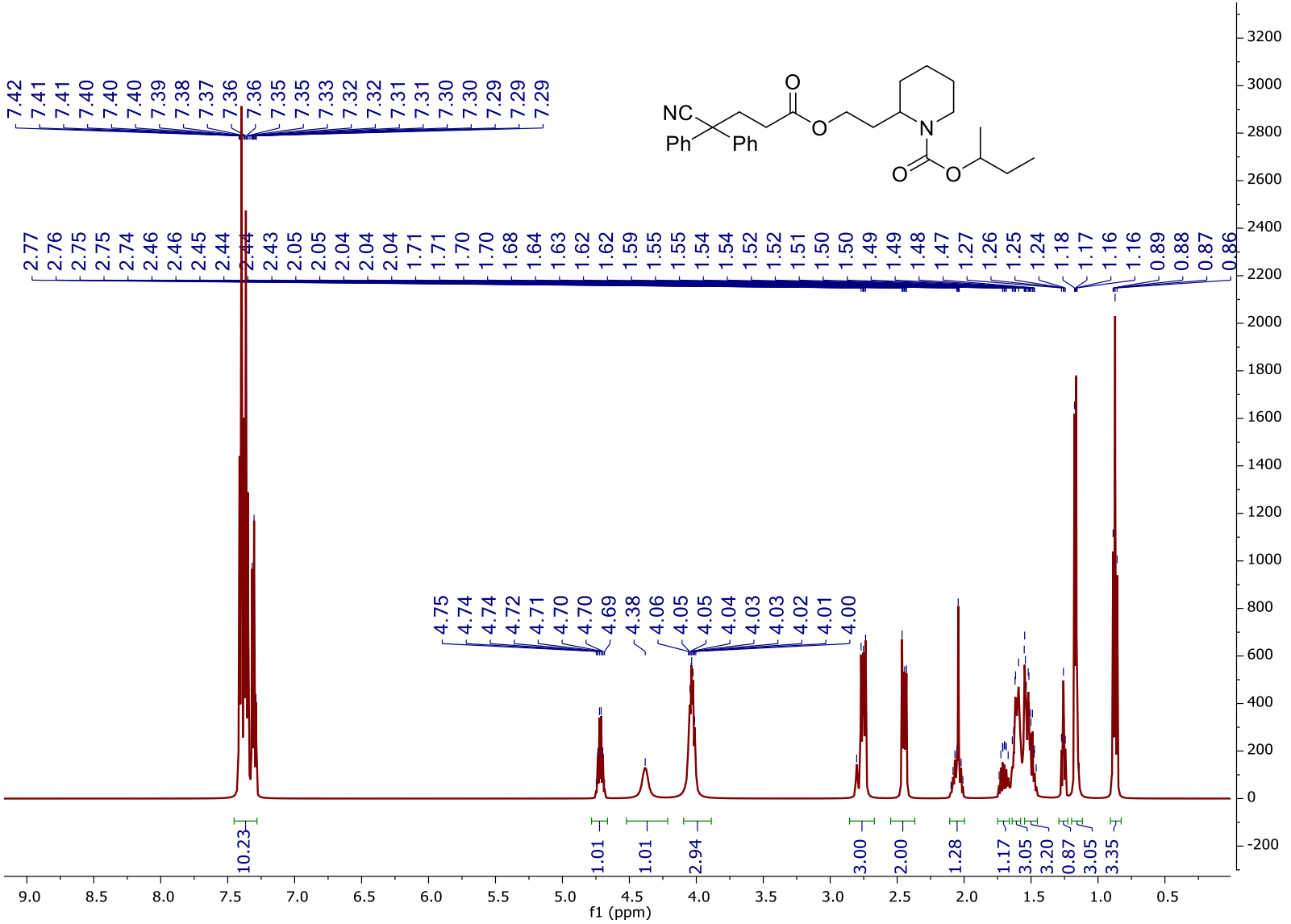
7.42 7.41 7.41 7.40 7.40 7.40 7.39 7.38 7.37 7.36 7.36 7.35 7.35 7.33 7.32 7.32 7.31 7.31 7.30 7.30 7.29 7.29 7.29
2.77 2.76 2.75 2.75 2.74 2.46 2.46 2.45 2.44 2.44 2.43 2.05 2.05 2.04 2.04 2.04 1.71 1.71 1.70 1.70 1.68 1.64 1.63 1.62 1.62 1.59 1.55 1.55 1.54 1.54 1.52 1.52 1.51 1.50 1.50 1.49 1.49 1.48 1.47 1.27 1.26 1.25 1.24 1.18 1.17 1.16 1.16 0.89 0.88 0.87 0.86
4.75 4.74 4.74 4.72 4.71 4.70 4.70 4.69 4.38 4.06 4.05 4.05 4.04 4.03 4.03 4.02 4.01 4.00
NC
Ph
Ph
O
O
N
O
O
10.23 1.01 1.01 2.94 3.00 2.00 1.28 1.17 3.05 3.20 0.87 3.05 3.35
f1 (ppm)

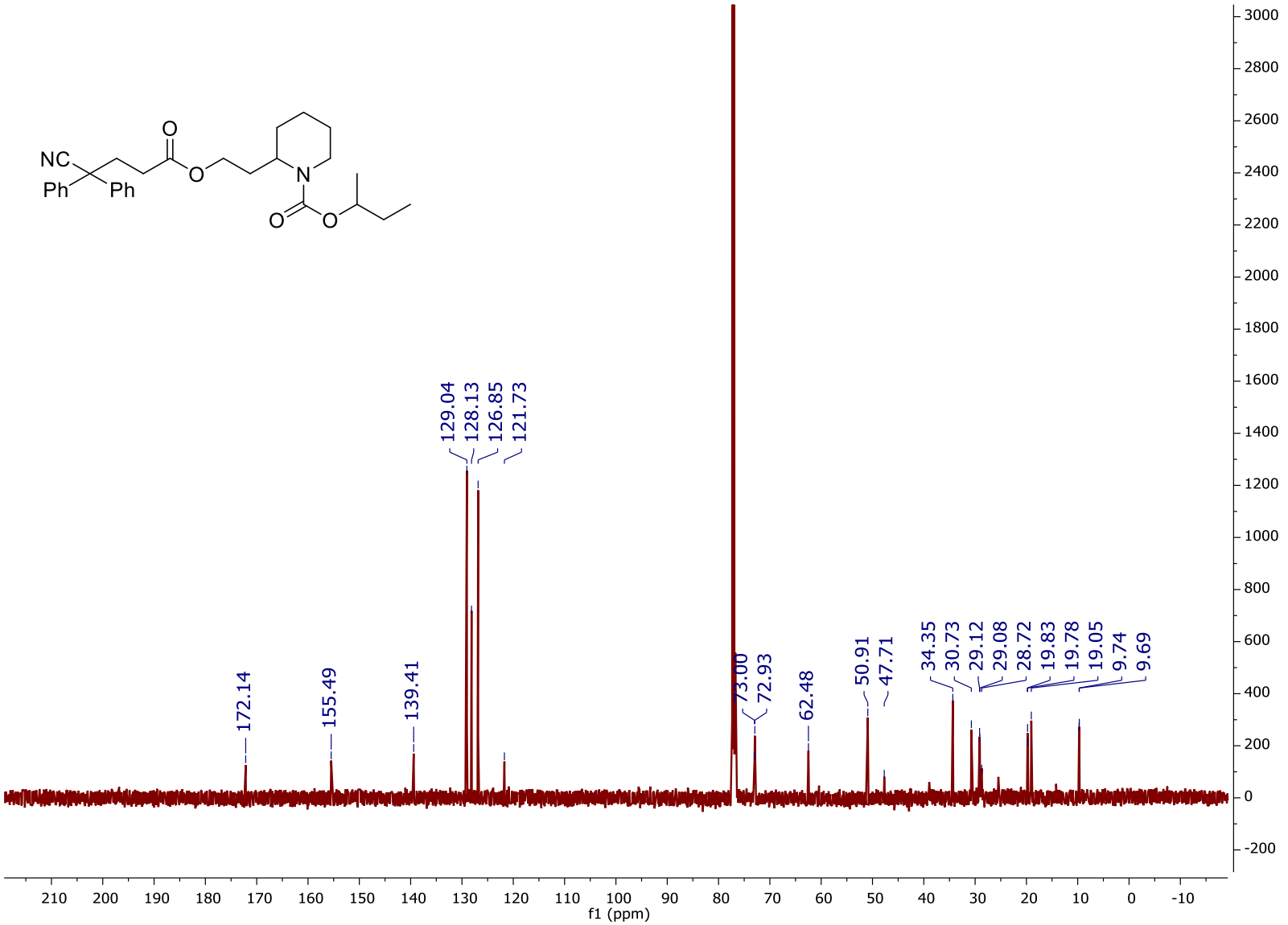
NC
Ph
Ph
O
O
N
O
O
172.14
155.49
139.41
129.04
128.13
126.85
121.73
73.00
72.93
62.48
50.91
47.71
34.35
30.73
29.12
29.08
28.72
19.83
19.78
19.05
9.74
9.69
f1 (ppm)

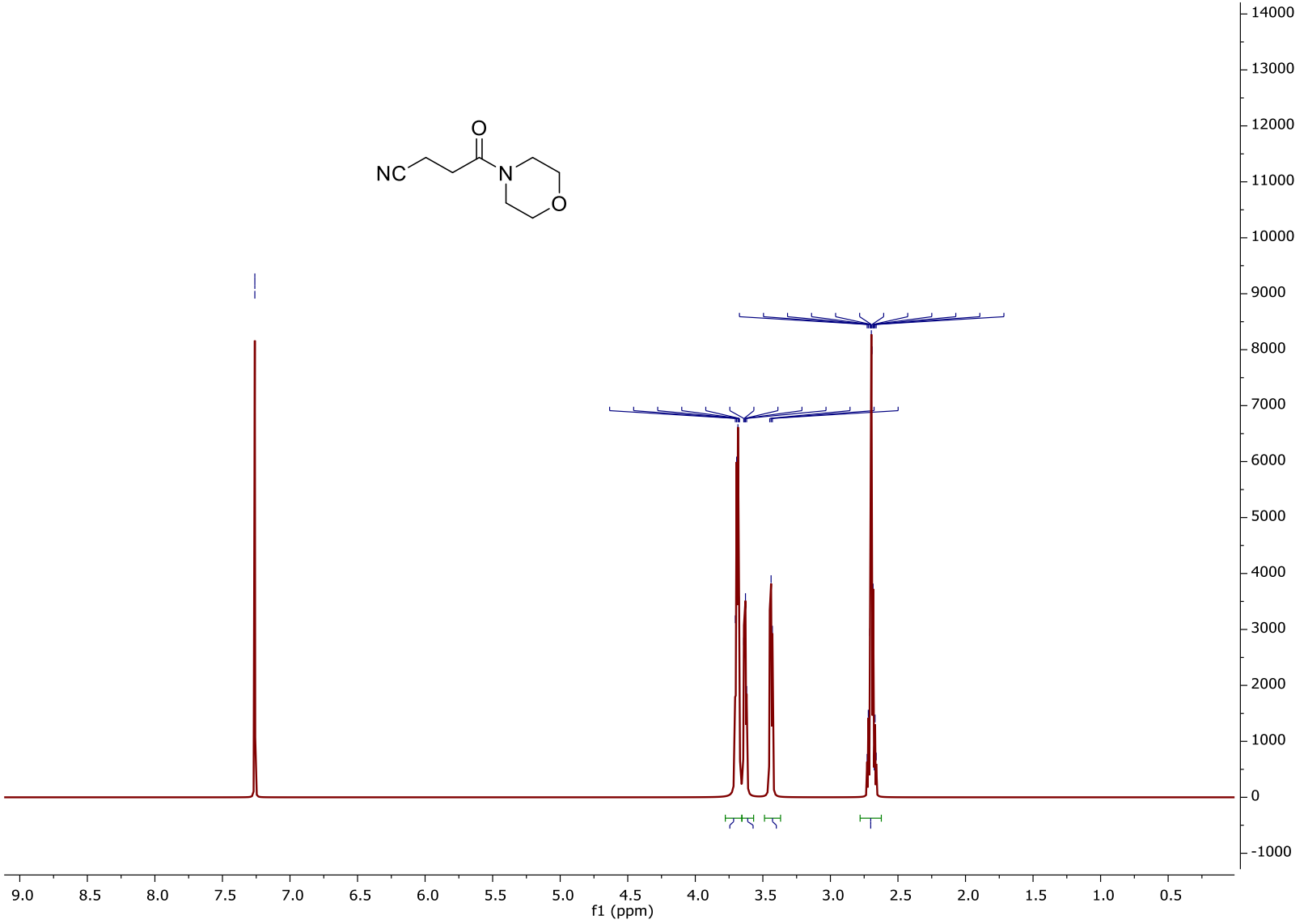
NC
O
N
O
14000
13000
12000
11000
10000
9000
8000
7000
6000
5000
4000
3000
2000
1000
0
-1000
9.0
8.5
8.0
7.5
7.0
6.5
6.0
5.5
5.0
4.5
4.0
3.5
3.0
2.5
2.0
1.5
1.0
0.5
f1 (ppm)

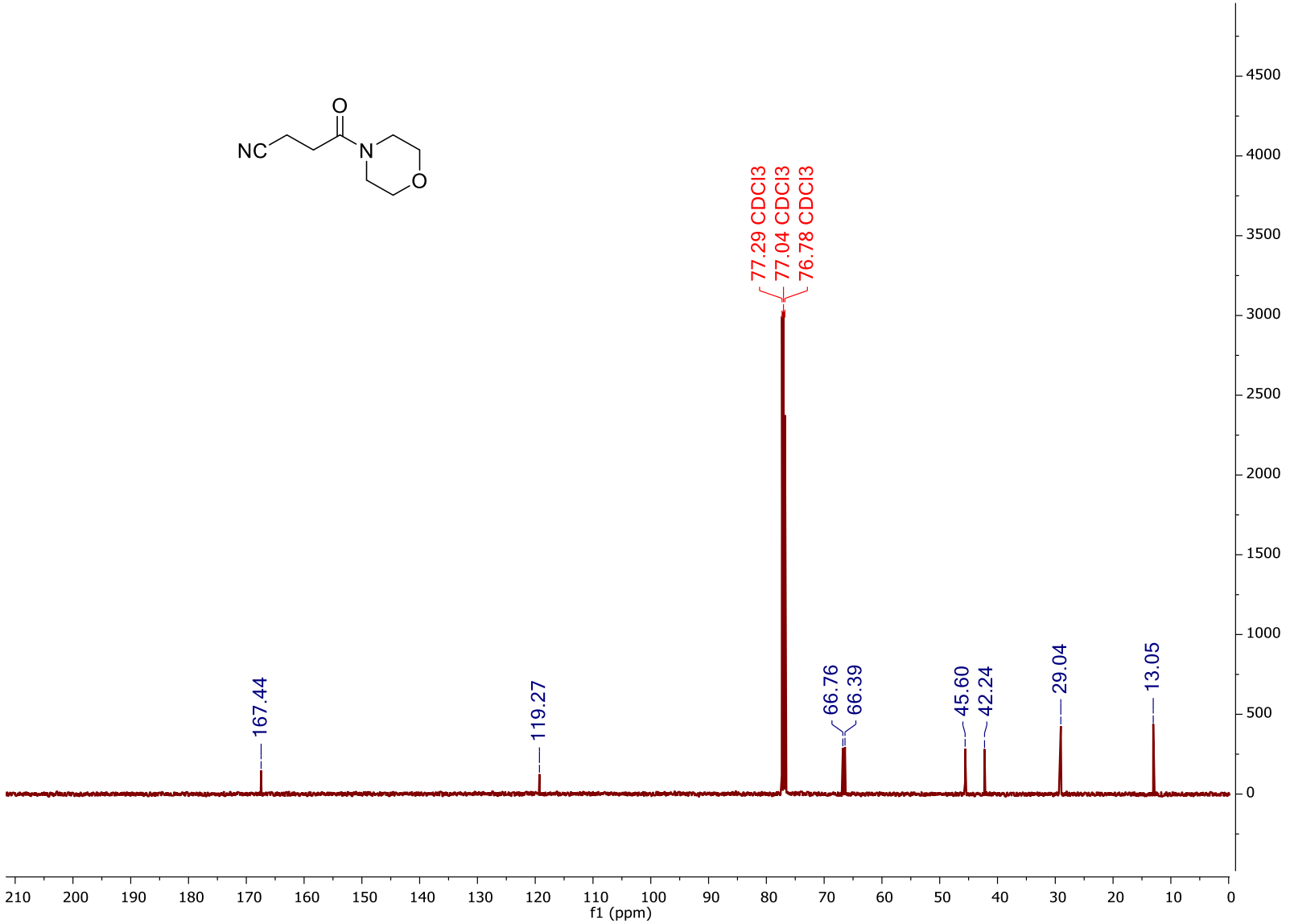
NC
O
N
O
77.29 CDCl3
77.04 CDCl3
76.78 CDCl3
167.44
119.27
66.76
66.39
45.60
42.24
29.04
13.05
4500
4000
3500
3000
2500
2000
1500
1000
500
0
210 200 190 180 170 160 150 140 130 120 110 100 90 80 70 60 50 40 30 20 10 0
f1 (ppm)

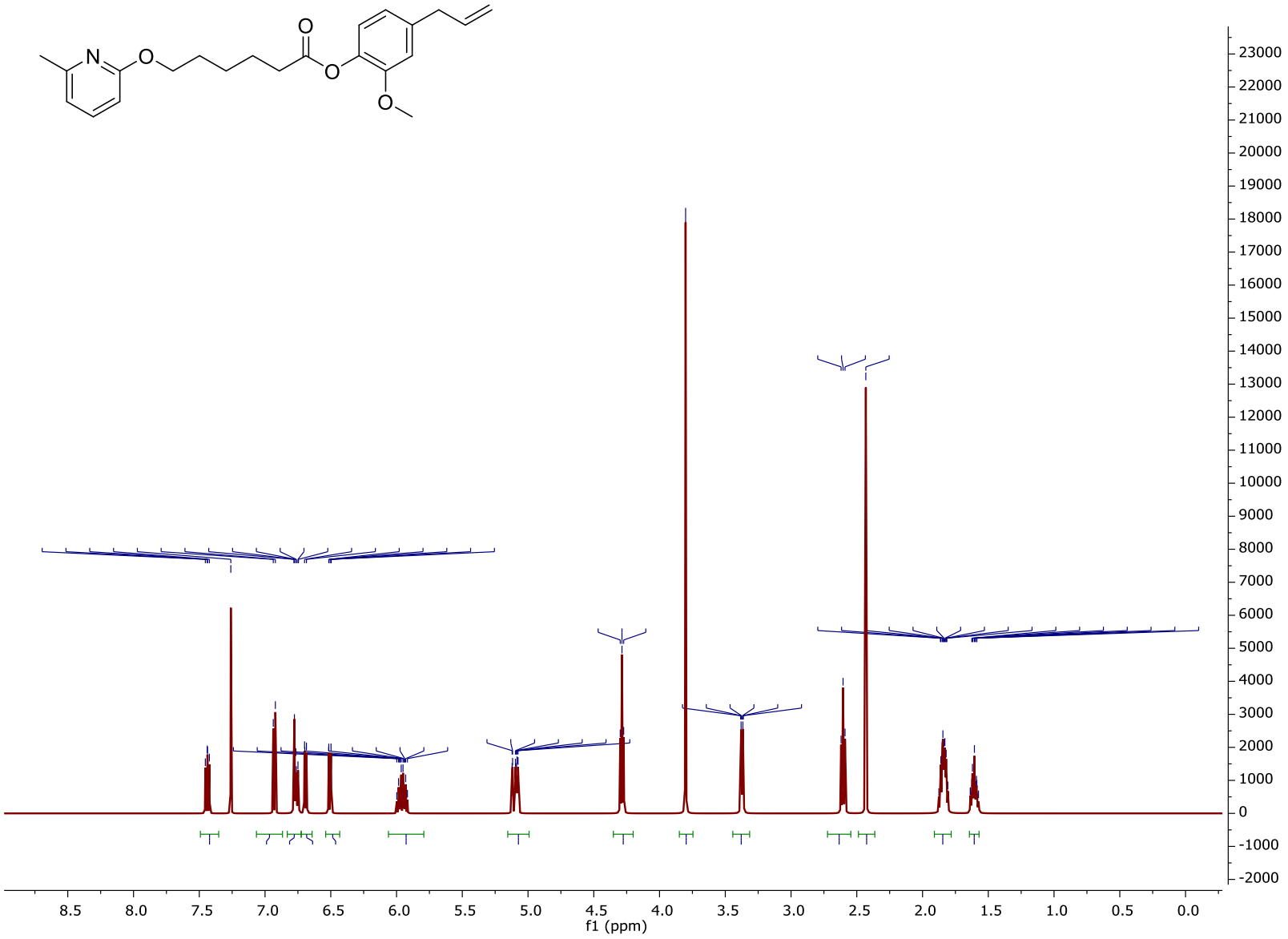
N
O
O
O
O
23000
22000
21000
20000
19000
18000
17000
16000
15000
14000
13000
12000
11000
10000
9000
8000
7000
6000
5000
4000
3000
2000
1000
0
-1000
-2000
8.5
8.0
7.5
7.0
6.5
6.0
5.5
5.0
4.5
4.0
3.5
3.0
2.5
2.0
1.5
1.0
0.5
0.0
f1 (ppm)

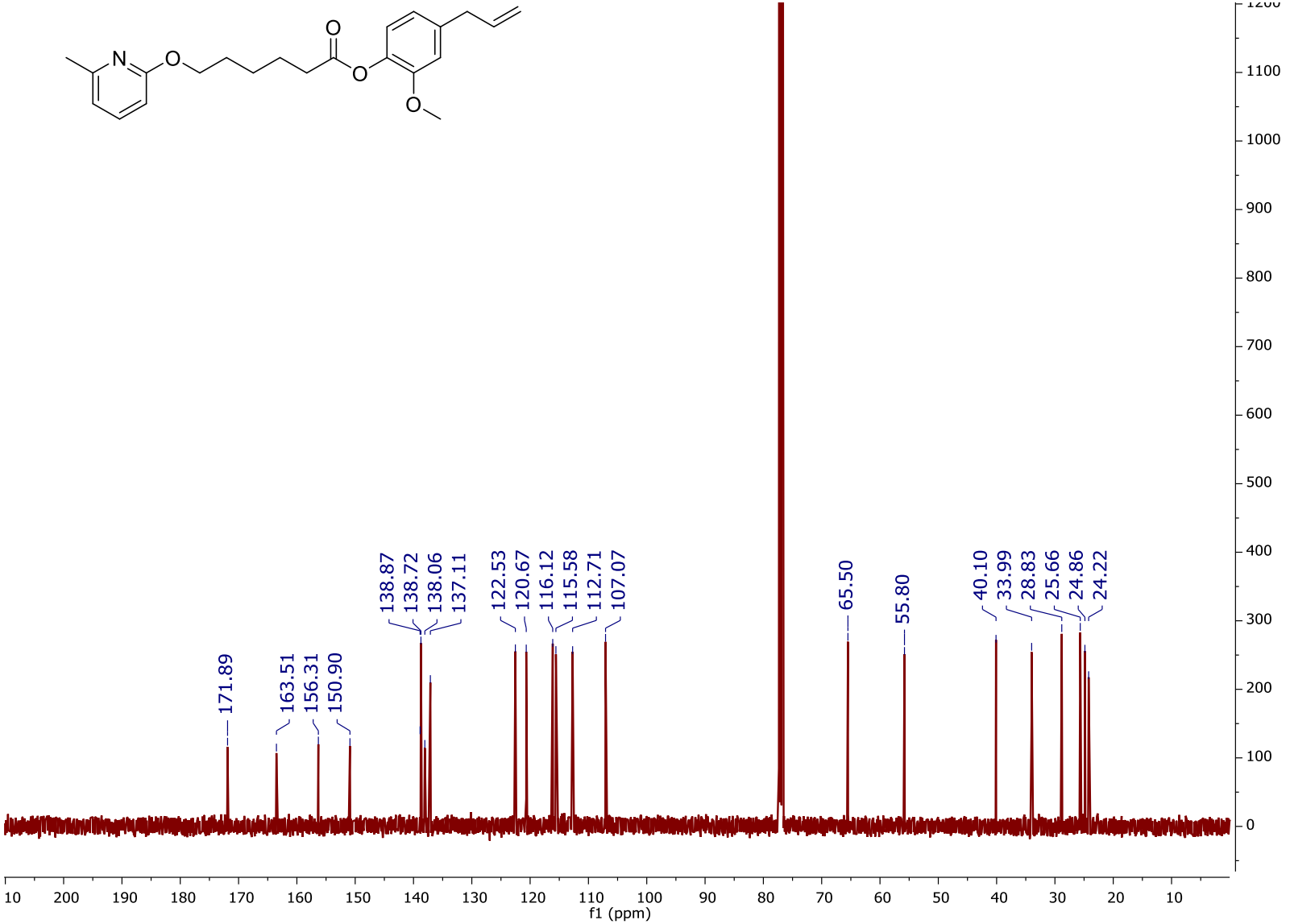
N
O
O
O
O
171.89
163.51
156.31
150.90
138.87
138.72
138.06
137.11
122.53
120.67
116.12
115.58
112.71
107.07
65.50
55.80
40.10
33.99
28.83
25.66
24.86
24.22
f1 (ppm)

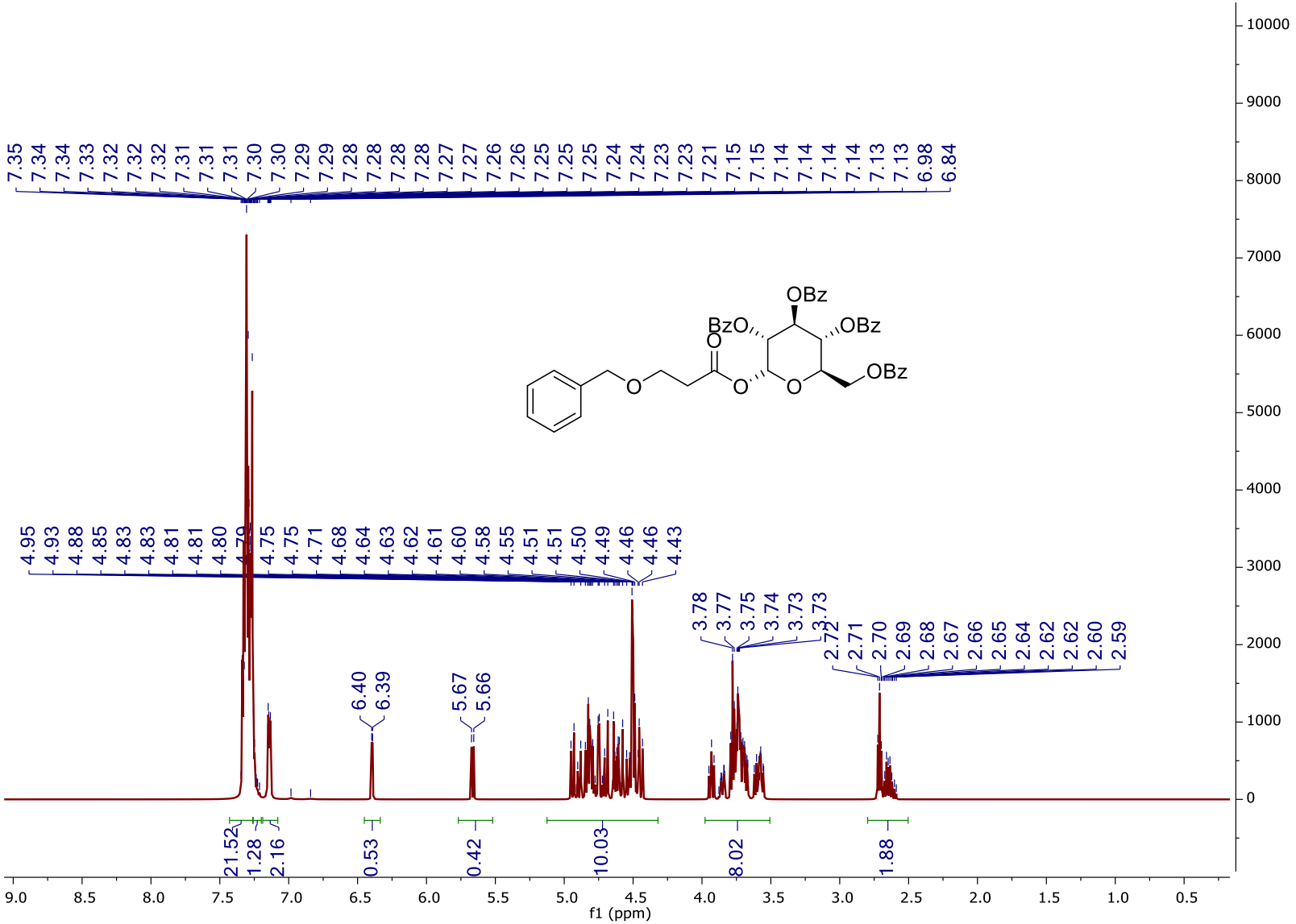
7.35 7.34 7.34 7.33 7.32 7.32 7.32 7.31 7.31 7.31 7.30 7.30 7.29 7.29 7.28 7.28 7.28 7.28 7.27 7.27 7.26 7.26 7.25 7.25 7.25 7.24 7.24 7.23 7.23 7.21 7.15 7.15 7.14 7.14 7.14 7.14 7.13 7.13 6.98 6.84
OBz
BzO
OBz
OBz
O
O
O
O
4.95 4.93 4.88 4.85 4.83 4.83 4.81 4.81 4.80 4.79 4.75 4.75 4.71 4.68 4.64 4.63 4.62 4.61 4.60 4.58 4.55 4.51 4.51 4.50 4.49 4.46 4.46 4.43
3.78 3.77 3.75 3.74 3.73 3.73 2.72 2.71 2.70 2.69 2.68 2.67 2.66 2.65 2.64 2.62 2.62 2.60 2.59
6.40 6.39
5.67 5.66
21.52 1.28 2.16 0.53 0.42 10.03 8.02 1.88
9.0 8.5 8.0 7.5 7.0 6.5 6.0 5.5 5.0 4.5 4.0 3.5 3.0 2.5 2.0 1.5 1.0 0.5
f1 (ppm)
10000 9000 8000 7000 6000 5000 4000 3000 2000 1000 0

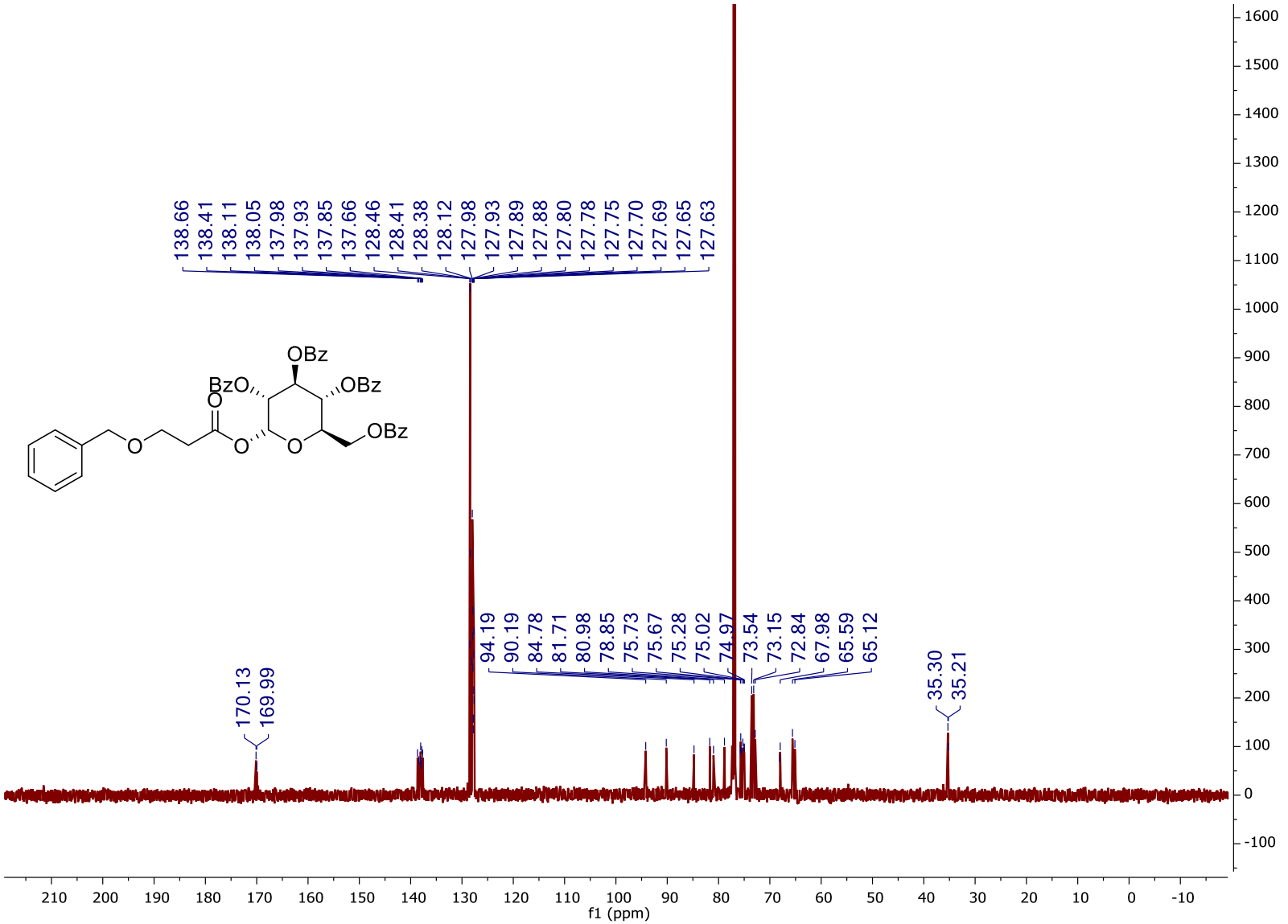
138.66
138.41
138.11
138.05
137.98
137.93
137.85
137.66
128.46
128.41
128.38
128.12
127.98
127.93
127.89
127.88
127.80
127.78
127.75
127.70
127.69
127.65
127.63
94.19
90.19
84.78
81.71
80.98
78.85
75.73
75.67
75.28
75.02
74.97
73.54
73.15
72.84
67.98
65.59
65.12
170.13
169.99
35.30
35.21
OBz
BzO
OBz
OBz
O
O
O
O
f1 (ppm)

4.12 Experimental References

(1) Y. Liu, C. Zhou, M. Jiang, B. Arndtsen. Versatile Palladium-Catalyzed Approach to Acyl Fluorides and Carbonylations by Combining Visible Light- and Ligand-Driven Operations *J. Am. Chem. Soc.* **2022**, *144*, 9413–9420.

(2) Bruker. *APEX3*; Bruker AXS Inc.: Madison, Wisconsin, USA, 2012

(4) V., Kunuru, D., Chanti Babu, B., Dokuburra, B., Tatipamula Vinay, R. A., Bunce, C. B., Rao, Y., Venkateswarlu, Synthesis of n-alkyl terminal halohydrin esters from acid halides and cyclic ethers or thioethers under solvent- and catalyst-free conditions. *RSC Adv.* **2014**, *4*, 51991-51994.

(5) M. A., Hossain, N., Sattenapally, H. I., Parikh, W., Li, K. P., Rumbaug, N. A., German, Design, synthesis, and evaluation of compounds capable of reducing Pseudomonas aeruginosa virulence. *Eur. J. Med. Chem.* **2020**, *185*, 111800.

(6) Y. Zhao, G. Chen. Palladium-Catalyzed Alkylation of *ortho*-C(sp^2)–H Bonds of Benzylamide Substrates with Alkyl Halides**.** *Org. Lett.* 2011, 13, 18, 4850–4853

(7) A., Baber, J. D., de Vries, A. G., Orpen, P. G., Pringle, K., von der Luehe, Allosteric effects in asymmetric hydrogenation catalysis? Asymmetric induction as a function of the substrate and the backbone flexibility of C1-symmetric diphosphines in rhodium-catalysed hydrogenations. *Dalton Trans*. **2006**, 4821-4828.

(8) D. Solé, A. Amenta, F. Mariani, M.-L. Bennasar, I. Fernández, *Adv. Synth. Catal.* **2017**, *359*, 3654.

(11) C. M., Brian, E. A. Cynthia.; R. A. Flowers, Synthesis of γ-halogenated ketones via the Ce(IV)-mediated oxidative coupling of cyclobutanols and inorganic halides.*Tetrahedron Lett.* **2009**, *50*, 1264-1266.

(12) R., Sina, D., Vijayarajan, D. A., Watson, Nickel-Catalyzed C-Alkylation of Nitroalkanes with Unactivated Alkyl Iodides. *J. Am. Chem. Soc.* **2017**, *139*, 8110-8113.

(13) Hernán-Gómez, M. Rodríguez, T. Parella, M. Costas, *Angew. Chem. Int. Ed.* **2019**, *58*, 13904.

(14) F. Zhou, J. Zhu, Y. Zhang, S. Zhu, *Angew. Chem. Int. Ed.* **2018**, *57*, 4058.

(15) S. Pache, M. Lautens, Palladium-Catalyzed Sequential Alkylation−Alkenylation Reactions: New Three-Component Coupling Leading to Oxacycles. *Org. Lett.* **2003**, *5*, 4827 4830.

(16) P.-C. Chiang, Y. Kim, J. W. Bode, Catalytic amide formation with α′-hydroxyenones as acylating reagents. *Chem. Commun.* **2009**, 4566-4568.

(17) K. B., Ling, A. D., Smith, α-Aroyloxyaldehydes: scope and limitations as alternatives to α-haloaldehydes for NHC-catalyzed redox transformations. *Chem. Commun*. **2011**, *47*, 373-375.

(18) D. Lafrance, P. Bowles, K. Leeman, R. Rafka, Mild Decarboxylative Activation of Malonic Acid Derivatives by 1,1'-Carbonyldiimidazole. *Org. Lett.* **2011**, *13*, 2322-2325.

(19) S. C., Ghosh, S. Muthaiah, Y. Zhang, X. Xu, H. Soon, Direct Amide Synthesis from Alcohols and Amines by Phosphine-Free Ruthenium Catalyst Systems. *Adv. Synth. Catal.* **2009**, *351*, 2643- 2649.

(20) I. Shiina, Y. Kawakita, The effective use of substituted benzoic anhydrides for the synthesis of carboxamides. *Tetrahedron*. **2004**, *60*, 4729-4733.

(21) J. W. Bode, S. S. Sohn, N-Heterocyclic Carbene-Catalyzed Redox Amidation of α-Functionalized Aldehydes with Amines. *J. Am. Chem. Soc.* **2007**, *129*, 13798-13799.

(22) D. G., Hewitt, G. L., Newland, Organophosphorus compounds. P-Arylated perhydro-1,2-azaphosphorines. *Aust. J. Chem.* **1977**, *30*, 579-587.

(23) V. Gandon, P. Bertus, J. Szymoniak, New transformations from a 3-silyloxy-2-aza-1,3-diene: consecutive Zr-mediated retro-Brook rearrangement and reactions with electrophiles. *Tetrahedron*. **2000**, *56*, 4467-4472.

(24) M. Cloutier, M. Roudias, J.-F., Paquin, Regioselective Gold-Catalyzed Hydration of CF3- and SF5-alkynes. *Org. Lett*. **2019**, *21*, 3866-3870.

(25) K. Geoghegan, S. Kelleher, P. Evans, An investigation into the one-pot Heck olefination-hydrogenation reaction. *J. Org. Chem.* **2011**, *76*, 2187-2194.

(26) Bruker. *APEX3*; Bruker AXS Inc.: Madison, Wisconsin, USA, 2012

(27) L. Krause, R. Herbst-Irmer, G. M. Sheldrick, D. Stalke, Comparison of Silver and Molybdenum Microfocus X-Ray Sources for Single-Crystal Structure Determination. *J. Appl. Cryst.* **2015**, *48*, 3–10.

(28) a) G. M. Sheldrick Crystal structure refinement with SHELXL *Acta Cryst.* **C71**, 3-8 (2015). b) C. B. Hübschle, G. M. Sheldrick, B. Dittrich ShelXle: a Qt graphical user interface for SHELXL *J. Appl. Cryst.* **2011**, *44*, 1281−1284.

(29) C. F. Macrae, I. Sovago, S. J. Cottrell, P. T. A. Galek, P. McCabe, E. Pidcock, M. Platings, G. P. Shields, J. S. Stevens, M. Towler, P. A. Wood, Mercury 4.0: from visualization to analysis, design and prediction *J. Appl. Cryst.* **2020** *53*, 226−235.

(30) O. V. Dolomanov, L. J. Bourhis, R. J. Gildea, J. A. K. Howard, H. Puschmann, H. OLEX2: A complete structure solution, refinement and analysis program. *J. Appl. Cryst*. **2009** *42*, 339−341.